

Nonlinear macroscopic description of liquid crystalline elastomers in external fields

Von der Universität Bayreuth
zur Erlangung des Grades eines
Doktors der Naturwissenschaften (Dr. rer. nat.)
genehmigte Abhandlung

vorgelegt von

Andreas Menzel

geboren in München/Bayern

1. Gutachter:	Prof. Dr. H. R. Brand
2. Gutachter:	Prof. Dr. H. Pleiner
Tag der Einreichung:	21.10.2008
Tag des Kolloquiums:	04.02.2009

Contents

Zusammenfassung	v
1 Introduction	1
1.1 Liquid crystals	2
1.2 Polymers and elastomers	6
1.3 Liquid crystalline elastomers	8
1.4 Scope of this work	14
2 Linear macroscopic description	17
2.1 State variables	18
2.2 Variables contributing to the generalized energy density	20
2.3 Generalized energy density	24
2.4 Other approaches	29
3 Rotatoelectricity in cholesteric side-chain liquid single crystal elastomers	31
3.1 Geometry and corresponding generalized energy density	32
3.2 Rotations of the director	36
3.3 Experimental observation of rotatoelectricity	40
3.4 Discussion and conclusion	43
4 Dielectric effects in cholesteric side-chain liquid single crystal elastomers	45
4.1 Geometry and macroscopic equations	45
4.2 Laterally homogeneous solution	50
4.3 Laterally inhomogeneous solutions	54
4.4 Discussion and conclusion	61
5 Mechanical deformations of cholesteric side-chain liquid single crystal elastomers	67
5.1 Macroscopic equations	68

5.2	Compression and dilation parallel to the helical axis	69
5.3	Lateral compression and dilation	71
5.4	Discussion and conclusion	76
6	Nonlinear macroscopic description	79
6.1	Motivation for the extension of the model to the nonlinear regime	80
6.2	Two coupled preferred directions and nonlinear relative rotations	84
6.3	Exact expressions for the nonlinear variables of relative rotations	90
6.4	Connection to the linear description	92
6.5	Discussion and perspective	93
7	Finite shear deformation of a nematic side-chain liquid single crystal elastomer	97
7.1	Geometry and generalized energy density	98
7.2	Analysis of the shear deformation	101
7.3	Discussion	104
8	Nonlinear stress-strain behavior of nematic side-chain liquid single crystal elastomers	107
8.1	Generalized energy density	108
8.2	Geometry and Eulerian description	109
8.3	Reorientation of the director field	115
8.4	Stress-strain curves	118
8.5	Including shear deformations	123
8.6	Discussion and perspective	127
9	Conclusions	131
A	Variational derivatives of the generalized energy	135
B	Electrostrictive effects in cholesteric side-chain liquid single crystal elastomers	139
C	Symmetry relations and an alternative definition of relative rotations	141
D	Finite shear deformation of an elastically anisotropic nematic side-chain liquid single crystal elastomer	145
E	Highly ordered patterns of parabolic focal conics in lamellar lyotropic systems	149
E.1	Introduction	149

<i>Contents</i>	iii
E.2 Sample preparation	151
E.3 Experimental observations on the parabolic focal conical structures	151
E.4 Discussion	158
E.5 Conclusions	164
Bibliography	167

Zusammenfassung

Im Hauptteil dieser Arbeit befassen wir uns mit der Modellierung des makroskopischen Verhaltens von Monodomänen flüssigkristalliner Seitenkettenelastomere. Dabei konzentrieren wir uns auf den Einfluss, den statische (bzw. quasistatische), von außen angelegte elektrische und mechanische Felder auf diese Materialien haben. Die Herleitung einer nichtlinearen makroskopischen Modellbeschreibung bildet den Kern dieser Arbeit.

Zu Beginn werden die untersuchten Materialien in Kapitel 1 genauer vorgestellt. Flüssigkristalline Seitenkettenelastomere entstehen durch die chemische Vernetzung von Polymerketten, an welche flüssigkristalline Einheiten als Seitenketten gebunden werden. In nematischen und cholesterischen Seitenkettenelastomeren ordnen sich diese flüssigkristallinen Einheiten dann lokal entlang einer mittleren Vorzugsrichtung an. Man beschreibt die Orientierung dieser Vorzugsrichtung mit Hilfe des Direktorfeldes. Durch spezielle Syntheseverfahren erhält man Monodomänen der Direktoranordnung, die sich über die gesamte Probe erstrecken. Die entsprechenden Materialien werden mit dem Kürzel SCLSCEs bezeichnet, welches für „side-chain liquid single crystal elastomers“ steht. Im Grundzustand nematischer SCLSCEs ist der Direktor räumlich homogen über die gesamte Probe orientiert, im cholesterischen Fall ist die Direktoranordnung zu einer helixartigen Struktur verdrillt. Wie in Kapitel 1 erklärt, besitzen flüssigkristalline Elastomere einzigartige Materialeigenschaften. Sie kombinieren nicht nur die Eigenschaften flüssigkristalliner Phasen mit der elastischen Verformbarkeit gummiartiger Festkörper, sondern koppeln diese auch aneinander. So können sie durch eine erzwungene Reorientierung des Direktors, etwa durch Anlegen eines äußeren elektrischen Feldes, elastisch deformiert werden. Umgekehrt lässt sich auch durch eine erzwungene elastische Verzerrung der Direktor reorientieren. Aufgrund dieser Eigenschaften sind verschiedene technologische Anwendungen der Materialien vorstellbar. Beispielsweise wurde ihre Verwendung zur Herstellung künstlicher Muskeln diskutiert.

Wir beschränken uns in dieser Arbeit auf die Charakterisierung des makroskopischen Verhaltens nematischer und cholesterischer SCLSCEs. Dabei

nehmen wir die Kopplung zwischen Direktororientierung und mechanischer Verformbarkeit der Materialien explizit in unsere Beschreibung auf. Dies geschieht, indem wir Relativrotationen zwischen der Direktororientierung und dem Polymernetzwerk als eigenständige makroskopische Variable berücksichtigen. Ein lineares Modell dieser Art wurde bereits durch de Gennes für nematische Elastomere vorgeschlagen. Wir geben in Kapitel 2 einen entsprechenden Ausdruck für die generalisierte Energiedichte cholesterischer Elastomere an, wobei auch der Einfluss eines äußeren elektrischen Feldes berücksichtigt wird. Dieser Ausdruck für die generalisierte Energiedichte dient als Grundlage unserer linearisierten Untersuchungen cholesterischer SCLSCEs in den drei darauffolgenden Kapiteln. Den Systemzustand charakterisieren wir jeweils durch die Komponenten des Direktorfeldes und des mechanischen Verschiebungsfeldes.

In den Kapiteln 3 und 4 untersuchen wir zunächst die Auswirkungen, welche ein homogenes externes elektrisches Feld auf cholesterische SCLSCEs hat. Dazu nehmen wir an, dass die Materialien elektrisch isolierend sind, was für gewöhnliche SCLSCEs eine gute Näherung darstellt. Wir betrachten eine Geometrie, in der das von außen angelegte elektrische Feld parallel zur Achse der cholesterischen Helix orientiert ist. Weiterhin berücksichtigen wir nur den Einfluss derjenigen Oberflächen, deren Normalen parallel zur cholesterischen Helixachse ausgerichtet sind. Insbesondere zur Beschreibung von Filmen cholesterischer SCLSCEs ist ein solches Vorgehen angebracht.

Zuerst konzentrieren wir uns in Kapitel 3 auf Effekte, die linear in der Amplitude des elektrischen Feldes sind. Für die beschriebene Geometrie erhalten wir im Rahmen unseres Modells ein verblüffendes Ergebnis. Erhöht oder erniedrigt man die Amplitude des elektrischen Feldes quasistatisch, so kann dies zu einer Rotation der Direktoranordnung um die cholesterische Helixachse führen. Dabei dreht sich die flüssigkristalline Vorzugsrichtung relativ zum makroskopisch fixierten Polymernetzwerk. Der Rotationswinkel ist proportional zur Feldamplitude und zur Wellenzahl, welche die cholesterische Helixstruktur kennzeichnet. Das bedeutet insbesondere, dass für unterschiedliche Händigkeit der cholesterischen Helix Direktorrotationen in entgegengesetzte Richtungen zu erwarten sind. Insgesamt wird der Effekt als rotatoelektrisch bezeichnet und kann als spezifisch für cholesterische SCLSCEs angesehen werden. Im Rahmen unseres Modells wird er durch die Variablen der Relativrotationen erzeugt. Da der Effekt experimentell noch nicht untersucht wurde, diskutieren wir einzelne Aspekte, welche für entsprechende Experimente wichtig werden können. Insbesondere berücksichtigen wir den Einfluss unterschiedlicher Randbedingungen für die Direktororientierung an den Probenoberflächen.

Im weiteren Verlauf untersuchen wir in Kapitel 4 das Verhalten choleste-

rischer SCLSCEs in derselben Geometrie, jedoch für den Fall höherer elektrischer Feldstärken. Dann werden die dielektrischen Eigenschaften der Materialien wichtig, wenn sich der Direktor vorzugsweise parallel zum externen Feld orientiert. Als Ergebnis einer linearen Stabilitätsanalyse erhalten wir, dass die ursprüngliche Direktororientierung bei einer kritischen elektrischen Feldstärke instabil wird. Wir finden zwei mögliche, qualitativ verschiedene Instabilitäten in der Direktoranordnung, welche aufgrund der spezifischen Eigenschaften der Materialien mit einer elastischen Verformung einhergehen. Eine der beiden möglichen Instabilitäten ist räumlich homogen in den Richtungen senkrecht zur cholesterischen Helixachse. Sie entspricht daher der Instabilität, welche auch am Fréedericksz-Übergang in gewöhnlichen niedermolekularen Flüssigkristallen beobachtet wird. Sowohl die Randbedingungen für die Direktororientierung an den Probenrändern, als auch die cholesterische Direktoranordnung und die Verankerung des Direktors im Polymernetzwerk bestimmen den Wert der kritischen elektrischen Feldamplitude. Die zweite mögliche, qualitativ verschiedene Instabilität ist durch Undulationen in der Direktororientierung und Verzerrung des Elastomers in mindestens einer Richtung senkrecht zur Helixachse gekennzeichnet. Für das Zustandekommen dieser Undulationen spielen wieder die Relativrotationen eine entscheidende Rolle.

Es stellt sich natürlich die Frage, welche der beiden Instabilitäten am kritischen Punkt tatsächlich auftritt. Als Antwort finden wir, dass die für die undulatorische Instabilität ermittelte kritische elektrische Feldamplitude nur dann einen niedrigeren Wert aufweisen kann, wenn einer der Materialparameter ein bestimmtes Vorzeichen besitzt. Es ist dies derjenige Materialparameter, welcher im Ausdruck der generalisierten Energiedichte die makroskopische Verzerrung der Materialien und die Relativrotationen koppelt. Wir stellen weiterhin fest, dass im Rahmen unseres linearen Modells Werte von Materialparametern auftreten können, welche eine Direktorreorientierung ohne mechanische Verzerrung des entsprechenden Elastomers erlauben würden.

Die Ergebnisse dieses Kapitels werden formal identisch erhalten, wenn man von einem äußeren Magnetfeld anstelle eines elektrischen Feldes ausgeht.

Als Beispiele für erzwungene mechanische Verformungen untersuchen wir in Kapitel 5 das Verhalten einer cholesterischen Probe, welche parallel bzw. senkrecht zur cholesterischen Helixachse komprimiert oder gedehnt wird. Im Fall der Kompression oder Dehnung senkrecht zur Helixachse wird aufgrund der materialspezifischen Kopplungen im Allgemeinen auch die Struktur der cholesterischen Direktoranordnung verformt. Wir erhalten ein Szenario, das man als Auf- oder Abwickeln der cholesterischen Helix beschreiben könnte. Wird die Probe senkrecht zur Helixachse in zwei orthogonalen Richtun-

gen gleich stark gedehnt bzw. komprimiert, so finden wir eine Kompression bzw. Dehnung der cholesterischen Helixstruktur parallel zur Helixachse. Wie wir erklären, hat dieser Effekt bereits eine Anwendung in der Herstellung spiegelloser Laser gefunden, deren Wellenlänge durch Stauchung und Dehnung der Helixstruktur durchstimmbare ist.

Durch die Untersuchungen in den Kapiteln 3 bis 5 wird die Bedeutung der Relativrotationen für die Charakterisierung von SCLSCEs deutlich. Im Ausdruck der in Kapitel 2 hergeleiteten generalisierten Energiedichte zur linearisierten Beschreibung des makroskopischen Verhaltens der Materialien sind zwei Materialparameter enthalten, welche direkt mit den Relativrotationen verknüpft sind. Bislang konnten deren Werte jedoch nicht unmittelbar auf experimentellem Weg bestimmt werden, da direkte Messmethoden unbekannt sind. Wir schlagen deshalb experimentelle Möglichkeiten zur Abschätzung ihrer Werte vor. Überhaupt ist uns die experimentelle Überprüfung der beschriebenen Effekte ein großes Anliegen, da bisher insbesondere der Einfluss der elektrischen Felder auf cholesterische SCLSCEs wenig untersucht wurde.

Wie erwähnt wird also in den Kapiteln 2 bis 5 ein linearisiertes Modell zur Charakterisierung des makroskopischen Verhaltens der Materialien vorgestellt und angewandt. Im Allgemeinen ist dieses Modell natürlich auf die Beschreibung von Zuständen kleiner Amplituden der mechanischen Verformung und der Relativrotationen beschränkt. Damit wir auch die spezifischen nichtlinearen Eigenschaften von SCLSCEs untersuchen können, stellen wir die Herleitung einer nichtlinearen makroskopischen Modellbeschreibung in Kapitel 6 in den Mittelpunkt dieser Arbeit.

Wir erklären dabei zunächst unser verallgemeinertes Bild, welches wir von den Materialien haben. In nematischen und cholesterischen SCLSCEs liegen lokal zwei gekoppelte Vorzugsrichtungen vor. Die eine ist durch die mittlere Orientierung der mesogenen Einheiten und damit durch die lokale Orientierung des Direktors gegeben. Die zweite Vorzugsrichtung ergibt sich als Folge des jeweiligen Syntheseverfahrens zur Herstellung der Materialien und beschreibt diejenige Orientierung, welche der Direktor einnimmt, wenn keine äußeren Felder anliegen. Dabei nehmen wir an, dass diese zweite Vorzugsrichtung mit der mechanischen Verformung des jeweiligen Elastomers verknüpft ist. Als nichtlineare makroskopische Variable verwenden wir dann die Relativrotationen zwischen den beiden gekoppelten Vorzugsrichtungen, wobei sich aus Symmetriegründen zwei verschiedene Variable ergeben. Im Weiteren leiten wir Ausdrücke für die nichtlinearen Relativrotationen her, indem wir sie als Funktionen derjenigen makroskopischen Variablen angeben, welche den momentanen Zustand des SCLSCE festlegen. Es sind dies wiederum die Komponenten des Direktorfeldes und des mechanischen Verschiebungsfeldes.

Wir zeigen, dass unser nichtlineares Modell für kleine Abweichungen vom energetischen Grundzustand mit der linearen Beschreibung durch de Gennes übereinstimmt.

In Kapitel 7 wenden wir unser nichtlineares Modell zunächst an, um eine endliche statische oder quasistatische Scherdeformation eines nematischen SCLSCE zu untersuchen. Hierbei sollen die Scherkräfte so an das Material angelegt werden, dass die Scherebene die Direktororientierung enthält. Dadurch ergibt sich eine Reorientierung des Direktors in der Scherebene als linearer Effekt, der bereits früher beschrieben wurde. Aufgrund der Kopplung durch die Relativrotationen führt diese Direktorreorientierung jedoch zusätzlich zu Dehnungen und Stauchungen des Elastomers. Letzteres sind nichtlineare Effekte. Wir heben die zentrale Rolle der Relativrotationen für die makroskopische Charakterisierung der Materialien hervor, indem wir explizit zeigen, dass die erwähnten Effekte ausschließlich auf die Kopplung durch die Relativrotationen zurückzuführen sind. Für die entsprechenden Untersuchungen wird ein kubischer Ausdruck der generalisierten Energiedichte hergeleitet und verwendet. Es stellt sich jedoch heraus, dass die angeführten Effekte qualitativ bereits durch die quadratischen Terme der generalisierten Energiedichte beschrieben werden. Dazu müssen wir in diese quadratischen Terme unsere Ausdrücke für die nichtlinearen Relativrotationen einsetzen. Auf diese Weise wird die Bedeutung unserer Ausdrücke für die nichtlinearen Relativrotationen unterstrichen.

Als weiteres Beispiel untersuchen wir in Kapitel 8 eine der bekanntesten nichtlinearen Eigenschaften nematischer SCLSCEs unter Verwendung unseres Modells. Es wurde in Experimenten, in welchen nematische SCLSCEs senkrecht zu ihrer ursprünglichen Direktororientierung gedehnt werden, beobachtet, dass sich der Direktor in Richtung der Zugachse reorientiert. Mit dieser Reorientierung des Direktors ist eine deutlich reduzierte Steigung der zugehörigen Spannungsdehnungskurve verknüpft. Wir zeigen, dass unser nichtlineares Modell diese experimentellen Beobachtungen beschreibt. Dabei konzentrieren wir uns auf die Untersuchung kürzlich veröffentlichter Ergebnisse von Urayama et al. Es stellt sich wiederum heraus, dass die Relativrotationen die entscheidende Rolle für das Auftreten der erwähnten Effekte spielen. Durch sie wird auch die geringere Steigung der Spannungsdehnungskurve mit der Reorientierung des Direktors in Zusammenhang gesetzt. Wir stellen jedoch auch fest, dass derjenige Teil der elastischen Antwort der Materialien, welcher nicht mit einer Reorientierung des Direktors und den Relativrotationen zusammenhängt, einen qualitativen Einfluss auf das Verhalten der Elastomere hat. Dieser Teil der elastischen Antwort dominiert das Gesamterscheinungsbild der Spannungsdehnungskurve und wird durch lokalisierte Prozesse erzeugt. Deshalb können wir unsere Untersuchungen auf

die Beschreibung des Verhaltens eines einzelnen repräsentativen Volumenelements reduzieren. Weiterhin erklären wir, dass Scherdeformationen während des Reorientierungsprozesses nur quantitativen Einfluss auf die Form der Spannungsdehnungskurve haben. Insgesamt ergibt sich, dass beide Variable, mit denen wir die nichtlinearen Relativrotationen beschreiben, zu einer vollständigen Charakterisierung der experimentellen Ergebnisse nötig sind.

Schließlich fassen wir unsere Ergebnisse in Kapitel 9 zusammen und geben darin auch einen Ausblick.

Zur besseren Übersicht wurden einzelne Punkte der Arbeit in die Anhänge A bis D ausgelagert. In einem weiteren Anhang E berichten wir von der Untersuchung der Entstehung hochgeordneter Strukturen parabolischer Fokalkegel in Tensidsystemen. Dieses Projekt entstand in Zusammenarbeit mit Dr. Christian Wolf (Bayreuther Zentrum für Kolloide und Grenzflächen (BZKG), Physikalische Chemie I). Wir führen eine einfache Analyse der beobachteten Muster durch und geben eine Erklärung für die Entstehung der Fokalkegel. Als Ergebnis zeigt sich unter anderem ein universeller Charakter der Muster in dem Sinn, dass in allen untersuchten Proben weitgehend dieselbe Fokalkegelstruktur räumlich isotrop gedehnt oder gestaucht vorlag.

Chapter 1

Introduction

Liquid crystalline elastomers form a new class of materials. Through their synthesis it has become possible to combine in one substance the properties of two components of high technological and industrial importance. These are liquid crystals on the one hand, as well as polymers and elastomers on the other hand. Furthermore the coupling of both of these components in one material leads to new additional and unique features. Consequently, it may be expected that liquid crystalline elastomers will gain an increasing degree of significance for technological applications in the future. At the moment of writing this thesis, the fields of soft actuators and artificial muscles are certainly among the most promising ones to be mentioned in this context [1–4].

In order to understand what the outstanding features of liquid crystalline elastomers are, where they come from, and how they may be characterized, we have to turn to some general considerations in the beginning. Our first step will therefore be to identify important features of liquid crystalline elastomers that can be clearly assigned to either their liquid crystalline or polymeric component. After that we will explain what in fact makes up the outstandingly new properties of these materials. Since closely connected to this question, we will also address one special route of synthesizing liquid crystalline elastomers which has become of crucial importance to the field.

Later on, during the major part of this thesis, we will focus on the investigation and description of the macroscopic behavior of liquid crystalline elastomers from the point of view of modeling. In this context, we are predominantly interested in the influence of external electric and mechanical fields. We have put the development of a nonlinear continuum characterization of the materials into the center of this work. This step becomes necessary in order to qualitatively understand some of the features of liquid crystalline elastomers from a macroscopic point of view. In addition, it gives

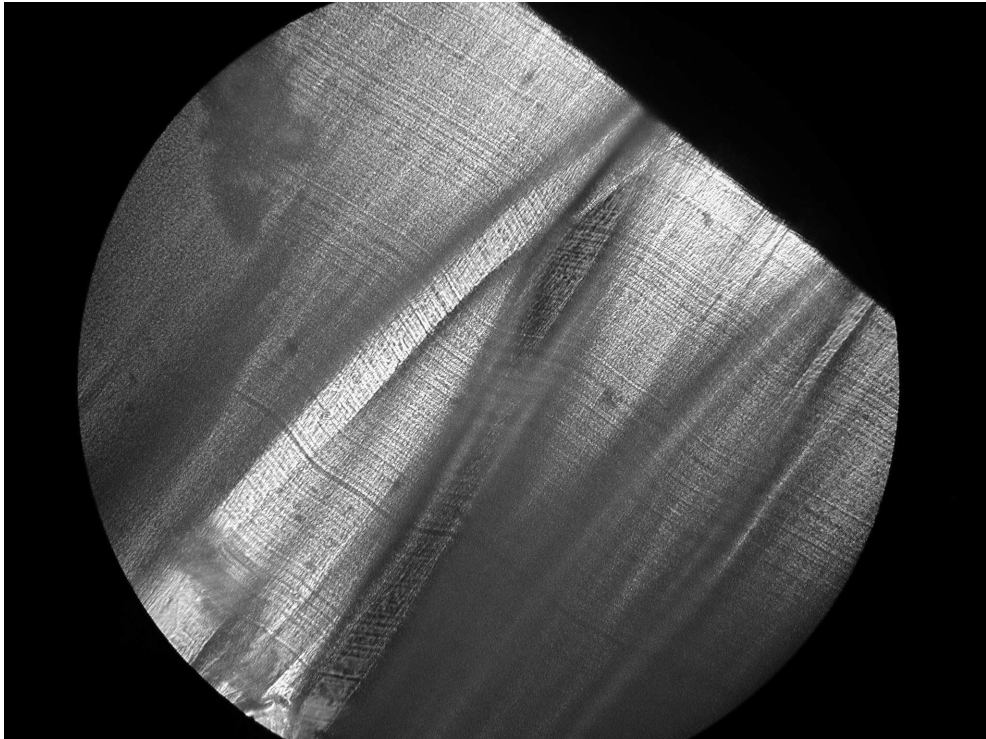


Figure 1.1: Transmission polarization microscope picture of a nematic side-chain liquid single crystal elastomer (SCLSCE). Polarizer and analyzer were crossed and oriented in horizontal and vertical direction. In this case, the sample was stretched by about 25 % of the original length. The stretching direction was oriented perpendicular to the clamped sample edges, one of which is visible in the upper right part of the picture.

us the possibility of a more profound comparison of experimental results to the model predictions.

1.1 Liquid crystals

We start our considerations by having a look at Fig. 1.1. What is shown there is a transmission polarization microscope picture of a thin film of a so-called nematic side-chain liquid single crystal elastomer (SCLSCE). In the course of this chapter we will explain what kind of material is described by this term. Important for us at the moment is the following fact. When this picture was taken, polarizer and analyzer of the polarization microscope were oriented perpendicular to each other. Nevertheless, the sample does not appear completely dark.

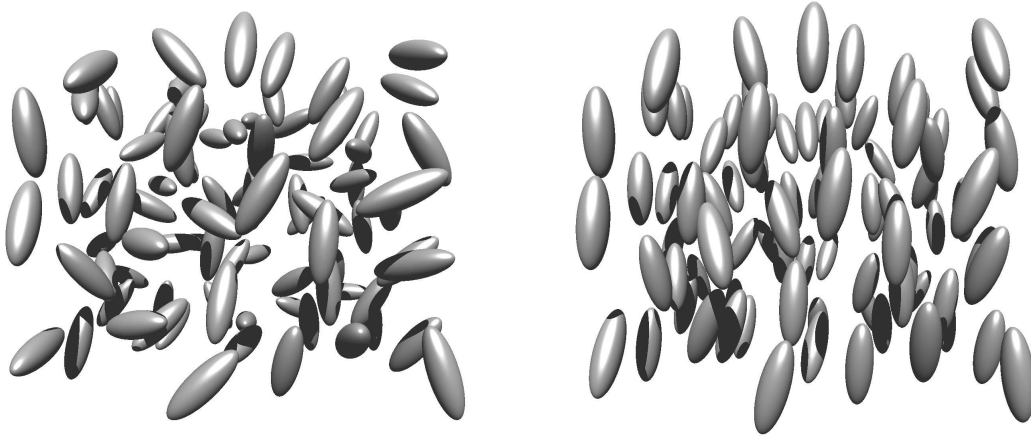


Figure 1.2: Sketch of a nematic liquid crystal in the isotropic (left) and nematic phase (right).

We can find the reason for this feature in the nematic liquid crystalline state of the SCLSC, which turns the sample locally uniaxial. This optical uniaxiality is a characteristic feature of liquid crystals in the nematic phase. It arises from the collective ordering of the constituents of the materials. In order to elucidate this fact we turn to the more instructive example of a conventional low molecular weight liquid crystal (LMWLC) like 5CB (4-cyano-4'-n-pentylbiphenyl). For our purposes we can think of this material as being composed of elongated, rod-like molecules.

At high temperatures this material behaves like an isotropic liquid. It is optically isotropic and transparent. Apparently, in this phase there is no long range order between the molecules, neither of a positional nor of an orientational kind. We have sketched this state in Fig. 1.2 on the left. When we decrease the temperature below a certain critical value T_{NI} (in the case of 5CB this value is $T_{NI} = 35.5$ °C under atmospheric pressure), the mechanical properties of the LMWLC are still fluid-like. However, the substance becomes turbid. This change in the optical properties indicates that some crucial change in the structure of the material has occurred. Further inspections reveal that we have passed through a phase transition of weakly first order by lowering the temperature from above to below its critical value T_{NI} .

When these facts were observed for the first time, they led to quite some confusion. Obviously, the substance did not pass from the isotropic liquid phase to a crystalline phase. The latter would be characterized by a long-range positional order given by a three dimensional lattice structure. Such an arrangement on a crystalline lattice, however, strongly contradicts the observed ability to flow.

As we know today, the explanation for these observations is that a phase in between the isotropic liquid and the crystalline phase is observed – a so-called mesophase. The materials that are able to show such a mesophase have been termed mesogens [5], or, in another way, liquid crystals [6] (see, e.g., Ref. [7] for an extensive review on the physics of liquid crystals). What happens in the case of 5CB at the temperature T_{NI} is that the substance passes from the isotropic liquid phase to a mesophase, which is called nematic. Here, the arrangement of the molecules does not show long-range positional order as in a crystal. However, we find the arrangement sketched on the right of Fig. 1.2. Of course, there are thermal fluctuations, but on average the molecules orient the direction of their elongation parallel to each other. They show a long-range orientational order.

This orientational order gives rise to optical anisotropy. We can identify one local optical axis, which coincides with the direction of the average orientation of the molecules. In continuum descriptions of nematic liquid crystals this orientation is characterized by a unit vector $\hat{\mathbf{n}}$, the so-called director. Care has to be taken in such a description to ensure that the director cannot distinguish between head and tail, corresponding to the appearance of the optical axis.

It is important to notice that in an ideal case the emergence of the optical axis at the isotropic-to-nematic phase transition corresponds to the spontaneous breaking of a continuous symmetry (see, e.g., Ref. [8]). In practice the orientation of the director may be influenced for example by grain boundaries, surface coating of the sample walls, electric, magnetic or mechanical static or dynamical fields. It is possible that in these situations we cannot talk of a spontaneous breaking of the symmetry any more. Such influences may even cause the isotropic-nematic phase transition not to be of first order any more. Later on, this will become an important issue.

When the sample contains chiral mesogenic molecules and it is not a racemic mixture, a different liquid crystalline phase is observed. The latter has been termed the cholesteric phase and actually was the one first identified historically. In contrast to the nematic phase, which shows a spatially homogeneous director orientation in the ground state, the ground state director in the cholesteric phase features a twisted, helical structure. As usual, this helix can be characterized by a corresponding wavenumber q_0 . The sign of q_0 thereby denotes the handedness of the helix, whereas its magnitude determines the helical pitch $2L = \frac{2\pi}{q_0}$.

The helical structure of cholesteric phases leads to interesting optical properties, as for example illustrated in Fig. 1.3. There, we consider a situation in which a cholesteric liquid crystal is illuminated in a direction parallel to the helical axis by circularly polarized light. If the handedness of the cir-

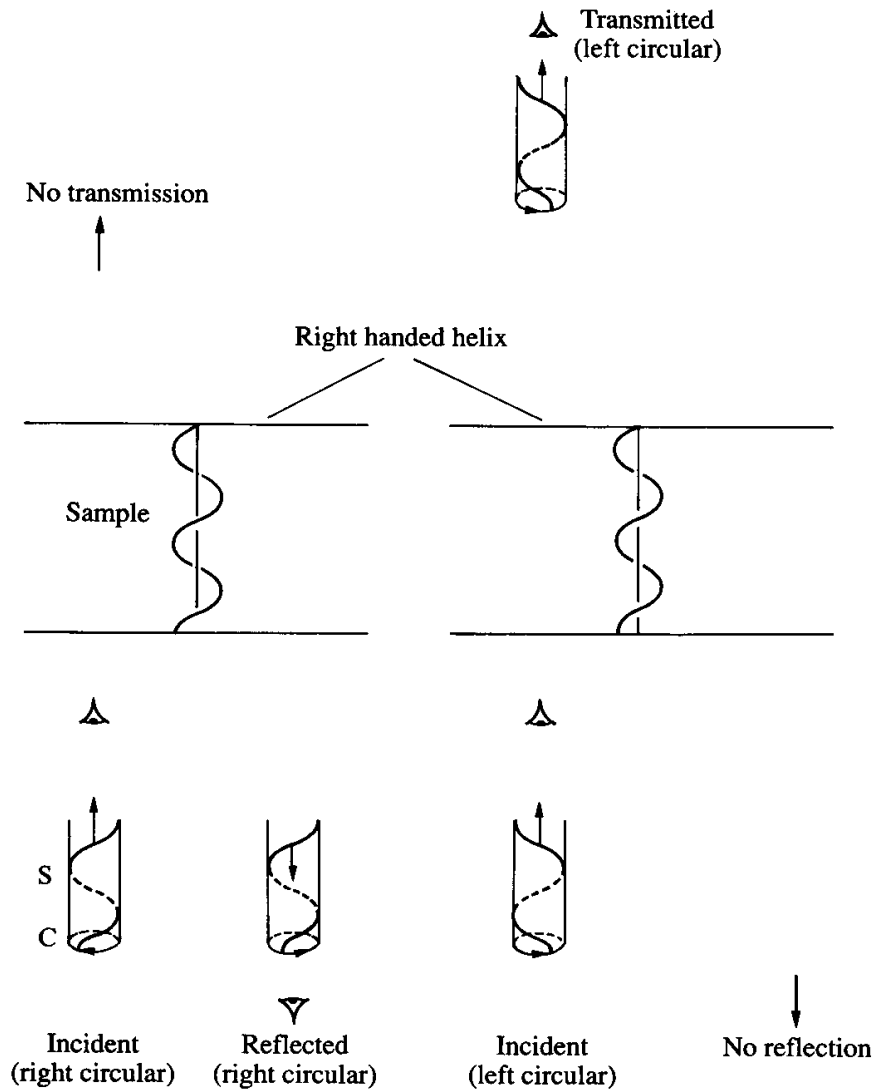


Figure 1.3: Right and left circularly polarized light illuminating a right handed cholesteric helical structure. The direction of illumination is oriented parallel to the cholesteric helical axis. It is assumed that the wavelength of the light approximately coincides with the pitch of the cholesteric helix. The figure has been reproduced from Ref. [7].

cularly polarized light coincides with the handedness of the cholesteric helix, and if simultaneously the wavelength of the illuminating light approximately matches the pitch of the cholesteric helix, the light will be reflected. In the other cases transmission prevails.

These properties lead to a colorful appearance of the samples when the wavelength of the reflected light is located within the visible regime. Oriented cholesteric samples then show a bandgap in their optical transmission spectrum. This feature can be exploited for various applications, one of them being the construction of mirrorless lasers [9–11].

For both, the nematic and the cholesteric phase, the director field $\hat{\mathbf{n}}(\mathbf{r})$ describes the local average orientation of the mesogenic molecules. However, it does not contain any information on the local degree of orientational ordering of the molecules. The degree of order may be characterized by a scalar order parameter S . By convention the latter takes the value $S = 0$ in an isotropic, disordered state of the system, and $S = 1$ in a perfectly ordered state. Its value can be determined experimentally (see, e.g., Ref. [12]). The whole information may be captured by a symmetric, traceless tensorial order parameter, the components of which read $Q_{ij} = S(n_i n_j - \frac{1}{3}\delta_{ij})$. Here, as in the remaining part of this work, δ_{ij} denotes the Kronecker delta, with $\delta_{ij} = 1$ if $i = j$, and $\delta_{ij} = 0$ otherwise.

Apart from the nematic and the cholesteric phase, a large number of other liquid crystalline phases has been identified. The various smectic liquid crystalline phases capture all kinds of examples of combinations of quasi long-range or long-range positional order with orientational order. However, only the nematic and cholesteric phases will be treated in the major part of this thesis, except for appendix E, where we will report our investigations on lamellar lyotropic systems.

1.2 Polymers and elastomers

Having addressed some of the remarkable optical features, we now turn to the mechanical properties of the material shown in Fig. 1.1. What cannot be inferred directly from the picture is that at the moment of taking this photograph, the depicted film had been uniaxially stretched. The direction of stretching was oriented perpendicular to the two clamped edges, one of which is visible in the upper right part of the photograph. In this case, the sample was stretched by about 25 % of its original length. Such a degree of deformation would be out of reach for most crystalline solids, no need to mention that it would be highly irreversible. Not so, however, for the pictured elastomer. It can be stretched even further, the overall deformation

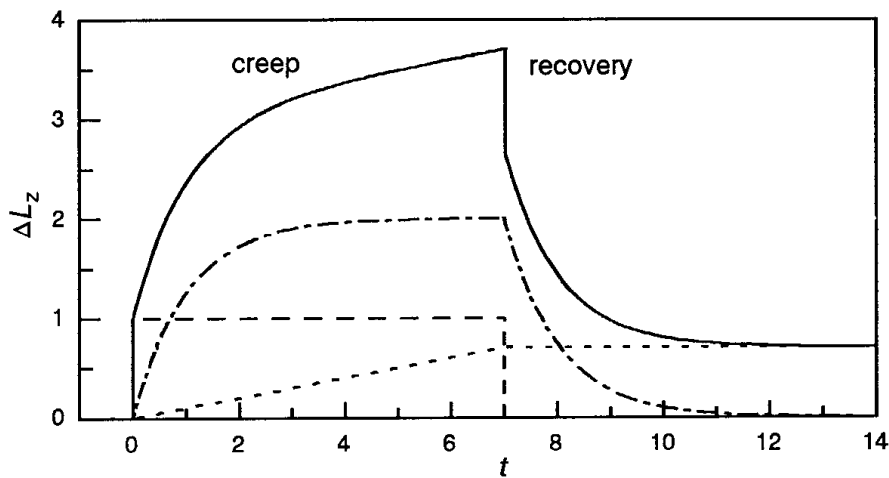


Figure 1.4: Typical mechanical response of a polymer sample during a creep experiment. A constant force is instantaneously applied at $t = 0$ and released at $t = 7$. The curves show the resulting overall elongation of the sample and the different contributions to this response (further explanation can be found in the main text). This figure has been reproduced from Ref. [13].

still remaining reversible.

Of course, it is the internal structure of polymeric materials that underlies this mechanical feature. In the simplest case, these materials consist of linear polymer chains, which themselves are synthesized by chemically connecting a large number of single monomer repeat units. The number of monomers on a polymer chain is then called the degree of polymerization.

With increasing degree of polymerization the respective sample becomes more and more viscous. Entanglements between the polymer chains become important and qualitatively influence the linear mechanical behavior of the respective material.

A sketch of the typical linear mechanical response of a polymer sample to a constant external mechanical force is depicted in Fig. 1.4. What we find illustrated in this figure is the resulting elongation during a so-called creep experiment. At $t = 0$ the constant external force is applied to the sample. When we have a look at the linear mechanical response from a macroscopic point of view, we can in general distinguish between three different components. First, the sample reacts instantaneously to the applied external force. This component is identified with the elastic part of the linear mechanical response, which is completely reversible (dashed line). Secondly, there exists a so-called anelastic part of the response, which although being retarded, is

also completely reversible (dash-dotted line). At least one relaxation time is connected to this process. Finally, the third component consists of a viscous flow, which is irreversible (dotted line). When at $t = 7$ the external force is released, the elongation due to the viscous flow remains. However, we find an instantaneous reversion of the elastic part of the elongation, as well as a relaxing contraction due to the anelastic component.

Adding crosslinking agents to a polymer melt, the polymer chains can be chemically crosslinked to form a permanent polymer network. From an idealized point of view, this chemical crosslinking suppresses the viscous flow in the mechanical response. In this case, the mechanical response of the sample becomes in principle reversible. On the other hand, when the crosslinking density is not too high, reversible mechanical deformations of large magnitude can be observed. We call such a material an elastomer.

For us, it is important to notice the following. Let us assume that we are only interested in measuring in an experiment the static, relaxed state of an elastomer which is exposed to a static external field. Then, from the recorded data it is not possible for us to distinguish between the elastic and the anelastic part of the response of the material to the external force. The same is true for the “quasistatic” case, in which the variation of the respective external field occurs on a time scale sufficiently long compared to the dominating relaxation time of the anelastic processes. We could also say that on a sufficiently long time scale the mechanical response of the elastomer appears elastic. Therefore, it is possible to use classical elasticity theory in order to describe the mechanical response in the static and quasistatic case [14].

1.3 Liquid crystalline elastomers

The contents of the two previous sections provides us with the information in order to characterize the current appearance of the nematic SCLSCE shown in Fig. 1.1. This stretched thin film of nematic SCLSCE was to a good approximation residing in a static state. However, fundamental additional information is connected to the process that led to the state of appearance of the sample in Fig. 1.1.

In the unconstrained ground state, the director orientation of the pictured thin film of nematic SCLSCE was an essentially different one. To first approximation it was spatially homogeneous and aligned parallel to the two clamped edges of the sample. In this state, the sample appeared dark under the polarization microscope when its clamped edges were aligned parallel to the analyzer or polarizer, respectively. However, when we align the edges

of the now stretched sample depicted in Fig. 1.1 parallel to the analyzer or polarizer, we still observe some bright regions. Therefore, we must conclude that the director is not aligned in its ground state orientation any more in the stretched state of the sample. Apparently, only through stretching the elastomer, here in the direction perpendicular to the initial director orientation, the director rotated out of its initial orientation. Strikingly, the externally imposed mechanical deformation couples to the orientation of the director and leads to a rotation of the director field. In the case shown in Fig. 1.1 this does not happen in a spatially homogeneous way across the pictured film. Noticing, however, the spatial heterogeneity of the film, such a spatially inhomogeneous scenario may be expected.

In essence, we can infer the outstanding property of liquid crystalline elastomers of statically coupling the liquid crystalline order, including the director orientation, to the elastic mechanical deformation of the materials. Having identified this remarkable feature of liquid crystalline elastomers, we can now address the question of how to produce them. In particular, we will concentrate on the synthesis of nematic and cholesteric SCLSEs, the materials mainly under consideration in this work.

As outlined in the previous section, the first step of this procedure consists of course of the synthesis of the uncrosslinked polymer chains. In order to obtain liquid crystalline polymers, the segments making up the polymer chains must contain the respective mesogenic units. There are basically two approaches to reach this goal, which lead to qualitatively different materials. In one case, which is shown on the left of Fig. 1.5, the mesogenic units become part of the backbone of the synthesized polymer chains. Such materials were named “main-chain” liquid crystalline polymers to stress the location of the mesogenic units in the polymer chain. The other possibility is sketched on the right of Fig. 1.5. Here, the mesogenic units are attached as side groups to the backbone of the polymer chains. Consequently these materials are called “side-chain” liquid crystalline polymers.

In the year 1978, Finkelmann et al. reported a special procedure to synthesize side-chain liquid crystalline polymers in a way that the formation of the liquid crystalline phase is facilitated [15]. They chemically attached the mesogenic units to the monomers in a quite flexible way. This was achieved via hydrocarbon chains, consisting of two to six hydrocarbon units, the so-called spacers (see Fig. 1.5). After the polymerization, the spacers reduce the orientational constraint imposed onto the mesogenic units by the polymer backbones. Therefore, the spacers add to the average orientation of the mesogenic units along a preferred direction. Performing the synthesis in this way, liquid crystalline phases can clearly be observed.

The additional step on the way of generating liquid crystalline elastomers

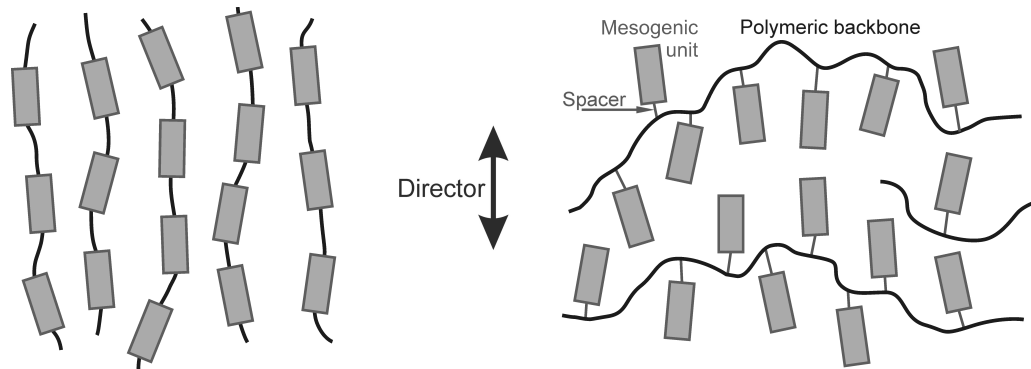


Figure 1.5: Sketch of a main-chain (left) and side-chain (right) liquid crystalline polymer structure. The average orientation of the mesogenic units, indicated by the rectangular boxes, is identified with the director orientation. In the main-chain case the mesogenic units are part of the polymeric backbone, whereas they are attached to the backbone via flexible spacers in the side-chain case.

consists of chemically crosslinking the corresponding polymers. Finkelmann et al. reported on the first synthesis of side-chain liquid crystalline elastomers in 1981 [16]. Nematic, smectic, as well as cholesteric states of the elastomers could be identified.

However, without further effort, we cannot recover an optical ground state corresponding to the one of the material shown in Fig. 1.1. In fact, unstrained materials produced as described above are optically turbid. Their ground state is characterized by a polydomain structure with different director orientation in each domain. Consequently, they are referred to as polydomain liquid crystalline elastomers.

On the other hand, in order to obtain a material which shows a homogeneous ground state director in a monodomain across the whole sample, special routes of synthesis are necessary. Performing this step is important from a basic as well as from an applied point of view. Starting from side-chain liquid crystalline polymers then leads to materials which are called side-chain liquid single crystal elastomers (SCLSCEs), the word “single” in this term referring to the monodomain of the ground state director orientation.

Küpfer et al. presented a route of generating nematic SCLSCEs in 1991 [17]. Their idea was to use a two step crosslinking procedure, which is illustrated in Fig. 1.6. They started with a melt containing the components of the reaction. This melt includes two kinds of bifunctional crosslinkers, one that reacts fast at both ends, and one that reacts slow at one end. Chemical groups which react quickly are indicated by an open circle (○) in Fig. 1.6,

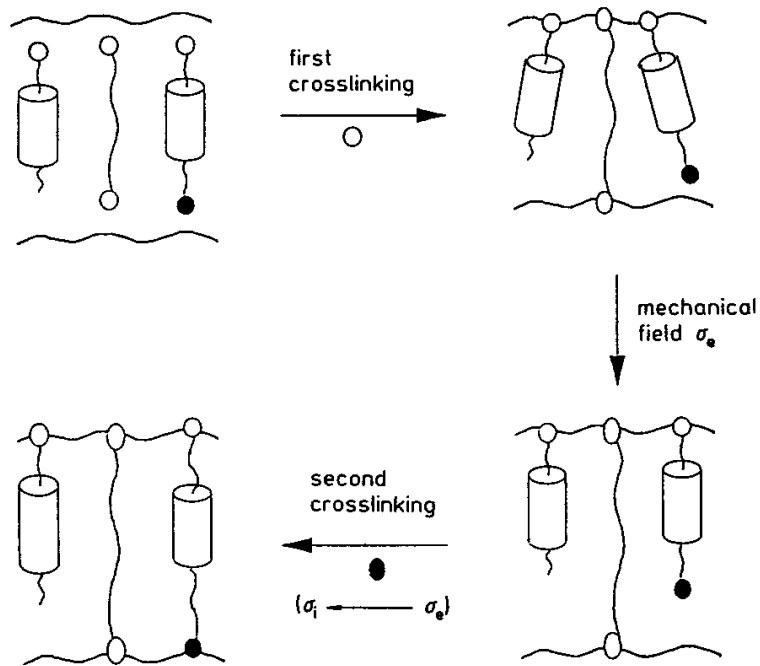


Figure 1.6: Sketch of the two step crosslinking procedure used to generate nematic SCLSCEs. The cylinders represent the mesogenic units, open circles represent groups that react quickly, and closed circles those with longer reaction times (further explanation in the main text). This figure has been reproduced from Ref. [18].

those which take a longer reaction time by a closed circle (●). After the fast chemical reaction has taken place during a first crosslinking step, a weakly crosslinked side-chain liquid crystalline elastomer is obtained. Now, an effect is put to use, which is related to the one we have introduced above when describing the appearance of the elastomer pictured in Fig. 1.1. After the first crosslinking step has occurred, a mechanical stress field σ_e is applied to the weakly crosslinked sample. The orientation of the mesogenic units couples to the strain field, so that on average they orient in one preferred direction. Then the major part of the slow chemical reactions is completed under the influence of the external stress field σ_e . During this second crosslinking step some part of the external stress field σ_e is converted to an internal stress σ_i , which is locked in the material. Then, even when the external stress field is released, the homogeneous director orientation across the sample remains fixed. It has been “frozen” into the sample. From further analysis, Küpfer et al. concluded that the anisotropy in these samples gets mainly locked in the vicinity of the crosslinking points [18].

Above, in section 1.1, we have included a short remark on the tensorial order parameter Q_{ij} describing the liquid crystalline order of a liquid crystalline state. In an analogous way, a second tensorial order parameter P_{ij} with related properties has been introduced to characterize the state of the permanent “frozen-in orientational order” [19, 20].

In the example presented in Fig. 1.6, bifunctional crosslinkers were used, which in part contained mesogenic units themselves. It has been demonstrated in the meantime that the nature and concentration of the crosslinkers can qualitatively affect the macroscopic behavior of the materials [21]. In this context, for example the influence of crosslinkers of higher functionality has been investigated [21, 22].

Furthermore, apart from the presented two step crosslinking process, other routes of synthesis have been developed. For instance, one possibility is to align the mesogenic units on average during crosslinking by applying an external magnetic field [23, 24]. Cholesteric SCLSCEs have been produced for example by a two step crosslinking process, during which first a weakly crosslinked elastomer is swollen and afterwards anisotropically deswollen. While this anisotropic deswelling occurs, a transition to the cholesteric monodomain state takes place, and the latter is chemically locked by a second crosslinking process. The result is a cholesteric SCLSCE with uniform Grandjean texture over the whole sample [25]. A later route of synthesizing consists of photo-crosslinking a sample in which the mesogenic units have been oriented macroscopically by surface interactions [3, 26, 27]. Via the latter method, glass-supported or free-standing films of SCLSCEs can be realized. These can for instance have a thickness of about 25 μm or less [28]. For

the cholesteric films synthesized in this way it has been demonstrated that they feature a larger liquid crystalline order than the films synthesized by anisotropic deswelling, which is reflected by their optical properties [29].

It is important to note that the continuous orientational symmetry is not spontaneously broken in SCLSCEs produced in these ways. The symmetry breaking has been induced from outside during the special routes of synthesis and has been locked in the materials. This is clearly demonstrated by the fact that reorientations of the director field like the one shown in Fig. 1.1 are reversible. When the external stress is released, the sample will relax to its initial length, and its initial ground state director orientation is recovered.

In conclusion, we have observed in Fig. 1.1 the consequences of the following fundamental feature of SCLSCEs. The orientation of a special preferred direction, characterized by the director field, couples to the mechanical deformation of the material. Therefore, as a consequence of stretching the elastomer, we have found a reorientation of the director field. More precisely, a static elastic deformation of the material was observed to lead to a static reoriented state of the director field.

However, the coupling between elastic mechanical deformation and director orientation also implies that the opposite effect may occur. This means that a reorientation of the director field can lead to a mechanical deformation of the elastomer. Such a behavior has been demonstrated for example by Urayama et al., who investigated a nematic SCLSCE swollen with a nematic LMWLC exposed to an external electric field [3]. Fig. 1.7 illustrates their experimental results. The swollen film has been observed under a polarization microscope with crossed analyzer and polarizer and the initial director orientation as indicated in the central picture of the figure. An external electric field has been applied perpendicularly to the plane of the film as indicated on the right of Fig. 1.7. For the chosen material, the director tends to orient parallel to the electric field direction. Therefore, the sample observed by the polarization microscope gets darker under the influence of the external electric field, which can be inferred by comparing the central and right picture of Fig. 1.7. Simultaneously, the sample contracts in the vertical direction as indicated in the figure. This contraction is again a direct consequence of the fact, that in SCLSCEs the director orientation and the elastic mechanical deformation of the material are coupled to each other.

With this picture of SCLSCEs in mind, we will turn to their macroscopic characterization. This will make up the major remaining part of this thesis.

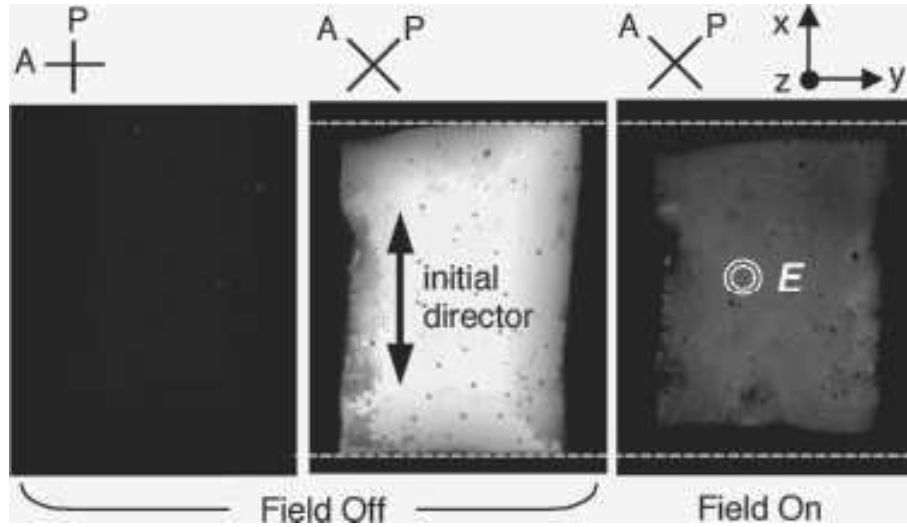


Figure 1.7: Swollen nematic SCLSCSCE exposed to an external electric field. The mesogenic molecules tend to align parallel to the electric field direction. Therefore, the director orientation differs from its initial state (center) when the electric field has been switched on (right). Coupling between director orientation and elastic deformation of the elastomer leads to the indicated contraction of the film. This figure has been reproduced from Ref. [3].

1.4 Scope of this work

The scope of this thesis can be clearly defined: we want to derive a non-linear continuum description which models the characteristic features of the macroscopic behavior of SCLSCSEs. We start in the next chapter by giving an overview on the linear continuum model that has been used so far in order to characterize the materials. In particular we will introduce the variables of linear relative rotations, which play a crucial role in this picture. Chapters 3, 4, and 5 are devoted to illustrate the diversity of predictions on the macroscopic behavior of SCLSCSEs which can be made already by using the linear description. For this purpose, we will study the reaction of cholesteric SCLSCSEs to static or quasistatic external electric fields in chapters 3 and 4, and to external mechanical fields in chapter 5. In this context, we will investigate qualitatively new effects and instabilities shown by the materials. Furthermore, we will demonstrate, how some of the values of the material parameters involved in our characterization could be inferred from corresponding experiments. From these considerations, also the limitations of the linear picture will become evident. Consequently, we will come to the point in chapter 6 and present our generalization of the model to the

nonlinear regime. Above all, this chapter will be dominated by the introduction of nonlinear expressions for the variables of relative rotations. We will use our nonlinear concept first in order to study the weakly nonlinear regime of a static or quasistatic shear deformation of a nematic SCLSCE in chapter 7. After that, we will demonstrate that our nonlinear model predicts the specific mechanical and optical behavior found experimentally for a nematic SCLSCE when the latter is stretched perpendicularly to its initial director orientation. For this purpose, in chapter 8 we will interpret the results obtained from recent corresponding stress-strain measurements, using our model. This investigation will also lead to a qualitatively new picture for the elastic behavior that can be observed for nematic SCLSCEs during such experiments. Finally, we will conclude in chapter 9. In order to keep our presentation compact, we have shifted several technical details of our work to the appendices. We have also added one appendix in which we describe our investigations on the formation of highly ordered patterns of parabolic focal conics in surfactant systems.

Chapter 2

Linear macroscopic description

In this chapter we will present the elements of the linear continuum model that has already been successfully applied in order to characterize the macroscopic behavior of SCLSCEs [30–35]. Referring to an early idea by de Gennes this model includes relative rotations [36], as will be further elucidated below. Although we will mainly consider static or quasistatic phenomena, the energy functional we will derive may be taken as a starting point for a dynamical description in the spirit of generalized hydrodynamics [8, 37, 38]. A first step in the latter direction has already been performed in Ref. [39] for nematic SCLSCEs.

Our plan for deriving the linear continuum model is the following. First, we will identify the appropriate minimal set of independent macroscopic variables which are necessary to characterize the current state of the respective material. These variables correspond to the degrees of freedom of the system under consideration. For simplicity, let us call these variables the “state variables” of the system. We will use as a framework to identify and classify them the concepts of generalized hydrodynamics. As a second step, we will identify the macroscopic variables that can contribute to the generalized energy density of the system. They will have to be expressed in terms of the state variables of the system. Finally, since we will deal with static or quasistatic external electric, magnetic, and mechanical fields, the following procedure applies. Combining the variables of the second kind using symmetry arguments we obtain an expression for the generalized energy density F of the respective system. Minimizing the generalized energy of the system $\mathcal{F} = \int F d^3r$ with respect to the independent state variables leads us to equations with the help of which we determine the current state of the elastomer.

2.1 State variables

The actual macroscopic state of a nematic or cholesteric SCLSCE under the influence of a static external field is identified by the following independent variables.

First, there are the variables connected to the quantities that can already be found in the hydrodynamic description of a simple fluid. These are the density of mass ρ , the density of linear momentum \mathbf{g} , and the density of energy ε . Since they are characterized by conservation laws, they are called conserved quantities [8, 38]. For example, the conservation law for the mass density ρ reads

$$\frac{\partial \rho}{\partial t} + \nabla \cdot \mathbf{g} = 0. \quad (2.1)$$

Here, the density of linear momentum \mathbf{g} acts as the current associated with the conservation of the density of mass ρ . As an example for another conserved quantity, which has to be included e.g. in the hydrodynamic description of binary mixtures, we may mention the concentration c of one of the two components [38, 40].

Furthermore, we have to take into account the variables associated with a spontaneous breaking of continuous symmetries [8, 38].

If we consider the case of a crystalline solid characterized by a three dimensional crystalline lattice structure, it is clear that we find the continuous translational symmetry being spontaneously broken in three independent spatial directions. However, also our case of elastic polymeric solids corresponds to a situation of a threefold breaking of the continuous translational symmetry [39]. When we think of the materials as being made up of infinitesimal volume elements, we can associate the three components of the displacement field $\mathbf{u}(\mathbf{r}) = \mathbf{r} - \mathbf{a}(\mathbf{r})$ with this threefold symmetry breaking [8, 37, 39, 41, 42]. Here, \mathbf{r} denotes the actual positions of the volume elements of the polymer network in the final deformed state. By the initial field $\mathbf{a}(\mathbf{r})$ we specify their positions in the initial undeformed state. Obviously, we can also take the components of $\mathbf{a}(\mathbf{r})$ as independent variables instead. The difference between the two choices of $\mathbf{u}(\mathbf{r})$ and $\mathbf{a}(\mathbf{r})$ will be discussed later on [41, 42]. As we will see below, the three components of the displacement field $\mathbf{u}(\mathbf{r})$ describe local strains and rotations of the polymer network. The same is true for the three components of the initial field $\mathbf{a}(\mathbf{r})$.

When we refer to the initial positions of the volume elements by the field $\mathbf{a}(\mathbf{r})$, we express the initial positions as a function of the final positions \mathbf{r} . In this way, also the displacement field $\mathbf{u}(\mathbf{r})$ is given as a function of the final positions \mathbf{r} . This approach of characterizing the material with respect to its final state corresponds to the Euler point of view and is the appropriate one in

a hydrodynamic description [40–43]. Considering the situation from the point of view of the initial, undeformed state of the respective material corresponds to the Lagrange picture, which will not be pursued in the following [14].

On the other hand, there are two independent variables associated with the breaking of the continuous rotational symmetry in nematic and in cholesteric SCLSCEs. We find the reason in the local uniaxial character of these two liquid crystalline states. The local orientation of the preferred axis is characterized by the director field $\hat{\mathbf{n}}(\mathbf{r})$. Since $\hat{\mathbf{n}}$ is a unit vector, two independent variables determine the current state of the director field $\hat{\mathbf{n}}(\mathbf{r})$, corresponding to the twofold rotational symmetry breaking. The ground state conformation of the director field will be denoted as $\hat{\mathbf{n}}_0(\mathbf{r})$.

In the linear regime, we can take the two angles that characterize deviations from the ground state director orientation as the appropriate macroscopic broken symmetry variables we are looking for. They are given by variations of the director $\delta\mathbf{n}$, defined by $\hat{\mathbf{n}}(\mathbf{r}) = \hat{\mathbf{n}}_0(\mathbf{r}) + \delta\mathbf{n}(\mathbf{r})$, and satisfy $\hat{\mathbf{n}} \cdot \delta\mathbf{n} = \hat{\mathbf{n}}_0 \cdot \delta\mathbf{n} = 0$ in the linear regime.

We mention at this point that in a strictly hydrodynamic sense all the effects under consideration should appear on much larger length scales than the inherent length scales of the system. It has been demonstrated that in this case only one broken symmetry variable contributes to the hydrodynamic behavior of a cholesteric phase [44]. However, in the following we will study systems of cholesteric pitch larger than or comparable to the thickness of the sample. This is the reason why we choose the local description of the cholesteric phase outlined above, using the deviations of the director field $\delta\mathbf{n}(\mathbf{r})$ as macroscopic variables.

Our description of the behavior of nematic and cholesteric SCLSCEs will be restricted to a regime far away from any transition to another liquid crystalline or the isotropic state. Therefore, we assume that the scalar degree of local liquid crystalline order S introduced in the previous chapter is approximately constant. Consequently, we will not include it explicitly as a macroscopic variable. Its magnitude implicitly contributes to the values of the material parameters that will enter the model.

In summary, we have identified five independent variables connected to the breaking of continuous symmetries. They correspond to the three components of the displacement field $\mathbf{u}(\mathbf{r})$ and the two independent components of the director orientation $\hat{\mathbf{n}}(\mathbf{r})$. These variables do not characterize conserved quantities of the system. Consequently, their dynamical behavior is not described by conservation laws. However, dynamic balance equations of a similar kind can be derived [37–39]. For the components of the director

field they for instance have the form

$$\frac{\partial \hat{\mathbf{n}}}{\partial t} + \mathbf{Y} = 0. \quad (2.2)$$

Here, \mathbf{Y} is called quasicurrent.

2.2 Variables contributing to the generalized energy density

When we want to construct an expression for the generalized energy density of the respective system, we notice that the state variables specified in the previous section cannot be included in this expression directly. The functional of the generalized energy has to satisfy certain conditions. For example, it has to be invariant under a rigid rotation or translation of the sample under consideration. The values of the state variables given for instance by $\hat{\mathbf{n}}$ or \mathbf{u} , however, change their magnitude when the sample is rigidly rotated or translated, respectively. Consequently our next step is to derive macroscopic variables that can directly contribute to the expression for the generalized energy density. These variables must reflect the modifications of state which change the magnitude of the generalized energy density. We will have to express these variables as functions of the state variables. Our focus will be on the variables connected to the broken symmetries.

In the linear regime, it is straightforward to perform this step in view of the variables characterizing the current director orientation. Only the gradient tensor $\nabla \hat{\mathbf{n}}$ is taken into account as a macroscopic variable which can contribute to the energy density of the system directly. In this way, rigid rotations of the whole system do not affect its generalized energy density via the terms that describe the current energetic state of the director field.

When we consider purely elastic mechanical deformations of the material, the following picture holds. The magnitude of the generalized energy should not be influenced by rigid translations or rotations of the material. Only when the distance between different volume elements of the sample is modified, we expect a contribution to the generalized energy density. The corresponding deformations are called deformations of strain. They are characterized by the strain tensor $\boldsymbol{\varepsilon}$. This tensor consequently measures the changes in the distance of the volume elements of the material and is defined by

$$dr_i^2 - da_i^2(\mathbf{r}) = 2dr_i dr_j \varepsilon_{ij}(\mathbf{r}) \quad (2.3)$$

in the Euler picture (see previous section) [41, 43]. The linear expressions for

the components of $\boldsymbol{\varepsilon}$ read

$$\varepsilon_{ij} = \frac{1}{2} [(\partial_i u_j) + (\partial_j u_i)]. \quad (2.4)$$

Here, $\boldsymbol{\varepsilon}$ and \mathbf{u} are functionals of \mathbf{r} , and ∂_i denotes the partial derivative $\frac{\partial}{\partial r_i}$ ($i = 1, 2, 3$).

We can see that $\boldsymbol{\varepsilon}$ is a function of the tensor of distortions $\nabla \mathbf{u}$. Consequently, rigid translations of the material do not contribute to the generalized energy density of the system through $\boldsymbol{\varepsilon}$. In addition, we find from Eq. (2.4) that the strain tensor $\boldsymbol{\varepsilon}$ coincides with the symmetric part of the distortion tensor $\nabla \mathbf{u}$ in the linear regime. This guarantees that rigid rotations of the whole system can neither contribute to the generalized energy density of the system. We mention at this point, that the form of the linear expression of the strain tensor in the Lagrange picture is identical [14].

With $\nabla \hat{\mathbf{n}}$ and $\boldsymbol{\varepsilon}$ we have introduced the macroscopic variables that separately arise from the liquid crystalline state and the elastic mechanical response of the materials, and which influence the generalized energy density. The crucial point is now to take into account the special features of liquid crystalline elastomers. In particular, this means that the coupling between the local elastic mechanical deformation and the local orientation of the director field has to be reflected by our description. For this purpose, we adopt an idea by de Gennes and introduce the variables of relative rotations. Remarkably, this concept had been presented before the first SCLSCEs have been synthesized [36].

It is most illustrative to introduce the concept of relative rotations in the following context. When we consider SCLSCEs of low enough crosslinking density, the respective isotropic and liquid crystalline states can clearly be distinguished from each other. This was demonstrated for instance for nematic SCLSCEs in Ref. [45]. In this case we may think of the elastomers as being made up of two coupled components or subsystems, respectively. One of these shows the liquid crystalline state, the other one behaves like a mechanically elastic medium. In a simplified picture, we may for illustrative purposes identify the first component with the entity of the mesogenic units. The second component would then be identified with the crosslinked network of polymeric backbone chains. It is clear that both subsystems are coupled to each other, already from the fact that the mesogenic units are chemically bound to the polymeric backbones via the flexible spacer groups.

Due to this coupling an energetic contribution will arise, when the material is not rotated rigidly as a whole, but when the two subsystems are rotated in different ways. For illustration we have sketched a two dimensional example of such a situation in Fig. 2.1 (we have used the same symbols as in

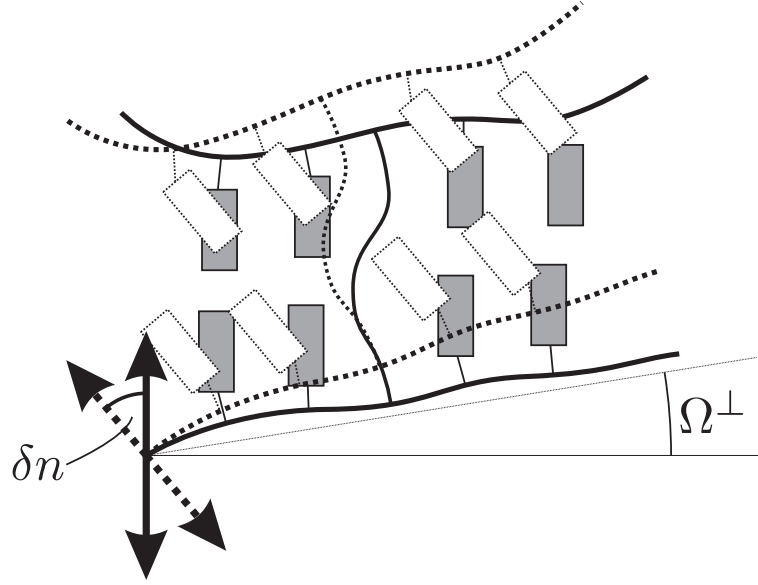


Figure 2.1: Illustrative two dimensional sketch of a situation in which a relative rotation has occurred. The entity of mesogens has been rotated by an angle δn , which differs from the rotation angle Ω^\perp of the crosslinked polymeric backbones.

Fig. 1.5). In this sketch, the mesogenic units have on average been rotated from the state indicated by the solid boxes to the one given by the dotted boxes. This rotation is reflected by the reorientation of the director by an angle δn . On the other hand, the polymer backbones have been rotated by a different angle Ω^\perp , which we obtain by comparing the orientation of the solid and the dotted lines. In effect, since $\delta n \neq \Omega^\perp$, one of the two subsystems has been rotated with respect to the other one. Or, in other words, it has been rotated relatively to the other one.

More generally, we should think of relative rotations as the director re-orientation with respect to the polymer network. As we have seen in the previous chapter, the continuous rotational symmetry is not broken spontaneously in nematic and cholesteric SCLSCs. Therefore, the broken symmetry variable $\delta \mathbf{n}$ is not purely hydrodynamic in these materials. The ground state director orientation is imprinted into the materials, or frozen in, respectively, during the synthesis. Relative rotations describe the deviations of the director orientation from its ground state anchoring direction within the polymer network. This is our concept, which we will also use in order to generalize the expressions of relative rotations to the nonlinear regime in chapter 6.

Clearly, such deviations of the director orientation from the anchoring direction within the polymer network are connected to a change of the generalized energy of the system. We therefore have to include relative rotations as macroscopic variables that can contribute to the generalized energy density. An appropriate expression for linear relative rotations in a three dimensional description can be found in the following way.

Rotations can be described by axial vectors. With the two vectors $\boldsymbol{\omega}^n$ and $\boldsymbol{\omega}^{nw}$ denoting the local rotations of the director and the polymer network, respectively, the expression $(\boldsymbol{\omega}^n - \boldsymbol{\omega}^{nw}) \times \hat{\mathbf{n}}$ describes relative rotations between the two subsystems in the linear regime. This is the way relative rotations have been introduced in Ref. [36]. The use of $\hat{\mathbf{n}}$ and $\hat{\mathbf{n}}_0$ in this expression is indistinguishable in the linear regime, so we could as well write

$$\tilde{\boldsymbol{\Omega}} = (\boldsymbol{\omega}^n - \boldsymbol{\omega}^{nw}) \times \hat{\mathbf{n}}_0 \quad (2.5)$$

for the vector of relative rotations. We have chosen the superscript “nw” as an abbreviation for polymeric “network”.

In Ref. [39] the notation has been modified and relative rotations have been defined by

$$\tilde{\boldsymbol{\Omega}} = \delta \mathbf{n} - \boldsymbol{\Omega}^\perp. \quad (2.6)$$

This expression refers to the linear regime. Here, $\delta n_i = n_i - n_{0,i}$ and $\Omega_i^\perp = n_j \Omega_{ji}$, where in linear order the latter expression cannot be distinguished from $n_{0,j} \Omega_{ji}$. $\boldsymbol{\Omega}$ denotes the antisymmetric tensor that describes linear rigid rotations of the polymer network. Therefore, it cannot contribute directly to the generalized energy density of the system. We obtain $\boldsymbol{\Omega}$ in the linear regime from the distortion tensor $\nabla \mathbf{u}$ by an additive decomposition:

$$\boldsymbol{\Omega}_{ij} = (\partial_i u_j) - \varepsilon_{ij} = \frac{1}{2} (\partial_i u_j - \partial_j u_i). \quad (2.7)$$

The vector $\boldsymbol{\Omega}^\perp$ can then be interpreted as the vector of rigid rotations of the polymer network perpendicular to the director [39]. This interpretation only accounts for the linear regime as we will see in chapter 6. It can also be interpreted as the variation of the director orientation that would take place if the director was rigidly anchored within the polymer network.

The consistency of Eqs. (2.5) and (2.6) follows from $\delta n_i = \varepsilon_{ijk} \omega_j^n n_{0,k}$ and $\omega_i^{nw} = \frac{1}{2} \varepsilon_{ijk} \Omega_{jk}$, where ε_{ijk} denotes the Levi-Civita tensor. Eqs. (2.5) and (2.6) imply that in the linear regime

$$n_i \tilde{\Omega}_i = 0. \quad (2.8)$$

Relative rotations will play a central role throughout the remaining major part of this work. In our picture they are the crucial variables. They

include the specific features of liquid crystalline elastomers and couple the local director orientation to the mechanical deformations. However, this concept is not restricted to the characterization of liquid crystalline elastomers. Relative rotations occur whenever two or more coupled components of a complex system are globally or locally rotated relatively to each other, or when a component is rotated relatively to a surrounding anchoring matrix. For example, also the macroscopic behavior of magnetic gels has been described successfully using the variables of relative rotations [46, 47].

When we will extend our model to the nonlinear regime in chapter 6, our major task will be to derive nonlinear expressions for the variables of relative rotations.

2.3 Generalized energy density

Our next step is now to derive an expression for the generalized energy density F of the system. For this purpose, we combine the macroscopic variables that have been introduced in the previous section. In particular, these are the gradient of the director field $\nabla \hat{\mathbf{n}}$, the strain tensor $\boldsymbol{\varepsilon}$, and the variables of relative rotations $\tilde{\boldsymbol{\Omega}}$. We will also include the influence of a homogeneous static external electric field \mathbf{E} , assuming that the material under consideration is a perfect electric insulator. This is a good approximation for common nematic and cholesteric SCLSCEs.

F as a scalar function has to be invariant under parity, time reversal, Galilei transformation, and inversion of the director field $\hat{\mathbf{n}} \rightarrow -\hat{\mathbf{n}}$. The terms contributing to the series expansion of the generalized energy density must reflect this behavior under symmetry transformations. Since we will restrict ourselves to a linearized model, it is sufficient to expand F up to quadratic order in the variables given above. Implying summation over repeated indices, the result reads

$$\begin{aligned}
F &= F'_0 + c_1 \varepsilon_{ij} \varepsilon_{ij} + \frac{1}{2} c_2 \varepsilon_{ii} \varepsilon_{jj} \\
&\quad + \frac{1}{2} D_1 \tilde{\Omega}_i \tilde{\Omega}_i + D_2 \tilde{\Omega}_i \varepsilon_{ij} n_j \\
&\quad + \frac{1}{2} K_1 (\nabla \cdot \hat{\mathbf{n}})^2 + \frac{1}{2} K_2 [\hat{\mathbf{n}} \cdot (\nabla \times \hat{\mathbf{n}}) + q_0]^2 + \frac{1}{2} K_3 [\hat{\mathbf{n}} \times (\nabla \times \hat{\mathbf{n}})]^2 \\
&\quad + e_1 (n_i E_i) (\partial_j n_j) + e_2 E_i (n_j \partial_j) n_i + \gamma_1 (n_i E_i) (\partial_j \tilde{\Omega}_j) + \gamma_2 E_i (n_j \partial_j) \tilde{\Omega}_i \\
&\quad + \zeta^{(R)} q_0 \varepsilon_{ijk} E_i n_j \tilde{\Omega}_k \\
&\quad - \frac{1}{2} \epsilon_a (n_i E_i)^2 + \tilde{\chi}_{ijkl}^E E_i E_j \varepsilon_{kl}.
\end{aligned} \tag{2.9}$$

In this expression we have not explicitly listed the terms that contain variables already present in the hydrodynamic description of simple liquids. As mentioned in section 2.1, these variables are given by the density of mass ρ , the density of linear momentum \mathbf{g} , and the density of energy ε . The corresponding terms are represented by the character F'_0 at the beginning of the formula. We assume that their contributions are not decisive for the effects studied in the following. Consequently their influence is neglected. This approach reduces the number of independent state variables, by which a certain state of the system can be identified, to five: the three components of the displacement field $\mathbf{u}(\mathbf{r})$ plus the two variables that describe the field of director orientation $\hat{\mathbf{n}}(\mathbf{r})$.

The rest of the first line of Eq. (2.9) reflects the energetic contributions of elastic strain deformations [14]. Whereas the material parameter c_2 is only related to compressions and dilations, c_1 also reflects the influence of shear deformations. Here, the elastic behavior is assumed to be isotropic for simplicity. In general, this is of course an approximation, although the anisotropy of solely the mechanical elastic behavior of the materials is not too pronounced. If one takes into account the anisotropy of the elastic behavior, one has to add three terms to Eq. (2.9) in the uniaxial case. They can be written in the form $c_3 n_i \varepsilon_{ij} n_j \varepsilon_{kk}$, $c_4 n_i \varepsilon_{ij} \varepsilon_{jk} n_k$, and $c_5 n_i \varepsilon_{ij} n_j n_k \varepsilon_{kl} n_l$ [14, 48]. However, we will mainly be interested in the description of qualitatively new effects, which arise from the coupling of the director orientation to the elastic behavior of the materials. For the description of these effects, the anisotropy of the elastic response in the absence of relative rotations plays a minor role. Therefore, we set the elastic coefficients c_3 , c_4 , and c_5 equal to zero in order to obtain the isotropic case. We note, however, that an anisotropy of the elasticity leads to quantitative corrections.

In the second line of Eq. (2.9), we have listed the terms containing the variables of relative rotations that have been introduced in Ref. [36]. These are the crucial contributions in our description, because they include the specific properties of SCLSCEs. Namely, they represent the coupling of the director orientation to the elastic mechanical deformations. Two material parameters are involved in these terms. On the one hand, D_1 is related to the magnitude of the relative rotations. It expresses the energetic penalty arising directly from the occurrence of a relative rotation. On the other hand, D_2 couples the vector of relative rotations to the strain tensor.

Next, the third line includes the Frank energy density familiar from the macroscopic description of cholesteric LMWLCs [7]. This part of F is solely connected to deformations of the homogeneous director orientation, which result in gradients of the director field $\nabla \hat{\mathbf{n}}$. Neglecting surface contributions,

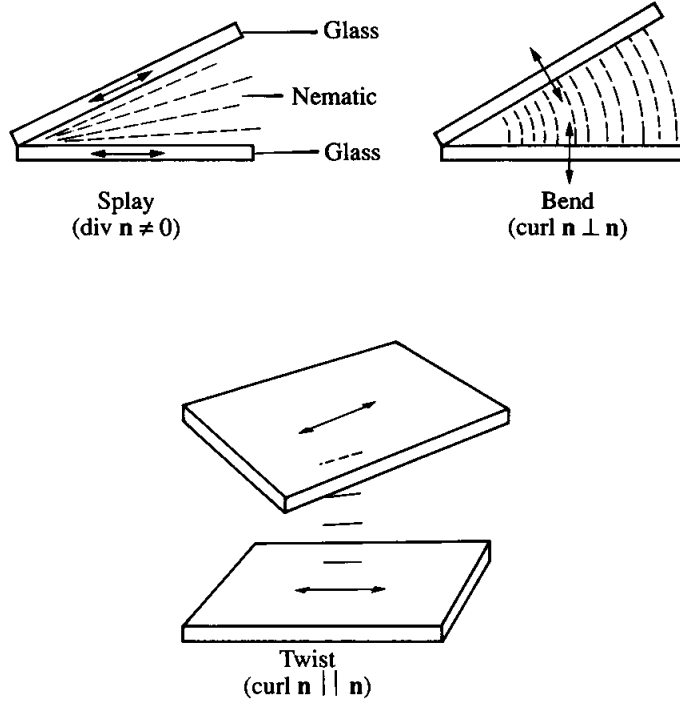


Figure 2.2: Illustration of the splay, twist, and bend deformation of the director field. The director is assumed to be strongly anchored on the surfaces of the sketched glass plates in the depicted orientation. This figure has been reproduced from Ref. [7].

there are the three independent deformations in the linear regime depicted in Fig. 2.2. Namely, these are the splay, twist, and bend deformation, corresponding in this order to the three terms in Eq. (2.9) with the Frank coefficients K_1 , K_2 , and K_3 , respectively. Since the cholesteric director field is twisted in the ground state, the cholesteric wave number q_0 explicitly appears in the twist term with the coefficient K_2 .

Finally, the contributions of the homogeneous static external electric field \mathbf{E} are included. We have listed the terms linear in the electric field first, whereas the terms quadratic in \mathbf{E} make up the last line of Eq. (2.9).

The leading contributions linear in \mathbf{E} with the coefficients e_1 and e_2 are called flexoelectric. They arise because splay and bend deformation of liquid crystals can lead to a polarization [7]. In our case of a spatially homogeneous external electric field, the two flexoelectric terms can be reduced to one for the bulk of the system by neglecting surface contributions. It can be written as $\bar{e}n_j(\partial_j n_i)E_i$, where $\bar{e} = -e_1 + e_2$. The terms with the coefficients γ_1 and

γ_2 have already been presented in Ref. [39] for nematic SCLSCs. Their structure is analogous to the flexoelectric contributions but involves relative rotations.

Next we have included the term with the coefficient $\zeta^{(R)}$, which has been named rotatoelectric [49, 50]. It has not been presented before this work for the local description of cholesteric elastomers [50]. Using vector notation we can rewrite it as $\zeta^{(R)} q_0 \mathbf{E} \cdot (\hat{\mathbf{n}} \times \tilde{\mathbf{\Omega}})$. The presence of this term has astonishing consequences, which seem to be unique for cholesteric SCLSCs. Chapter 3 is mainly devoted to expand on this issue.

The last line of Eq. (2.9) starts with the dielectric contribution. ϵ_a denotes the dielectric anisotropy and can be written as $\epsilon_a = \epsilon_{\parallel} - \epsilon_{\perp}$. Here, ϵ_{\parallel} is the dielectric constant of the material measured parallel and ϵ_{\perp} the dielectric constant measured perpendicular to the director [7]. A term $-\frac{1}{2}\epsilon_{\perp}E^2$ has been incorporated into F'_0 because it does not depend on any of our state variables, but only on the magnitude of the externally applied electric field.

Finally, we have taken into account electrostrictive effects in Eq. (2.9) by the term $\tilde{\chi}_{ijkl}^E E_i E_j \varepsilon_{kl}$. Here, $\tilde{\chi}_{ijkl}^E$ denotes the electrostrictive tensor [48]. Actually, this term is already of cubic order, but we will include a short discussion of its qualitative influence on the results presented in chapter 4.

Altogether, the terms in Eq. (2.9) have been obtained by assuming local uniaxial symmetry of the system, with the symmetry axis given by the director $\hat{\mathbf{n}}$. This only excludes the elastic contributions, as has been discussed above, and the electrostrictive term. The latter will be expanded for the case of uniaxial symmetry at a later stage.

We want to point out that the case of a homogeneous static external magnetic field is formally identically described if we only set the flexoelectric coefficients e_1 and e_2 , the coefficients γ_1 and γ_2 , as well as the rotatoelectric coefficient $\zeta^{(R)}$ equal to zero, replace $\epsilon_a E^2$ by $\chi_a H^2$, and $\tilde{\chi}_{ijkl}^E E_i E_j \varepsilon_{kl}$ by $\tilde{\chi}_{ijkl}^H H_i H_j \varepsilon_{kl}$. Then, χ_a and $\tilde{\chi}_{ijkl}^H$ denote the anisotropy of the magnetic susceptibility and the magnetostrictive tensor, respectively. Both, for an external electric or magnetic field, we obtain the corresponding nematic case from Eq. (2.9) simply by setting $q_0 = 0$.

The thermodynamic stability conditions arising from Eq. (2.9) read $c_1 > 0$, $2c_1 + 3c_2 > 0$, $D_1 > 0$, $D_2^2 < 4c_1 D_1$, $K_1 > 0$, $K_2 > 0$, and $K_3 > 0$ [7, 14, 36].

We obtain the generalized energy \mathcal{F} of the system via spatial integration of the expression for the generalized energy density (2.9),

$$\mathcal{F} = \int_V F d^3r. \quad (2.10)$$

Here, V denotes the volume of the system.

A standard procedure of finding the current state of the material under investigation then consists of minimizing the generalized energy \mathcal{F} . It is of major importance to perform this minimization with respect to the independent state variables that characterize the current state of the system. They correspond to the degrees of freedom of the system under consideration. Following this procedure, it is clear that a realistic situation is described, for which conditions of compatibility as known from solving problems of elasticity theory are satisfied automatically.

In our case, the five independent state variables are given by $\mathbf{u}(\mathbf{r})$, or $\mathbf{a}(\mathbf{r})$, respectively, and by the two variables that specify the orientation of $\hat{\mathbf{n}}(\mathbf{r})$. We have not explicitly included the components of an electric displacement field \mathbf{D} as thermodynamic variables separately. In our situation of a static electric field \mathbf{E} applied to the system externally it is more convenient to take the components of the electric field E_i as thermodynamic variables. Technically speaking the connection between both ways of description is given by a Legendre transformation (more details on this point can be found, e.g., in Ref. [39] for nematic SCLSCes).

Since in our case the electric field is applied externally, we do not minimize the generalized energy of the system \mathcal{F} with respect to the components E_i . In this way, for example the famous Fréedericksz transition and the flexoelectric effect of LMWLCs have successfully been analyzed [7]. Indirectly we do, however, minimize \mathcal{F} with respect to the components of the electric displacement field \mathbf{D} , because they are given from Eq. (2.9) by

$$D_i = \frac{\partial F}{\partial E_i} = e_1(\partial_j n_j)n_i + e_2(n_j \partial_j)n_i + \gamma_1(\partial_j \tilde{\Omega}_j)n_i + \gamma_2(n_j \partial_j)\tilde{\Omega}_i + \zeta^{(R)} q_0 \epsilon_{ijk} n_j \tilde{\Omega}_k - \epsilon_a (n_j E_j)n_i + 2\tilde{\chi}_{ijkl}^E E_j \epsilon_{kl}. \quad (2.11)$$

This expression is a combination of our five independent state variables.

Having introduced our model and explained our scheme to characterize the state of the materials, we will use this macroscopic description in order to investigate the reaction of cholesteric SCLSCes to static external fields in the next three chapters. Whereas the influence of a homogeneous static external electric field is studied in the following two chapters, we will turn to external mechanical fields in chapter 5. Before we start our considerations, however, we will give a short overview on other approaches that have been proposed to describe liquid crystalline elastomers.

2.4 Other approaches

A different macroscopic characterization has been proposed for example in Ref. [51] for nematic elastomers. The main focus of this approach is, however, on materials which show “soft” elastic distortions [52]. In essence, this term refers to anisotropic materials which show a vanishing linear elastic shear modulus when they are sheared within a plane containing a preferred direction. The feature is based on a spontaneous breaking of the continuous rotational symmetry through the emergence of this preferred direction. Since the rotational symmetry is not broken spontaneously in SCLSCEs, but a preferred direction is locked in during the process of synthesis, we conclude that SCLSCEs behave in a different way. In fact, shear experiments using piezorheometry have demonstrated that shear deformations of SCLSCEs in a plane containing the director orientation cost energy, the linear shear modulus being manifestly different from zero [32,34,53]. The possibility of a locked in uniaxial direction has been mentioned and shortly discussed in Ref. [51]. Relative rotations, the crucial variables in our model, however, have not been included in this description explicitly.

“Soft” elastic deformations also play a central role in a semi-microscopic approach, based on rubber elasticity [54]. There, an anisotropic Gaussian distribution function for the end-to-end vectors of the polymer chains between the crosslinking points is assumed. The anisotropy is implied to result from the orientation of the mesogenic units. Consequently, the axis of orientation of the mesogenic units and the axis of anisotropy of the polymer network are identified with each other (and are assumed to remain identical during deformations). Entanglements of the polymer chains are not included, and there is only one independent parameter. Later on, a second independent parameter has been added, and the model has been extended to comprise “semi-soft” elastic distortions [54]. A nonvanishing, but small linear elastic shear modulus for the geometry mentioned above can be obtained in this way. Interpreting the results of macroscopic experiments in the framework of a semi-microscopic model of this kind is difficult, because one has to make the assumption that affine deformations of single unentangled polymer chains between crosslinking points reflect the macroscopic behavior of the materials [55]. Naturally, including the possibility of macroscopically spatially inhomogeneous solutions is also problematic in a semi-microscopic approach. Again, the results obtained from piezorheological shear experiments contradict the association of “soft” elastic shear deformations with the observed behavior of SCLSCEs [32,34,53].

We want to mention, that also a manifestly different semi-microscopic model has been proposed [56,57]. The latter includes constitutive equations

and does not involve the notion of “soft elasticity”.

In the course of this work, we will shortly relate and compare the results obtained by our model to those obtained by the other approaches, if possible and appropriate. The basis of a recently proposed biaxial picture of nematic SCLSCEs [58], which we have not referred to in this section, will be outlined at the beginning of chapter 6.

Chapter 3

Rotatoelectricity in cholesteric side-chain liquid single crystal elastomers

As mentioned in the last chapter, we will start our considerations by investigating the effect of a static or quasistatic homogeneous external electric field on the macroscopic state of cholesteric SCLSCEs. We begin by studying the consequences of electric fields of low amplitudes in the following. Higher electric field amplitudes will be taken into account during the course of the next chapter.

The effect we want to put into the main focus of this chapter arises directly from the coupling of the director to the polymer network. It is connected to the term with the coefficient $\zeta^{(R)}$ in the generalized energy density (2.9) and has been called rotatoelectricity [49, 50]. Furthermore, it represents a unique feature of cholesteric SCLSCEs and leads to perhaps surprising but certainly fascinating consequences: we apply a homogeneous static external electric field parallel to the helical axis of a cholesteric SCLSCE; increasing the electric field amplitude in a quasistatic way then can result in a rotation of the director around the helical axis. The director in this case reorients within the planes perpendicular to the external electric field. As we will see, the director reorientation may occur in this way even if the electric anisotropy is positive.

This chapter is organized as follows. First, we will specify the geometry investigated and give the explicit expression for the corresponding generalized energy density. After that we will show that the generalized energy density describes a rotation of the director in the liquid crystalline state – the effect already mentioned above. In section 3.3, we will propose an experiment in which the consequences of rotatoelectricity should be observable, and finally,

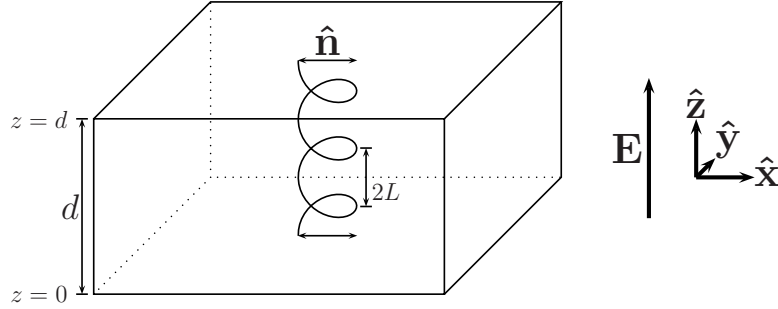


Figure 3.1: Geometry of the system investigated.

in the last section, we will discuss our results. Concerning the presentation of the subject we closely follow the one which we have given in Ref. [50].

3.1 Geometry and corresponding generalized energy density

Our first step is to specify the geometry of the system we want to investigate. For this purpose, we choose the z -axis of our Cartesian coordinate system to be parallel to the ground state cholesteric helical axis. We have depicted this choice in Fig. 3.1.

The ground state conformation $\hat{\mathbf{n}}_0(\mathbf{r})$ of the director field can then be parameterized by

$$\hat{\mathbf{n}}_0(\mathbf{r}) = \begin{pmatrix} n_{ox}(z) \\ n_{oy}(z) \\ 0 \end{pmatrix} = \begin{pmatrix} \cos(q_0 z) \\ \sin(q_0 z) \\ 0 \end{pmatrix}. \quad (3.1)$$

As introduced in chapter 1, q_0 denotes the wave number of the rotation of the cholesteric helix. q_0 is equal to $\frac{\pi}{L}$, $2L$ being the cholesteric pitch (see Fig. 3.1). The sign of q_0 reflects the screw sense of the helix. Since the latter does not change under parity, q_0 must be a pseudoscalar.

Variations of the director field w.r.t. its ground state conformation can then be expressed by

$$\begin{aligned} \delta\mathbf{n}(\mathbf{r}) = \hat{\mathbf{n}}(\mathbf{r}) - \hat{\mathbf{n}}_0(\mathbf{r}) &= \begin{pmatrix} \cos(q_0 z + \Delta(\mathbf{r})) \cos(n_z(\mathbf{r})) \\ \sin(q_0 z + \Delta(\mathbf{r})) \cos(n_z(\mathbf{r})) \\ \sin(n_z(\mathbf{r})) \end{pmatrix} - \begin{pmatrix} \cos(q_0 z) \\ \sin(q_0 z) \\ 0 \end{pmatrix} \\ &\approx \begin{pmatrix} -n_{oy}(z)\Delta(\mathbf{r}) \\ n_{ox}(z)\Delta(\mathbf{r}) \\ n_z(\mathbf{r}) \end{pmatrix}. \end{aligned} \quad (3.2)$$

Here, $n_z(\mathbf{r})$ characterizes a local tilt of the director out of the planes perpendicular to the helical axis, whereas $\Delta(\mathbf{r})$ denotes local variations of the phase angle of the helicoidal director orientation and thus local rotations of the director around the helical axis. Therefore, $n_z(\mathbf{r})$ and $\Delta(\mathbf{r})$ correspond to the two independent broken rotational symmetry variables that we have pointed at in section 2.1. They follow from the local uniaxial symmetry of the material for a large cholesteric pitch.

Consequently, we can now explicitly list the five independent state variables which characterize the current state of our system: the three components of the displacement field $u_x(\mathbf{r})$, $u_y(\mathbf{r})$, and $u_z(\mathbf{r})$, as well as the two variables resulting from the broken rotational symmetry, $n_z(\mathbf{r})$ and $\Delta(\mathbf{r})$. We will not continue to explicitly note the spatial dependence of these variables in the following, and neither the z -dependence of the abbreviations $n_{ox}(z)$ and $n_{oy}(z)$ introduced in Eq. (3.1).

Combining Eqs. (2.6), (3.1), and (3.2) leads us to an expression for the variables of relative rotations in the linearized regime,

$$\tilde{\mathbf{\Omega}} = \begin{pmatrix} -\Delta \sin(q_0 z) + \Omega_{xy} \sin(q_0 z) \\ \Delta \cos(q_0 z) - \Omega_{xy} \cos(q_0 z) \\ n_z - \Omega_{xz} \cos(q_0 z) - \Omega_{yz} \sin(q_0 z) \end{pmatrix} = \begin{pmatrix} -\Delta n_{oy} + \Omega_{xy} n_{oy} \\ \Delta n_{ox} - \Omega_{xy} n_{ox} \\ n_z - \Omega_{xz} n_{ox} - \Omega_{yz} n_{oy} \end{pmatrix}. \quad (3.3)$$

From Eqs. (3.1), (3.2), and (3.3) we can now also explicitly confirm the property $n_i \tilde{\Omega}_i = 0$ of linear relative rotations, which we have noted in Eq. (2.8).

As we have mentioned above, the main focus in this chapter, is on the term $\zeta^{(R)} q_0 \mathbf{E} \cdot (\hat{\mathbf{n}} \times \tilde{\mathbf{\Omega}})$ in Eq. (2.9). We can see from the structure of this term that the consequences of its presence must be unique features of cholesteric SCLSCEs. On the one hand, the term is proportional to the wave number q_0 associated with the cholesteric helix, leading to the fact that it can only be present in the characterization of a macroscopically chiral state. q_0 is a pseudoscalar, which is essential for the existence of the term because the whole term must be even under parity. In turn, this means that in chiral phases lacking symmetry under parity the effects of rotatoelectricity cannot be observable. On the other hand, the main feature of SCLSCEs of coupling the director orientation to the elastic mechanical behavior enters the rotatoelectric term via the relative rotations. Without this coupling, the rotatoelectric term must vanish.

It is interesting to compare the rotatoelectric term of Eq. (2.9) with the one in Ref. [49], where rotatoelectricity has been discussed for the first time. We have noted in section 2.1 that we will include in our picture the director field $\hat{\mathbf{n}}(\mathbf{r})$ in order to characterize the local uniaxial state of the cholesteric

elastomer. This is because we refer to systems of cholesteric pitch larger than or comparable to the thickness of the sample. It leads to the introduced form $\zeta^{(R)} q_0 \mathbf{E} \cdot (\hat{\mathbf{n}} \times \tilde{\mathbf{\Omega}})$ of the rotatoelectric term. The approach in Ref. [49] has been based on the truly hydrodynamic description of cholesteric SCLSCes. This means that the effects under consideration are of much larger wavelengths than the inherent lengths of the system. The cholesteric phase is then properly characterized by the direction of orientation of the helical axis $\hat{\mathbf{p}}(\mathbf{r})$ instead of the director field [44].

Consequently, in Ref. [49] the rotatoelectric term has been introduced as

$$\zeta^{(R)} [\delta\phi - p_i \Omega_i] q_0 p_j E_j. \quad (3.4)$$

There, $\delta\phi$ corresponds to our Δ and denotes the phase variable characterizing the rotation of the director around the helical axis. The components p_i of $\hat{\mathbf{p}}$ give the orientation of the helical axis, and Ω_i are the components of the vector of rigid rotations of the polymer network, defined by $\Omega_i = \frac{1}{2} \epsilon_{ijk} \Omega_{jk} = \frac{1}{2} \epsilon_{ijk} (\partial_j u_k)$. Using this definition on the one hand and Eq. (3.3) on the other hand and remembering that our coordinate system has been chosen to satisfy $\hat{\mathbf{p}} \parallel \hat{\mathbf{z}}$, we can rewrite the two rotatoelectric terms of Eqs. (2.9) and (3.4) in the case of $\mathbf{E} = E \hat{\mathbf{z}}$:

$$\begin{aligned} \bullet \quad & \zeta^{(R)} q_0 \epsilon_{ijk} E_i n_j \tilde{\Omega}_k &= & \zeta^{(R)} [\Delta - \Omega_{xy}] q_0 E, \\ \bullet \quad & \zeta^{(R)} [\delta\phi - p_i \Omega_i] q_0 p_j E_j &= & \zeta^{(R)} [\delta\phi - \Omega_{xy}] q_0 E. \end{aligned} \quad (3.5)$$

From the comparison of the two terms we can see that for $\mathbf{E} \parallel \hat{\mathbf{z}}$ the truly hydrodynamic and the local description of cholesteric SCLSCes are equivalent concerning rotatoelectricity. However, in general, when \mathbf{E} has also nonvanishing components in the directions perpendicular to $\hat{\mathbf{z}}$, the local description offers more information on the behavior of the system. This especially becomes important when the cholesteric pitch is comparable to the extension of the system in the direction of the helical axis, as it is the case in the situation we will investigate here.

Since we want to study in this chapter only effects linear in the external electric field \mathbf{E} , we expand the expression for the generalized energy density Eq. (2.9) up to quadratic order in $\partial_i u_j$ ($i, j = x, y, z$), n_z , Δ , and the components of the external electric field E_i ($i = x, y, z$). We have added to this expression the dielectric contribution in view of later inspections, but we put it into squared brackets in order to stress that it will not be considered in the investigations of the current chapter (it is quadratic in \mathbf{E}). Neglecting contributions to the generalized surface energy of the system, we obtain

$$F = c_1 \left\{ (\partial_x u_x)^2 + (\partial_y u_y)^2 + (\partial_z u_z)^2 + \frac{1}{2} \left((\partial_y u_x) + (\partial_x u_y) \right)^2 \right.$$

$$\begin{aligned}
& + \frac{1}{2} \left((\partial_z u_x) + (\partial_x u_z) \right)^2 + \frac{1}{2} \left((\partial_z u_y) + (\partial_y u_z) \right)^2 \Big\} \\
& + \frac{1}{2} c_2 \left\{ (\partial_x u_x) + (\partial_y u_y) + (\partial_z u_z) \right\}^2 \\
& + \frac{1}{2} D_1 \left\{ \left[\Delta + \frac{1}{2} \left((\partial_y u_x) - (\partial_x u_y) \right) \right]^2 \right. \\
& \quad \left. + \left[n_z + \frac{1}{2} n_{ox} \left((\partial_z u_x) - (\partial_x u_z) \right) + \frac{1}{2} n_{oy} \left((\partial_z u_y) - (\partial_y u_z) \right) \right]^2 \right\} \\
& + D_2 n_{ox} n_{oy} \left\{ - (\partial_x u_x) \left[\Delta + \frac{1}{2} \left((\partial_y u_x) - (\partial_x u_y) \right) \right] \right. \\
& \quad + (\partial_y u_y) \left[\Delta + \frac{1}{2} \left((\partial_y u_x) - (\partial_x u_y) \right) \right] \\
& \quad \left. + \frac{1}{2} \left((\partial_z u_x) (\partial_z u_y) - (\partial_x u_z) (\partial_y u_z) \right) \right\} \\
& + \frac{1}{2} D_2 n_{ox}^2 \left\{ \left((\partial_y u_x) + (\partial_x u_y) \right) \left[\Delta + \frac{1}{2} \left((\partial_y u_x) - (\partial_x u_y) \right) \right] \right. \\
& \quad \left. + \frac{1}{2} \left[(\partial_z u_x)^2 - (\partial_x u_z)^2 \right] \right\} \\
& + \frac{1}{2} D_2 n_{oy}^2 \left\{ - \left((\partial_y u_x) + (\partial_x u_y) \right) \left[\Delta + \frac{1}{2} \left((\partial_y u_x) - (\partial_x u_y) \right) \right] \right. \\
& \quad \left. + \frac{1}{2} \left[(\partial_z u_y)^2 - (\partial_y u_z)^2 \right] \right\} \\
& + \frac{1}{2} D_2 n_z \left\{ n_{ox} \left((\partial_z u_x) + (\partial_x u_z) \right) + n_{oy} \left((\partial_z u_y) + (\partial_y u_z) \right) \right\} \\
& + \frac{1}{2} K_1 \left\{ n_{ox} (\partial_y \Delta) - n_{oy} (\partial_x \Delta) + (\partial_z n_z) \right\}^2 \\
& + \frac{1}{2} K_2 \left\{ n_{ox} (\partial_y n_z) - n_{oy} (\partial_x n_z) - (\partial_z \Delta) \right\}^2 \\
& + \frac{1}{2} K_3 \left\{ \left(n_{ox} n_{oy} (\partial_y \Delta) + n_{ox}^2 (\partial_x \Delta) + q_0 n_{ox} n_z \right)^2 \right. \\
& \quad + \left(n_{ox} n_{oy} (\partial_x \Delta) + n_{oy}^2 (\partial_y \Delta) + q_0 n_{oy} n_z \right)^2 \\
& \quad \left. + \left(n_{ox} (\partial_x n_z) + n_{oy} (\partial_y n_z) \right)^2 \right\} \\
& + (e_1 - e_2) q_0 \left\{ E_x n_{oy} - E_y n_{ox} \right\} n_z \\
& - \frac{1}{4} \gamma_1 q_0 \left\{ \left[-2 E_x n_{ox} n_{oy} + E_y (n_{ox}^2 - n_{oy}^2) \right] (\partial_z u_x) \right. \\
& \quad \left. + \left[E_x (n_{ox}^2 - n_{oy}^2) + 2 E_y n_{ox} n_{oy} \right] (\partial_z u_y) \right\} \\
& + \gamma_1 q_0 \left\{ E_x n_{oy} - E_y n_{ox} \right\} n_z
\end{aligned}$$

$$\begin{aligned}
& -\frac{1}{4}\zeta^{(R)}q_0\left\{\left[-2E_xn_{ox}n_{oy}+E_y(n_{ox}^2-n_{oy}^2)\right](\partial_zu_x)\right. \\
& \quad \left.+ \left[E_x(n_{ox}^2-n_{oy}^2)+2E_y n_{ox}n_{oy}\right](\partial_zu_y)\right\} \\
& +\zeta^{(R)}q_0\left\{E_xn_{oy}-E_y n_{ox}\right\}n_z \\
& +\zeta^{(R)}q_0E_z\Delta \\
& \left[-\frac{1}{2}\epsilon_a\left\{E_x(n_{ox}-n_{oy}\Delta)+E_y(n_{oy}+n_{ox}\Delta)+E_zn_z\right\}^2\right]. \tag{3.6}
\end{aligned}$$

It is very interesting to note that in the regime where we concentrate on the generalized bulk energy density and where the amplitude of the external electric field is considered to be small enough, only the component of the external electric field parallel to the helical axis leads to a new contribution resulting explicitly from rotatoelectricity. The other rotatoelectric terms can be combined with the flexoelectric terms and the γ_1 -terms. If E_z vanishes, the remaining terms containing the electric field can be combined to two terms with coefficients $\bar{c}_1 = e_1 - e_2 + \gamma_1 + \zeta^{(R)}$ and $\bar{c}_2 = \gamma_1 + \zeta^{(R)}$, respectively. Then rotatoelectricity does not lead to qualitatively new effects. However, if larger amplitudes and thus higher orders of \mathbf{E} are taken into account, for example via the dielectric term, the situation will, in general, be different.

As mentioned above, small amplitudes of the external electric field \mathbf{E} are investigated in this chapter, and we choose a geometry in which the external electric field is applied parallel to the helical axis (see Fig. 3.1). Then $E_x = 0 = E_y$ and the electric field contributes to the generalized energy density in Eq. (3.6) in linear order only via the rotatoelectric term. In this case we can study the phenomenon of rotatoelectricity explicitly.

3.2 Rotations of the director

Following the procedure described in the previous chapter, we now derive the equations that characterize the macroscopic state of the material under the influence of the respective static or quasistatic external electric field. For this purpose, we determine the variational derivatives of the generalized energy $\mathcal{F} = \int F d^3r$ of the system w.r.t. the five independent state variables and set the resulting expressions equal to zero. The latter step leads us to Eqs. (A.1)-(A.5) listed in appendix A. We note that in the regime of small external electric field amplitudes, to which we restrict ourselves in this chapter, the influence of the dielectric term in Eq. (2.9) will not be investigated. Therefore, we have put the dielectric contribution between squared brackets in Eqs. (A.4) and (A.5), in the same way as in Eq. (3.6).

Only terms linear in E_i ($i = x, y, z$) enter the inspection of Eqs. (A.1)-(A.5) in this chapter.

As we have mentioned at the end of the last section, we want to investigate a situation in which $\mathbf{E} = E\hat{\mathbf{z}}$ is parallel to the cholesteric helical axis. The cholesteric SCLSCE can, for this purpose, be assumed to be confined between two parallel plates with a distance d , located at $z = 0$ and $z = d$, as illustrated in Fig. 3.1. For simplicity we consider the plates to be infinitely extended in $\hat{\mathbf{x}}$ and $\hat{\mathbf{y}}$ direction.

If we impose no boundary conditions onto the system, the simplest solution to the problem is a spatially homogeneous one. Eqs. (A.1)-(A.5) show that in this case the variable Δ decouples from the other variables. Since, however, Eq. (A.5) is the only equation in which the external electric field $\mathbf{E} = E\hat{\mathbf{z}}$ enters, the field \mathbf{E} acts exclusively on the phase angle Δ . We therefore can set all the other variables equal to zero, without loss of generality,

$$u_x = u_y = u_z = n_z = 0. \quad (3.7)$$

Eq. (A.5) reduces to

$$D_1\Delta + \zeta^{(R)}q_0E = 0, \quad (3.8)$$

which leads us to the solution

$$\Delta = -\frac{\zeta^{(R)}}{D_1}q_0E. \quad (3.9)$$

On the other hand, if we assume the director to be strongly anchored to the plates, which may result, for example, from the way films of cholesteric SCLSCEs are synthesized [26], we obtain as boundary conditions:

$$\begin{aligned} n_z(z=0) &= n_z(z=d) = 0, \\ \Delta(z=0) &= \Delta(z=d) = 0. \end{aligned} \quad (3.10)$$

Then we have to treat the problem as z -dependent, but again we look for a solution which is spatially homogeneous in the lateral directions $\hat{\mathbf{x}}$ and $\hat{\mathbf{y}}$, meaning that we set $\partial_x = 0 = \partial_y$ in Eqs. (A.1)-(A.5). As before, a decoupling of Δ from the other variables arises, and the influence of the external electric field remains restricted to Δ . Thus Eq. (3.7) continues to be valid without loss of generality, and Eq. (A.5) now reduces to

$$D_1\Delta - K_2\partial_z^2\Delta + \zeta^{(R)}q_0E = 0. \quad (3.11)$$

From that, together with the boundary conditions, a z -dependent solution for Δ is derived,

$$\Delta = \frac{\zeta^{(R)}}{D_1} \left[\frac{\cosh\left(\sqrt{\frac{D_1}{K_2}}\left(z - \frac{d}{2}\right)\right)}{\cosh\left(\sqrt{\frac{D_1}{K_2}}\frac{d}{2}\right)} - 1 \right] q_0E. \quad (3.12)$$

If we calculate from this result the mean value of Δ over the sample thickness d , we obtain

$$\langle \Delta \rangle = \frac{1}{d} \int_0^d \Delta(z) dz = \frac{\zeta^{(R)}}{D_1} \left[\frac{2}{d} \sqrt{\frac{K_2}{D_1}} \tanh \left(\sqrt{\frac{D_1 d}{K_2 2}} \right) - 1 \right] q_0 E. \quad (3.13)$$

For large sample thicknesses d this expression again yields the result given by Eq. (3.9), which is consistent because for large values of d the major part of the bulk of the system is not hindered by the constraints of strong anchoring at the sample surfaces.

At this point we want to focus on what our solutions imply. From the physics of LMWLCs, we are used to the dielectric effects that an external electric field induces [7]. We will introduce a corresponding example of diamagnetic effects in the case of an external magnetic field at the beginning of the next chapter. For our purposes at the moment, it is sufficient to have a look at the dielectric term in the expression for the generalized energy density F (2.9). This term implies that in the case of a dielectric anisotropy $\epsilon_a < 0$ the mesogenic units try to orient on average perpendicular to an external electric field. On the contrary, in the case of $\epsilon_a > 0$, they try to orient parallel to the external electric field direction. This leads, for example, to the typical splay, bend, or twist deformations of the director field, if the director is strongly anchored at the boundaries of the system [7]. We recall that dielectric effects result from contributions quadratic in \mathbf{E} to the generalized energy density of the system.

What we observe in the regime linear in $\mathbf{E} = E\hat{\mathbf{z}}$ is rather different from these dielectric effects. Since Δ denotes the phase shift of the director orientation around the helical axis, Eqs. (3.9) and (3.12) describe a rotation of the director around the cholesteric helical axis when compared to the ground state of $\mathbf{E} = \mathbf{0}$, no matter whether $\epsilon_a < 0$ or $\epsilon_a > 0$. Without any boundary conditions for the director, this rotation occurs homogeneously over the whole sample as given by Eq. (3.9) and depicted in Fig. 3.2. There, the situation is sketched for a sample of a cholesteric pitch larger than the sample thickness d . If strong anchoring of the director prevails at the surfaces, the rotation is hindered at the boundaries as given by Eq. (3.12).

In both cases the amplitude of the rotation is proportional to the amplitude of the external electric field, to the rotatoelectric coefficient $\zeta^{(R)}$, as well as to the wave number of the cholesteric helix q_0 . We also note that the larger the coupling between the director and the polymer network of the respective SCLSCE, reflected by the coefficient D_1 , the smaller is the amplitude of the rotatoelectric rotation. This is consistent with Eq. (3.7), which implies vanishing local rigid rotations of the polymer network and in turn leads to

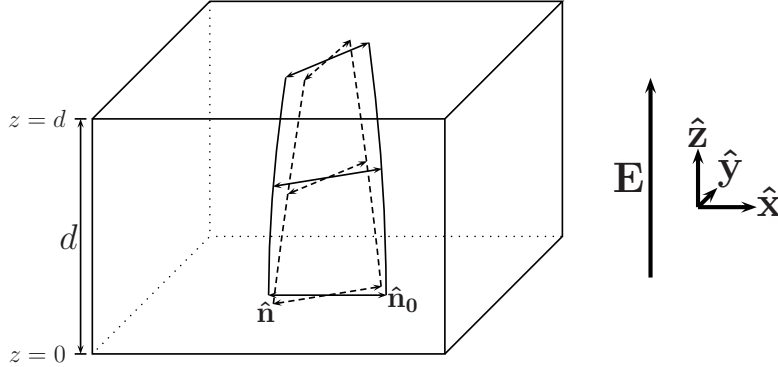


Figure 3.2: In the case depicted, the director is not anchored at the boundaries of the system and the cholesteric pitch is larger than the sample thickness d . The external electric field \mathbf{E} induces a rotation of the director from its ground state conformation $\hat{\mathbf{n}}_0$ (solid lines) to its end position $\hat{\mathbf{n}}$ (dashed lines).

a large amplitude of the relative rotations of $\tilde{\Omega} = \Delta$. The latter enters the expression for the generalized energy density of the system in Eq. (2.9) via the positive definite term $D_1 \tilde{\Omega}_i \tilde{\Omega}_i$. Consistently, in Eqs. (3.9), (3.12), and (3.13) D_1 appears in the denominator and thus reduces the amplitude of the rotatoelectric reorientation of the director.

For illustration we have plotted in Fig. 3.3 the y -component of the director field across the sample for the three introduced cases. The y -component of the director is given by $n_{oy}(z) = \sin(q_0 z)$ from Eq. (3.1) without an external electric field \mathbf{E} applied (solid line in Fig. 3.3). On the other hand, the two cases of boundary conditions we have studied are represented by the two dashed lines for nonvanishing \mathbf{E} . $n_{y,na}(z)$ describes the y -component of a director which is not anchored at the surfaces of the system, whereas $n_{y,sa}(z)$ gives the y -component of a director which is strongly anchored at the bottom and top boundaries. We have obtained the lines by inserting the expressions for Δ from Eqs. (3.9) and (3.12) into $n_y(z) = \sin(q_0 z + \Delta)$. For reasons of clarity, we have chosen a very large value of $\frac{\zeta^{(R)}}{D_1} q_0 E = 0.5$, a ratio $\sqrt{\frac{D_1}{K_2}} = 10^7 \text{ m}^{-1}$, a sample thickness $d = 25 \text{ }\mu\text{m}$, and a cholesteric wave number $q_0 = \frac{4\pi}{d}$. As the two dashed lines demonstrate, the effect of the boundaries remains restricted to the region near the surfaces.

On the whole, the fascinating feature of the rotatoelectric rotation is of course that the resulting force imposed by the external electric field acts perpendicularly to the direction of the external electric field. As described above, it leads to a reorientation of the director within the planes perpendicular to

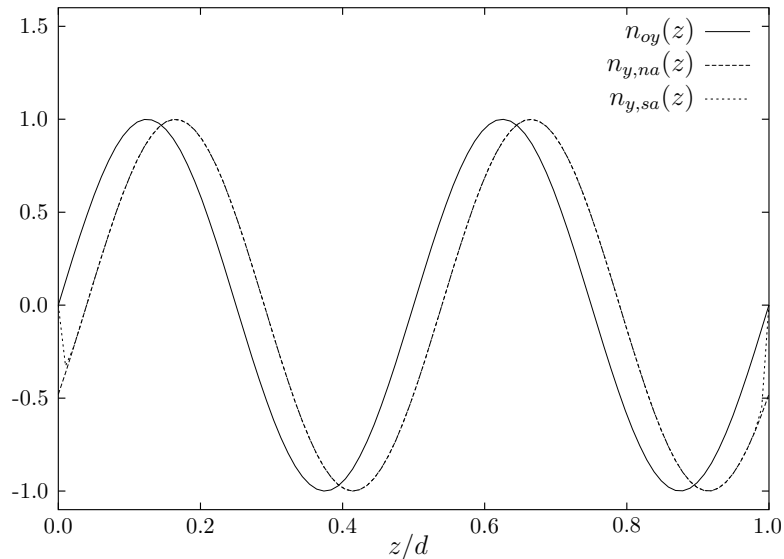


Figure 3.3: $n_{oy}(z)$, $n_{y,na}(z)$, and $n_{y,sa}(z)$ represent the y -component of the director field across the sample for $\mathbf{E} = \mathbf{0}$, for $\mathbf{E} \neq \mathbf{0}$ and vanishing anchoring at the boundaries, and for $\mathbf{E} \neq \mathbf{0}$ and strong anchoring, respectively. The values of the parameters involved have been chosen as described in the text.

the helical axis. Such a behavior is reminiscent of the precession during a gyroscopic motion in the gravitational field. There, the resulting mechanical force inducing the motion of precession is also oriented perpendicular to the external field direction.

3.3 Experimental observation of rotatoelectricity

In the last section we have shown that rotatoelectricity implies interesting effects, which should be observable in an experiment using a rather simple set-up. Therefore we present in this section some expressions that might be helpful for a comparison with experimental results.

The set-up we propose is identical with the geometry depicted in Fig. 3.2. If thin films of cholesteric SCLSCEs are investigated, for which the cholesteric pitch is large compared to the sample thickness d , then the director orientation in such samples should be observable by optical measurements using polarization microscopy. The viewing direction is assumed to be parallel to the helical axis and thus parallel to the direction of the external electric field. In particular, in experiments during which irradiation of very

small wavelengths is applied (x-ray), the mean director orientation should be probed.

Since we think that the condition of strong anchoring of the director to the sample surfaces leads to more realistic boundary conditions, we will use the result given by Eq. (3.12) for the calculations below. We choose the orientation of our coordinate system in such a way that at the bottom plate at $z = 0$ the strongly anchored director points into the $\hat{\mathbf{x}}$ direction, which means $\hat{\mathbf{n}}(z = 0) \parallel \hat{\mathbf{x}}$. Due to the requirement of a cholesteric pitch large compared to the sample thickness d , we assume in the following that across the whole sample the phase angle of the director orientation around the helical axis satisfies the condition

$$q_0 z + \Delta(z) \leq \frac{\pi}{2}. \quad (3.14)$$

In this section, we may rewrite the cholesteric wave number q_0 as

$$q_0 = \frac{\alpha\pi}{d}, \quad (3.15)$$

α being a constant of a value that guarantees the validity of inequality (3.14).

We have noted before, that also the mean values of the director orientation may be observed. Because of this we list the expressions for the components of the director averaged over the sample thickness d . Using relation (3.15) for the cholesteric wave number q_0 , the mean values of the x - and y -components of the ground state director orientation are given by

$$\langle n_{ox} \rangle = \frac{1}{d} \int_0^d n_{ox} dz = \frac{1}{\alpha\pi} \sin(\alpha\pi), \quad (3.16)$$

$$\langle n_{oy} \rangle = \frac{1}{d} \int_0^d n_{oy} dz = \frac{1}{\alpha\pi} [1 - \cos(\alpha\pi)]. \quad (3.17)$$

Similarly, the values of the components of the director variation in the planes perpendicular to the helical axis, namely δn_x and δn_y in Eq. (3.2), averaged over the sample thickness, lead to the following expressions:

$$\begin{aligned} \langle \delta n_x \rangle &= \frac{1}{d} \int_0^d \delta n_x dz \\ &= - \frac{\zeta^{(R)} E \sqrt{\frac{D_1}{K_2}} \sin(\alpha\pi) \tanh\left(\sqrt{\frac{D_1}{K_2}} \frac{d}{2}\right) + \frac{D_1}{K_2} \frac{d}{\alpha\pi} [\cos(\alpha\pi) - 1]}{D_1 \frac{D_1}{K_2} d^2 + (\alpha\pi)^2} \alpha\pi, \end{aligned} \quad (3.18)$$

$$\begin{aligned}
\langle \delta n_y \rangle &= \frac{1}{d} \int_0^d \delta n_y dz \\
&= \frac{\zeta^{(R)} E}{D_1} \frac{\sqrt{\frac{D_1}{K_2}} [\cos(\alpha\pi) + 1] \tanh\left(\sqrt{\frac{D_1}{K_2}} \frac{d}{2}\right) - \frac{D_1}{K_2} \frac{d}{\alpha\pi} \sin(\alpha\pi)}{\frac{D_1}{K_2} d^2 + (\alpha\pi)^2} \alpha\pi.
\end{aligned} \tag{3.19}$$

In the case of a large cholesteric pitch, that is for small values of α , the mean values of the components of the director variation are obtained from the previous expressions to first order in α as

$$\langle \delta n_x \rangle = 0, \tag{3.20}$$

$$\langle \delta n_y \rangle = \frac{\zeta^{(R)} E}{D_1} \left[\frac{2}{d} \sqrt{\frac{K_2}{D_1}} \tanh\left(\sqrt{\frac{D_1}{K_2}} \frac{d}{2}\right) - 1 \right] \frac{\alpha\pi}{d}. \tag{3.21}$$

From the second equation we can infer that for a large cholesteric pitch and a constant sample thickness d the magnitude of the rotatoelectric rotation increases linearly with the wave number of the cholesteric sample. This is because $\langle \delta n_y \rangle$ increases linearly with q_0 .

The mean values of the components of the director $\hat{\mathbf{n}}$ follow from the above equations, because

$$\langle n_x \rangle = \langle n_{ox} \rangle + \langle \delta n_x \rangle, \tag{3.22}$$

$$\langle n_y \rangle = \langle n_{oy} \rangle + \langle \delta n_y \rangle. \tag{3.23}$$

In an experiment, one challenge consists of the selection of the most suitable values for the cholesteric pitch and the thickness of the sample. The relative contributions of three ingredients must be optimized. On the one hand, we have seen that the rotatoelectric rotation increases linearly with q_0 , so that a pronounced cholesteric character of the sample favors the rotatoelectric effect. On the other hand, the sample must not be too thick compared to the cholesteric pitch, because then the determination of the director orientation across the sample using polarization microscopy (or x-ray) does not lead to results that are easy to interpret. Furthermore, however, if the cholesteric film is too thin and strong anchoring governs the surfaces of the system, rotatoelectric effects might not be observable at all due to the strong anchoring at the boundaries. Thus a compromise must be found in order to maximize the observable rotatoelectric effects.

The experiment itself should first of all demonstrate the existence of the rotatoelectric effect discussed here, which has not been done yet. We predict that the phase angle Δ of the rotation and its mean $\langle \Delta \rangle$, as well as

the amplitude of the director reorientation and its mean, depend linearly on the amplitude of the external electric field. These relations are given by Eqs. (3.2), (3.12), (3.13), and (3.18)-(3.21). In addition, it would be very interesting to check for samples of different cholesteric pitch the linear dependence of Δ and/or $\langle \Delta \rangle$ on the cholesteric wave number q_0 as predicted by Eqs. (3.12) and (3.13). Here, in particular, the direction of rotation of the director should change, when samples of different handedness of the cholesteric helix, implying a different sign of q_0 , are investigated. A control experiment with a nematic SCLSCE ($q_0 = 0$) is expected to give no effect, since rotatoelectricity is a novel phenomenon only associated with SCLSCEs of macroscopic handedness.

Furthermore, as can be inferred from Eqs. (3.16)-(3.23), measurements of samples with different sample thicknesses d should allow an estimate of the ratio $\zeta^{(R)}/D_1$. This is the ratio of the rotatoelectric material parameter to the material parameter that determines the contribution to the generalized energy density of the system due to relative rotations exclusively.

3.4 Discussion and conclusion

It is very important to address the question, whether the reaction of a cholesteric SCLSCE in the geometry of Fig. 3.1 to an external electric field with strong anchoring boundary conditions occurs laterally homogeneously, or whether spatial modulations in the lateral directions $\hat{\mathbf{x}}$ and $\hat{\mathbf{y}}$ might complicate the experimental observation of rotatoelectricity. Therefore it is instructive to compare our situation with that of an external electric field $\mathbf{E} = E\hat{\mathbf{z}}$ of larger magnitude. Then the dielectric term becomes important in Eq. (2.9) and leads to an additional contribution $-\epsilon_a E^2 n_z$ in Eq. (A.4).

In the case of $\epsilon_a < 0$ we do not expect an instability arising from the dielectric term at all, because the ground state orientation of the director within the planes perpendicular to the helical axis is stabilized. Such a stabilization of the director adds to the rotation of the director around the helical axis within these planes due to rotatoelectricity.

On the other hand, we will study the situation of $\epsilon_a > 0$ in chapter 4, where we will neglect the rotatoelectric term, the terms with the coefficients γ_i ($i = 1, 2$), and the flexoelectric terms as effects linear in \mathbf{E} . At the moment, for us the most important result of this inspection is the following. Below a critical threshold field amplitude $|E_c|$ the system remains laterally spatially homogeneous. Even above this critical amplitude, the system keeps the lateral spatial homogeneity for the bigger part of the parameter range investigated. We estimate $|E_c|$ to be of the order of $30 \text{ V } \mu\text{m}^{-1}$ for $\epsilon_a = \epsilon_0$. These

facts support our assumption that a major group of cholesteric SCLSCEs in the geometry sketched in Fig. 3.1 should react to the external electric field by a laterally homogeneous solution, which makes us confident that the effect of rotatoelectricity can be observed in an experiment.

Concerning the interval of external electric field amplitudes suitable to detect the rotatoelectric effect we expect no difficulties, because rotatoelectricity describes a phenomenon linear in \mathbf{E} . Therefore, the relevant field amplitudes must be smaller by orders of magnitude compared to the threshold field amplitude $|E_c|$ of the instabilities that arise from the dielectric term.

In summary, we have demonstrated that rotatoelectricity is an intrinsic and unique property of cholesteric SCLSCEs and leads to interesting effects. By quasistatically increasing the amplitude of an external electric field applied parallel to the cholesteric helical axis, the director can rotate in a plane perpendicular to the external field direction. We have proposed an experiment in which rotatoelectricity should be observable, and we hope that such experiments will be carried out in the future to find out more about the consequences of this phenomenon.

Chapter 4

Dielectric effects in cholesteric side-chain liquid single crystal elastomers

In this chapter, we will continue to study the macroscopic consequences that arise for a cholesteric SCLSCE when exposed to a homogeneous static or quasistatic external electric field \mathbf{E} . We will investigate the same set-up as introduced in the previous chapter and illustrated in Fig. 3.1. The difference arises from the magnitude of the external electric field considered. Whereas an effect linear in the electric field amplitude has been studied in the previous chapter, we now put into the focus the dielectric behavior of the materials. Our treatment of the subject is closely connected to the one we have presented in Ref. [59].

We will start with some general remarks in the next section, including a short review of the Fréedericksz transition observed for LMWLCs [7]. After that, we will investigate the geometry depicted in Fig. 3.1 in detail. As a consequence of the dielectric response of the systems, we will find two kinds of instabilities. Whereas the one presented in section 4.2 can be viewed as the analog to the Fréedericksz instability in LMWLCs, we will detect a qualitatively new instability in section 4.3. Finally, we will shortly discuss our results.

4.1 Geometry and macroscopic equations

Throughout this chapter, we will assume the dielectric anisotropy ϵ_a to be positive. The reason has already been explained in section 3.2. Only if $\epsilon_a > 0$ will the electric field impose a torque onto the director orientation.

This can lead to a reorientation of the director, because then the director tends to align parallel to the external electric field for energetic reasons. We can infer this fact directly from Eq. (2.9). If $\epsilon_a < 0$, the director tends to align perpendicularly to the external electric field direction and the result is a stabilization of the director orientation within the planes perpendicular to the cholesteric helical axis. Again, we suppose that the material under consideration is a perfect electric insulator.

For nematic LMWLCs, the geometry we want to investigate in this chapter has become quite famous. In the situation corresponding to Fig. 3.1, the LMWLC is confined between two glass plates separated by a distance d . Special treatment of the plate surfaces leads to strong anchoring of the director in one fixed direction at the top and bottom boundaries, within the boundary planes. Consequently, in the ground state the director of the nematic liquid crystal is homogeneously oriented in this preferred direction across the whole sample. We will assume that an external magnetic field is applied to the low molecular weight nematic sample, instead of an external electric field [7]. The corresponding energy density describing this system then reads

$$F_{LMW} = \frac{1}{2}K_1(\nabla \cdot \hat{\mathbf{n}})^2 + \frac{1}{2}K_2[\hat{\mathbf{n}} \cdot (\nabla \times \hat{\mathbf{n}})]^2 + \frac{1}{2}K_3[\hat{\mathbf{n}} \times (\nabla \times \hat{\mathbf{n}})]^2 - \frac{1}{2}\chi_a(H_i n_i)^2. \quad (4.1)$$

The anisotropy of the magnetic susceptibility is considered to be positive, $\chi_a > 0$ [7], and, in analogy to Fig. 3.1, we assume $\mathbf{H} = H\hat{\mathbf{z}}$ perpendicular to $\hat{\mathbf{n}}_0$.

Then, from this energy density, we find a clear competition between two effects. On the one hand, the external magnetic field tries to align the director perpendicular to its initial orientation. On the other hand, the director is fixed in its original orientation at the sample boundaries. Therefore, a reorientation of the director leads to spatial inhomogeneities of the director orientation. The latter cost energy because in this case $\nabla \hat{\mathbf{n}} \neq \mathbf{0}$.

A linear stability analysis yields the following results. For low magnetic field amplitudes, the homogeneous ground state director orientation is preserved. The energetic gain by orienting the director parallel to the magnetic field cannot balance the energy which is necessary to distort the homogeneous director field. There exists, however, a critical external field amplitude, at which this situation changes. When the field amplitude is increased beyond this threshold value, the spatially homogeneous director orientation becomes unstable with respect to a spatially inhomogeneous state. Therefore, the director starts to reorient. From an analysis of Eq. (4.1), the critical magnetic

field amplitude is found to be

$$|H_c| = \frac{\pi}{d} \sqrt{\frac{K_1}{\chi_a}}, \quad (4.2)$$

whereas the shape of the instability at threshold reads

$$\delta \mathbf{n}(\mathbf{r}) = N \sin\left(\frac{\pi}{d}z\right) \hat{\mathbf{z}}. \quad (4.3)$$

N is the amplitude of the instability and cannot be determined in a linear stability analysis.

The corresponding transition can be detected optically. It is an example of the famous Fréedericksz transition of nematic LMWLCs [7]. Since only the Frank constant K_1 characterizing splay deformations (see Fig. 2.2) is involved in the expression for $|H_c|$, the described set-up is suitable for measuring this material parameter in an experiment. For obvious reasons, the geometry has been named splay geometry.

On the way to the macroscopic investigation of the analogous geometry for cholesteric SCLSCEs exposed to an external electric field, we are already well prepared. In Eq. (3.6) of the previous chapter we have listed the explicit expression for the generalized energy density which characterizes the geometry under consideration. Of course, we now include the dielectric term noted in squared brackets at the end of Eq. (3.6). The independent state variables defining the current state of the system remain the same as in the previous chapter, u_x , u_y , u_z , n_z , and Δ , namely. Also the macroscopic equations which characterize the current state of the material under the influence of the external electric field have already been derived. They are given by the five coupled partial differential equations (A.1)-(A.5) listed in appendix A. Again, we now have to include the dielectric contributions added to Eqs. (A.4) and (A.5) in squared brackets.

When we inspect Eqs. (2.9) and (3.6), we find that the dielectric term describes an effect quadratic in \mathbf{E} . We expect that the dielectric effect in cholesteric SCLSCEs should occur at rather elevated values of the electric field amplitude. We will therefore concentrate exclusively on the dielectric term in this chapter and neglect the contributions linear in \mathbf{E} . That is, we set $e_1 = e_2 = \gamma_1 = \gamma_2 = \zeta^{(R)} = 0$ in this chapter (and $\bar{c}_1 = \bar{c}_2 = \zeta^{(R)} = 0$ in appendix A). In fact, we will confirm our approach by estimations of typical electric field amplitudes at a later stage of this chapter.

We also expect elevated electric field amplitudes for the dielectric effects to become observable when we compare to the analogous case of LMWLCs. Our goal is to investigate the nature of director reorientations by a static

external electric field applied parallel to the cholesteric helical axis. Because of the specific coupling in SCLSCEs, in general this will also lead to an elastic mechanical deformation of the respective sample. Since the mechanical deformation costs energy, we expect a much higher electric threshold field for director reorientations in cholesteric SCLSCEs than in the case of LMWLCs.

From the special geometry we want to study (see Fig. 3.1), a further simplification of our task arises. Due to the orientation of the electric field $\mathbf{E} = E\hat{\mathbf{z}}$, the dielectric contributions to Eqs. (A.4) and (A.5) reduce to only one term $-\epsilon_a E_z^2 n_z$ in Eq. (A.4).

On the other hand, we will also neglect the electrostrictive term of Eq. (2.9) in the main text of this chapter and discuss its influence separately in appendix B. The reason for this approach lies with the comparatively small contributions to the mechanical deformations by electrostriction, as will be further explained in the appendix. There, we also show that electrostrictive effects will not change the results of our calculations qualitatively.

As indicated in Fig. 3.1, the bottom surface of the sample under consideration will be located at $z = 0$, and the top surface at $z = d$. We will impose the following restrictions onto these boundaries of the system.

First, in analogy to the Fréedericksz geometry of LMWLCs described above, the director is assumed to be strongly anchored at the top and bottom boundaries. Consequently

$$n_z(z = 0) \equiv n_z(z = d) \equiv 0, \quad (4.4)$$

$$\Delta(z = 0) \equiv \Delta(z = d) \equiv 0. \quad (4.5)$$

In addition, we require

$$u_z(z = 0) \equiv u_z(z = d) \equiv 0. \quad (4.6)$$

The reason for this boundary condition is that a sample compressed between two plates should not penetrate these plates or detach from them.

During mechanical deformations of the elastomer, mechanical stress will arise in the bulk and on the surfaces of the sample under consideration. When we have found a certain state of the material, which is given by a specific displacement field $\mathbf{u}(\mathbf{r})$ and director field $\hat{\mathbf{n}}(\mathbf{r})$, this mechanical stress can be characterized by a mechanical stress tensor

$$\sigma_{ij}^{mech} = \frac{\partial F}{\partial \varepsilon_{ij}} = 2c_1 \varepsilon_{ij} + c_2 \varepsilon_{kk} \delta_{ij} + \frac{1}{2} D_2 (\tilde{\Omega}_i n_j + \tilde{\Omega}_j n_i). \quad (4.7)$$

No tangential mechanical shear stresses should occur on the surfaces of the sample at $z = 0$ and $z = d$. This means that the components $\sigma_{xz}^{mech} = \sigma_{zx}^{mech}$

and $\sigma_{yz}^{mech} = \sigma_{zy}^{mech}$ of the mechanical stress tensor have to vanish on these surfaces. We therefore obtain as boundary conditions

$$(\partial_z u_x)(z=0) \equiv (\partial_z u_x)(z=d) \equiv 0, \quad (4.8)$$

$$(\partial_z u_y)(z=0) \equiv (\partial_z u_y)(z=d) \equiv 0. \quad (4.9)$$

For simplicity, in this chapter we will assume that the system is infinitely extended in the lateral directions $\hat{\mathbf{x}}$ and $\hat{\mathbf{y}}$.

In the derivation of Eqs. (A.1)-(A.5) we have neglected energetic contributions of the sample surfaces and concentrated on the energetic contributions of the bulk. For the lateral directions, this is justified by the dimensions of the systems under consideration. We take into account the effect of the surfaces at $z=0$ and $z=d$ by the boundary conditions we have imposed.

Before coming to the details of our analysis, we want to include a general remark concerning the treatment of Eqs. (A.1)-(A.5). We notice that the resulting set of equations can be solved by an ansatz that separates the z -dependence of the solution from the lateral dependences, which are the x - and y -dependences:

$$\begin{aligned} u_x(\mathbf{r}) &= \cos(k_x x + k_y y + \varphi) \tilde{u}_x(z), \\ u_y(\mathbf{r}) &= \cos(k_x x + k_y y + \varphi) \tilde{u}_y(z), \\ u_z(\mathbf{r}) &= \sin(k_x x + k_y y + \varphi) \tilde{u}_z(z), \\ n_z(\mathbf{r}) &= \cos(k_x x + k_y y + \varphi) \tilde{n}_z(z), \\ \Delta(\mathbf{r}) &= \sin(k_x x + k_y y + \varphi) \tilde{\Delta}(z). \end{aligned} \quad (4.10)$$

This solution contains lateral undulations in $\hat{\mathbf{x}}$ and $\hat{\mathbf{y}}$ direction, where φ is an arbitrary phase angle that only becomes important if both of the wave numbers k_x and k_y are zero. It will be one of the goals of our work to find out, whether instabilities with nonvanishing wave numbers k_x and k_y could be identified when minimizing the generalized energy of the system \mathcal{F} . Such an instability would be of qualitatively different character when compared to the introduced LMWLC Fréedericksz instability.

The possible separation of the z -dependence from the lateral x - and y -dependences of the solutions proposes the following approach. First we will treat the problem only z -dependent, which means that we are looking for solutions that are homogeneous over the whole sample in lateral directions $\hat{\mathbf{x}}$ and $\hat{\mathbf{y}}$. In a second step we will demonstrate that, depending on the material parameters, laterally inhomogeneous solutions may occur and can be energetically favored over the homogeneous solution.

4.2 Laterally homogeneous solution

Looking for only z -dependent solutions, we can set $\partial_x \equiv 0 \equiv \partial_y$ in Eqs. (A.1)-(A.5) or equally $k_x = 0 = k_y$ in ansatz (4.10).

Strong anchoring of the director at $z = 0$ and $z = d$ is maintained, and all pitches of the cholesteric helix are allowed in the ground state independent of the sample thickness d . Consequently, the director orientation at the bottom and top surfaces can be written as

$$\begin{aligned} \hat{\mathbf{n}}(z=0) &\equiv \begin{pmatrix} 1 \\ 0 \\ 0 \end{pmatrix} \quad \text{and} \\ \hat{\mathbf{n}}(z=d) &\equiv \begin{pmatrix} n_{ox}(d) \\ n_{oy}(d) \\ 0 \end{pmatrix} \equiv \begin{pmatrix} \cos(q_0 d) \\ \sin(q_0 d) \\ 0 \end{pmatrix}, \end{aligned} \quad (4.11)$$

where

$$q_0 = m \frac{\pi}{d}, \quad m \in \mathbb{R}. \quad (4.12)$$

Since we are looking for only z -dependent solutions, we infer from Eqs. (A.1)-(A.5) that in this case the variables $u_z(z)$ and $\Delta(z)$ completely decouple from the respective other variables. Taking into account Eqs. (4.5) and (4.6), and minimizing \mathcal{F} , we can set $u_z(z)$ and $\Delta(z)$ equal to zero:

$$u_z(z) = 0, \quad (4.13)$$

$$\Delta(z) = 0. \quad (4.14)$$

We can now solve the remaining system of equations (A.1), (A.2), and (A.4) explicitly. Making use of the boundary conditions (4.8) and (4.9) leads us to the general solution of Eqs. (A.1) and (A.2), which is given by

$$(\partial_z u_x) = \frac{\alpha}{\beta} n_{ox} n_z, \quad (4.15)$$

$$(\partial_z u_y) = \frac{\alpha}{\beta} n_{oy} n_z, \quad (4.16)$$

with the abbreviations

$$\alpha = -\frac{1}{2}(D_1 + D_2), \quad (4.17)$$

$$\beta = \frac{1}{4}(4c_1 + D_1 + 2D_2). \quad (4.18)$$

Substituting this into Eq. (A.4) together with $\mathbf{E} = E\hat{\mathbf{z}}$, we obtain an ordinary differential equation for n_z ,

$$\left(-\epsilon_a E^2 + D_1 + K_3 q_0^2 - \frac{\alpha^2}{\beta}\right) n_z - K_1 (\partial_z^2 n_z) = 0. \quad (4.19)$$

In order to satisfy the boundary conditions resulting from (4.11), we solve this differential equation by a Fourier series, keeping only the sin-terms:

$$n_z = \sum_{n \in \mathbb{N}} N_n \sin\left(n \frac{\pi}{d} z\right). \quad (4.20)$$

There always exists the trivial solution of Eq. (4.19) where all the N_n vanish and $n_z \equiv 0$. For small amplitudes of the electric field $|E|$ this is the only possible solution in real space. However, when E reaches a certain threshold value E_c , nontrivial solutions of Eq. (4.19) exist and lead to a lower generalized energy of the system than does $n_z \equiv 0$. In our case this threshold value corresponds to the mode of $n = 1$ in Eq. (4.20), and it is given by

$$\epsilon_a E_c^2 = K_1 \left(\frac{\pi}{d}\right)^2 + K_3 q_0^2 + \frac{4c_1 D_1 - D_2^2}{4c_1 + D_1 + 2D_2}. \quad (4.21)$$

The value of the amplitude of the external electric field given by this expression is the lowest value of $|E|$ for which we expect a deviation of the system from its ground state on the basis of the linear stability analysis we have performed. The final solution of the set of Eqs. (A.1)-(A.5) for $E = E_c$ is then obtained by integration of Eqs. (4.15) and (4.16) as

$$u_x = N_1 \frac{\alpha}{2\beta} \left\{ \frac{\cos[(q_0 - \frac{\pi}{d})z]}{q_0 - \frac{\pi}{d}} - \frac{\cos[(q_0 + \frac{\pi}{d})z]}{q_0 + \frac{\pi}{d}} \right\}, \quad (4.22)$$

$$u_y = N_1 \frac{\alpha}{2\beta} \left\{ \frac{\sin[(q_0 - \frac{\pi}{d})z]}{q_0 - \frac{\pi}{d}} - \frac{\sin[(q_0 + \frac{\pi}{d})z]}{q_0 + \frac{\pi}{d}} \right\}, \quad (4.23)$$

$$n_z = N_1 \sin\left(\frac{\pi}{d} z\right), \quad (4.24)$$

where N_1 is the amplitude of director reorientation and remains undetermined in a linear stability analysis.

In essence, what we have found is a critical threshold value of the electric field amplitude $|E_c|$, at which the original orientation of the director becomes unstable with respect to a tilting of the director out of the planes perpendicular to the helical axis. Since all the terms in Eq. (4.21) are positive because of conditions of thermodynamic stability, there are four competing effects.

On the one hand the external electric field tends to align the director parallel to itself, which would lead to a tilting of the director out of its original position. This is given by the left-hand side of Eq. (4.21). On the other hand there are three effects that try to keep the director fixed in its ground state position and thus within the planes perpendicular to the helical axis. These effects show up in the terms on the right-hand side of Eq. (4.21):

First, the boundaries of the system impose a torque which acts to fix the director in its original position as known from the common Fréedericksz transition in the case of nematic LMWLCs [7] and from the Fréedericksz-like or undulatory instabilities predicted for nematic SCLSCes [33, 35]. It is the term $K_1(\frac{\pi}{d})^2$ which expresses this effect. Its contribution is due to a splay deformation of the director field, and its influence vanishes with increasing distance of the boundaries d in the same way as indicated for the Fréedericksz transition of nematic LMWLCs in Eq. (4.2). Secondly, the cholesteric helix structure of the director opposes to a reorientation of the director by a bend deformation of the director field, given by the term $K_3 q_0^2$. The more pronounced the cholesteric structure, that means the larger q_0^2 , the larger is the influence of this effect. As a third effect, the coupling of the director to the polymer network also increases $|E_c|$, which is included by the last term on the right of Eq. (4.21). It arises because due to this coupling the elastomer has to be deformed as implied by Eqs. (4.22) and (4.23) when the director is reoriented.

The first two of the three effects contributing to the right-hand side of Eq. (4.21) also show up for a common cholesteric LMWLC in the same geometry. This case is included in our equations and occurs if the coupling between director and polymer network vanishes, which means $D_1 \rightarrow 0$ and $D_2 \rightarrow 0$. We then obtain from Eq. (A.4) as an instability in the corresponding low molecular weight system

$$n_z(z) = N_1 \sin\left(\frac{\pi}{d}z\right) \quad (4.25)$$

at a critical electric threshold field given by

$$\epsilon_a E_c^2 = K_1 \left(\frac{\pi}{d}\right)^2 + K_3 q_0^2. \quad (4.26)$$

Except for the term $K_3 q_0^2$ arising from the cholesteric structure and the consideration of an external electric field, these results correspond to the ones presented in Eqs. (4.2) and (4.3) for the Fréedericksz transition of nematic LMWLCs.

If we want to estimate values of the critical field amplitude from Eq. (4.21), we consider the third term on the right-hand side being the dominating

one. Assuming $c_1 > -D_2/2$ as it seems appropriate for common cholesteric SCLSCEs, this term strictly increases for growing values of D_1 . In the limit of $D_1 \rightarrow \infty$ we obtain the same result as has been found for nematic SCLSCEs in Ref. [33],

$$|E_c| \lesssim 2\sqrt{\frac{c_1}{\epsilon_a}}. \quad (4.27)$$

For typical values of c_1 in the range of $10^4 - 10^6$ Pa and for $\epsilon_a = \epsilon_0$ this yields maximal values for the amplitude of $|E_c|$ in the range of $70 - 700$ V μm^{-1} , for $\epsilon_a = 10\epsilon_0$ in the range of $20 - 200$ V μm^{-1} . If we more realistically set $D_1 = 10^4$ Pa, for example, we obtain $|E_c| \approx 30$ V μm^{-1} in the case of $\epsilon_a = \epsilon_0$ and $|E_c| \approx 10$ V μm^{-1} in the case of $\epsilon_a = 10\epsilon_0$, quite independently of the values of c_1 and D_2 . These are field amplitudes that certainly can be realized in an experiment nowadays.

As we can see from Eqs. (4.22) and (4.23), the cases $q_0 = \pm\frac{\pi}{d}$, where the cholesteric helix makes exactly one half turn from one boundary at $z = 0$ to the other at $z = d$, are special. In these cases, with $n_z = N_1 \sin(\frac{\pi}{d}z)$, we obtain by integrating Eqs. (4.15) and (4.16), and from Eq. (4.21),

$$u_x = \mp N_1 \frac{\alpha}{4q_0\beta} [\cos(2q_0z)], \quad (4.28)$$

$$u_y = \pm N_1 \frac{\alpha}{4q_0\beta} [2q_0z - \sin(2q_0z)], \quad (4.29)$$

$$n_z = \pm N_1 \sin(q_0z), \quad (4.30)$$

$$\epsilon_a E_c^2 = (K_1 + K_3)q_0^2 + \frac{4c_1 D_1 - D_2^2}{4c_1 + D_1 + 2D_2}. \quad (4.31)$$

Calculating the expressions for u_x and u_y by taking the limit $q_0 \rightarrow \pm\frac{\pi}{d}$ in Eqs. (4.22) and (4.23), one term in the expression for u_x diverges,

$$\lim_{q_0 \rightarrow \pm\frac{\pi}{d}} \frac{\cos[(q_0 \mp \frac{\pi}{d})z]}{q_0 \mp \frac{\pi}{d}} = \lim_{a \rightarrow 0} \frac{\cos(az)}{a} = \lim_{a \rightarrow 0} \frac{1}{a} = \infty. \quad (4.32)$$

However, this divergence does not depend on the value of z , and since here only the spatial derivative of u_x in $\hat{\mathbf{z}}$ direction is important for the physical behavior of the system we may drop this term.

At the end of this section we want to have a closer look at the mechanical deformation of the elastomer. The solutions obtained here are only z -dependent and thus constant within the planes perpendicular to the helical axis. As u_z vanishes over the whole sample the mechanical deformation of the elastomer is then identical to a shearing of the different layers perpendicular to the helical axis against each other. We can calculate the shear \mathbf{S}

of the boundary layer at $z = d$ against the boundary layer at $z = 0$ by using Eqs. (4.22) and (4.23):

$$\mathbf{S} = D_x \hat{\mathbf{x}} + D_y \hat{\mathbf{y}}, \quad (4.33)$$

where

$$D_x = u_x(d) - u_x(0) = -N_1 \frac{\alpha}{\beta} \frac{\pi}{d} \frac{1}{q_0^2 - (\frac{\pi}{d})^2} [1 + \cos(q_0 d)], \quad (4.34)$$

$$D_y = u_y(d) - u_y(0) = -N_1 \frac{\alpha}{\beta} \frac{\pi}{d} \frac{1}{q_0^2 - (\frac{\pi}{d})^2} \sin(q_0 d). \quad (4.35)$$

In the case of $q_0 = \pm \frac{\pi}{d}$, we obtain

$$D_x = u_x(d) - u_x(0) = 0, \quad (4.36)$$

$$D_y = u_y(d) - u_y(0) = \pm N_1 \frac{\alpha}{2\beta} d. \quad (4.37)$$

With the help of these equations we can identify the following special cases for \mathbf{S} :

- $\mathbf{S} = \mathbf{0}$ if $q_0 = m \frac{\pi}{d}$, $m = \pm 3, \pm 5, \dots$
- $\mathbf{S} \parallel \hat{\mathbf{x}}$ if $q_0 = m \frac{\pi}{d}$, $m = \pm 2, \pm 4, \dots$
- $\mathbf{S} \parallel \hat{\mathbf{y}}$ if $q_0 = \pm \frac{\pi}{d}$.

If we now consider for example a system satisfying the condition $q_0 = \pm \frac{\pi}{d}$, and if the amplitude N_1 of the director reorientation n_z can be measured, the value of

$$\frac{\alpha}{2\beta} = - \frac{D_1 + D_2}{4c_1 + D_1 + 2D_2} \quad (4.38)$$

can be determined from Eq. (4.37). In this way, a relation between the material parameters D_1 and D_2 can be obtained when c_1 is measured in another experiment.

4.3 Laterally inhomogeneous solutions

Finally, we have studied solutions that also depend on the x - and/or y -coordinate, in addition to the z -coordinate, by introducing ansatz (4.10) into the set of partial differential equations (A.1)-(A.5). These solutions are characterized by undulations of the director orientation as well as of the displacement of the elastomer in at least one of the lateral directions $\hat{\mathbf{x}}$ and $\hat{\mathbf{y}}$. Furthermore, the displacement of the elastomer parallel to the helical axis, given by u_z , and the reorientation of the director around the helical axis, described by Δ , do not decouple from the other variables. Therefore,

the solutions inspected in the following qualitatively differ from the laterally homogeneous solution of the previous section.

The resulting set of z -dependent ordinary differential equations has been solved numerically for different values of the material parameters and of the lateral wave numbers k_x and k_y . For this purpose we have chosen the sign of the dominant second order z -derivatives in Eqs. (A.1)-(A.5) to be positive and used a relaxation method. The resulting equations are dominated by the diffusive terms and have been developed forward in time according to the FTCS scheme [60] on a discrete lattice of $N + 1$ points with a lattice constant dz . We have mainly investigated situations which correspond to a sample thickness of $d = 25 \mu\text{m}$ by setting $N = 250$ and $dz = 10^{-7}$.

Values of the material parameters in our numerical studies have been chosen as follows. For the Frank constants we have assumed different values of about 10^{-10} Pa, which is one order of magnitude larger than typical corresponding low molecular weight values. Thereby, the influence of the exact values of the Frank constants has been found to be negligible. The behavior of the system is dominated by the material parameter c_1 associated with the elastic behavior of the material in the absence of any relative rotation, and by the two material parameters D_1 and D_2 that determine the coupling of the director to the polymer network. We have varied c_1 in the range of $10^4 - 10^6$ Pa, which corresponds to typical values for common networks, and we have set $D_1 = 10^4$ Pa, so that D_1 does neither become much smaller than $|D_2|$ nor much larger than c_1 (to our knowledge so far only for one specific nematic SCLSCE the ratio of D_2^2/D_1 has been estimated to be roughly 5×10^4 Pa [32]). D_2 has then been varied over the whole range of values allowed by the thermodynamic stability condition $D_2^2 < 4c_1D_1$. On the other hand, the influence of the material parameter c_2 associated with the compressibility of the system was found to be quite small. Increasing c_2 over four orders of magnitude affected the amplitude of the critical external field by not more than a few per cent, no matter whether $c_2 < c_1$ or $c_2 > c_1$. In order to account for the low compressibility of common SCLSCEs, we have always chosen $c_2 = 10^4 c_1$ in what follows.

As boundary conditions we have again assumed the director to be strongly anchored at the bottom and top surface of the sample. However, it should now be aligned in parallel directions on both surfaces. We have chosen, without loss of generality,

$$\hat{\mathbf{n}}(z = 0) \parallel \hat{\mathbf{n}}(z = d) \parallel \hat{\mathbf{x}}. \quad (4.39)$$

This implies

$$q_0 = m \frac{\pi}{d}, \quad \text{with} \quad m = \pm 1, \pm 2, \pm 3, \dots \quad (4.40)$$

To simplify the notation we will restrict ourselves to positive values of q_0 in the following. Concerning the displacement field we have kept the conditions given by Eqs. (4.6), (4.8), and (4.9).

By means of linear stability analysis, we could then determine the amplitude of the critical electric field necessary in order to realize a certain solution with wave numbers k_x and k_y for the given set of material parameters. In particular, we could compare this amplitude with the corresponding value for the laterally homogeneous solution given by Eq. (4.21). From this comparison we can infer whether there exist situations in which at onset an instability including lateral undulations in $\hat{\mathbf{x}}$ and/or $\hat{\mathbf{y}}$ direction occurs instead of the laterally homogeneous instability of the previous section.

Some of the results obtained in this way are depicted in Figs. 4.1 (a)-(f). They show maps in the D_2 - c_1 -plane for different values of q_0 indicated in the figures, keeping the sample thickness $d = 25 \mu\text{m}$ fixed. On the ordinate we give the respective value of the material parameter c_1 on a logarithmic scale, where c_1 ranges from 10^4 Pa to 10^6 Pa as described above. The special form of the maps results as the abscissa labels on a linear scale the values of D_2 , which for the respective value of c_1 are limited by the condition of thermodynamic stability $D_2^2 < 4c_1D_1$. The black lines indicate $D_2 = 0$. In Figs. 4.1 (a)-(c) we refer to solutions with $k_y = 0$ and nonvanishing values of k_x as specified in the respective figures; in Figs. 4.1 (d)-(f) we refer to solutions with $k_x = 0$ and nonvanishing values of k_y . For comparison, in figures corresponding to systems of the same cholesteric pitch, the values of the nonzero wave numbers k_x and k_y were taken to be equal, and they have been chosen to minimize the amplitude of the critical external electric field $|E_c|$. Of course the latter cannot be achieved by exactly one value of k_x or k_y over the whole range of c_1 and D_2 , but this fact is negligible for what we want to demonstrate here. In the darker regions of Figs. 4.1 (a)-(f) we find undulatory instabilities with wave numbers as indicated to have a lower $|E_c|$ than the laterally homogeneous instability. Therefore we are sure that in these regions at onset an undulatory instability will be observed instead of the laterally homogeneous one. The differences in $|E_c|$ for the two types of solutions thereby can get quite remarkable. In the parameter range inspected, we have recorded values for the undulatory instabilities which are about 25% lower than the corresponding values for the laterally homogeneous instability.

When decreasing the cholesteric pitch or increasing the cholesteric wave number q_0 , respectively, we have detected an increase of the value of $|E_c|$ of the respective undulatory instability compared to the homogeneous solution. This is also reflected by Figs. 4.1 (a)-(c) and (d)-(f), where in this order the area of the dark regions gets smaller, respectively. As indicated in the

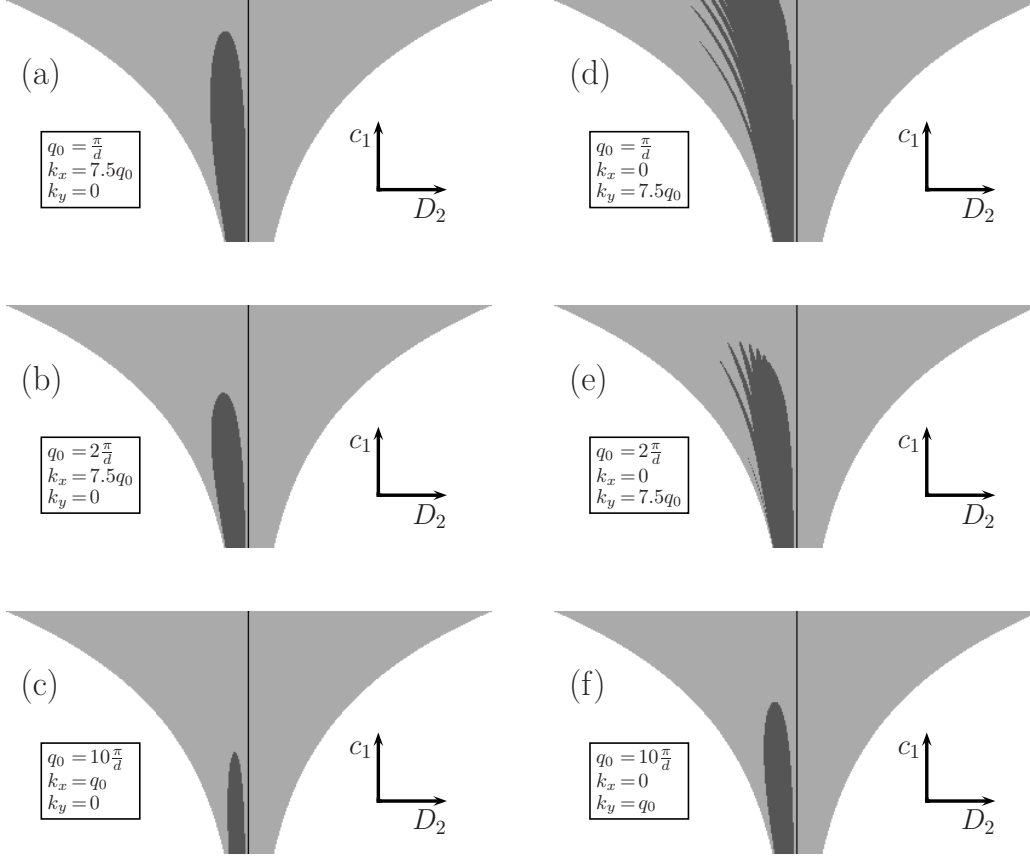


Figure 4.1: Maps of the D_2 - c_1 -plane, in which we have indicated by the darker regions where we expect undulations at onset with certainty. (a)-(c) show a series of increasing q_0 for $k_x \neq 0$ and $k_y = 0$, (d)-(f) for $k_x = 0$ and $k_y \neq 0$. In the respective map, c_1 increases vertically from $10^4 - 10^6$ Pa on a logarithmic scale; horizontally we label D_2 on a linear scale in the range of thermodynamic stability. The nonzero values of the lateral wave numbers have been chosen to minimize the amplitude of the critical external electric field; the values of the remaining parameters have been set at fixed values as discussed in the text.

figures, we have also observed a decrease of the relative values of the lateral wave numbers at which the minimum of $|E_c|$ occurs with increasing q_0 .

For every set of values for the material parameters inspected, we have determined the nonzero critical wave numbers k_x or k_y to be of the order of q_0 . Furthermore, we have always found those undulations most favored that appear perpendicular to the orientation of the strongly anchored director at the system boundaries. For situations of $k_x \neq 0$ and $k_y = 0$, and for situations in which both k_x and k_y are nonzero, always a larger value of $|E_c|$ has been found than for situations of $k_x = 0$ and $k_y \neq 0$. This shows up in Figs. 4.1 (a)-(f), where in maps corresponding to systems with the same cholesteric pitch the dark regions are always larger in area for $k_x = 0$ than for $k_y = 0$.

As a main result also represented by Figs. 4.1 (a)-(f), we find that regions where we expect an undulatory instability at onset only occur when the value of the material parameter D_2 is negative. Actually we have not observed any undulations at onset for any set of material parameters as long as D_2 was positive. Our explanation for this fact is the following. In the maps of Figs. 4.1 (a)-(f) the areas of undulatory instabilities at onset are always located around the line of $D_2 = -D_1$. This value of D_2 , however, is special. If we inspect Eqs. (A.1)-(A.5) setting $D_2 = -D_1$, we find for the laterally homogeneous solution that not only u_z and Δ decouple from the other variables and vanish as given by Eqs. (4.13) and (4.14), but also the lateral components of the displacement field u_x and u_y decouple from n_z . Since n_z , which describes the tilting of the director out of the planes perpendicular to the helical axis, is the only variable directly connected to the external electric field, we can set $u_x \equiv 0$ and $u_y \equiv 0$. Because of this, the laterally homogeneous solution and the expression for the corresponding critical external electric field in Eqs. (4.13), (4.14), and (4.21)-(4.24) now turn into the simple form of

$$\mathbf{u} \equiv \mathbf{0}, \quad (4.41)$$

$$n_z = N_1 \sin\left(\frac{\pi}{d}z\right), \quad (4.42)$$

$$\Delta \equiv 0, \quad (4.43)$$

$$\epsilon_a E_c^2 = K_1 \left(\frac{\pi}{d}\right)^2 + K_3 q_0^2 + D_1. \quad (4.44)$$

Furthermore, the strain tensor and the tensor describing the rigid rotations of the polymer network vanish, $\boldsymbol{\varepsilon} \equiv \mathbf{0} \equiv \boldsymbol{\Omega}$, so that the relative rotations read $\tilde{\boldsymbol{\Omega}} = (0, 0, n_z)$. This makes the magnitude of the relative rotations become very large, which increases the value of the term $\frac{1}{2}D_1\tilde{\Omega}_i\tilde{\Omega}_i$ in the generalized energy density F of the system in Eq. (2.9). In contrast, the

term $D_2 \tilde{\Omega}_i \varepsilon_{ij} n_j$ vanishes due to $\varepsilon \equiv \mathbf{0}$. However, apart from some terms included in F'_0 and those terms containing the external electric field, the D_2 -term is the only contribution to the expression for F that is not positive definite. Altogether these facts lead to an increase of the generalized energy of the system \mathcal{F} and thus of the amplitude of the critical external electric field $|E_c|$ compared to the cases in which D_2 clearly differs from $-D_1$. On the contrary, if the system is undulated, none of the variables completely decouples from n_z . Then, by nonvanishing components of the tensors ε and Ω , the magnitude of the relative rotations can be lowered. Because of that the contribution of the positive definite term $\frac{1}{2} D_1 \tilde{\Omega}_i \tilde{\Omega}_i$ in the generalized energy density decreases, and additionally the term $D_2 \tilde{\Omega}_i \varepsilon_{ij} n_j$ can further reduce the generalized energy of the system \mathcal{F} . Both effects resulting from undulations in the system can lead to a lower value of $|E_c|$ than the one expected for the laterally homogeneous solution. Due to these reasons, undulations should really occur at onset if the value of D_2 is close to $-D_1$.

For practical purposes this means that an experiment can indicate the sign of the material parameter D_2 : if undulations are detected at onset, it is quite certain that for the sample under investigation D_2 is negative. Furthermore, we find that the occurrence of the undulations in cholesteric SCLSCEs is governed in the first place by the kind of coupling of the director to the polymer network, described by the material parameters D_1 and D_2 . Without this coupling, which implies a vanishing value of D_2 , undulations are not expected at onset as can also be seen from Figs. 4.1 (a)-(f).

The reason why we do not find any undulations for large values of c_1 can now also be explained. Undulatory instabilities imply a distortion of the elastomer and thus nonvanishing components of the strain tensor ε . In particular, these components enter the expression for the generalized energy density F in Eq. (2.9) by the positive definite terms $c_1 \varepsilon_{ij} \varepsilon_{ij}$. If the coefficient c_1 becomes too large, the values of the generalized energy of the system \mathcal{F} and the amplitude of the critical external electric field $|E_c|$ increase over the corresponding values for the laterally homogeneous solution. Then the laterally homogeneous instability arises at onset in the case of $D_2 = -D_1$, also shown by the maps in Figs. 4.1 (a)-(f). What this means is that within our approach there is a clear indication that theoretically cholesteric SCLSCEs could be synthesized which allow the reorientation of the director without any macroscopic distortion of the elastomer.

If in our equations we take the limit of an infinite cholesteric pitch or of a vanishing wave number q_0 , respectively, we end up with the situation of a nematic SCLSCE in a classical splay geometry. The latter situation has been investigated in Ref. [33]. There, undulatory instabilities likewise are

expected only for one specific sign of D_2 . Furthermore, if in the respective equations of Ref. [33] we also investigate the case of $D_2 = -D_1$, we find that theoretically it should be equally possible to synthesize nematic SCLSCes allowing the reorientation of the director without any macroscopic distortion of the polymer network.

After that, we want to have a short look at the spatial symmetries of the z -dependent part of the solutions, marked by the \sim in ansatz (4.10). We find from Eqs. (A.1)-(A.5) and from our numerical investigations in the case of $q_0 = \frac{\pi}{d}$ the spatial symmetries as listed in the following table:

	$\tilde{u}_x(z)$	$\tilde{u}_y(z)$	$\tilde{u}_z(z)$	$\tilde{n}_z(z)$	$\tilde{\Delta}(z)$
$k_x \neq 0, k_y = 0$	+	-	-	+	-
$k_x = 0, k_y \neq 0$	+	-	+	+	+

Here “+” means “symmetric in $\hat{\mathbf{z}}$ direction with respect to $z = \frac{d}{2}$ ” and “-” means “antisymmetric in $\hat{\mathbf{z}}$ direction with respect to $z = \frac{d}{2}$ ”. If both $k_x \neq 0$ and $k_y \neq 0$, the symmetries get mixed up.

We give an example for the z -dependent part of the solutions obtained for $q_0 = 2\frac{\pi}{d}$, $k_x = 0$, $k_y = 7.5q_0$, $c_1 = 10^5$ Pa, and $D_2 = -\sqrt{c_1 D_1}$ in Fig. 4.2. The amplitudes of the variables have been rescaled as indicated in the caption of the figure. One of the amplitudes remains undetermined in a linear stability analysis.

Finally, in order to study the effect of an increasing cholesteric wave number q_0 , we have chosen $k_x = 0$, $c_1 = 10^4$ Pa, as well as $D_2 = -\sqrt{c_1 D_1}$, and again the sample thickness was kept fixed at $d = 25$ μm . As can be seen from Figs. 4.1 (d)-(f), these values of the material parameters strongly favor the undulations to occur. We have increased q_0 from $\frac{\pi}{d}$ to $10\frac{\pi}{d}$ by steps of $\frac{\pi}{d}$ in order to satisfy the boundary conditions, and the results we have obtained are depicted in Fig. 4.3. What we have observed is that on the one hand the lateral wave number $k_{y,c}$ describing the solution with the minimal amplitude of the corresponding external electric field increases with increasing q_0 as depicted by the first set of data points. On the other hand, the second set of data points once again shows that with increasing q_0 the undulatory solution becomes less favored with respect to the laterally homogeneous solution. The values of the points give the ratio of $\epsilon_a E_c^2(k_y = k_{y,c})$ determined numerically for the undulatory instability to the respective value of $\epsilon_a E_c^2(k_y = 0)$ for the laterally homogeneous solution calculated from Eq. (4.21). Considering the absolute values of $\epsilon_a E_c^2(k_y = k_{y,c})$ for the undulatory solutions, we have found an increase approximately linear in q_0 , in contrast to the laterally homogeneous solution where the term $K_3 q_0^2$ in Eq. (4.21) leads to an increase quadratic in q_0 .

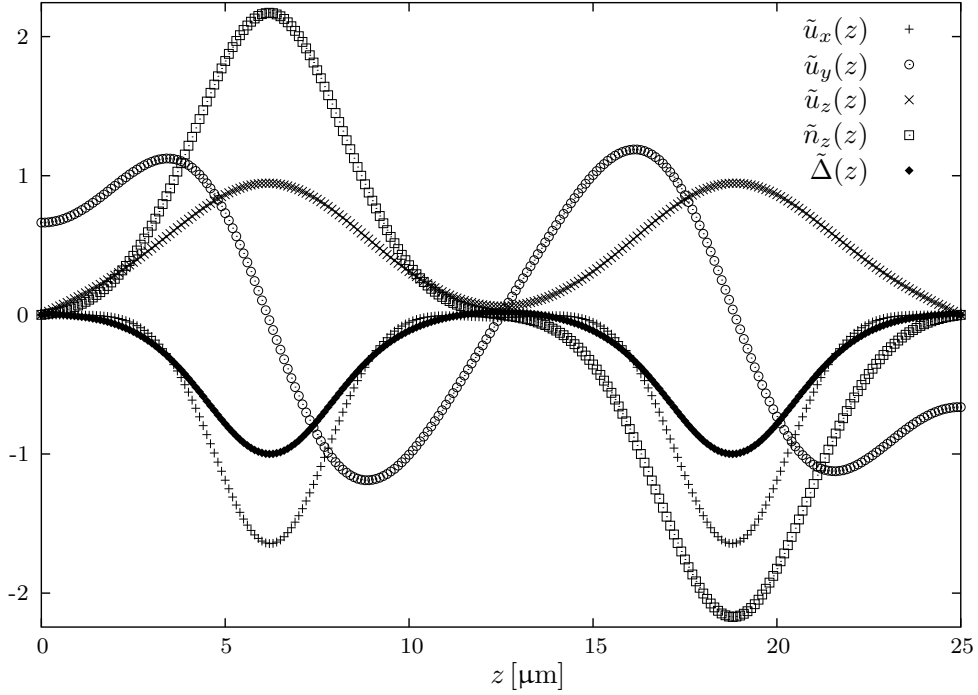


Figure 4.2: Example for the z -dependent part of the laterally inhomogeneous solution in the case of $q_0 = 2\frac{\pi}{d}$. In the plot $\tilde{u}_x(z)$, $\tilde{u}_y(z)$, $\tilde{u}_z(z)$, $\tilde{n}_z(z)$, and $\tilde{\Delta}(z)$ have been rescaled by $2\Upsilon \times 10^{-8}$ m, $2\Upsilon \times 10^{-7}$ m, $2\Upsilon \times 10^{-6}$ m, 30Υ , and Υ , respectively, where Υ denotes the amplitude of $\tilde{\Delta}(z)$. The material parameters have been selected as specified in the main text.

Interestingly, decreasing the sample thickness from $d = 100 \mu\text{m}$ to $d = 5 \mu\text{m}$ with the same values of the material parameters and a constant value of $q_0 = \frac{\pi}{d}$ induces an approximately quadratic increase of $\epsilon_a E_c^2(k_y = k_{y,c})$, which is also the case for the laterally homogeneous solution due to the term $K_1(\frac{\pi}{d})^2$ in Eq. (4.21).

4.4 Discussion and conclusion

In this chapter, we have investigated the dielectric reaction of a cholesteric SCLSCE which is exposed to a homogeneous static or quasistatic external electric field oriented parallel to the helical axis (Fig. 3.1). We have detected a threshold value of the field amplitude at which the ground state conformation of the system becomes unstable. At onset we have found two qualitatively different types of instabilities, one of which takes place homogeneously over the whole sample in the directions perpendicular to the cholesteric helical

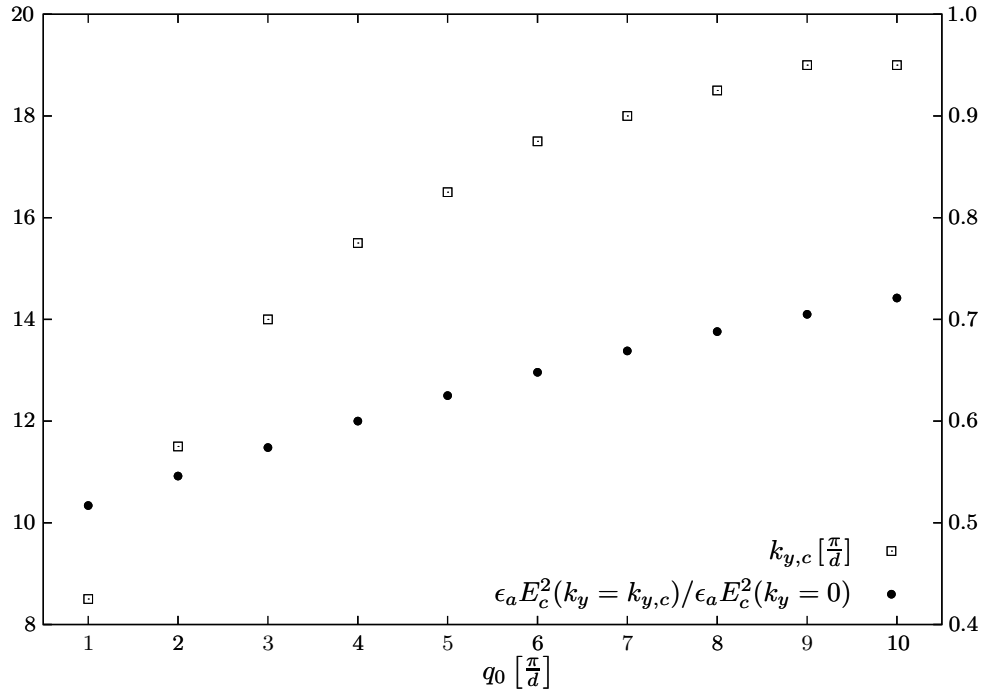


Figure 4.3: Increase of the lateral wave number $k_{y,c}$, which minimizes the amplitude of the critical external electric field $|E_c|$, and increase of the ratio $\epsilon_a E_c^2(k_y = k_{y,c})/\epsilon_a E_c^2(k_y = 0)$ for $k_x = 0$ when q_0 is increased. The values of $k_{y,c}$ have been determined to an accuracy of $\frac{\pi}{2d}$, those of $\epsilon_a E_c^2(k_y = k_{y,c})/\epsilon_a E_c^2(k_y = 0)$ to an accuracy of 0.001. Labels on the left of the frame correspond to $k_{y,c}$, those on the right to $\epsilon_a E_c^2(k_y = k_{y,c})/\epsilon_a E_c^2(k_y = 0)$.

axis (section 4.2) while the other one corresponds to undulations in these directions (section 4.3).

As a reorientation of the director, the first of these two instabilities only contains a tilting of the director out of the planes perpendicular to the cholesteric helical axis. We have shown that the boundaries of the system, the cholesteric helical structure, and the coupling to the polymer network oppose to this reorientation of the director, whereas its amplitude remains undetermined in the linear stability analysis performed here. Together with the reorientation of the director, a shearing of the layers perpendicular to the helical axis occurs, from which a relation between the so far undetermined material parameters D_1 and D_2 could be estimated.

The other type of instability is characterized by undulations perpendicular to the cholesteric helical axis that result from the coupling of the director orientation to the mechanical deformations of the materials. Here, additionally a distortion of the elastomer parallel to the helical axis and a reorientation of the director within the planes perpendicular to the helical axis occur. Low values of the elastic coefficient c_1 favor undulations. Furthermore, only for negative values of the material parameter D_2 we have found this undulatory type of instability to have a lower amplitude of the corresponding threshold field than has the laterally homogeneous instability. Therefore, in an experiment the observation of undulations at onset in general indicates a negative sign of the material parameter D_2 for the sample investigated. For a situation in which the director is strongly anchored at the top and the bottom of the sample with same orientation we have found that undulations perpendicular to this direction of anchoring are favored. Small cholesteric pitches favor the laterally homogeneous instability at onset. Our results are consistent with those obtained in the limit of large cholesteric pitches, where we end up in the case of the splay geometry of nematic SCLSCEs, a situation that has been investigated in Ref. [33].

Finally, we have concluded that theoretically it should be possible to synthesize cholesteric and nematic SCLSCEs in which only the director is reoriented when the sample is put into an external electric field, whereas the polymer network is not macroscopically distorted. This case can occur if the material parameter D_2 takes the value of $-D_1$.

We would like to add a few remarks. As a first point, we want to stress that in our macroscopic description the boundary conditions play an important role concerning the form of the respective solution. However, we are sure that the boundary conditions chosen reflect the actual constraints in corresponding experimental set-ups and/or can easily be realized.

Next, we mention that similar geometries to the ones studied here have been investigated for cholesteric SCLSCEs by the semi-microscopic approach

introduced in section 2.4 [61]. The major limitation of the semi-microscopic inspections is, however, that thereby obtained solutions are spatially homogeneous. Therefore, the qualitatively new solution of an undulatory instability predicted here has not been obtained by using the semi-microscopic model. In addition, the influence of the system boundaries is not included as a constraint imposed only onto the surfaces, neither are the effects of the classical Frank distortion energy incorporated. However, for systems in which the director is fixed at the boundaries, terms resulting from these contributions to the internal energy are essential. Furthermore, in the investigation of cholesteric SCLSCEs in Ref. [61], the cholesteric structure is only accounted for as a rotated nematic layer structure. Turning to the situation of an external electric field applied parallel to the helical axis of a cholesteric SCLSCE, the result would be that in our expression for the threshold field of director reorientation in Eq. (4.21), the first two terms would be missing. However, these are the terms we already expect for LMWLCs in the same geometry. If we then, for comparison, also incorporate another consequence of the semi-microscopic model, namely “soft elasticity” of SCLSCEs, we have to set $D_2^2 = 4c_1D_1$ for the material parameter that couples elastic strain to the relative rotations. In this way, the value of D_2 is pushed to the boundaries of the region of thermodynamic stability. As a consequence, which we have already pointed at in section 2.4, there result “soft” elastic deformations of liquid crystalline elastomers in general, which do not change the free energy of the system [54]. In Ref. [61] no “soft” deformations have been found for cholesteric SCLSCEs in the geometries inspected.

On the whole, the result would be a completely vanishing threshold field in Eq. (4.21). This is proposed in Ref. [61], where the influence of an external electric field applied parallel to the cholesteric helical axis is studied theoretically by the semi-microscopic approach. However, we know already from the Fréedericksz transition of nematic LMWLCs in the corresponding geometry that there exists a critical threshold field for the director reorientation in case of nonvanishing anchoring of the director at the boundaries. When, in addition, the director reorientation is restricted due to a cholesteric helical structure and coupling to a polymer network, it would be very surprising if the amplitude of the threshold field were even lower. In essence, we believe that the approach by a macroscopic continuum model is appropriate in describing the experimental realization of the geometries investigated.

To conclude, it would be of major interest to check in an experiment whether a threshold value of an external electric field applied parallel to the cholesteric helical axis can be detected, and whether the undulatory instabilities predicted theoretically in this chapter can be observed. Furthermore, the proposed experimental access to the material parameters can help to reveal

their values, most of which are still unknown so far.

Chapter 5

Mechanical deformations of cholesteric side-chain liquid single crystal elastomers

In the course of the two previous chapters, we have investigated the influence of an external electric field on the state of a cholesteric SCLSCE. Now, we will turn to a different topic: mechanical deformations of the materials will be the subject of this chapter. We will start with some general considerations.

A major focus on cholesteric liquid crystalline phases from the application point of view is due to their specific optical properties. We have already indicated in section 1.1 of the introduction that cholesteric phases show a photonic bandgap. The reason for the occurrence of this bandgap can be found in the spatially twisted arrangement of the director and the resulting birefringence. Circularly polarized light with the same handedness as the cholesteric helix and a wavelength comparable to the cholesteric pitch is strongly reflected when irradiated parallel to the helical axis [7]. As a consequence, films of cholesteric phases doped with a fluorescent dye, the maximum of emission of which is located in the photonic bandgap, can act as mirrorless lasers with a low lasing threshold [10]. The cholesteric film then replaces the cavity of a common laser. There exist also cholesteric liquid crystals that additionally act as the active lasing medium themselves [11].

In the same way as the LMWLC films, also films of cholesteric SCLSCEs doped with a suitable fluorescent dye show lasing activity. However, as a major advance of using free-standing films of cholesteric SCLSCEs, lasing cannot only be achieved by means of a mirrorless cavity. In addition, the wavelength of the emitted light also becomes mechanically tunable over a range of about 100 nm [29,62]. Tuning is realized by stretching the sample in two orthogonal directions perpendicular to the helical axis.

We will investigate the latter situation as a special case in this chapter. More generally, we will study the behavior of cholesteric SCLSCes when exposed to static or quasistatic external mechanical fields. The corresponding macroscopic equations will be specified in the next section. After that, we will begin by investigating the influence of compressive and dilative forces applied parallel to the cholesteric helical axis in section 5.2. Closely related to this issue is the investigation of the influence of static compressive and dilative forces applied perpendicularly to the cholesteric helical axis in section 5.3. There, we will address the geometry relevant for the mechanically tunable mirrorless lasers as a special case. In this context, we will find that our results obtained in this respect fully agree with the corresponding experimental observations [29, 62]. We will summarize and shortly discuss our results in section 5.4.

In essence, in this chapter we are predominantly interested in the effects that mechanical deformations of the elastomer have on the orientation of the director in cholesteric SCLSCes. Again, our presentation of the topic in this chapter closely follows the one we have given in Ref. [59].

5.1 Macroscopic equations

The orientation of our Cartesian coordinate system w.r.t. the cholesteric SCLSCe investigated will be kept the same as in the two previous chapters. It is illustrated in Fig. 3.1. Without loss of generality, we again locate the bottom of the sample at $z = 0$ and the top at $z = d$. The only difference in comparison to the geometry depicted in Fig. 3.1 arises from the fact that now the external electric field has to be set equal to zero, $\mathbf{E} = \mathbf{0}$.

As a consequence, we can use the same macroscopic equations already derived in chapter 3 and appendix A in order to characterize our system. A certain state of the system is defined by the respective values of the five independent variables u_x , u_y , u_z , n_z , and Δ . The latter values are calculated from the five coupled linear partial differential equations (A.1)-(A.5) listed in appendix A, setting $\mathbf{E} = \mathbf{0}$. In addition, we may specify appropriate boundary conditions.

We will assume that the director is oriented in parallel directions at the bottom and at the top of the sample. Without loss of generality, we orient the director in $\hat{\mathbf{x}}$ direction on these surfaces,

$$\hat{\mathbf{n}}(z = 0) \parallel \hat{\mathbf{n}}(z = d) \parallel \hat{\mathbf{x}}. \quad (5.1)$$

The assumption of a strong anchoring of the director on the bottom and top surfaces is certainly justified for the films synthesized by photo-crosslinking

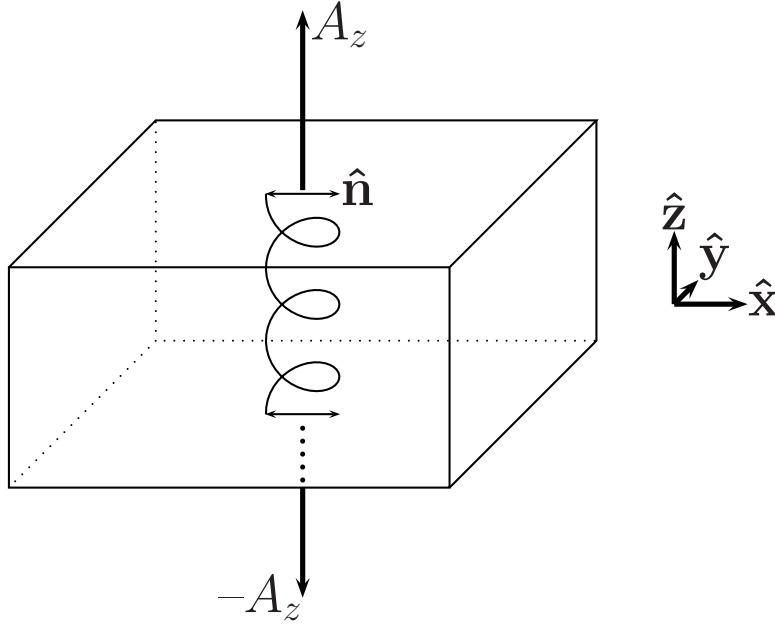


Figure 5.1: Compression and dilation of a cholesteric SCLSCE by external mechanical forces parallel to the cholesteric helical axis.

[26]. In this case, the polymer network gets covalently bound to the substrate during the crosslinking process, if supported films are produced. If free-standing films are synthesized, the polymer network gets covalently bound to a sacrificial layer, by which the substrate is coated. Most of the sacrificial layer is dissolved in water afterwards in order to separate the film from the substrate. In the following, we will only investigate situations which on the surfaces maintain the director orientations given by Eq. (5.1).

In the ground state of the system, the cholesteric pitch $2L$ (see Fig. 3.1) for homogeneous structures then satisfies the condition $d = mL$ with $m = 1, 2, 3, \dots$. The wave number for the rotation of the cholesteric helix can therefore be written as

$$q_0 = m \frac{\pi}{d}, \quad \text{with} \quad m = \pm 1, \pm 2, \pm 3, \dots \quad (5.2)$$

5.2 Compression and dilation parallel to the helical axis

The first geometry that we want to inspect is the one depicted in Fig. 5.1. By static external mechanical forces the system is compressed or dilated parallel to the axis of the cholesteric helix, and we denote the applied force

densities (per unit area) by \mathcal{A} . The corresponding surfaces of the sample under consideration are oriented by surface vectors $\hat{\mathbf{s}}$. According to Fig. 5.1, in this geometry $\mathcal{A} = (0, 0, \pm A_z)$ on the surfaces oriented by the surface vectors $\hat{\mathbf{s}} = (0, 0, \pm 1)$, and $\mathcal{A} = (0, 0, 0)$ on the surfaces oriented by the surface vectors $\hat{\mathbf{s}} = (\pm 1, 0, 0)$ and $\hat{\mathbf{s}} = (0, \pm 1, 0)$. For $A_z < 0$ we obtain a situation of compression, for $A_z > 0$ the system is dilated.

Using the tensor of mechanical stress introduced in Eq. (4.7), we connect surface vectors and mechanical force densities on the sample surfaces by

$$\hat{\mathbf{s}} \cdot \boldsymbol{\sigma}^{mech} = \mathcal{A}. \quad (5.3)$$

As boundary conditions, we assume Eq. (5.1) for the director orientation at $z = 0$ and $z = d$, and, in addition,

$$u_z(z = 0) \equiv 0 \quad \text{and} \quad u_z(z = d) \equiv C_z d \quad (5.4)$$

for the displacement field. Here, C_z denotes what is usually called the compression or dilation in this context. The reason for the boundary conditions (5.4) is that a sample compressed between two plates should not penetrate these plates or detach from them.

We solve Eqs. (A.1)-(A.5) by the ansatz

$$\begin{aligned} u_x(\mathbf{r}) &= C_x x, \\ u_y(\mathbf{r}) &= C_y y, \\ u_z(\mathbf{r}) &= C_z z, \\ n_z(\mathbf{r}) &= 0, \\ \Delta(\mathbf{r}) &= 0. \end{aligned} \quad (5.5)$$

This describes a homogeneous distortion of the system, by which the director conformation remains unchanged and the origin of the coordinate system is kept fixed without loss of generality. The coefficients C_x , C_y , and C_z give the compression or dilation in the respective direction of space ($C_i = \partial_i u_i$, $i = x, y, z$; no summation over i in this formula).

From Eq. (A.5), it follows that $C_x = C_y$ as it should be due to symmetry reasons. The relation between the mechanical force density \mathcal{A} and the coefficients is obtained from Eqs. (4.7) and (5.3),

$$C_x = C_y = -\frac{c_2 A_z}{2c_1(2c_1 + 3c_2)}, \quad (5.6)$$

$$C_z = \frac{(c_1 + c_2) A_z}{c_1(2c_1 + 3c_2)}. \quad (5.7)$$

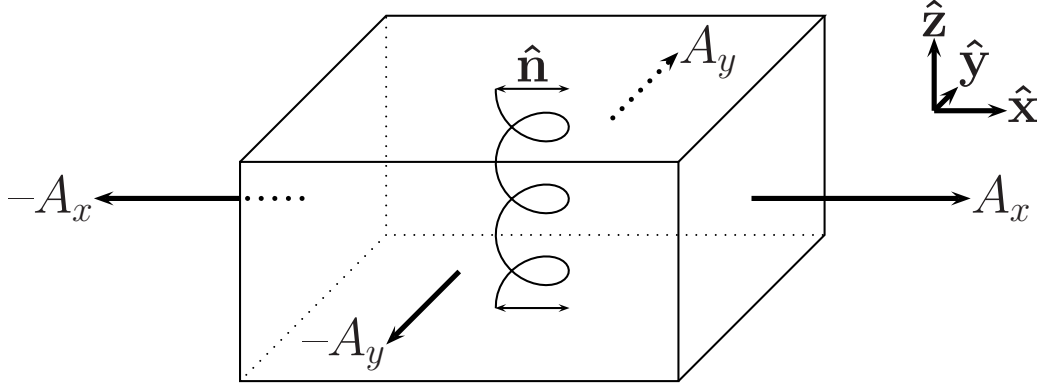


Figure 5.2: Lateral compression and dilation of a cholesteric SCLSCE by external mechanical forces.

As we can see, this is the same result we also obtain for a common elastic body. For incompressible systems, which are characterized by $c_2 \rightarrow \infty$ in the expression for the generalized energy density (2.9), the trace of the strain tensor $\boldsymbol{\varepsilon}$ correctly tends to zero,

$$\text{Tr}(\boldsymbol{\varepsilon}) = \varepsilon_{ii} = \frac{A_z}{2c_1 + 3c_2} \xrightarrow{c_2 \rightarrow \infty} 0. \quad (5.8)$$

Because of the homogeneous distortion also the cholesteric helix gets homogeneously compressed or stretched along its axis. The change of half of the cholesteric pitch $\Delta L = C_z L$ results in a shift of the photonic bandgap to smaller wavelengths for compression and to larger wavelengths for dilation of the sample, which is proportional to the applied force density.

We have tested the solution (5.5) numerically up to strains of a magnitude of $\pm 10\%$. Thereby, we have probably exceeded the domain of validity of our linearized model, however, there was no indication of an instability.

5.3 Lateral compression and dilation

A situation of lateral compression and dilation is achieved by applying external mechanical forces in $\hat{\mathbf{x}}$ and $\hat{\mathbf{y}}$ direction to the lateral sample surfaces, as depicted in Fig. 5.2. Again the surface force densities (per unit area) are denoted by \mathcal{A} , where now $\mathcal{A} = (\pm A_x, 0, 0)$ on the surfaces oriented by the surface vectors $\hat{\mathbf{s}} = (\pm 1, 0, 0)$, $\mathcal{A} = (0, \pm A_y, 0)$ on the surfaces oriented by $\hat{\mathbf{s}} = (0, \pm 1, 0)$, and $\mathcal{A} = (0, 0, 0)$ on the surfaces oriented by $\hat{\mathbf{s}} = (0, 0, \pm 1)$.

Then we solve the system of partial differential equations (A.1)-(A.5) by

the following ansatz:

$$\begin{aligned}
u_x(\mathbf{r}) &= C_x x, \\
u_y(\mathbf{r}) &= C_y y, \\
u_z(\mathbf{r}) &= C_z z, \\
n_z(\mathbf{r}) &= 0, \\
\Delta(\mathbf{r}) &= D_\Delta \sin(2q_0 z).
\end{aligned} \tag{5.9}$$

As in the previous section, the components of $\mathbf{u}(\mathbf{r})$ describe a homogeneous deformation of the system, where the coefficients C_x , C_y , and C_z denote the compression or dilation in the respective direction of space. The origin of the coordinate system is again kept fixed without loss of generality. n_z is set equal to zero, which means that the director does not tilt out of the planes perpendicular to $\hat{\mathbf{z}}$. This corresponds to what is observed in the analogous situation for nematic SCLSCEs under external mechanical stress below a certain threshold stress [31]. Δ as given by solution (5.9) keeps the initial parallel director orientation of Eq. (5.1), which follows in combination with Eq. (5.2). The coefficient D_Δ can be calculated from Eq. (A.5), and the result reads

$$D_\Delta = \frac{D_2(C_x - C_y)}{2D_1 + 8K_2q_0^2}. \tag{5.10}$$

In order to find the coefficients in solution (5.9), we take into account the conditions (5.3), which the tensor of mechanical stress from Eq. (4.7) has to satisfy on the sample surfaces. This leads us to the following expressions:

$$C_x = +fgA_x - fhA_y, \tag{5.11}$$

$$C_y = -fhA_x + fgA_y, \tag{5.12}$$

$$C_z = -\frac{c_2}{2c_1(2c_1 + 3c_2)}(A_x + A_y), \tag{5.13}$$

with the abbreviations

$$f = [4c_1(2c_1 + 3c_2)(8c_1D_1 + 32c_1K_2q_0^2 - D_2^2)]^{-1}, \tag{5.14}$$

$$g = 32c_1(c_1 + c_2)(D_1 + 4K_2q_0^2) - (2c_1 + c_2)D_2^2, \tag{5.15}$$

$$h = 16c_1c_2(D_1 + 4K_2q_0^2) + (2c_1 + c_2)D_2^2. \tag{5.16}$$

From Eqs. (5.9) we see at once that the strain tensor $\boldsymbol{\varepsilon}$ has no off-diagonal components. Its trace is given by the sum of the coefficients C_x , C_y , and C_z , and with the help of Eqs. (5.11)-(5.16) it turns out to vanish for incompressible systems,

$$Tr(\boldsymbol{\varepsilon}) = \varepsilon_{ii} = \frac{A_x + A_y}{(2c_1 + 3c_2)} \xrightarrow{c_2 \rightarrow \infty} 0. \tag{5.17}$$

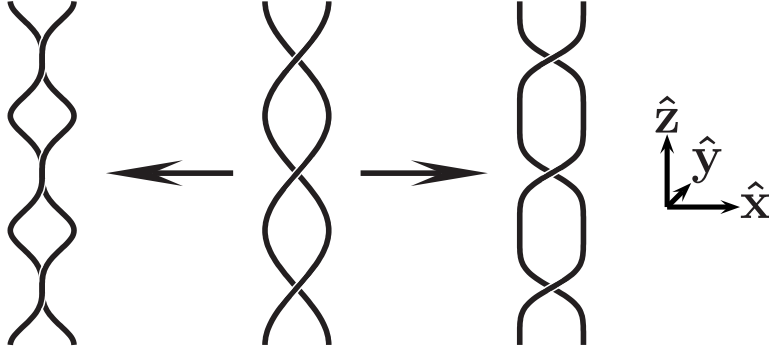


Figure 5.3: Beginning of twisting and untwisting of the cholesteric helix as given by $\Delta(\mathbf{r})$ in Eq. (5.18).

A further remark concerns the mechanical stress tensor $\boldsymbol{\sigma}^{mech}$. All its off-diagonal components vanish, except for $\sigma_{xy}^{mech} = \sigma_{yx}^{mech} \propto \sin(4q_0z)$. However, the latter also vanishes on average, so that on average no mechanical shear forces are involved.

An interesting result is obtained for the angle of director reorientation around the cholesteric helical axis,

$$\Delta(\mathbf{r}) = \frac{2D_2(A_y - A_x)}{8c_1D_1 + 32c_1K_2q_0^2 - D_2^2} \sin(2q_0z). \quad (5.18)$$

What is described by this equation is the beginning of a twisting or an untwisting of the cholesteric helix as it is known from LMWLCs, to which an external magnetic field is applied perpendicularly to the helical axis [7]. Here, by twisting the helix we denote a situation as shown on the left of Fig. 5.3 and by untwisting a situation as depicted on the right. The cholesteric pitch is not free to adjust because of the boundary conditions and because of the coupling to the polymer network.

The expression for $\Delta(\mathbf{r})$ in Eq. (5.18) is significant, because the material parameter D_2 plays a decisive role in it. Thermodynamic stability requires the denominator to be positive. As a consequence, for a positive sign of D_2 the prefactor of the sin-term becomes positive if only dilative external forces in $\hat{\mathbf{y}}$ direction or only compressive external forces in $\hat{\mathbf{x}}$ direction are applied. The helix is then twisted as shown on the left of Fig. 5.3. If the sign of D_2 is negative, the forces have to be applied just in the opposite directions in order to twist the helix, that is a compression in $\hat{\mathbf{y}}$ direction or a dilation in $\hat{\mathbf{x}}$ direction has to be imposed. Other combinations of the signs of D_2 and the external forces lead to an untwisting of the helix as depicted on the right of Fig. 5.3. It should be noted that these relations offer a possibility of determining the sign of D_2 directly from an experiment.

In addition to being twisted or untwisted, the cholesteric helix also becomes compressed or stretched parallel to its axis, due to the compression or dilation of the whole elastomer and according to the respective sign of C_z .

If the system is dilated or compressed both in $\hat{\mathbf{x}}$ and $\hat{\mathbf{y}}$ direction by equal force densities A_x and A_y , the cholesteric helix is neither twisted nor untwisted, but the whole sample gets only homogeneously distorted in accordance with section 5.2. In particular, the cholesteric helix gets only homogeneously compressed or stretched parallel to its axis, respectively. This is the situation of applying two orthogonal external mechanical forces perpendicularly to the helical axis as investigated in Refs. [29] and [62]. There, a linear relationship has been measured between the thickness of the sample and the wavelength λ_R of the reflected circularly polarized light irradiated parallel to the cholesteric helical axis. Since λ_R is proportional to the pitch of the helix $2L$, a homogeneous compression of the cholesteric helix parallel to its axis under the enforced dilation of the elastomer follows from these experiments and demonstrates the significance of our solution.

Finally, it is worthwhile to have a closer look at the amplitudes of the components of the displacement field. First, we find that in Eqs. (5.11)-(5.13) the situations of applied mechanical forces either in $\hat{\mathbf{x}}$ or in $\hat{\mathbf{y}}$ direction are completely identical, which we expect for symmetry reasons.

We then consider the system as being incompressible ($c_2 \rightarrow \infty$) and concentrate on a situation in which external forces are only applied in $\hat{\mathbf{x}}$ direction ($A_y = 0$). In this case, the compressions and dilations read

$$C_x = U_x A_x = + \tilde{f} [32c_1(D_1 + 4K_2q_0^2) - D_2^2] A_x, \quad (5.19)$$

$$C_y = U_y A_x = - \tilde{f} [16c_1(D_1 + 4K_2q_0^2) + D_2^2] A_x, \quad (5.20)$$

$$C_z = U_z A_x = - \tilde{f} [16c_1(D_1 + 4K_2q_0^2) - 2D_2^2] A_x, \quad (5.21)$$

with

$$\tilde{f} = [12c_1(8c_1D_1 + 32c_1K_2q_0^2 - D_2^2)]^{-1}. \quad (5.22)$$

What we recognize from these equations is that there are two kinds of contributions to the compressions and dilations in the squared brackets. The terms $\sim c_1(D_1 + 4K_2q_0^2)$ describe a homogeneous uniaxial compression or dilation of the system by external forces parallel to the $\hat{\mathbf{x}}$ direction, which leads to a dilation or compression of half of the magnitude in $\hat{\mathbf{y}}$ as well as in $\hat{\mathbf{z}}$ direction. Such a behavior corresponds to the one of a macroscopically isotropic body. However, our system is not isotropic, on average there is one special direction marked by the helical axis. This is expressed by the terms $\sim D_2^2$ in the squared brackets: in the direction parallel to the helical axis, that is in $\hat{\mathbf{z}}$ direction, the imposed distortion is by the amount $3\tilde{f}D_2^2A_x$ smaller than in $\hat{\mathbf{y}}$ direction, perpendicular to the helical axis. That means

the cholesteric helix slightly impedes the imposed distortion, and thus the system is a little bit stiffer in the direction parallel to the cholesteric helical axis than perpendicular to it ($\tilde{f} > 0$ for reasons of thermodynamic stability). It is very interesting to note that the coupling parameter D_2 plays this significant isolated role in the behavior of the system, because until now there is no experimental set-up known where D_2 is directly accessible. Consequently, the value of D_2 has not been directly measured so far.

For practical purposes this means the following. In an experiment the coefficients U_x , U_y , and U_z can be directly measured, where U_z becomes accessible for example by the methods used in Ref. [29]. From that,

$$U_1 = U_x + 2U_z = -(U_x + 2U_y) = 3\tilde{f}D_2^2 \quad (5.23)$$

can be calculated. On the other hand we realize that Eq. (5.18) may be written in the form

$$\Delta(\mathbf{r}) = -24c_1\tilde{f}D_2A_x\sin(2q_0z) = -U_2A_x\sin(2q_0z). \quad (5.24)$$

Here, U_2 should be accessible by x-ray measurements. Defining the angle of the local director orientation as

$$\theta(\mathbf{r}) = \arctan\left(\frac{n_y(\mathbf{r})}{n_x(\mathbf{r})}\right), \quad (5.25)$$

U_2 can be determined with the help of the distribution function $f(\theta)$, which for small values of U_2A_x becomes

$$f(\theta) = \frac{1}{q_0d} [1 + 2U_2A_x \cos(2\theta)] + \mathcal{O}[(U_2A_x)^2]. \quad (5.26)$$

From the results, the ratio

$$\frac{U_1}{U_2} = \frac{D_2}{8c_1} \quad (5.27)$$

can be calculated and finally D_2 can be derived, obtaining c_1 by common techniques without significant mistake. Further measurements on samples with different pitches and therefore different wave numbers of the cholesteric helix q_0 could then give information about the material parameters D_1 and K_2 , the values of which have also not been measured yet.

Because of the symmetry of the system, the whole procedure can also be conducted by external forces applied only in $\hat{\mathbf{y}}$ direction ($A_x = 0$), however, then U_2 changes sign as can be inferred from Eq. (5.18).

We have shown in this calculation that the coupling between the relative rotations and the strain tensor, represented by the material parameter D_2 in

the above equations, leads to an anisotropy of the overall strain of the system. We emphasize that our results have been obtained for the case of an isotropic elastic behavior of the materials in the absence of any relative rotation. If, however, an anisotropic elastic response of the material prevails also in the latter case, the resulting effects could quantitatively exceed the anisotropic behavior connected to the material parameter D_2 . Since the absolute value of D_2 may be small compared to the elastic coefficients, this must be taken into account when a corresponding experiment is performed.

5.4 Discussion and conclusion

In this chapter we have studied the reaction of cholesteric SCLSCEs to static or quasistatic external mechanical compressive and dilative forces, applied parallel or perpendicular to the cholesteric helical axis.

For the situation in which a compressive or dilative strain is applied parallel to the helical axis (Fig. 5.1 and section 5.2), we predict a homogeneous deformation of the whole system. This means that also the cholesteric helix is homogeneously compressed or stretched and its pitch changes proportionally to the external force density. The displacement field describing the mechanical deformation is not influenced by the liquid crystalline component at all and has the same analytical form as for a conventional elastic body.

In contrast, external compressive and dilative forces applied in only one direction perpendicular to the helical axis (Fig. 5.2 and section 5.3) lead to an anisotropic deformation of the system. We have shown for incompressible systems that, due to the influence of the liquid crystalline structure, the induced deformation parallel to the cholesteric helical axis is hindered with respect to the resulting deformation perpendicular to both the helical axis and the external force. The decisive material parameter controlling this anisotropy is the coefficient D_2 of the coupling between the strain deformation of the elastomer and the relative rotations between director and polymer network. In addition to the anisotropic deformation of the elastomer, a twisting or untwisting of the cholesteric helix arises (Fig. 5.3). As pointed out, both effects together offer the possibility of experimental access to the so far undetermined material parameter D_2 . In this context, it has to be noted that our calculations have been performed assuming an isotropic elastic behavior of the materials in the case of vanishing relative rotations. If an anisotropic elastic response prevails in the absence of relative rotations, the effect can be masked.

As a further result, we have found that a compression or dilation of the system in both directions perpendicular to the helical axis by equal force

densities leads to a homogeneous stretching or compression of the cholesteric helix, respectively. This is consistent with the observations during corresponding experiments [29,62]. In addition, experiments on the deformation of the cholesteric helix by external mechanical forces applied perpendicularly to the cholesteric helical axis have been performed [63]. The results of these experiments are in agreement with the results of our calculations.

We would like to close this chapter with a few remarks. First, we would like to recall that we have not included the scalar order parameter S into our considerations. We have assumed that during the mechanical deformations either the magnitude of S does not significantly vary, or, if there are changes in S , they do not have significant impact onto the physics of the respective system. Our assumption is corroborated by corresponding experimental observations for nematic SCLSCEs [64].

Next, as already mentioned before, our description should include the case of quasistatic external fields applied to the elastomers. In the case of external mechanical fields, this means, for example, that the frequency of the oscillating external force must be small enough so that the director associated with the orientational order can reorient properly.

Concerning the surfaces of the cholesteric SCLSCEs, we would like to emphasize that we have concentrated on geometries and solutions which are compatible with a parallel alignment of the director at the bottom and top boundaries of the sample.

Finally, we stress that we have proposed a way of interpreting corresponding experiments in order to determine still unknown values of the material parameters involved.

On the whole, however, we must note that the validity of our linear description is confined to cases in which the amplitudes of deformations are small. This restricts the applicability of our model to the interpretation of a limited number of experiments. In contrast, many of the unique features of SCLSCEs become evident mainly in the nonlinear regime. Probably, the most prominent example in this context is the pronounced nonlinear stress-strain behavior of nematic SCLSCEs, which can be observed when these materials are stretched perpendicularly to their ground state director orientation. The results of the corresponding experiment have first been reported in Ref. [17]. Our goal is to also interpret this nonlinear macroscopic behavior of SCLSCEs. Consequently, as a major step in this direction, we must extend our model to the nonlinear regime. This makes up the central part of our work. We will perform this step in the next chapter. The main effort in this context will consist of deriving nonlinear expressions for the variables of relative rotations. We will test our model in chapter 7 for a simple shear geometry. Finally, we will turn to the interpretation of the nonlinear stress-

strain experiments in chapter 8, where we will concentrate on the results of a more recent measurement [27]. Although the formalism will be derived in a more general way, we will confine ourselves to the case of nematic SCLSCEs in our investigations in chapters 7 and 8.

Chapter 6

Nonlinear macroscopic description

The first part of this work has been dominated by the linear macroscopic characterization of cholesteric SCLSCes. We have introduced the linear model in chapter 2 and investigated the reaction of cholesteric SCLSCes to static and quasistatic external fields in the preceding chapters. Whereas we have put our focus on the reaction of cholesteric SCLSCes to external electric fields in chapters 3 and 4, the influence of external mechanical fields has been studied in chapter 5.

As already announced at the end of the previous chapter, we will now turn to the extension of our model to the nonlinear regime. This step will be further motivated in the next section. Although we will concentrate on the description of nematic SCLSCes in the present and the next two chapters, the basic elements of our considerations can also be incorporated into the characterization of other liquid crystalline states. Cholesteric SCLSCes can be studied by the same formalism when the local description of the cholesteric state in terms of the orientation of the director field is chosen. Therefore, we will note conceptual deviations arising from the difference between nematic and cholesteric SCLSCes.

We have organized the further part of this chapter in the following way. In section 6.2 we will describe in detail our nonlinear picture of nematic SCLSCes. As we will explain, we think of nematic SCLSCes as materials of two coupled preferred directions. This concept leads us to nonlinear expressions for the variables of relative rotations. The analytical treatment necessary in order to connect the nonlinear variables of relative rotations to the independent variables characterizing a specific state of the system will be more involved than in the linear regime. We will derive expressions for the nonlinear relative rotations in the spirit of a series expansion, which will

mainly be appropriate for practical purposes. In the subsequent section, we will also show how to derive exact expressions for the nonlinear relative rotations. After that, in section 6.4, we will demonstrate that in the linear regime de Gennes' picture of the materials is recovered within the framework of our model. Finally, we will shortly summarize and discuss our results in section 6.5. We have added an appendix in which we expand on the importance of the symmetry relations that have to be taken into account when the materials are characterized (appendix C). In combination with the elucidation in this appendix, an alternative approach to the variables of relative rotations is presented and discussed in view of later applications in chapter 8.

Our presentation of the subject is closely connected to the ones we have given in Refs. [65] and [66].

6.1 Motivation for the extension of the model to the nonlinear regime

In the previous chapters we have repeatedly stressed the fact that SCLSCEs feature a coupling of macroscopic elastic mechanical deformation on the one hand and reorientation of the director field on the other hand. The first report of the synthesis of a monodomain nematic side-chain elastomer in Ref. [17] already contained the description of one characteristic experimental manifestation of this property.

We refer in this context to the observations made during a stress-strain experiment, in which a nematic SCLSCE is stretched perpendicularly to its original director orientation [17]. The result of the corresponding measurement is a stress-strain curve of pronounced nonlinear shape. In Fig. 6.1, the triangles (\triangle) reflect the stress-strain data reported in Ref. [17]. After a steep increase of the external stress for small elongations in region "A" of the plot, we find a significant decrease in the slope of the curve in region "B". In region "C", the stress again strongly increases with increasing strain.

In addition to measuring the stress-strain data, the authors of Ref. [17] have simultaneously recorded the values of the dichroic ratio which represents the current orientation of the director in the sample. These data are described by the stars (*) in Fig. 6.1. For region "A", the constant value of the dichroic ratio indicates that the director remains in its initial orientation perpendicular to the direction of the externally applied mechanical force. At a threshold strain on the boundary between the regions "A" and "B", a continuous reorientation of the director field sets in and appears to be closely connected to the decrease in the slope of the stress-strain curve. Finally,

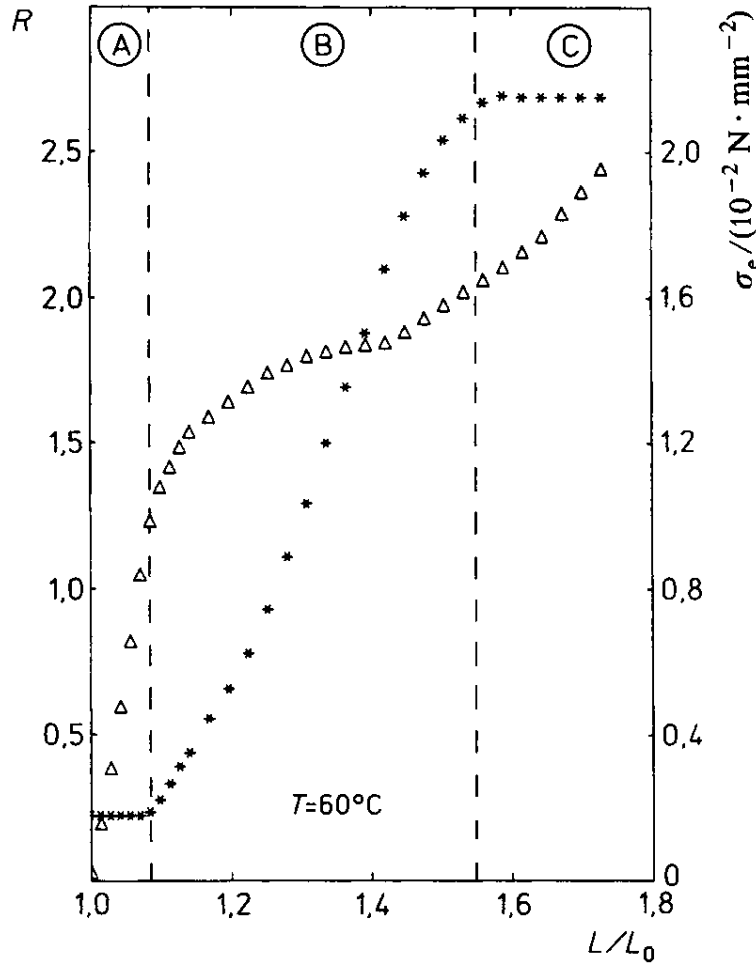


Figure 6.1: Data obtained from a stress-strain experiment, during which a nematic SCLSCE has been stretched perpendicularly to its initial director orientation. On the abscissa, the elongation L/L_0 is plotted, with L the current length of the sample in stretching direction and L_0 the corresponding initial length. Triangles (Δ), with scale on the right, denote values of the nominal stress applied externally, i.e. the applied force per initial cross-sectional area of the sample. Stars (*), with scale on the left, indicate the dichroic ratio which represents the current director orientation. Further explanations can be found in the main text. The figure has been reproduced from Ref. [17].

the value of the dichroic ratio is again constant in region “C”. This means that the director orientation remains essentially fixed in the reoriented state for high values of the elongation and does not change noticeably any more. Investigations by x-ray scattering reveal that in the final state of region “C” the director has rotated towards the stretching direction.

In various later experiments, this fascinating macroscopic stress-strain behavior of the materials has been recovered. It has been found to be characteristic for common nematic SCLSCEs investigated in this way. The photograph included in the introduction by Fig. 1.1 shows the state of a nematic SCLSCE in this geometry at intermediate values of elongation.

Furthermore, it has been reported that the reorientation can occur via a splitting of the director orientation into stripe domains [64,67]. These stripes were elongated into the stretching direction and distinguished by clockwise and counterclockwise rotation of the director during the reorientation process. Stripes in Refs. [64] and [67] could be observed only for samples which were clamped in a way that the stretching direction was oriented nearly perfectly perpendicular to the initial director orientation. In this context, domain walls between neighboring stripes of different orientation have been detected and their thickness has been estimated [30].

Since the early experiments have been performed, the topic is under thorough discussion from the point of view of modeling. We have introduced in section 2.4 the semi-microscopic approach based on Gaussian rubber elasticity [54]. Using this approach in order to investigate the geometry, it is possible to describe a plateau in the stress-strain curve which is connected to the reorientation of the director, and to give an explanation for the appearance of the stripe domains introduced above. This characterization of the materials has also been taken as a basis for numerical studies of the stress-strain geometry [68]. We have already explained in section 2.4 why we pursue a manifestly different approach to the problem.

An alternative, qualitatively different semi-microscopic model has been proposed in Refs. [56] and [57]. This model also addresses the appearance of the stripe domains, without including the notion of “soft” elastic distortions, and it recovers the experimental results.

More recently, a biaxial model has been proposed to describe the results of the nonlinear stress-strain experiments [58]. One of the two directions defining the biaxiality is assumed to arise from the internal stress imprinted into the materials during the process of synthesis. This internal stress may be related, for example, to the stress σ_i introduced in Fig. 1.6 of chapter 1. The second direction in this model is defined by the external stress applied to the material during the stress-strain experiment. Consequently, in this characterization, one of the two directions results from an internal property

of the materials, the other one from the force applied externally.

Our picture is different and has already been indicated when we have introduced the variables of relative rotations in section 2.2. Two coupled preferred directions will be identified for the elastomers. One of these two directions will coincide with the liquid crystalline director orientation, the other one with a preferred direction imprinted into the materials during the process of their synthesis. We will focus our considerations on the effects connected to the coupling of these two preferred directions. Within the framework of our model, we will find that this coupling is the reason for many of the specific properties of the materials. As demonstrated later on in chapter 8, the coupling, and consequently relative rotations between the two preferred directions, can lead to a pronounced nonlinear response during stress-strain measurements.

In our picture, the two preferred directions are internal properties of the materials, which makes a major difference compared to the model proposed in Ref. [58]. Furthermore, our model is macroscopic and can be understood as a starting point for a description of the materials in the spirit of generalized hydrodynamics. We keep our characterization general in the sense that we do not assign specific values to the material parameters from the beginning. In these ways, it differs from the approach given in Ref. [54].

Before coming to the details of our nonlinear description in the next section, we want to add some general remarks in advance. When we were describing the linear effects of SCLSCEs within the macroscopic model in the previous chapters, our procedure was the following. First, we have derived linear expressions for the variables that can contribute to the generalized energy density. These expressions have been given in terms of the independent state variables, which characterize a certain state of the system. Then, these linear expressions have been combined to symmetry-allowed quadratic terms, which have formed an expression for the generalized energy density.

If we want to keep the framework of this procedure and include nonlinear properties of the materials into the macroscopic characterization, the generalized energy density has to be supplemented by higher-order terms. But also the quadratic terms in the generalized energy density describe nonlinear effects, when nonlinear expressions are inserted for the macroscopic variables. Therefore, nonlinear expressions for the macroscopic variables have to be derived.

The corresponding result for the strain tensor $\boldsymbol{\varepsilon}$ is already well known and will be included in the next section. It is also straightforward to parameterize the tensor $\nabla \hat{\mathbf{n}}$ in the nonlinear regime. However, up to now, only a linear expression for the relative rotations in liquid crystalline elastomers has been given within the framework of the macroscopic model. Therefore, the

main task in the next section of this chapter will be to derive nonlinear expressions for the variables of relative rotations, within the framework of our macroscopic approach. The resulting formalism can then be used in order to describe the characteristic nonlinear features of liquid crystalline elastomers by our continuum model. This will be performed later on in chapters 7 and 8.

6.2 Two coupled preferred directions and nonlinear relative rotations

In this section, we present in detail the ingredients of our model describing the macroscopic physical behavior of the elastomers. As we have already mentioned before, we will first identify two coupled preferred directions associated with the materials. On the basis of these two preferred directions, we will then derive nonlinear expressions for the variables of relative rotations between the director field and the polymer network. We will first expand the corresponding expressions up to quartic order in the variables that characterize the actual state of the system. This procedure will mainly be appropriate for practical purposes and can systematically be generalized to any desirable order. After that, in section 6.3, we will show how an exact expression for the relative rotations can be found, and we will give the result for a two-dimensional system.

It is straightforward to identify one preferred direction associated with the current state of the materials. In the nematic and cholesteric state of the materials, the mesogens on average orient parallel to each other on the local scale. As usual, this preferred direction is characterized by the director field $\hat{\mathbf{n}}(\mathbf{r})$.

On the other hand, we can identify a separate, second preferred direction, which is connected to the way the materials are synthesized. We have described in section 1.3 that the continuous rotational symmetry is not spontaneously broken in nematic and cholesteric SCLSCEs. Instead, the original director orientation is imprinted into the materials during the respective process of synthesis, or, in other words, it is “frozen in” [19]. For example, materials generated by the two-step crosslinking procedure described in section 1.3 are macroscopically stretched after the major part of the first crosslinking step has been completed. As a consequence, the director aligns in one preferred direction across the whole elastomer [17, 18]. It has been demonstrated that during the second crosslinking step some anisotropy gets locked in the vicinity of the crosslinking points [18]. But also if the director is

macroscopically aligned by an external magnetic field [23, 24], by anisotropic deswelling [25], or by surface effects [3, 26, 27] before the crosslinking process is completed, the respective original orientation of the director field becomes imprinted into the polymer network. If the director of a nematic SCLSCE is reoriented during a stress-strain experiment or due to an external electric or magnetic field, it will relax back to its original imprinted orientation after the external force has been released. We therefore identify this imprinted direction as a second preferred direction of the materials. We denote this direction by $\hat{\mathbf{n}}^{\text{nw}}(\mathbf{r})$.

In the ground state of the materials, the two preferred directions are aligned parallel to each other. However, in our picture, the influence of an external field may lead to a misalignment of the orientations of the two preferred directions. Clearly, $\hat{\mathbf{n}}(\mathbf{r})$ and $\hat{\mathbf{n}}^{\text{nw}}(\mathbf{r})$ are energetically coupled to each other and a misalignment of the two orientations leads to a contribution to the generalized energy density of the system.

We note at this point that a situation in which the two coupled preferred directions become misaligned corresponds to a relative rotation between these two directions. Our assumption in the following will be that the rotations of the imprinted direction $\hat{\mathbf{n}}^{\text{nw}}(\mathbf{r})$ are connected to the rotations of the polymer network and can be tracked by the displacement field $\mathbf{u}(\mathbf{r})$. Then, situations of misalignment of the two preferred directions again describe relative rotations of the director with respect to the polymer network (the superscript “nw” has been chosen as an abbreviation for polymeric “network”).

In section 2.2, where we have introduced the variables of linear relative rotations, we have already made a corresponding remark. What we have called the ground state anchoring direction in section 2.2 is now denoted by the imprinted direction $\hat{\mathbf{n}}^{\text{nw}}(\mathbf{r})$. In this way, we may use the misalignment of the two orientations in order to construct nonlinear macroscopic variables which are suitable for a macroscopic, hydrodynamic-like description.

It is important that the macroscopic variables contributing to a hydrodynamic-like picture vanish when the system is in equilibrium and no external forces are applied. As suggested above, we take the misalignment in the orientations of the two preferred directions as a starting point for our description. This misalignment can be characterized by the difference between the two directions $\hat{\mathbf{n}}(\mathbf{r}) - \hat{\mathbf{n}}^{\text{nw}}(\mathbf{r})$. However, the difference $\hat{\mathbf{n}}(\mathbf{r}) - \hat{\mathbf{n}}^{\text{nw}}(\mathbf{r})$ cannot be taken directly as an expression of the macroscopic variables we are looking for due to the following reasons of symmetry.

In the physics of low molecular weight nematics the two directions $\hat{\mathbf{n}}(\mathbf{r})$ and $-\hat{\mathbf{n}}(\mathbf{r})$ cannot be distinguished. Therefore, an expression for the generalized energy density characterizing such a system must be invariant under the symmetry transformation $\hat{\mathbf{n}}(\mathbf{r}) \rightarrow -\hat{\mathbf{n}}(\mathbf{r})$. For this reason, when deriv-

ing an expression for the generalized energy density, it makes sense to use macroscopic variables that show a clear behavior of symmetry under the transformation $\hat{\mathbf{n}}(\mathbf{r}) \rightarrow -\hat{\mathbf{n}}(\mathbf{r})$.

Returning to locally uniaxial SCLSCEs, we have two separate preferred directions $\hat{\mathbf{n}}(\mathbf{r})$ and $\hat{\mathbf{n}}^{\text{nw}}(\mathbf{r})$. The generalized energy density must be invariant under the symmetry transformation $\hat{\mathbf{n}}(\mathbf{r}) \rightarrow -\hat{\mathbf{n}}(\mathbf{r})$ as well as under the symmetry transformation $\hat{\mathbf{n}}^{\text{nw}}(\mathbf{r}) \rightarrow -\hat{\mathbf{n}}^{\text{nw}}(\mathbf{r})$, separately (inversion of $\hat{\mathbf{n}}(\mathbf{r})$ does not imply inversion of $\hat{\mathbf{n}}^{\text{nw}}(\mathbf{r})$ and vice versa). Our macroscopic variables must show a definite behavior under these transformations of symmetry.

We thus define two sets of nonlinear relative rotations on the basis of the difference $\hat{\mathbf{n}}(\mathbf{r}) - \hat{\mathbf{n}}^{\text{nw}}(\mathbf{r})$. Taking the component of this difference that is perpendicular to $\hat{\mathbf{n}}^{\text{nw}}(\mathbf{r})$, we obtain as variables of relative rotations

$$\tilde{\mathbf{\Omega}}(\mathbf{r}) := \hat{\mathbf{n}}(\mathbf{r}) - [\hat{\mathbf{n}}(\mathbf{r}) \cdot \hat{\mathbf{n}}^{\text{nw}}(\mathbf{r})] \hat{\mathbf{n}}^{\text{nw}}(\mathbf{r}). \quad (6.1)$$

$\tilde{\mathbf{\Omega}}(\mathbf{r})$ is odd under the transformation $\hat{\mathbf{n}}(\mathbf{r}) \rightarrow -\hat{\mathbf{n}}(\mathbf{r})$ and even under the transformation $\hat{\mathbf{n}}^{\text{nw}}(\mathbf{r}) \rightarrow -\hat{\mathbf{n}}^{\text{nw}}(\mathbf{r})$. Systematically taking the component of $\hat{\mathbf{n}}(\mathbf{r}) - \hat{\mathbf{n}}^{\text{nw}}(\mathbf{r})$ which is perpendicular to $\hat{\mathbf{n}}(\mathbf{r})$, we obtain as a second set of variables of relative rotations

$$\tilde{\mathbf{\Omega}}^{\text{nw}}(\mathbf{r}) := -\hat{\mathbf{n}}^{\text{nw}}(\mathbf{r}) + [\hat{\mathbf{n}}(\mathbf{r}) \cdot \hat{\mathbf{n}}^{\text{nw}}(\mathbf{r})] \hat{\mathbf{n}}(\mathbf{r}). \quad (6.2)$$

$\tilde{\mathbf{\Omega}}^{\text{nw}}(\mathbf{r})$ is even under the transformation $\hat{\mathbf{n}}(\mathbf{r}) \rightarrow -\hat{\mathbf{n}}(\mathbf{r})$ and odd under the transformation $\hat{\mathbf{n}}^{\text{nw}}(\mathbf{r}) \rightarrow -\hat{\mathbf{n}}^{\text{nw}}(\mathbf{r})$. Later we will show that this formulation is in accordance with the linear description in the spirit of de Gennes [36], and we will comment on the role of the two sets of relative rotations in chapter 8.

As a next step, we must connect the orientations of $\hat{\mathbf{n}}(\mathbf{r})$ and $\hat{\mathbf{n}}^{\text{nw}}(\mathbf{r})$ to the variables which characterize the current macroscopic state of the system. In our model, the state of a nematic or cholesteric SCLSCE is completely defined by the orientation of the director field $\hat{\mathbf{n}}(\mathbf{r})$ and by the state of elastic distortion of the polymer network. Elastic distortions are described in terms of gradients of the displacement field $\mathbf{u}(\mathbf{r})$ in the framework of elasticity theory. More precisely, the initial field $\mathbf{a}(\mathbf{r})$ introduced in section 2.1 should be used in the Eulerian description instead of the displacement field $\mathbf{u}(\mathbf{r})$ [41, 42]. However, in a static picture, we may also perform our analysis in terms of $\mathbf{u}(\mathbf{r})$. We will come back to this point in the discussion.

In order to include the energy density resulting from the elastic distortions into our expression for the generalized energy density, we will have to use the nonlinear form of the strain tensor in the Euler notation [41, 43]. We have already defined the strain tensor in chapter 2 by Eq. (2.3). The complete

nonlinear expressions for the components of $\boldsymbol{\varepsilon}$ read

$$\varepsilon_{ij} = \frac{1}{2} [(\partial_i u_j) + (\partial_j u_i) - (\partial_i u_k)(\partial_j u_k)] = \frac{1}{2} [\delta_{ij} - (\partial_i a_k)(\partial_j a_k)]. \quad (6.3)$$

Here, $\boldsymbol{\varepsilon}$, \mathbf{u} , and \mathbf{a} are functionals of \mathbf{r} . We will not explicitly display the spatial dependence on \mathbf{r} in the following. The nonlinear expression for the strain tensor in the Lagrangian picture differs from the expression in Eq. (6.3) in the sign of the term $(\partial_i u_k)(\partial_j u_k)$ [43].

When we want to connect the preferred direction $\hat{\mathbf{n}}^{\text{nw}}$ to the elastic deformation, we start with the original, undistorted state of the system. Here, we find that the two macroscopic preferred directions are aligned in parallel directions. When we denote them as $\hat{\mathbf{n}}_0$ and $\hat{\mathbf{n}}_0^{\text{nw}}$, respectively, we may write $\hat{\mathbf{n}}_0 \parallel \hat{\mathbf{n}}_0^{\text{nw}}$.

For finite deformations, $\hat{\mathbf{n}}_0$ and $\hat{\mathbf{n}}_0^{\text{nw}}$ will in general be functionals of $\mathbf{u}(\mathbf{r})$ or $\mathbf{a}(\mathbf{r})$, respectively,

$$\hat{\mathbf{n}}_0 = \hat{\mathbf{n}}_0(\mathbf{a}(\mathbf{r})), \quad (6.4)$$

$$\hat{\mathbf{n}}_0^{\text{nw}} = \hat{\mathbf{n}}_0^{\text{nw}}(\mathbf{a}(\mathbf{r})). \quad (6.5)$$

We include this dependence on $\mathbf{a}(\mathbf{r})$ because the mesogenic units are chemically attached to the polymer backbone chains via flexible spacer groups. Under finite mechanical deformations, they are displaced together with the polymer network. In general, the ground state orientation $\hat{\mathbf{n}}_0$ at a certain position $\mathbf{a}(\mathbf{r})$ is known as an initial condition. What is not known is the initial field $\mathbf{a}(\mathbf{r})$. These dependences become important for instance in the nonlinear description of cholesteric SCLSCEs. The case simplifies in nematic SCLSCEs because of the spatially homogeneous orientation of $\hat{\mathbf{n}}_0$ and $\hat{\mathbf{n}}_0^{\text{nw}}$ in the ground state.

We now assume that the system has been exposed to the influence of some external field. When we consider the system in its final state, the director $\hat{\mathbf{n}}$ is obtained from $\hat{\mathbf{n}}_0$ via a rotation matrix \mathbf{S} . In general, for finite deformations, \mathbf{S} will also be a functional of \mathbf{r} and of $\mathbf{u}(\mathbf{r})$ or $\mathbf{a}(\mathbf{r})$, respectively, which is a consequence of Eq. (6.4),

$$n_i(\mathbf{a}(\mathbf{r})) = S_{ij}(\mathbf{a}(\mathbf{r}), \mathbf{r}) n_{0,j}(\mathbf{r}). \quad (6.6)$$

Because of this dependence, $\mathbf{S}(\mathbf{a}(\mathbf{r}), \mathbf{r})$ can describe how the mesogenic units have on average been rotated compared to their ground state orientation at their ground state position. In short, we can write Eq. (6.6) as

$$\hat{\mathbf{n}} = \mathbf{S} \cdot \hat{\mathbf{n}}_0. \quad (6.7)$$

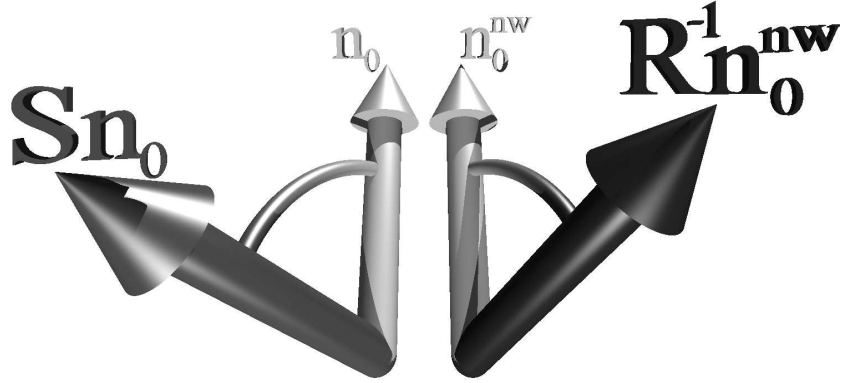


Figure 6.2: Two local rotations \mathbf{S} and \mathbf{R}^{-1} leading to a local misalignment of the two preferred directions $\hat{\mathbf{n}} = \mathbf{S}\hat{\mathbf{n}}_0$ and $\hat{\mathbf{n}}^{\text{nw}} = \mathbf{R}^{-1}\hat{\mathbf{n}}_0^{\text{nw}}$. In the initial state, the two directions $\hat{\mathbf{n}}_0$ and $\hat{\mathbf{n}}_0^{\text{nw}}$ have been oriented parallel to each other. Although we have drawn simple arrows for reasons of clearness, head and tail of the directions cannot be distinguished in the physics of the system.

We have included Fig. 6.2 in order to illustrate the corresponding rotation.

In the same way, also $\hat{\mathbf{n}}^{\text{nw}}$ is obtained from $\hat{\mathbf{n}}_0^{\text{nw}}$ via a rotation, which we denote as \mathbf{R}^{-1} ,

$$\hat{\mathbf{n}}^{\text{nw}} = \mathbf{R}^{-1} \cdot \hat{\mathbf{n}}_0^{\text{nw}}, \quad (6.8)$$

and which we have also included in our illustration in Fig. 6.2. As we have stated above, we identify the rotation matrix \mathbf{R}^{-1} with the matrix that describes the local rotations of the network of polymer backbones. Therefore, \mathbf{R}^{-1} is connected to the local elastic mechanical distortion of the elastomer. Consequently, our next task is to express the rotation matrix \mathbf{R}^{-1} in terms of the displacement field \mathbf{u} , or the initial field \mathbf{a} , respectively.

We derive an expression for the matrix \mathbf{R}^{-1} from a comparison between the initial state and the final state of the system,

$$da_i = dr_k (\partial_k a_i). \quad (6.9)$$

Here, $\partial_k a_i$ describes the local distortions of the elastomer. Using the polar decomposition theorem, $\partial_k a_i$ can be rewritten as a product of a rotation matrix and a symmetric matrix,

$$\partial_k a_i = R_{ij} \Xi_{jk}. \quad (6.10)$$

Altogether we obtain $da_i = R_{ij} \Xi_{jk} dr_k$. Ξ tells us how the polymer network in its final state locally has to be unstrained, and \mathbf{R} tells us how it locally has to be rotated back to retrieve its initial state. In Refs. [41] and [42] it

has been shown how to calculate Ξ from Eq. (6.10), and Ξ was given up to quadratic order in the components of $\nabla \mathbf{u}$. We now calculate Ξ up to quartic order and from that derive the rotation matrix \mathbf{R} .

From $R_{ij}R_{ik} = \delta_{jk}$ and from Eqs. (6.3) and (6.10) we find

$$\delta_{jk} - 2\varepsilon_{jk} = \Xi_{ij}\Xi_{ik}. \quad (6.11)$$

Inserting a power expansion of Ξ_{ij} with respect to ε into Eq. (6.11) we obtain

$$\Xi_{ij} = \delta_{ij} - \varepsilon_{ij} - \frac{1}{2}\varepsilon_{ik}\varepsilon_{kj} - \frac{1}{2}\varepsilon_{ik}\varepsilon_{kl}\varepsilon_{lj} - \frac{5}{8}\varepsilon_{ik}\varepsilon_{kl}\varepsilon_{lm}\varepsilon_{mj} + \mathcal{O}((\nabla \mathbf{u})^5). \quad (6.12)$$

Furthermore, by using $(\Xi^{-1})_{ij}\Xi_{jk} = \delta_{ik}$, we can show that

$$(\Xi^{-1})_{ij} = \delta_{ij} + \varepsilon_{ij} + \frac{3}{2}\varepsilon_{ik}\varepsilon_{kj} + \frac{5}{2}\varepsilon_{ik}\varepsilon_{kl}\varepsilon_{lj} + \frac{35}{8}\varepsilon_{ik}\varepsilon_{kl}\varepsilon_{lm}\varepsilon_{mj} + \mathcal{O}((\nabla \mathbf{u})^5). \quad (6.13)$$

This expression for Ξ^{-1} together with Eq. (6.10) can then be used to calculate the components of the rotation matrix \mathbf{R} . As we have noted above, we are interested in the way the network of polymer backbones has been rotated from the initial to the final state, and so we give the components of \mathbf{R}^{-1} ,

$$\begin{aligned} (R^{-1})_{ij} = R_{ji} &= \left(\delta_{ik} + \varepsilon_{ik} + \frac{3}{2}\varepsilon_{il}\varepsilon_{lk} + \frac{5}{2}\varepsilon_{il}\varepsilon_{lm}\varepsilon_{mk} \right. \\ &\quad \left. + \frac{35}{8}\varepsilon_{il}\varepsilon_{lm}\varepsilon_{mn}\varepsilon_{nk} \right) (\partial_k a_j) + \mathcal{O}((\nabla \mathbf{u})^5) \\ &= \delta_{ij} + \varepsilon_{ij} + \frac{3}{2}\varepsilon_{ik}\varepsilon_{kj} + \frac{5}{2}\varepsilon_{ik}\varepsilon_{kl}\varepsilon_{lj} + \frac{35}{8}\varepsilon_{ik}\varepsilon_{kl}\varepsilon_{lm}\varepsilon_{mj} \\ &\quad - (\partial_i u_j) - \varepsilon_{ik}(\partial_k u_j) - \frac{3}{2}\varepsilon_{ik}\varepsilon_{kl}(\partial_l u_j) \\ &\quad - \frac{5}{2}\varepsilon_{ik}\varepsilon_{kl}\varepsilon_{lm}(\partial_m u_j) + \mathcal{O}((\nabla \mathbf{u})^5), \end{aligned} \quad (6.14)$$

where we have made use of $\mathbf{a}(\mathbf{r}) = \mathbf{r} - \mathbf{u}(\mathbf{r})$ to obtain the final expression.

For a check of consistency we calculate the matrices $\tilde{\Xi}$ and $\tilde{\mathbf{R}}$, defined by $\partial_k a_i = \tilde{\Xi}_{ij}\tilde{R}_{jk}$. We multiply this equation by \tilde{R}_{lk} , and from the resulting equation we derive $\tilde{\Xi}_{li}\tilde{\Xi}_{im} = (\partial_k a_i)(\partial_n a_i)\tilde{R}_{lk}\tilde{R}_{mn}$. With the help of this expression and together with Eq. (6.3) we can verify that

$$\begin{aligned} \tilde{\Xi}_{ij} &= \tilde{R}_{ik}\tilde{R}_{jl} \left(\delta_{kl} - \varepsilon_{kl} - \frac{1}{2}\varepsilon_{km}\varepsilon_{ml} - \frac{1}{2}\varepsilon_{km}\varepsilon_{mn}\varepsilon_{nl} \right. \\ &\quad \left. - \frac{5}{8}\varepsilon_{km}\varepsilon_{mn}\varepsilon_{no}\varepsilon_{ol} \right) + \mathcal{O}((\nabla \mathbf{u})^5). \end{aligned} \quad (6.15)$$

Introducing $\tilde{\Xi}_{ij}$ into $\partial_p a_i = \tilde{\Xi}_{ij} \tilde{R}_{jp}$, taking into account that $\tilde{R}_{jp} \tilde{R}_{jl} = \delta_{lp}$, and convincing ourselves that the inverse of the expression in brackets in Eq. (6.15) is given by Eq. (6.13), we find $\tilde{\mathbf{R}} = \mathbf{R}$. There arises no problem from $\tilde{\Xi} \neq \Xi$, because in our description we will use the tensor $\boldsymbol{\varepsilon}$ as a macroscopic variable to include strain deformations, not Ξ .

In essence, Eqs. (6.3), (6.8), and (6.14) connect $\hat{\mathbf{n}}^{\text{nw}}$ to the displacement field \mathbf{u} , or the initial field \mathbf{a} , respectively.

At the beginning of this section, we have taken the misalignment $\hat{\mathbf{n}} - \hat{\mathbf{n}}^{\text{nw}}$ as a starting point for the construction of the variables of relative rotations in Eqs. (6.1) and (6.2). These expressions for the relative rotations can now be understood in the following manner, which recovers our previous remarks on the interpretation of relative rotations in SCLSCEs. Relative rotations give the difference between the way the director actually has been rotated starting from its ground state orientation (\mathbf{S}), and the way it would have been rotated if it were rigidly coupled to the polymer network (\mathbf{R}^{-1}). The latter rotation is described by the rotation of the preferred direction $\hat{\mathbf{n}}^{\text{nw}}$, and the connection between both rotations \mathbf{S} and \mathbf{R}^{-1} arises from the fact that $\hat{\mathbf{n}}_0^{\text{nw}} \parallel \hat{\mathbf{n}}_0$ in the ground state, or initial state, respectively, of the material. We have illustrated the connection between the two rotations \mathbf{S} and \mathbf{R}^{-1} in Fig. 6.2. Eqs. (6.7) and (6.8) together with the condition $\hat{\mathbf{n}}_0^{\text{nw}} \parallel \hat{\mathbf{n}}_0$ will guarantee rotational invariance with respect to the initial state of the system, when we will set up the expression for the generalized energy density.

We include some remarks concerning the technical approach to concrete problems. In general, the matrix \mathbf{S} does not have to be determined explicitly for practical purposes. This is because usually for a given problem the two independent variables that define the current state of $\hat{\mathbf{n}}(\mathbf{r})$ have to be found as a solution to the problem, and because the ground state conformation $\hat{\mathbf{n}}_0(\mathbf{a}(\mathbf{r}))$ is known as an initial condition in general. In addition, the three components of $\mathbf{a}(\mathbf{r})$, or those of $\mathbf{u}(\mathbf{r})$, respectively, must be determined in a separate step. This procedure is possible since via Eqs. (6.3) and (6.14) we have expressed the variables of relative rotations in the five independent variables describing the current state of the SCLSCE.

6.3 Exact expressions for the nonlinear variables of relative rotations

Combining Eqs. (6.1)-(6.3), (6.8), and (6.14), we have derived in the previous section expressions for the nonlinear variables of relative rotations in the sense of a series expansion. These expressions will mainly be useful for practical

purposes. In addition, we now want to derive an exact expression for the nonlinear variables of relative rotations. For this purpose we have to find an exact expression for \mathbf{R}^{-1} , which can then be introduced into Eqs. (6.8), (6.1) and (6.2).

Since Ξ is symmetric it follows from Eq. (6.11) that ε and Ξ are diagonalized by the same matrix \mathcal{R} ,

$$\varepsilon = \mathcal{R} \varepsilon^D \mathcal{R}^T, \quad \Xi = \mathcal{R} \Xi^D \mathcal{R}^T, \quad (6.16)$$

where in our notation diagonalized matrices are marked by \cdot^D and transposed matrices by \cdot^T . Since we know ε from Eq. (6.3), we can calculate exact expressions for its eigenvalues e_i ($i = 1, 2, 3$) and its eigenvectors. From the eigenvalues e_i the eigenvalues of Ξ follow with the help of Eq. (6.11) as $X_i = \sqrt{1 - 2e_i}$ ($i = 1, 2, 3$). The eigenvectors of ε lead us to an exact expression for \mathcal{R} .

Introducing all these ingredients into Eq. (6.10) we can calculate the exact expressions for the components of the rotation matrix \mathbf{R} :

$$R_{ij} = (\partial_k a_i) \mathcal{R}_{kl} ((\Xi^D)^{-1})_{lm} (\mathcal{R}^T)_{mj}. \quad (6.17)$$

Here, the components of the matrix $(\Xi^D)^{-1}$ are simply given by $((\Xi^D)^{-1})_{ij} = X_i^{-1} \delta_{ij}$ (no summation over i in this formula; $i, j \in \{1, 2, 3\}$). \mathbf{R}^{-1} then of course follows as $\mathbf{R}^{-1} = \mathbf{R}^T$.

Concerning the existence of the expressions above, no problems arise, and all expressions remain real. First, ε and Ξ are symmetric and thus can be diagonalized in real space. Next, we consider the relation $da_i = dr_k (\partial_k a_i)$ in the local principal frame of $\nabla \mathbf{a}$. It reads $da_i = \lambda_i^{-1} dr_i$ ($i = 1, 2, 3$; no summation over i in this formula), λ_i^{-1} being the eigenvalues of $\nabla \mathbf{a}$. Rewriting the latter equation as $dr_i = \lambda_i da_i$ implies that λ_i can be interpreted as the stretch of the system parallel to the i th principal axis ($i = 1, 2, 3$). For physical reasons, $0 < \lambda_i < \infty$ (for a discussion of this point in the Lagrangian description, see, e.g., Ref. [69]). Furthermore, in the principal frame of $\nabla \mathbf{a}$ no rotations occur and thus $(\nabla \mathbf{a})^D = \Xi^D$. Due to this fact, $X_i = \lambda_i^{-1}$, which includes $0 < X_i < \infty$ and $e_i < \frac{1}{2}$ ($i = 1, 2, 3$).

Applying this procedure in the two-dimensional case we can derive a result which still can be written in a manageable form:

$$\begin{aligned} \mathbf{R}^{-1} &= \frac{1}{2} \begin{pmatrix} A_- & \pm A_+ \\ \mp A_+ & A_- \end{pmatrix} \begin{pmatrix} X_1^{-1} & 0 \\ 0 & X_2^{-1} \end{pmatrix} \begin{pmatrix} A_- & \mp A_+ \\ \pm A_+ & A_- \end{pmatrix} \\ &\times \begin{pmatrix} \partial_x a_x & \partial_x a_y \\ \partial_y a_x & \partial_y a_y \end{pmatrix}. \end{aligned} \quad (6.18)$$

Here, we have used as abbreviations $A_{\pm} = \sqrt{1 \pm \alpha}$, with $\alpha = (\varepsilon_{xx} - \varepsilon_{yy})/e$ and $e = \sqrt{(\varepsilon_{xx} - \varepsilon_{yy})^2 + 4\varepsilon_{xy}^2}$. As defined above, we have $X_i = \sqrt{1 - 2e_i}$ ($i = 1, 2$), where the eigenvalues of $\boldsymbol{\varepsilon}$ read $e_{1;2} = \frac{1}{2}(\varepsilon_{xx} + \varepsilon_{yy} \mp e)$. From the multiple signs in Eq. (6.18) the upper sign has to be chosen in the case $\varepsilon_{xy} > 0$ and the lower one for $\varepsilon_{xy} < 0$ at the local position \mathbf{r} . This ensures the right-handedness of our coordinate system in the principal frame.

Introducing the rotation matrix into Eqs. (6.8), (6.1) and (6.2) then leads us to exact expressions for the nonlinear variables of relative rotations in the two-dimensional case.

6.4 Connection to the linear description

In this section, we want to check whether the description in the spirit of the nonlinear relative rotations is connected to the linear model which we have introduced in chapter 2. For this purpose, we demonstrate that in the linear regime of small strains and small magnitudes of the relative rotations we recover de Gennes' expression for the generalized energy density [36].

As a first step, we have to derive an expression for the generalized energy density. We proceed in the same way as in section 2.3, whereas now both variables of relative rotations $\tilde{\boldsymbol{\Omega}}$ and $\tilde{\boldsymbol{\Omega}}^{\text{nw}}$ contribute as macroscopic variables. The resulting expression must now not only be invariant with respect to the symmetry transformation $\hat{\mathbf{n}} \rightarrow -\hat{\mathbf{n}}$, but also with respect to the transformation $\hat{\mathbf{n}}^{\text{nw}} \rightarrow -\hat{\mathbf{n}}^{\text{nw}}$, separately. Since we are only interested in this section in the comparison to the linear regime, it is again sufficient to include only terms which are quadratic in the macroscopic variables contributing to the generalized energy density. Concentrating only on terms arising solely from contributions of the macroscopic variables $\boldsymbol{\varepsilon}$, $\tilde{\boldsymbol{\Omega}}$, and $\tilde{\boldsymbol{\Omega}}^{\text{nw}}$ we obtain

$$F = c_1 \varepsilon_{ij} \varepsilon_{ij} + \frac{1}{2} c_2 \varepsilon_{ii} \varepsilon_{jj} + \frac{1}{2} D_1 \tilde{\Omega}_i \tilde{\Omega}_i + D_2 n_i \varepsilon_{ij} \tilde{\Omega}_j + D_2^{\text{nw}} n_i^{\text{nw}} \varepsilon_{ij} \tilde{\Omega}_j^{\text{nw}}. \quad (6.19)$$

Due to $\tilde{\Omega}_i \tilde{\Omega}_i = \tilde{\Omega}_i^{\text{nw}} \tilde{\Omega}_i^{\text{nw}}$ we have not explicitly added the corresponding term containing only the variable $\tilde{\boldsymbol{\Omega}}^{\text{nw}}$.

Introducing into Eq. (6.19) the nonlinear expressions for the variables of relative rotations (6.1) and (6.2) and substituting $\hat{\mathbf{n}} = \hat{\mathbf{n}}_0 + \delta\mathbf{n}$ as well as $\hat{\mathbf{n}}^{\text{nw}} = \hat{\mathbf{n}}_0^{\text{nw}} + \delta\mathbf{n}^{\text{nw}}$ in the linear regime, we find

$$F^{(\text{lin})} = c_1 \varepsilon_{ij} \varepsilon_{ij} + \frac{1}{2} c_2 \varepsilon_{ii} \varepsilon_{jj} + \frac{1}{2} D_1 \tilde{\Omega}_i^{(\text{lin})} \tilde{\Omega}_i^{(\text{lin})} + \bar{D}_2 n_i \varepsilon_{ij} \tilde{\Omega}_j^{(\text{lin})}. \quad (6.20)$$

Here, $\bar{D}_2 = D_2 + D_2^{nw}$ and $\tilde{\mathbf{\Omega}}^{(\text{lin})} = \delta\mathbf{n} - \delta\mathbf{n}^{\text{nw}}$ (one has to take care of the parameterization in the case of antiparallel alignment of $\hat{\mathbf{n}}_0$ and $\hat{\mathbf{n}}_0^{\text{nw}}$). For isotropic elastic behavior, this expression of $F^{(\text{lin})}$ coincides with de Gennes' expression as noted in Ref. [36]. We obtain the conditions of thermodynamic stability $c_1 > 0$, $2c_1 + 3c_2 > 0$, $D_1 > 0$, and

$$4c_1 D_1 - \bar{D}_2^2 = 4c_1 D_1 - (D_2 + D_2^{nw})^2 > 0. \quad (6.21)$$

Furthermore, by construction, it follows from Eqs. (6.1) and (6.2) that

$$\hat{\mathbf{n}}^{\text{nw}} \cdot \tilde{\mathbf{\Omega}} = 0, \quad \hat{\mathbf{n}} \cdot \tilde{\mathbf{\Omega}}^{\text{nw}} = 0. \quad (6.22)$$

In the linear regime, this leads to the familiar condition $\hat{\mathbf{n}} \cdot \tilde{\mathbf{\Omega}}^{(\text{lin})} = 0$, or equivalently $\hat{\mathbf{n}}^{\text{nw}} \cdot \tilde{\mathbf{\Omega}}^{(\text{lin})} = 0$, $\hat{\mathbf{n}}_0 \cdot \tilde{\mathbf{\Omega}}^{(\text{lin})} = 0$, and $\hat{\mathbf{n}}_0^{\text{nw}} \cdot \tilde{\mathbf{\Omega}}^{(\text{lin})} = 0$.

When we compare our results in this section to Eqs. (2.8), (2.9), and to the thermodynamic stability conditions listed above Eq. (2.10) in chapter 2, we find that we can in fact consider our nonlinear picture as an extension of the model presented in chapter 2 to the nonlinear regime. Vice versa, we have demonstrated in this section that we should recover the same results as in the previous chapters when we confine our nonlinear description to the linear regime.

6.5 Discussion and perspective

In this chapter we have presented a picture of nematic and cholesteric SCLSCEs which allows the description of their nonlinear macroscopic behavior. We have proposed that two preferred directions $\hat{\mathbf{n}}$ and $\hat{\mathbf{n}}^{\text{nw}}$ are important for the nonlinear characterization of the materials. One of these directions has been connected to the liquid crystalline properties, the other one to the elastic mechanical behavior of the polymer network. From these two preferred directions, two sets of nonlinear relative rotations $\tilde{\mathbf{\Omega}}$ and $\tilde{\mathbf{\Omega}}^{\text{nw}}$ have been derived. The major problem in the latter step consisted of finding the matrix of local rotations of the polymer network \mathbf{R} . We have demonstrated how this matrix can be approximated by a series expansion and how it can be determined using a local transformation to the principal system of the strain tensor $\boldsymbol{\varepsilon}$. Finally, we have shown that for small deviations from the energetic ground state our picture is consistent with the previous characterization of the materials using only one set of relative rotations.

In section 6.2 we have postponed an explanation for our remark that we should use the initial field $\mathbf{a}(\mathbf{r})$ instead of the displacement field $\mathbf{u}(\mathbf{r})$ in order to formulate the expressions for our macroscopic variables. We will shortly comment on this issue at this point.

It has been shown in Ref. [41] that the use of the displacement field $\mathbf{u}(\mathbf{r})$ should be handled with care when dynamic deformations of anisotropic systems are investigated. This feature arises from the fact that the components of $\mathbf{u}(\mathbf{r}) = \mathbf{r} - \mathbf{a}(\mathbf{r})$ connect two different spaces [41, 42]. On the one hand, this is the space in which the initial/ground state of the system is described, and we call this space the initial space. The field $\mathbf{a}(\mathbf{r})$ is associated with the initial space. On the other hand, we have the space in which the final state of the material is characterized. We call this space the final space. The current positions \mathbf{r} of the volume elements of the material are associated with the final space. We can simply avoid the problems arising from the connection of the two spaces by replacing $\mathbf{u}(\mathbf{r})$ by $\mathbf{r} - \mathbf{a}(\mathbf{r})$ in the expressions for the macroscopic variables. In doing so we correctly distinguish between initial space and final space. This is the reason why we have given the expressions in Eqs. (6.3) and (6.14) also in terms of the initial field $\mathbf{a}(\mathbf{r})$ and not only in terms of the displacement field $\mathbf{u}(\mathbf{r})$.

Using the initial field $\mathbf{a}(\mathbf{r})$ instead of the displacement field $\mathbf{u}(\mathbf{r})$, we find that our macroscopic variables have a well defined symmetry behavior in the initial as well as in the final space, separately. For example, we infer from Eq. (6.3) that ε is even under parity in the initial space, when $\mathbf{a}(\mathbf{r}) \rightarrow -\mathbf{a}(\mathbf{r})$. Separately, ε is also even under parity in the final space, when together with $\mathbf{r} \rightarrow -\mathbf{r}$ also $\partial_i \rightarrow -\partial_i$, ($i = 1, 2, 3$).

We have added an appendix, in which we further expand on the consequences of the distinction between the two different spaces (appendix C). There, we discuss in particular the symmetry relations associated with the directions $\hat{\mathbf{n}}$ and $\hat{\mathbf{n}}^{\text{nw}}$ connected to the distorted state of the elastomer, and $\hat{\mathbf{n}}_0$ and $\hat{\mathbf{n}}_0^{\text{nw}}$ connected to the undistorted state. Furthermore, in combination with this discussion, we outline an alternative approach to the nonlinear variables of relative rotations.

In closing this chapter, we may conclude that we have for the first time explicitly derived nonlinear expressions for the variables of relative rotations within the framework of the macroscopic theory. We have formulated these expressions as a function of the variables $\mathbf{u}(\mathbf{r})$ (or $\mathbf{a}(\mathbf{r})$) and $\hat{\mathbf{n}}(\mathbf{r})$, which completely describe the state of the material. In the following two chapters, we will explicitly include the nonlinear variables of relative rotations into expressions for the generalized energy density in order to characterize the nonlinear macroscopic behavior of nematic SCLSCs.

As a perspective, we may emphasize that the nonlinear expressions for the relative rotations will also be helpful in the macroscopic description of other complex systems. For example, these expressions can directly be included in the macroscopic characterization of magnetic gels [46, 47]. In this case, the analog to the director orientation $\hat{\mathbf{n}}(\mathbf{r})$ in nematic SCLSCs is given by the

local magnetization $\mathbf{m}(\mathbf{r})$.

Chapter 7

Finite shear deformation of a nematic side-chain liquid single crystal elastomer

In the previous chapter, we have presented our picture of nematic and cholesteric SCLSCEs as materials of two coupled preferred directions. We have put our focus onto the derivation of nonlinear expressions for the variables of relative rotations.

One goal of the current chapter will be to demonstrate that our picture is appropriate as a basis for a nonlinear macroscopic description of nematic SCLSCEs. For this purpose, we will investigate the behavior of a nematic SCLSCE exposed to a static or quasistatic shear deformation. We will specify the geometry in the next section. There, in the same way as in chapter 2, we will also systematically derive an expression for the corresponding generalized energy density, now, however, up to cubic order. A crucial point of this procedure is that nonlinearities arise in the characterization from two different sources. On the one hand, they are included via the nonlinear terms in the expression for the generalized energy density. On the other hand, they are due to the nonlinear expressions of the macroscopic variables contributing to the generalized energy density. Including both kinds of nonlinearities, we will analyze the macroscopic behavior of a nematic SCLSCE under shear deformation in detail in section 7.2. The nonlinear description of the materials will reveal additional features of their reaction which are not covered by the linear model. In combination with appendix D, we again demonstrate that relative rotations play a decisive role in the macroscopic behavior of the elastomers. Finally, we shortly discuss our results and compare them to other approaches.

The presentation of the contents of this chapter closely follows the one

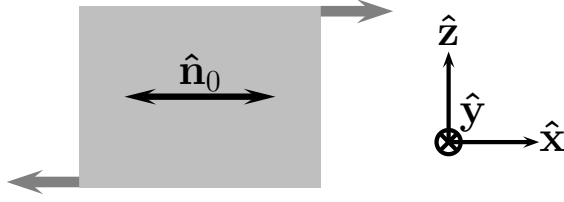


Figure 7.1: Geometry of the static or quasistatic shear deformation investigated. The bulk volume element of the nematic SCLSCE is oriented such that $\hat{\mathbf{n}}_0 \parallel \hat{\mathbf{x}}$. The shear is applied within the x - z -plane as indicated by the arrows.

we have given in Ref. [65].

7.1 Geometry and generalized energy density

In the course of this chapter, we will demonstrate that nonlinear effects attributed solely to the possibility of relative rotations can lead to qualitatively new information in comparison to the linear picture. For this purpose, we will go one order beyond the linear model in our nonlinear description of this chapter, which means, for instance, that we will expand the expression for the generalized energy density up to cubic order. As announced before, we will investigate the situation of a nematic SCLSCE exposed to a static or quasistatic shear deformation. The geometry we have in mind is depicted in Fig. 7.1.

As illustrated in the figure, the nematic elastomer in the ground state is oriented such that the mesogenic units are aligned on average parallel to the x -axis. Thus the director in the ground state conformation may be parameterized by

$$\hat{\mathbf{n}}_0 = (1, 0, 0). \quad (7.1)$$

This conformation is spatially homogeneous. Therefore, we do not have to explicitly account for an $\mathbf{a}(\mathbf{r})$ -dependence of $\hat{\mathbf{n}}_0$ according to Eq. (6.4), which simplifies the problem significantly. As we have noted in section 6.2, the direction $\hat{\mathbf{n}}_0^{\text{nw}}$ is oriented parallel to $\hat{\mathbf{n}}_0$ in the initial state.

In order to parameterize the current state of the director field, we set

$$\hat{\mathbf{n}} = \left([1 - \sin^2 n_y - \sin^2 n_z]^{1/2}, \sin n_y, \sin n_z \right). \quad (7.2)$$

Here, n_y and n_z describe the angles between the director orientation and the planes of $y = 0$ and $z = 0$, respectively. This parameterization is sufficient for an investigation of the problem up to cubic order.

On the other hand, we have to characterize the elastic mechanical deformations of the elastomer by three independent variables. We will use the three components of the more intuitive field $\mathbf{u}(\mathbf{r})$, rather than those of $\mathbf{a}(\mathbf{r})$.

Furthermore, for illustration, we will only study the bulk effect of an external shear imposed on the elastomer. In other words, we will neglect influences of the boundaries and only look for spatially homogeneous solutions of the director reorientation and the mechanical distortion. For this reason, terms containing components of $\nabla\hat{\mathbf{n}}$ are not explicitly listed below.

In the following, we will derive an expression for the generalized energy density F of the system up to cubic order. For this purpose, we will proceed in the same way as in section 2.3, whereas now, as an additional condition of symmetry, the final expression of F must also be invariant under the transformation $\hat{\mathbf{n}}^{\text{nw}} \rightarrow -\hat{\mathbf{n}}^{\text{nw}}$. We will concentrate on the terms made up by the three macroscopic variables $\boldsymbol{\varepsilon}$, $\tilde{\boldsymbol{\Omega}}$, and $\tilde{\boldsymbol{\Omega}}^{\text{nw}}$ that contribute to the generalized energy density. Minimizing the generalized energy $\mathcal{F} = \int F d^3r$ we then can find the current state of the elastomer under an imposed shear deformation.

Isotropic behavior is again assumed for all the terms that are solely connected to the elastic mechanical behavior in the case in which no reorientation of the director takes place. In this way, we guarantee that the behavior we will predict for the nematic SCLSCE is directly connected to the influence of relative rotations and cannot be found by simply including anisotropic elastic behavior via the terms made up only by the strain tensor $\boldsymbol{\varepsilon}$. (In appendix D, we demonstrate that our results are not changed qualitatively if, in addition, this kind of anisotropic elastic behavior is taken into account.)

It is then straightforward to write down a nonlinear convex expression for the generalized energy density of the system up to quartic order in the variables n_y, n_z , and in the components of $\nabla\mathbf{u}$. However, if, in the following, for demonstrative purposes we are only interested in the small-amplitude first order corrections to the linear theory, quartic terms are negligible. It is then a legitimate procedure to only consider terms up to cubic order. Furthermore, in the illustrative example we will investigate below, the amplitude of the solution will be imposed onto the system externally. This additionally guarantees the stability of our solution.

We obtain

$$\begin{aligned} F = & F_0 + c_1 \varepsilon_{ij} \varepsilon_{ij} + \frac{1}{2} c_2 \varepsilon_{ii} \varepsilon_{jj} \\ & + \frac{1}{2} D_1 \tilde{\Omega}_i \tilde{\Omega}_i \\ & + D_2 \tilde{\Omega}_i \varepsilon_{ij} n_j + D_{2,n} n_i \tilde{\Omega}_i n_j \varepsilon_{jk} n_k + D_{2,tr} n_i \tilde{\Omega}_i \varepsilon_{jj} \end{aligned}$$

$$\begin{aligned}
& + D_2^{nw} \tilde{\Omega}_i^{nw} \varepsilon_{ij} n_j^{nw} + D_{2,n}^{nw} n_i^{nw} \tilde{\Omega}_i^{nw} n_j^{nw} \varepsilon_{jk} n_k^{nw} \\
& + \zeta_1 \varepsilon_{ii} \varepsilon_{jj} \varepsilon_{kk} + \zeta_2 \varepsilon_{ii} \varepsilon_{jk} \varepsilon_{jk} + \zeta_3 \varepsilon_{ij} \varepsilon_{jk} \varepsilon_{ki} \\
& + \phi_1 n_i \varepsilon_{ij} \tilde{\Omega}_j \varepsilon_{kk} + \phi_2 n_i \varepsilon_{ij} \varepsilon_{jk} \tilde{\Omega}_k + \phi_3 n_i \varepsilon_{ij} \tilde{\Omega}_j n_k \varepsilon_{kl} n_l \\
& + \psi_1 \tilde{\Omega}_i \tilde{\Omega}_i \varepsilon_{jj} + \psi_2 \tilde{\Omega}_i \varepsilon_{ij} \tilde{\Omega}_j + \psi_3 \tilde{\Omega}_i \tilde{\Omega}_i n_j \varepsilon_{jk} n_k. \tag{7.3}
\end{aligned}$$

In the first line, F_0 incorporates all the terms that contain variables other than ε , $\tilde{\Omega}$, and $\tilde{\Omega}^{nw}$. As mentioned above, their influence will not be studied in this chapter.

What follows are the quadratic terms with the coefficients c_1 , c_2 , D_1 , and D_2 , which are already well known from the linear theory introduced in section 2.3 [36,39]. There are two new quadratic terms with the coefficients $D_{2,n}$ and $D_{2,tr}$ in addition to the linear theory because in the nonlinear regime Eq. (2.8) does not apply anymore. Furthermore, there arise the contributions with the coefficients D_2^{nw} and $D_{2,n}^{nw}$ in contrast to the linear theory, because in the nonlinear regime the preferred directions $\hat{\mathbf{n}}$ and $\hat{\mathbf{n}}^{nw}$ have to be distinguished, and two sets of relative rotations have to be included.

Next, we have listed the three cubic terms arising from the deformation of an isotropic elastic body [48] with coefficients ζ_i ($i = 1, 2, 3$), and afterward the cubic terms containing relative rotations are included with coefficients ϕ_i and ψ_i ($i = 1, 2, 3$). The terms $\sim \psi_1$ and $\sim \psi_3$ can be thought of as modifications of the contribution $\sim D_1$, while the terms $\sim \phi_1$ and $\sim \phi_3$ can be viewed as modifications of the contribution $\sim D_2$. The components of ε and $\tilde{\Omega}$ have to be introduced into the cubic terms only to linear order, and as a consequence Eq. (2.8) applies. For this reason we have not listed the cubic terms containing $n_i \tilde{\Omega}_i$.

Formally, further terms arise respecting the necessary conditions of symmetry. However, we have not explicitly noted the other symmetry allowed terms containing components of $\hat{\mathbf{n}}^{nw}$ and/or $\tilde{\Omega}^{nw}$. They are either formally identical to or linearly dependent on the expressions that we have listed in Eq. (7.3), or they are not distinguishable to the order that will be considered below. The possible qualitative impact of these terms is therefore already covered by the contributions included.

Before turning to our example of the sheared nematic SCLSCE, we want to recall once again that nonlinearities arising from Eq. (7.3) have two different sources. On the one hand, these are the explicitly nonlinear cubic terms in Eq. (7.3). On the other hand, the quadratic terms also contain nonlinear contributions, because the nonlinear expression for ε as well as the new nonlinear expressions for $\tilde{\Omega}$ and $\tilde{\Omega}^{nw}$ derived in the preceding chapter must be inserted into the quadratic terms. That is the reason why the material parameters c_1 , D_1 , D_2 , and also D_2^{nw} will significantly contribute to the

nonlinear results listed in the next section.

7.2 Analysis of the shear deformation

We now want to analyze the consequences of a shear deformation of the bulk of the nematic SCLSCE as indicated in Fig. 7.1. Denoting the shear amplitude by A_0 and looking only for homogeneous solutions due to the reasons elucidated in the previous section, we make the ansatz

$$u_x(\mathbf{r}) = A_0 z + A_1 x, \quad (7.4)$$

$$u_y(\mathbf{r}) = B_1 y, \quad (7.5)$$

$$u_z(\mathbf{r}) = C_1 z, \quad (7.6)$$

$$n_y(\mathbf{r}) = n_y, \quad (7.7)$$

$$n_z(\mathbf{r}) = n_z. \quad (7.8)$$

If we assume the system to be incompressible, which is a good approximation for the elastomers under investigation, we obtain

$$B_1 = \frac{A_1 C_1 - A_1 - C_1}{1 + A_1 C_1 - A_1 - C_1}. \quad (7.9)$$

Furthermore, the terms with the coefficients ζ_1 , ζ_2 , ϕ_1 , and ψ_1 are of higher order due to incompressibility and thus vanish in our consideration of the problem.

Since we study a spatially homogeneous solution, \mathcal{F} is minimized simultaneously with F . Thus we can find the actual state of the system by solving the set of equations $\frac{\partial F}{\partial A_1} = 0$, $\frac{\partial F}{\partial C_1} = 0$, $\frac{\partial F}{\partial n_y} = 0$, and $\frac{\partial F}{\partial n_z} = 0$. For this purpose we expand the coefficients in ansatz (7.4)-(7.8) in a small parameter ϵ up to quadratic order,

$$A_0 = A_0^{(1)} \epsilon, \quad (7.10)$$

$$A_1 = A_1^{(1)} \epsilon + A_1^{(2)} \epsilon^2, \quad (7.11)$$

$$C_1 = C_1^{(1)} \epsilon + C_1^{(2)} \epsilon^2, \quad (7.12)$$

$$n_y = n_y^{(1)} \epsilon + n_y^{(2)} \epsilon^2, \quad (7.13)$$

$$n_z = n_z^{(1)} \epsilon + n_z^{(2)} \epsilon^2, \quad (7.14)$$

and introduce them into the set of equations. Here, $A_0^{(1)} \epsilon$ has been used as input. Up to quadratic order in ϵ we obtain the following results, which are also depicted in Fig. 7.2.

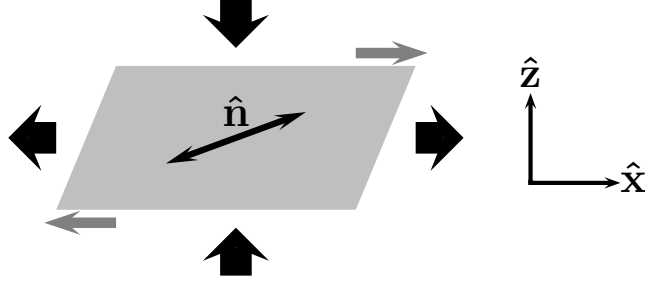


Figure 7.2: Consequences of a static or quasistatic mechanical shear deformation of a bulk volume element of a nematic SCLSCE. The director is rotated within the plane of the applied shear. In addition, dilative and compressive strains occur. The black arrows indicate one possible case of the resulting deformations. Relative rotations are the mediator between these effects.

The director $\hat{\mathbf{n}}$ acquires a z -component given by the angle

$$n_z = -\frac{D_1 + \bar{D}_2}{2D_1}A_0, \quad (7.15)$$

where we have introduced the abbreviation

$$\bar{D}_2 = D_2 + D_2^{nw}. \quad (7.16)$$

As we can see, this is an effect linear in the shear amplitude A_0 , and indeed this effect has already been predicted by the linear theory [32]. Up to the order investigated there is no correction to this result for n_z : $n_z^{(2)} = 0$. Furthermore, we find that the director remains oriented within the x - z -plane, which is not surprising for a spatially homogeneous solution due to reasons of symmetry:

$$n_y = 0. \quad (7.17)$$

It turns out that $A_1^{(1)}$ and $C_1^{(1)}$ vanish identically. Thus, in addition to the reorientation of the director, we observe a compression and/or dilation of the SCLSCE parallel to the $\hat{\mathbf{x}}$, $\hat{\mathbf{y}}$, and $\hat{\mathbf{z}}$ direction, described by

$$A_1 = \frac{A_0^2}{24c_1D_1^2}(4c_1D_1^2 + D_1\bar{D}_2^2 + \bar{D}_2^3 - 2\bar{D}_{2,n}\bar{D}_2^2 - 3\zeta_3D_1^2 + \phi_2D_1\bar{D}_2 + 2\phi_3D_1\bar{D}_2 + \psi_2\bar{D}_2^2 - 2\psi_3\bar{D}_2^2 + D_2^{nw}\bar{D}_2^2), \quad (7.18)$$

$$B_1 = \frac{A_0^2}{48c_1D_1^2}(-16c_1D_1^2 + 2D_1\bar{D}_2^2 + 2\bar{D}_2^3 + 2\bar{D}_{2,n}\bar{D}_2^2 + 12\zeta_3D_1^2 - 4\phi_2D_1\bar{D}_2 - 2\phi_3D_1\bar{D}_2 + 2\psi_2\bar{D}_2^2 + 2\psi_3\bar{D}_2^2 - 4D_2^{nw}\bar{D}_2^2), \quad (7.19)$$

$$\begin{aligned}
C_1 = & \frac{A_0^2}{48c_1D_1^2}(8c_1D_1^2 - 4D_1\bar{D}_2^2 - 4\bar{D}_2^3 + 2\bar{D}_{2,n}\bar{D}_2^2 - 6\zeta_3D_1^2 \\
& + 2\phi_2D_1\bar{D}_2 - 2\phi_3D_1\bar{D}_2 - 4\psi_2\bar{D}_2^2 + 2\psi_3\bar{D}_2^2 + 2D_2^{nw}\bar{D}_2^2). \quad (7.20)
\end{aligned}$$

The amplitudes given by these strain coefficients are proportional to the square of the shear amplitude A_0 . So they describe nonlinear effects, which cannot be predicted by a linear theory. In these expressions we have introduced another abbreviation, namely

$$\bar{D}_{2,n} = D_{2,n} - D_{2,n}^{nw}. \quad (7.21)$$

We can interpret these results in the following way. Due to the external mechanical shear deformation the director is reoriented. This is a linear effect which arises from the coupling between the mechanical deformation and the director orientation, mediated by the relative rotations. However, this reorientation of the director itself acts back onto the mechanical deformation and leads to compressive and/or dilative strains. From that point of view, the nonlinear character of the compressive and/or dilative strain deformations becomes clear. Again, this action of the director reorientation back onto the mechanical deformation is mediated by the relative rotations.

The described effects cannot be attributed to an anisotropy of the elastic mechanical behavior observed in the case that no reorientation of the director occurs. We have excluded anisotropy from all terms of F that are solely related to the elastic mechanical behavior. All the terms in Eqs. (7.15) and (7.18)-(7.20) directly depend on the coefficients of Eq. (7.3) that are connected to relative rotations.

If in those terms of Eq. (7.3) containing relative rotations we furthermore take into account the isotropy of the elastic mechanical behavior, we have to set $\bar{D}_{2,n}$, ϕ_3 , and ψ_3 equal to zero. However, this does not affect our results qualitatively.

On the other hand, as already mentioned, in appendix D we investigate the effect of an anisotropic elastic mechanical behavior explicitly. Up to the inspected order, we do not find a correction to the reorientation of the director field as given by Eqs. (7.15) and (7.17). The corrections to the expressions in Eqs. (7.18)-(7.20) do not change the results given above qualitatively. We also demonstrate in the appendix that concentrating only on an anisotropic elastic mechanical behavior and neglecting relative rotations one does not recover the compressive and/or dilative deformations described above.

The interesting physics of the geometry investigated mainly occurs in the x - z -plane of the system. In this plane the rotation of the director takes place, and the relative rotations between the director orientation and the direction

imprinted into the polymer network also occur within this plane. The compression or dilation in the $\hat{\mathbf{y}}$ direction only results from the incompressibility condition (7.9) and influences the coefficients A_1 and C_1 . We qualitatively obtain the same result concerning the physics in the x - z -plane, if we treat the system as two-dimensional. In this case and up to the order investigated, including incompressibility of the system, we obtain

$$n_z = -\frac{D_1 + \bar{D}_2}{2D_1}A_0, \quad (7.22)$$

$$A_1 = A_0^2 \frac{\bar{D}_2}{16c_1 D_1^2} (\bar{D}_2^2 + \bar{D}_2(D_1 - \bar{D}_{2,n}) + D_1\phi_3 + \bar{D}_2(\psi_2 - \psi_3)), \quad (7.23)$$

$$C_1 = -A_1. \quad (7.24)$$

Therefore, the director reorients in the same way as described for the three-dimensional geometry. In the two-dimensional case, compression or dilation in $\hat{\mathbf{x}}$ direction coincides with dilation or compression in $\hat{\mathbf{z}}$ direction, respectively. This is the situation indicated by the black arrows in Fig. 7.2.

7.3 Discussion

We want add one technical remark concerning our way of describing the shear deformation of the nematic SCLSCE. In this chapter, we have used the components of the displacement field $\mathbf{u}(\mathbf{r})$ instead of those of $\mathbf{a}(\mathbf{r})$ in order to characterize the current state of distortion of the material. We have made this choice, because $\mathbf{u}(\mathbf{r})$ gives the more intuitive and illustrative variables. This procedure is convenient when static deformations are considered. However, as we have noted in section 6.5, the use of $\mathbf{u}(\mathbf{r})$ should be handled with care when dynamic deformations of anisotropic systems are studied [41].

Next, we should shortly compare our model to other approaches proposed to describe the shear deformation of nematic elastomers. As mentioned in section 2.4, the macroscopic characterization in Ref. [51] to a big extent concentrates on “soft” elastic shear deformations connected to materials featuring a spontaneously broken continuous rotational symmetry. Our model qualitatively differs from the one proposed in Ref. [51]. We explicitly include nonlinear relative rotations as macroscopic variables when we obtain the expression for the generalized energy density of the system. For this purpose, we have derived for the first time explicit nonlinear expressions for the relative rotations within the framework of the macroscopic theory, which we have formulated in terms of the fields $\mathbf{u}(\mathbf{r})$ (or $\mathbf{a}(\mathbf{r})$) and $\hat{\mathbf{n}}(\mathbf{r})$.

When we compare our description to the semi-microscopic approach proposed in Ref. [54], we may note the following. It has been demonstrated

in Ref. [70] that the semi-microscopic model formally contains the D_1 - and D_2 -terms listed in Eq. (7.3); however, the material parameters D_1 and D_2 are not independent in this model. Also the terms $\sim \psi_2$ and $\sim \psi_3$ are shown to be included, but again with dependent coefficients [54]. We have not fixed the values of the material parameters so that they are still independent of each other. This renders the characterization of the materials more general. In particular, this means that our description is not restricted to “soft” or “semi-soft” elastic deformations.

Moreover, in Ref. [54] the linear expressions of relative rotations are used in the way they have been introduced in Ref. [36]. Consequently, it is concluded in Ref. [54] that the D_1 - and D_2 -terms cannot describe nonlinear effects, and cubic terms like the ones $\sim \psi_2$ and $\sim \psi_3$ in Eq. (7.3) must be incorporated in a macroscopic characterization. On the contrary, by our illustrative example we have demonstrated that already the D_1 - and D_2 -terms can model corresponding effects, when appropriate nonlinear expressions for the variables of relative rotations are inserted. (More precisely, in Ref. [54] a geometry corresponding to the experimental situation of, e.g., Refs. [24] and [64] is referred to. There, compressive or dilative mechanical strains couple to the reorientation of the director field. In the linear description, the D_2 -term in Eq. (7.3) does not contain this coupling because linear relative rotations are always perpendicular to $\hat{\mathbf{n}}(\mathbf{r})$, as given by Eq. (2.8). We have indicated in Eq. (7.3) and noted thereafter that relation (2.8) is, however, restricted to the linear regime.)

To conclude, we have demonstrated that we can account for additional effects not covered by our linear model when we include nonlinear expressions for the variables of relative rotations. In our example of shearing a bulk volume element of a nematic SCLSCE, the compressive and dilative strain deformations have been identified with these additional effects. They arise as a consequence of the relative rotations that occur when a reorientation of the director is enforced by an imposed shear deformation. The latter effect is already described by the linear characterization of nematic SCLSCEs.

Again, the variables of relative rotations have played a central role in our investigations. We will study a second nonlinear example of a mechanically distorted nematic SCLSCE in the next chapter. In doing so, we will once more underline the importance of relative rotations for the macroscopic description of the materials.

Chapter 8

Nonlinear stress-strain behavior of nematic side-chain liquid single crystal elastomers

In this chapter, we will analyze the geometry of stretching a nematic SCLSCE perpendicularly to its original director orientation, which leads to a reorientation of the director field. Thus we will come back to the kind of experiment described in section 6.1, and to the photograph presented in the introduction in Fig. 1.1. We will include a semi-quantitative comparison of the predictions of our model to the results obtained from recent corresponding reorientation experiments. The main goal of this procedure will be to reveal the dominating underlying processes which from a macroscopic point of view take place during the reorientation of the director field.

We will first derive an expression for the generalized energy density which is appropriate in order to characterize the macroscopic processes underlying the reorientation experiment. Next, in section 8.2, we will further specify the geometry and connect our variables to the set-up under investigation. In particular, since we want to compare the predictions of our model to the experimental results, we must link our Eulerian picture to the quantities measured during a stress-strain experiment. After that, we will perform our major inspection of the subject in three steps. First, we will concentrate on the reorientation process of the director in section 8.3. Then, we will turn to the nonlinear stress-strain behavior, where we will first suppress elastic shear deformations in section 8.4, whereas we will include them in section 8.5. Finally, we will summarize and discuss our results and give a short perspective in the last section.

Before we start our analysis, we want to stress that the nonlinearities in the stress-strain behavior in our investigations will be associated directly

with the reorientation of the director field. We will not include any nonlinearity of the elastic mechanical behavior that can appear without reorienting at least one of the two preferred directions. Consequently, as might be expected, relative rotations will again play the major role in our analysis in this chapter. The comparison with the experimental results reported in Ref. [27] will corroborate our concept.

We will closely follow in this chapter the presentation of the analysis which we have given in Ref. [66].

8.1 Generalized energy density

In this chapter, we will concentrate on the investigation of strain-induced reorientation processes at constant temperature. It has been observed for this situation that within domains of one orientation of the director, the scalar order parameter S is either slightly decreasing or constant within the experimental error bar [64]. Due to this fact, we will not take into account the scalar degree of ordering S of the mesogens, but only deal with the orientation of the macroscopic director field.

Using symmetry arguments, we derive in this section an expression for the generalized energy density of the system which will be shown to cover the basic features of the materials underlying the strain-induced reorientation process. We follow the same procedure as described in section 2.3. The macroscopic variables that can contribute to the generalized energy density comprise the conserved quantities of mass density ρ , density of momentum \mathbf{g} , and density of energy ε , as well as the macroscopic variables of strain $\boldsymbol{\varepsilon}$, given by Eq. (6.3), relative rotations $\tilde{\mathbf{\Omega}}$ and $\tilde{\mathbf{\Omega}}^{\text{nw}}$, given by Eqs. (6.1) and (6.2), and gradient fields like $\nabla\hat{\mathbf{n}}$. We combine these variables to contributions which satisfy the symmetry requirements, such as invariance under parity and under the transformations $\hat{\mathbf{n}} \rightarrow -\hat{\mathbf{n}}$ and $\hat{\mathbf{n}}^{\text{nw}} \rightarrow -\hat{\mathbf{n}}^{\text{nw}}$, separately. In the following, we will assume that for the investigation of the stress-strain geometry the strains $\boldsymbol{\varepsilon}$ and the relative rotations $\tilde{\mathbf{\Omega}}$ and $\tilde{\mathbf{\Omega}}^{\text{nw}}$ play the dominant role. Therefore, only terms composed of $\boldsymbol{\varepsilon}$, $\tilde{\mathbf{\Omega}}$, and $\tilde{\mathbf{\Omega}}^{\text{nw}}$ are taken into consideration. In particular, this means that we assume that spatial heterogeneities such as the stripe domains reported in Refs. [64] and [67] do not play a generic role for the effects described in this chapter. The comparison to the experimental results will corroborate our assumption, and we will comment on this issue later in section 8.6. As a consequence, it will turn out that the following expression for the generalized energy density is appropriate for our

studies in this chapter:

$$\begin{aligned}
F &= c_1 \varepsilon_{ij} \varepsilon_{ij} + \frac{1}{2} c_2 \varepsilon_{ii} \varepsilon_{jj} \\
&+ \frac{1}{2} D_1 \tilde{\Omega}_i \tilde{\Omega}_i + D_1^{(2)} (\tilde{\Omega}_i \tilde{\Omega}_i)^2 + D_1^{(3)} (\tilde{\Omega}_i \tilde{\Omega}_i)^3 \\
&+ D_2 n_i \varepsilon_{ij} \tilde{\Omega}_j + D_2^{nw} n_i^{nw} \varepsilon_{ij} \tilde{\Omega}_j^{nw} \\
&+ D_2^{(2)} n_i \varepsilon_{ij} \varepsilon_{jk} \tilde{\Omega}_k + D_2^{nw,(2)} n_i^{nw} \varepsilon_{ij} \varepsilon_{jk} \tilde{\Omega}_k^{nw}. \tag{8.1}
\end{aligned}$$

In appendix C we have introduced an alternative definition of the nonlinear variables of relative rotations. We have demonstrated in this appendix that these alternatively defined nonlinear relative rotations lead to the same expression for the generalized energy density.

Again, in expression (8.1), the elastic behavior of the elastomer is assumed to be isotropic in the case that no relative rotations occur. This can be inferred from the first two terms of Eq. (8.1). We will comment on this point in section 8.6. The terms with the coefficients D_1 , $D_1^{(2)}$, and $D_1^{(3)}$ include energetic contributions only related to relative rotations. For symmetry reasons, namely the required invariance under the transformations $\hat{\mathbf{n}} \rightarrow -\hat{\mathbf{n}}$ and $\hat{\mathbf{n}}^{\text{nw}} \rightarrow -\hat{\mathbf{n}}^{\text{nw}}$, only even powers of the relative rotations may appear in these terms. Due to $\tilde{\Omega}_i \tilde{\Omega}_i = \tilde{\Omega}_i^{nw} \tilde{\Omega}_i^{nw}$ we did not explicitly add the corresponding terms containing only the variable $\tilde{\Omega}^{\text{nw}}$. What comes next in expression (8.1) are the terms that couple the relative rotations to the strain of the elastomer. As we can see, the terms with the coefficients D_2 and D_2^{nw} couple to the strain tensor in a linear way, whereas the terms with the coefficients $D_2^{(2)}$ and $D_2^{nw,(2)}$ couple to the strain tensor quadratically. An additional term $\varepsilon_{ij} \varepsilon_{ij} \tilde{\Omega}_k \tilde{\Omega}_k$ can be included in order to model an effective change of the elastic coefficient c_1 with increasing relative rotations between the director and the polymer network. However, we will not need this term for the following discussion. For all terms, strain is only included up to quadratic order. The motivation for this approach will become more transparent during the procedure of our further inspections.

8.2 Geometry and Eulerian description

We begin this section by further specifying the geometry under consideration, which is illustrated in Fig. 8.1. The $\hat{\mathbf{z}}$ direction of our Cartesian coordinate system will be oriented parallel to the externally applied stretching force \mathbf{F}_{ext} . Furthermore, the initial directions $\hat{\mathbf{n}}_0$ and $\hat{\mathbf{n}}_0^{\text{nw}}$ are chosen to be oriented

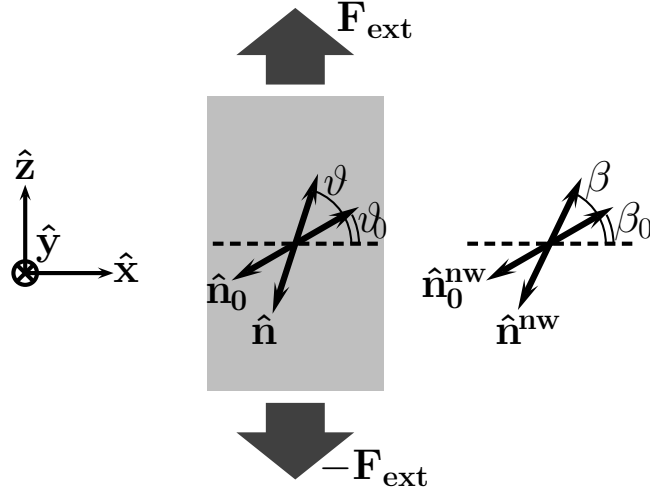


Figure 8.1: Geometry of the system investigated. An external force \mathbf{F}_{ext} is applied parallel to the z -axis, the initial directions $\hat{\mathbf{n}}_0$ and $\hat{\mathbf{n}}_0^{\text{nw}}$ are oriented in the x - z -plane. The angles between the x -axis and $\hat{\mathbf{n}}_0$, $\hat{\mathbf{n}}$, $\hat{\mathbf{n}}_0^{\text{nw}}$, and $\hat{\mathbf{n}}^{\text{nw}}$ are called ϑ_0 , ϑ , β_0 , and β , respectively.

parallel within the x - z -plane, so that we can denote them as

$$\hat{\mathbf{n}}_0 = \begin{pmatrix} \cos(\vartheta_0) \\ 0 \\ \sin(\vartheta_0) \end{pmatrix}, \quad \hat{\mathbf{n}}_0^{\text{nw}} = \begin{pmatrix} \cos(\beta_0) \\ 0 \\ \sin(\beta_0) \end{pmatrix}, \quad \vartheta_0 = \beta_0 + n\pi, \quad n \in \mathbb{Z}. \quad (8.2)$$

When we set $\vartheta_0 = 0$ we obtain the case of stretching the elastomer exactly perpendicularly to the original director orientation. Then, $\hat{\mathbf{n}}_0$ and $\hat{\mathbf{n}}_0^{\text{nw}}$ are oriented parallel to the $\hat{\mathbf{x}}$ direction.

It is straightforward to study an inhomogeneous deformation and to include, e.g., heterogeneous initial director orientations. However, in this chapter we will adopt the assumption of a homogeneous deformation, which includes a homogeneous orientation of the initial directions $\hat{\mathbf{n}}_0$ and $\hat{\mathbf{n}}_0^{\text{nw}}$. One should rather think of the homogeneous deformation of a characteristic volume element, not of the whole sample, a concept which we will further motivate later on.

In this spirit, we take as an ansatz for the displacement field

$$u_z = Az + Sx, \quad (8.3)$$

$$u_x = Bx + Tz, \quad (8.4)$$

$$u_y = Cy. \quad (8.5)$$

Here, the amplitudes A , B , C , S , and T reflect the strain deformation of the

elastomer. We know from the experiments that the reaction of the director field to the external forces is mainly determined by a reorientation within the x - z -plane. Previous calculations in the spirit of our model, for example in Ref. [32] and in chapter 7, show that within this plane the reorientation of the director is closely connected to a shear deformation of the elastomer. This relation has also been found from other models. In ansatz (8.3)-(8.5), we therefore allow for a shear deformation in the x - z -plane and discuss its role later.

We start our calculations by deriving an expression for the matrix \mathbf{R}^{-1} , which describes the elastic rotational deformation of the elastomer. For this purpose, we introduce ansatz (8.3)-(8.5) into Eqs. (6.3) and (6.14). Up to quartic order in the deformation amplitudes we obtain

$$\mathbf{R}^{-1} = \begin{pmatrix} \cos(\beta - \beta_0) & 0 & -\sin(\beta - \beta_0) \\ 0 & 1 + \mathcal{O}(C^5) & 0 \\ \sin(\beta - \beta_0) & 0 & \cos(\beta - \beta_0) \end{pmatrix}, \quad (8.6)$$

where

$$\begin{aligned} \beta - \beta_0 &= -\frac{1}{2} \left(1 + \frac{1}{2}(A + B) + \frac{1}{4}(A + B)^2 + \frac{1}{8}(A + B)^3 \right) (T - S) \\ &+ \frac{1}{24} \left(1 + \frac{3}{2}(A + B) \right) (T - S)^3 + \mathcal{O}(|^5). \end{aligned} \quad (8.7)$$

Here, $\mathcal{O}(|^5)$ represents terms of quintic or higher order in the deformation amplitudes A , B , C , S , and T .

We add four remarks. First, we see from Eqs. (8.6) and (8.7) that in the absence of any shear deformation (i.e. $S = T = 0$) we do not find any elastic rotational deformation. The same is true for equal shear amplitudes $S = T$. Furthermore, in the linear regime we recover the fact that shear and rotational elastic deformations are equivalent: $\beta - \beta_0 = -\frac{1}{2}(T - S)$. Finally, only the shear amplitudes S and T determine the degree of elastic rotational deformation in the case of $B = -A$ and $C = 0$ (which is often referred to as a “pure shear” deformation; see, e.g., Ref. [71]).

Using Eqs. (6.8), (8.6), and (8.7) we can now parameterize $\hat{\mathbf{n}}^{\text{nw}}$ in terms of the deformation amplitudes. On the other hand, we have to include a further degree of freedom ϑ , which is connected to the reorientation of the director $\hat{\mathbf{n}}$ within the x - z -plane. More precisely, $\vartheta - \vartheta_0$ is denoting the angle by which the director has rotated from its original orientation $\hat{\mathbf{n}}_0$ to its final orientation $\hat{\mathbf{n}}$. We obtain

$$\hat{\mathbf{n}} = \begin{pmatrix} \cos(\vartheta) \\ 0 \\ \sin(\vartheta) \end{pmatrix}, \quad \hat{\mathbf{n}}^{\text{nw}} = \begin{pmatrix} \cos(\beta) \\ 0 \\ \sin(\beta) \end{pmatrix}. \quad (8.8)$$

It is a very good approximation to assume that common nematic SCLSCEs do not change their volume during the deformations investigated in the following. We include this feature, which is also denoted as incompressibility, by setting

$$C = \frac{-A - B + AB}{1 - A - B + AB}. \quad (8.9)$$

In particular, this expression for the amplitude C implies that up to cubic order in the strain amplitudes the term with the coefficient c_2 does not contribute to Eq. (8.1).

We can now obtain an expression for the generalized energy density F which is a function only of the strain amplitudes A , B , C , S , and T , as well as of the reorientation angle ϑ . For this purpose, we have to introduce expressions (6.1)-(6.3), (8.3)-(8.5), and (8.7)-(8.9) into Eq. (8.1). We want to stress at this point that we will only take into account the strains up to quadratic order in the generalized energy density (8.1). The quadratic term of the strain tensor (6.3) enters F only in the terms with the coefficients D_2 and D_2^{nw} , and Eq. (8.7) is reduced to $\beta - \beta_0 = -\frac{1}{2}(T - S)$. This way we make sure that the nonlinear stress-strain behavior we will recover in the following originates solely from the influence of the relative rotations. There will be no terms included in the final form of expression (8.1) that can describe a nonlinear elastic behavior when no reorientation of the director occurs.

In our approach, we then have to minimize the generalized energy $\mathcal{F} = \int_V F d^3r$ of the system, V being the volume of the respective sample. This means that we treat the system in a static or quasistatic way. We consider the respective elongation of the sample in $\hat{\mathbf{z}}$ direction to be imposed onto the system externally. Therefore, since we are dealing with a spatially homogeneous deformation, the value of the strain amplitude A is considered to be fixed from outside. For every value of A we determine the equilibrium state of the system.

Following this procedure, we have to minimize the generalized energy density F with respect to the strain amplitudes B , C , S , and T , as well as to the reorientation angle ϑ . From this minimization we obtain the values of B , C , S , T , and ϑ as a function of A . Consequently, also the generalized energy density F can be expressed as a function of A . From the change of the generalized energy density F with respect to A , that is from the derivative $\frac{dF}{dA}$, we can then deduce the value of the externally applied force F_{ext} . F_{ext} is connected to the external stress amplitude, and it is the cause of the respective elongation characterized by A . In this way our picture is closed.

Since we want to compare the results obtained from our model to experimental results, we should address two more issues before we start to evaluate the expression for F .

On the one hand, a completely spatially homogeneous deformation of the entire sample can of course not be realized in an experiment. This results already from the geometrical constraints connected to the respective experimental set-up, in interplay with the low compressibility of the materials. Especially near the top and bottom edges, where the samples are usually clamped during reorientation experiments, the strain deformation is quite heterogeneous. Because of this, a spatially homogeneous characterization can only describe the behavior of one volume element of the sample. Only if the geometry of the sample investigated is chosen such that most of the regions of the sample react in a similar way, and only if the behavior of a characteristic volume element can reflect the overall behavior of the sample, then this approach is meaningful.

Furthermore, for polymer materials it is difficult to map the overall boundary conditions of a clamped sample to one volume element. It seems plausible that shear deformations characterized by $T \neq 0$ play a minor role. This is also suggested by the observations of the stripe domains, which are oriented parallel to the direction of the externally applied force [64, 67]. As a consequence, we will set

$$T = 0 \quad (8.10)$$

during the rest of our considerations. The discussion is not as clear for shear deformations described by $S \neq 0$. Narrow stripes of alternating shear deformation $S > 0$ and $S < 0$, respectively, do not lead to a large deviation from the boundary conditions imposed by the clamps. We will therefore study the case of $S = 0$ first, however, we will also discuss the influence of a nonvanishing shear deformation $S \neq 0$.

On the other hand, we have to connect the variables the values of which are measured during the experiments to the variables that appear in our hydrodynamic-like Eulerian picture. Usually, in the experiments the value of the current macroscopic dimension l of the respective sample in the direction of the externally applied force is recorded step by step. Comparing to the initial dimension l_0 of the sample in this direction, the ratio

$$\lambda = \frac{l}{l_0} \quad (8.11)$$

is determined and taken as a measure of the induced strain. Sometimes, like for instance in Ref. [27], the so-called true strain $\epsilon = \ln(\lambda)$ is taken as a variable. We will choose our Cartesian coordinate system such that the externally applied force is oriented parallel to the $\hat{\mathbf{z}}$ direction (Fig. 8.1). Then, $\lambda \equiv \lambda_z$, $l \equiv l_z$, and $l_0 \equiv l_{z,0}$. In the same way, we define the current dimensions l_x and l_y as well as the initial dimensions $l_{x,0}$ and $l_{y,0}$ of the

respective sample in the lateral directions. Stresses are recorded either as true stress

$$\sigma_{ext} = \frac{F_{ext}}{l_x l_y} \quad (8.12)$$

or as nominal stress

$$\sigma_{ext}^N = \frac{F_{ext}}{l_{x,0} l_{y,0}}, \quad (8.13)$$

where F_{ext} again denotes the magnitude of the force externally applied to the sample edges in $\hat{\mathbf{z}}$ direction. Underlying these definitions is, of course, the assumption that the sample deforms in a spatially homogeneous way. Naturally, from the experimental point of view the initial dimension l_0 is considered to be constant and the current sample dimension l is changed.

In the hydrodynamic-like picture, however, the situation is different. Here, we have to adopt an Eulerian point of view. Therefore, the current dimension of the sample l is considered to be constant, and what changes is the initial dimension l_0 .

Because of $l_{z,0} = l_z - Al_z$, in a spatially homogeneous deformation we obtain

$$\lambda = \frac{1}{1 - A}. \quad (8.14)$$

Furthermore, from

$$d\mathcal{F} = F_{ext}d(l_z - l_{z,0}) = -F_{ext}dl_{z,0} \stackrel{!}{=} l_x l_y l_z \frac{dF}{dA} dA \quad (8.15)$$

we find

$$\sigma_{ext} = \frac{F_{ext}}{l_x l_y} = \frac{dF}{dA}, \quad (8.16)$$

$$\sigma_{ext}^N = \frac{F_{ext}}{l_{x,0} l_{y,0}} = (1 - A) \frac{dF}{dA}. \quad (8.17)$$

Here, the expressions on the left of Eqs. (8.16) and (8.17) are given as functions of λ , the expressions on the right as functions of A . The connection between both follows from Eq. (8.14).

In the following, we will continue our considerations in three steps. First, we will focus on the reorientation of the director field. In this context, we can elucidate the different roles of the two sets of relative rotations. After that, we will address the stress-strain curves. Here, we will first completely exclude shear deformations from our considerations in section 8.4 ($S = 0$), and then allow for shear deformations in section 8.5 ($S \neq 0$). We keep in mind that the reorientation of the director field and the nonlinear shape of the respective stress-strain curve are closely connected to each other.

8.3 Reorientation of the director field

For illustration we will suppress shear elastic deformations in this section, that is we set $S = T = 0$. Therefore, no rotation of the polymer network occurs and $\beta = \beta_0$. Furthermore, we will only take into account the quadratic terms with the coefficients c_1 , D_1 , D_2 , D_2^{nw} , as well as the term with the coefficient $D_1^{(2)}$. Only the linear components of the strain tensor (6.3) will be included in the beginning, so the strain tensor adopts the very simple form $\varepsilon_{xx} = B$, $\varepsilon_{yy} = C$, $\varepsilon_{zz} = A$, and $\varepsilon_{ij} = 0$ for $i \neq j$.

As explained before, we then have to solve the system of equations $\frac{dF}{dB} = \frac{dF}{dC} = 0$. For the values of the material parameters, we choose $c_1 = 121 \times 10^3 \text{ J m}^{-3}$, $D_1 = 12 \times 10^3 \text{ J m}^{-3}$, $D_2 = -32 \times 10^3 \text{ J m}^{-3}$, $D_2^{nw} = -32 \times 10^3 \text{ J m}^{-3}$, and $D_1^{(2)} = 4.5 \times 10^3 \text{ J m}^{-3}$. In general, c_1 is obtained from the initial slope of the respective stress-strain curve before any reorientation of the director takes place. The choice of the other material parameters can be motivated in the following way. From a stability analysis for $\vartheta_0 = 0^\circ$, we find that the original orientation of the director $\vartheta = \vartheta_0 = 0^\circ$ becomes unstable at a critical strain given by $A = A_c$,

$$A_c = -\frac{D_1}{2D_2 + D_2^{nw}}. \quad (8.18)$$

With increasing $A > A_c$ the director continuously rotates and reaches an orientation of $\vartheta = 90^\circ$ at $A = A_r$,

$$A_r = A_c - \frac{8c_1 D_1^{(2)} - (D_2^{nw})^2}{2c_1(2D_2 + D_2^{nw})}. \quad (8.19)$$

For $A > A_r$ the director remains at this orientation of $\vartheta = 90^\circ$.

We can infer from Eq. (8.18) that $2D_2 + D_2^{nw} \stackrel{!}{<} 0$, if a rotation of the director shall occur ($D_1 > 0$). Furthermore, if the values of D_2 and D_2^{nw} are set and the value of A_c is adopted from an experiment, we can estimate the value of D_1 . On the contrary, estimate (8.19) has to be taken with care. The experiments show that the strain amplitudes corresponding to a saturation of the director reorientation are rather high so that nonlinear effects will probably play a major role. Therefore, Eq. (8.19) should mainly be considered as an estimate for the order of magnitude of the value of $D_1^{(2)}$.

As a result, we obtain the curves depicted in Fig. 8.2, where the orientation angle of the director ϑ is plotted against the externally applied strain A (in the corresponding calculations the strain amplitudes have been taken into account up to quadratic order). The different curves correspond to different initial orientation angles $\vartheta_0 = 0^\circ, 0.1^\circ, 2^\circ, 10^\circ$ to 80° in steps of 10° , and

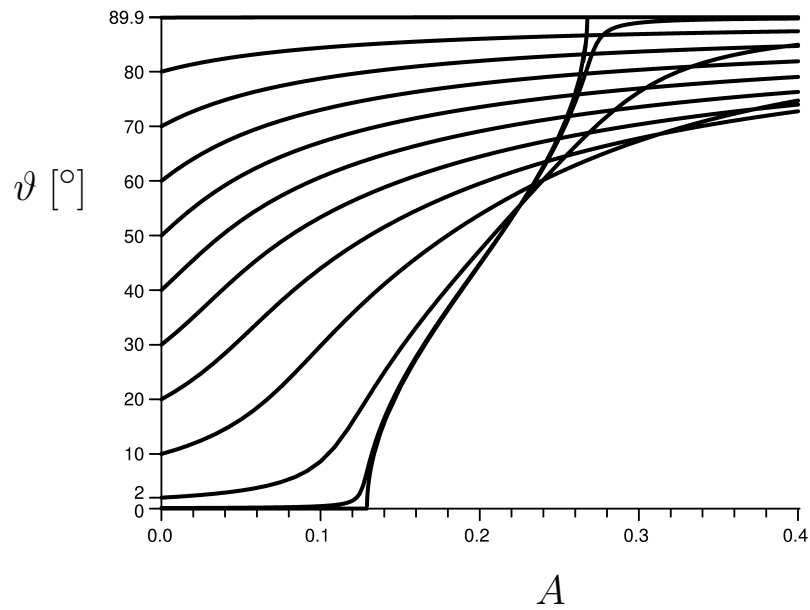


Figure 8.2: Angle ϑ between the director orientation and the x -axis under the influence of an externally applied strain A . The initial director orientations for $A = 0$ were given by $\vartheta(A = 0) = \vartheta_0 = 0^\circ, 0.1^\circ, 2^\circ, 10^\circ$ to 80° in steps of 10° , and 89.9° , respectively. They can be inferred from the scaling labels on the ordinate (the value $\vartheta_0 = 0.1^\circ$ has not been marked explicitly). For $\vartheta_0 = 0^\circ$ a pronounced threshold behavior is found (values of the material parameters as specified in the main text).

89.9°, respectively, which can be inferred from the scaling labels on the ordinate (the value of $\vartheta_0 = 0.1^\circ$ has not been marked explicitly). At small and large strain amplitudes the curves for $\vartheta_0 = 0^\circ$ and $\vartheta_0 = 0.1^\circ$ nearly coincide. Significantly, for an external force applied perfectly perpendicularly to the initial director orientation, that is for $\vartheta_0 = 0^\circ$, we find a pronounced threshold at a critical strain $A_c \approx 0.13$. However, the curve strongly smoothes out already for the small value of $\vartheta_0 = 0.1^\circ$. Naturally, when the director is already aligned parallel to the externally applied force ($\vartheta_0 \approx 90^\circ$), practically no further reorientation occurs.

It is interesting to note that we find a complete alignment of the director parallel to the external force direction, that is $\vartheta = 90^\circ$ at finite strains, only for the perfectly perpendicular geometry of $\vartheta_0 = 0^\circ$. In order to understand this point, we have a look at the terms with the coefficients D_2 and $D_2^{(nw)}$, which induce the reorientation of the director field. For the geometry investigated, they read

$$D_2 n_i \varepsilon_{ij} \tilde{\Omega}_j + D_2^{nw} n_i^{nw} \varepsilon_{ij} \tilde{\Omega}_j^{nw} = (D_2 n_x \varepsilon_{xx} \tilde{\Omega}_x + D_2^{nw} n_z^{nw} \varepsilon_{zz} \tilde{\Omega}_z^{nw}) \\ + (D_2 n_z \varepsilon_{zz} \tilde{\Omega}_z + D_2^{nw} n_x^{nw} \varepsilon_{xx} \tilde{\Omega}_x^{nw}). \quad (8.20)$$

The two terms in the first bracket are always positive, whereas the two terms in the second bracket are always negative. This follows from definitions (6.1) and (6.2), as well as from $\varepsilon_{xx} < 0$ and $\varepsilon_{zz} > 0$. In general, the energetic penalty arising from the first two terms inhibits a complete alignment of the director parallel to the external force direction. However, these terms vanish in a geometry in which the external stress is always oriented perfectly perpendicular to $\hat{\mathbf{n}}^{nw}$ ($\vartheta_0 = 0^\circ$, $S = T = 0$). More illustratively, we can say that the stretching of the elastomer given by $\varepsilon_{zz} > 0$ enforces, whereas the induced contraction described by $\varepsilon_{xx} < 0$ hinders the director reorientation via the relative rotations $\tilde{\Omega}$. The opposite is true for the role of the relative rotations $\tilde{\Omega}^{nw}$: here the stretching $\varepsilon_{zz} > 0$ hinders and the induced contraction $\varepsilon_{xx} < 0$ enforces the director reorientation. Only in the case of the perfectly perpendicular geometry without shear deformation, Eq. (8.20) solely leads to contributions that drive the director to $\vartheta = 90^\circ$. In all the other cases, additional contributions leading to the opposite effect arise. This is the reason for the very different appearances of the curves in Fig. 8.2.

For the special case of $\vartheta_0 = 0^\circ$ and $S = T = 0$, we can further elucidate the roles of the two sets of relative rotations $\tilde{\Omega}$ and $\tilde{\Omega}^{nw}$. $\tilde{\Omega}$ directly couples to the externally imposed strain $\varepsilon_{zz} = A$, and this coupling induces the reorientation of the director field. On the other hand, $\varepsilon_{zz} > 0$ results in a contraction $\varepsilon_{xx} < 0$, which couples to $\tilde{\Omega}^{nw}$. Then, $\tilde{\Omega}^{nw}$ also enforces the director reorientation. Because of the coupling between $\tilde{\Omega}^{nw}$ and ε_{xx} , however,

the material parameter D_2^{nw} simultaneously influences the magnitude of the lateral contraction ε_{xx} .

When we want to compare the shape of the curves in Fig. 8.2 to the ones obtained during measurements, we have to rescale the abscissa via Eq. (8.14), introducing λ as a variable. This procedure stretches the shape of the curves for higher strains, a tendency which is also observed experimentally [67]. In our model, it is possible to fine-tune the shape of the curves especially for larger angles ϑ via the values of the material parameters $D_1^{(2)}$ and $D_1^{(3)}$ (and using terms in the expression for F of even higher order in the relative rotations, if necessary). We note that for values $D_1 > 0$, $D_1^{(2)} < 0$, and $D_1^{(3)} > 0$ our model predicts a jump of the orientation angle ϑ to higher values at a certain strain amplitude. A related behavior has been reported, for example, in Ref. [24].

8.4 Stress-strain curves

In this section we will use our model in order to study the mechanical stress-strain behavior of nematic SCLSCEs deformed in a geometry as described above. For this purpose we will compare the results of our model with data measured during recent stress-strain experiments.

We have decided to focus on the stress-strain curve shown in Fig. 8.3. It has been measured by Urayama et al. and it is reproduced from Fig. 5 of Ref. [27]. The authors of Ref. [27] have investigated a thin film of nematic SCLSCE of homeotropic ground state director alignment. At 70°C the film was deeply in the nematic state and showed a pronounced decrease in the slope of the stress-strain curve at intermediate strain amplitudes (Fig. 8.3). The reasons for us to focus on these data are of different kinds. For one thing, the data curve apparently represents a material which has sufficiently equilibrated for each step of increasing the strain. In particular, besides the stress-strain data, also measurements revealing the orientation of the director field as well as measurements on the dimensional shape change of the sample during the strain deformation are presented for the same material and thus give a complete picture.

Two important facts can be extracted from the region of high strain amplitudes in Fig. 8.3. We can see that the elastomer reacts in a well defined way to the imposed strain deformation. A fairly linear relationship has been found between the nominal stress σ_{ext}^N and the logarithm of the elongation $\ln(\lambda)$ for these high strain amplitudes. This especially applies to the data points in the regime $0.4 < \epsilon < 0.5$. For $\epsilon > 0.5$ the data points start to scatter and slightly deviate from this linear relationship. We interpret this

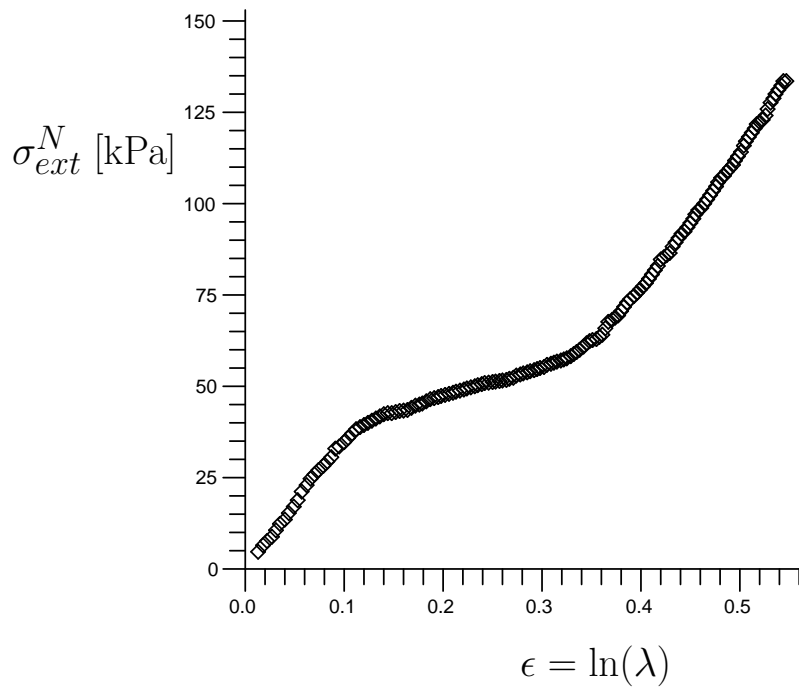


Figure 8.3: Nominal stress σ_{ext}^N versus the true strain $\epsilon = \ln(\lambda)$, measured for a nematic SCLSCE by Urayama et al. The data points were acquired for a thin film of homeotropic alignment at 70°C. This figure has been reproduced from Fig. 5 of Ref. [27].

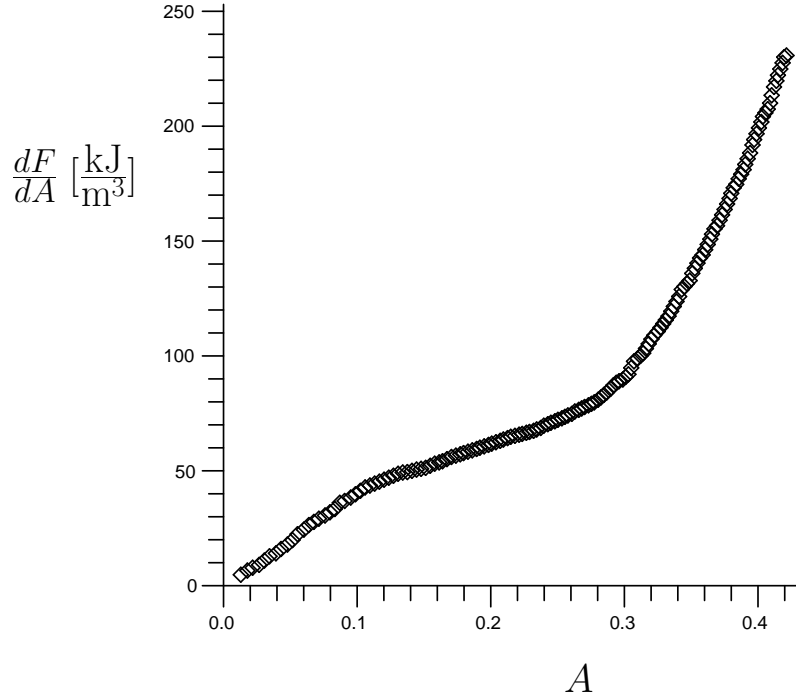


Figure 8.4: Stress-strain data from Fig. 8.3 measured by Urayama et al., transferred to the representation in terms of A and $\frac{dF}{dA}$.

fact as the onset of a qualitatively different behavior at very high strain amplitudes. Therefore, we will restrict our considerations to the regime of $\epsilon < 0.5$. The authors of Ref. [27] could further demonstrate by infrared dichroism measurements that in the regime of high strain amplitudes ($\epsilon > 0.4$) the director reorientation has been completed and practically no further reorientation occurs. Moreover, the slope of the stress-strain curve for $0.4 < \epsilon < 0.5$ is roughly as large as for low strain amplitudes.

In order to compare with our model, we have to convert the stress-strain curve from Fig. 8.3 to the corresponding representation in terms of the variables A and $\frac{dF}{dA}$. We perform this step with the help of Eqs. (8.14) and (8.17). As a result, we obtain the curve depicted in Fig. 8.4.

Furthermore, we remember that in our approach we have derived the expression for the generalized energy density F by means of a series expansion in the strain tensor $\boldsymbol{\varepsilon}$. As mentioned before, in our calculations pure elastic strain is explicitly included only to quadratic order. Nonlinear behavior of the stress-strain curve predicted by our expression for the generalized energy density F always has to be connected to a reorientation process of the director field. If the director orientation remains constant w.r.t. the polymer network,

we will find a linear relationship between A and $\frac{dF}{dA}$.

A nonlinear behavior of the stress-strain curve in a regime of constant director orientation (and constant relative rotations) has to arise solely from an intrinsic nonlinear elastic behavior, resulting from stretching the network of polymer backbones. We will subtract this nonlinear elastic behavior from the stress-strain curve. For this purpose we have fitted the linear regime of high strains in Fig. 8.3 by a straight line. With the help of Eqs. (8.14) and (8.17), we could transfer this straight line from the $\ln(\lambda)$ - σ_{ext}^N representation of Fig. 8.3 to the A - $\frac{dF}{dA}$ representation of Fig. 8.4. We obtain $\frac{dF}{dA}$ as a power series of A , $\frac{dF}{dA} = a_0 + a_1A + a_2A^2 + a_3A^3 + \dots$. As mentioned above, the authors of Ref. [27] have demonstrated that for these high strain amplitudes no reorientation process of the director occurs. The nonlinear contributions in A must therefore result from intrinsic nonlinear purely elastic contributions resulting from stretching the network of polymer backbones. Since these effects are not included in the characterization by our model, we can exclude them from our considerations: we subtract the values $a_2A^2 + a_3A^3 + \dots$ from the data points of our stress-strain curve in the A - $\frac{dF}{dA}$ representation. This is possible on the basis of our approach in the spirit of a series expansion, in which every effect is connected to a limited number of terms. As a result, we obtain the curve of data points shown by Fig. 8.5.

We have to note that, as a consequence of this procedure, we make a small error in the following sense. Terms, like for instance $\varepsilon_{ij}\varepsilon_{jk}\varepsilon_{ki}\tilde{\Omega}_l\tilde{\Omega}_l$, include the strain to higher than quadratic order and couple, for example, to relative rotations. At low strain amplitudes the term may vanish due to $\tilde{\Omega} = \mathbf{0}$. On the contrary, it may lead to a contribution nonlinear in A for higher strain amplitudes when $\tilde{\Omega} = \mathbf{const} \neq \mathbf{0}$. In this case, we may subtract the nonlinear influence of this term from the A - $\frac{dF}{dA}$ curve only for the higher strain amplitudes where $\tilde{\Omega} = \mathbf{const} \neq \mathbf{0}$, not for the lower strain amplitudes of $\tilde{\Omega} = \mathbf{0}$. However, we have checked that the error resulting from these deviations is only minor. For this purpose, we have repeated the whole procedure, now fitting the linear regime of small strains of the $\ln(\lambda)$ - σ_{ext}^N plot with a straight line. Eventually, after subtracting the elastic nonlinearities resulting from this regime, we have obtained almost the same curve as before. In short: we have verified that our procedure of fitting the original stress-strain curve leads essentially to the same results for both regimes, small and large amplitudes of strain.

As mentioned above, as a first step in order to investigate the stress-strain behavior, we suppress elastic shear deformations completely by setting $S = T = 0$. This means that $\hat{\mathbf{n}}^{\text{nw}} \parallel \hat{\mathbf{n}}_0^{\text{nw}}$ during the whole deformation. We solve the equations $\frac{dF}{dB} = \frac{dF}{d\vartheta} = 0$, and we obtain B and ϑ as a function of A .

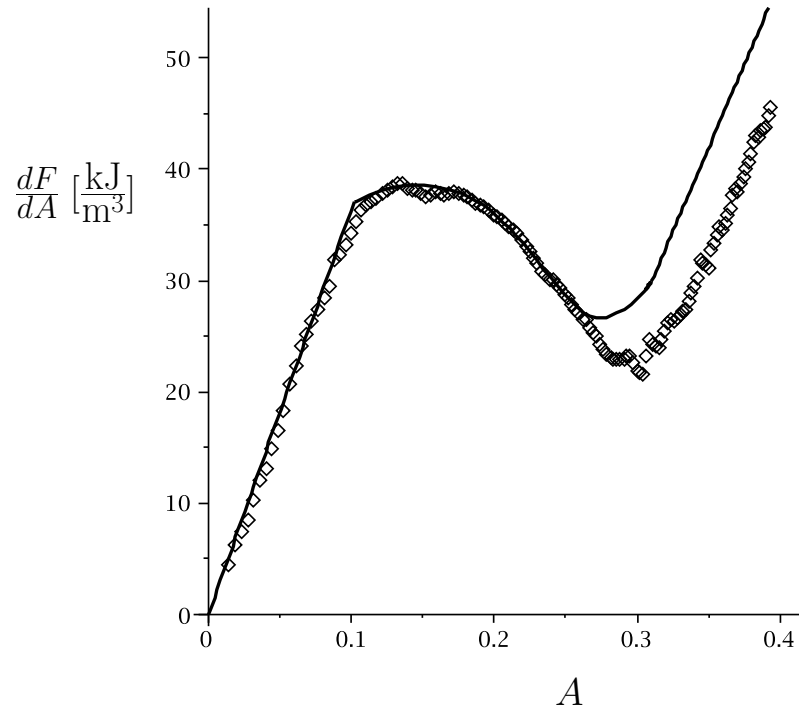


Figure 8.5: Same stress-strain data as in Fig. 8.4 with nonlinear purely elastic contributions by the network of polymer backbones subtracted. The exact procedure behind this subtraction is described in the main text. A curve that has been obtained with the help of our model is also shown. In this case, the amplitude S of the shear deformation has been free to adjust (material parameters characterizing this curve as specified in the main text).

As a result, by choosing appropriate values for the material parameters, we obtain curves for $\frac{dF}{dA}(A)$ which qualitatively correspond to the arrangement of the data points in Fig. 8.5. When we choose $\vartheta_0 = 0^\circ$ for the angle of initial director orientation, corresponding to $\hat{\mathbf{n}}^{\text{nw}} \parallel \hat{\mathbf{x}}$, we find pronounced cusps in the A - $\frac{dF}{dA}$ curve. These cusps are located at the strain amplitudes where the director orientation starts and ends. They correspond to the kinks in the curve of $\vartheta_0 = 0^\circ$ in Fig. 8.2. It is not surprising that such a threshold behavior occurs in the perfectly perpendicular geometry. We could demonstrate that a pretilt in the initial director orientation ($\vartheta_0 \neq 0^\circ$) smoothes out the stress-strain curves. Simultaneously, however, it leads to an increase of the slope in the intermediate strain region. Spatial heterogeneities of the materials also play a major role in this context. They correspond to a spatial variation of the values of the material parameters in our model. As a qualitative estimate, we have taken simple averages over stress-strain curves obtained for different values of only one material parameter. The result indicates that the curves will be strongly smoothed under the influence of spatial variations.

Comparing the curves obtained in this way for $S = 0$ to the data points in Fig. 8.5, there is a major difference: the length of the interval of negative slope cannot be quantitatively reproduced. The reasons for this fact may comprise additional effects induced by spatial heterogeneities, which then would have to be included in our model. Furthermore, nonlinear contributions not considered up to now (such as, for example, described by higher order coupling terms of strain and relative rotations) can extend the width of the interval. However, the suppression of the shear deformation by setting $S = 0$ also plays a major role, as will be demonstrated in the following.

8.5 Including shear deformations

When we want to inspect the situation of $S \neq 0$, we have to solve the system of equations given by $\frac{dF}{dB} = \frac{dF}{dS} = \frac{dF}{d\vartheta} = 0$. As a result, we obtain B , S , and ϑ as a function of A , noting that the corresponding algebra becomes quite complex. Here, we have investigated the situation of an initial director orientation given by $\vartheta_0 = 0^\circ$. An example for the stress-strain curves we obtain by this procedure is shown in Fig. 8.5. In addition, we have plotted the corresponding angle of director orientation as a function of the strain A in Fig. 8.6. We find that the threshold strain at which the director reorientation starts shifts to a lower value, when compared to the situation of $S = 0$. Significantly, the strain interval over which the director reorientation takes place becomes considerably longer when the shear amplitude S is free to adjust.

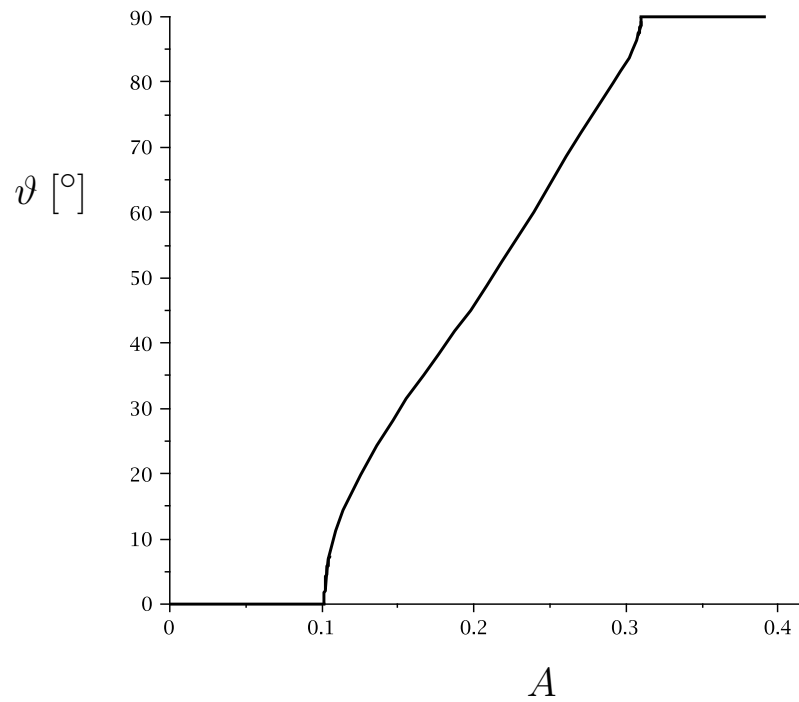


Figure 8.6: Angle of director orientation ϑ during the strain deformation which corresponds to the solid line in Fig. 8.5. The shear amplitude S has been free to adjust in this case (material parameters as given in the main text).

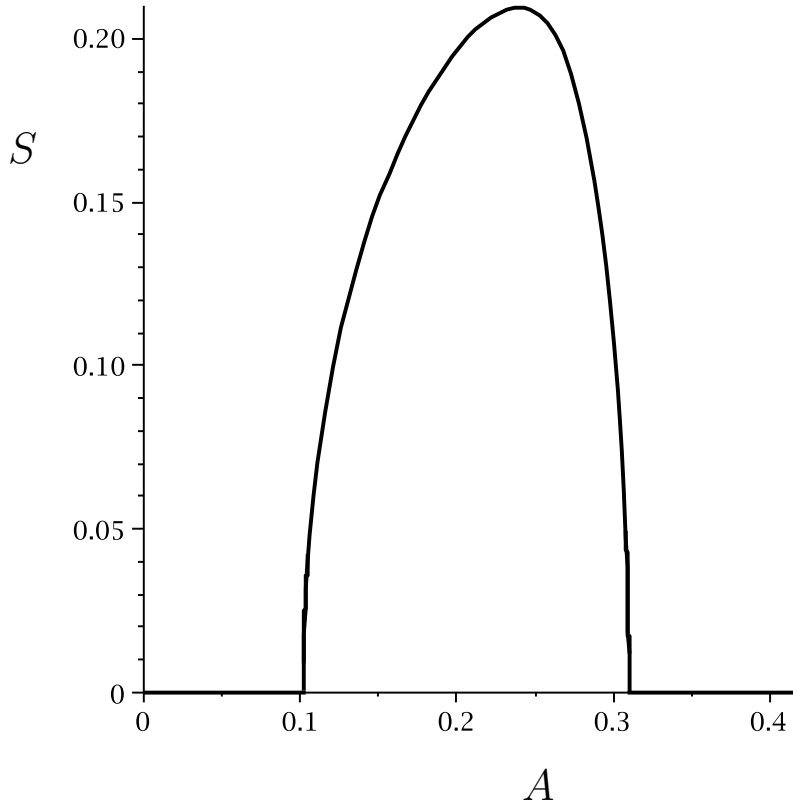


Figure 8.7: Shear deformation of a volume element exposed to a strain A , during which the shear amplitude S is free to adjust (material parameters as specified in the main text).

The shear amplitude S connected to the corresponding deformation is depicted in Fig. 8.7. We can see that no shear deformation occurs below threshold. When the threshold strain amplitude has been passed and the director starts to reorient, the shear deformation steeply increases. It steeply decreases again when the reorientation angle of the director comes close to 90° . In the reoriented state we find no shear deformation, as it has been the case for the low strain amplitudes.

We have plotted the evolution of the strain amplitude B corresponding to the resulting contraction in $\hat{\mathbf{x}}$ direction in Fig. 8.8. This is the direction parallel to the original orientations $\hat{\mathbf{n}}_0$ and $\hat{\mathbf{n}}_0^{\text{nw}}$. The dependence of the amplitude B on the externally imposed strain A reflects well the experimental observations [27]. For low strain amplitudes $A < A_c$ we obtain the linear isotropic elastic behavior of an incompressible material, characterized by $B = -\frac{1}{2}A$. As soon as the director reorientation sets in, however, this behavior changes qualitatively. We find that during the reorientation of the director

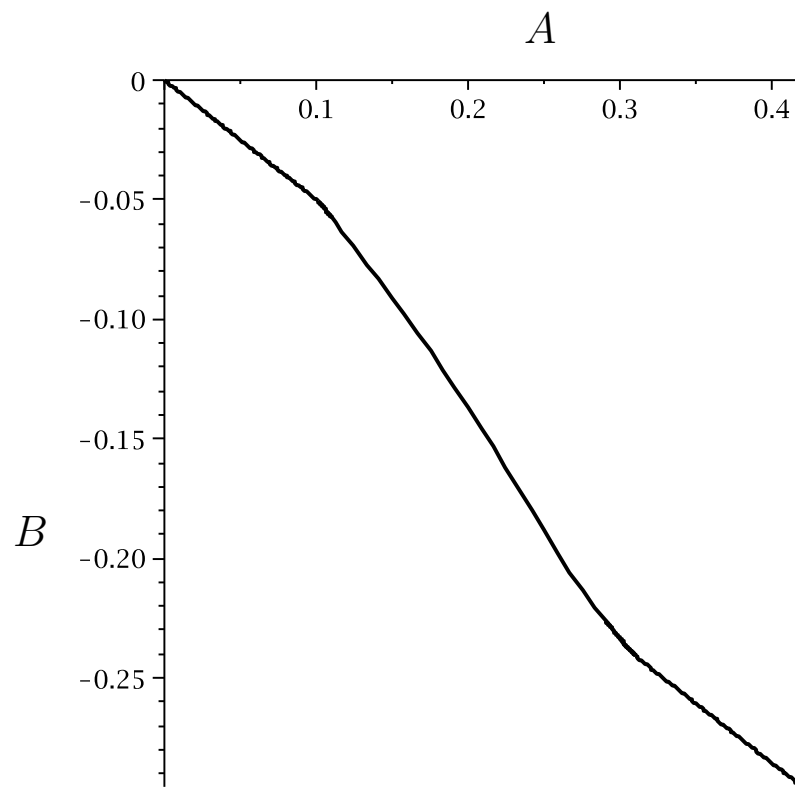


Figure 8.8: Amplitude B describing the lateral contraction of a volume element exposed to a strain A , where the shear amplitude S is free to adjust (material parameters as specified in the main text).

field the lateral contraction mainly occurs in $\hat{\mathbf{x}}$ direction and can be described approximately by $B \approx -A$. This means that the elastic deformation occurs mainly in the plane of the director reorientation. Consequently, the material in this regime reacts approximately in a two dimensional way, which agrees well with the experimental observation [3, 27]. This kind of deformation is often referred to as a “pure shear” deformation [71]. When the reorientation process has been completed, we again find a behavior close to $B = -\frac{1}{2}A$. We would like to stress at this point that the respective magnitudes of the lateral contractions for $A > A_c$ are mainly determined by the influence of the relative rotations $\tilde{\Omega}^{nw}$. When this second set of relative rotations is neglected, the elastic behavior of the materials is not recovered correctly. Related remarks have already been included in the discussion below Eq. (8.20).

In order to obtain the curves presented in Figs. 8.5 - 8.8, the values of the material parameters have been set to $c_1 = 121 \times 10^3 \text{ J m}^{-3}$, $D_1 = 22.9 \times 10^3 \text{ J m}^{-3}$, $D_1^{(2)} = 3.5 \times 10^3 \text{ J m}^{-3}$, $D_1^{(3)} = 0.9 \times 10^3 \text{ J m}^{-3}$, $D_2 = -42.0 \times 10^3 \text{ J m}^{-3}$, $D_2^{nw} = -42.2 \times 10^3 \text{ J m}^{-3}$, $D_2^{(2)} = -53.5 \times 10^3 \text{ J m}^{-3}$, and $D_2^{(2),nw} = -22.0 \times 10^3 \text{ J m}^{-3}$. Here, the value of c_1 follows from a fit of the initial slope of the stress-strain curve resulting from the experimental data points. As explained above, the relationship between D_1 , D_2 , and D_2^{nw} strongly influences the value of the threshold strain amplitude at which the reorientation of the director starts. $D_1^{(2)}$ and $D_1^{(3)}$ affect the length of the reorientation interval and the shape of the curve during this interval to a large extent. The same is true for $D_2^{(2)}$ and $D_2^{(2),nw}$, whereas D_2 and D_2^{nw} mainly influence the shape of the curve. As has already been mentioned above, the relative rotations $\tilde{\Omega}^{nw}$ and therefore the values of the material parameters D_2^{nw} and $D_2^{(2),nw}$ strongly affect the magnitude of the lateral contractions. We have carefully adjusted the values of the material parameters. However, small deviations from these values qualitatively lead to the same results.

Finally, we note that the slope of the stress-strain curve for high strain amplitudes is lower than for small strain amplitudes. This means that the generalized energy of the system increases less with increasing strain. If this were not the case, there would be no reason for the director to remain in the reoriented position.

8.6 Discussion and perspective

In this chapter, we have demonstrated that the experimentally observed process of director reorientation and the connected decrease in the slope of the stress-strain curves can be described by our model. In this context, we have explained that the two sets of relative rotations $\tilde{\Omega}$ and $\tilde{\Omega}^{nw}$ are necessary

so that the overall behavior of the materials can be recovered correctly. In addition, we have pointed out that one has to take into account explicitly the contribution of the nonlinear elastic behavior of the materials which is not connected to any reorientation of the director field. This plays a significant role for the interpretation of the stress-strain curves.

From our investigations, it is difficult to judge to what degree the shear described by $S \neq 0$ may be observed for a volume element which behaves in a representative way. We have found that both a deformation without shear $S = 0$ as well as a deformation including the shear $S \neq 0$ can qualitatively reproduce the stress-strain behavior observed in the experiments. When we allow for a shear deformation $S \neq 0$ to occur, the interval of the stress-strain curve with lower slope increases, or in other words, the strain interval during which the director reorients becomes larger. On the other hand we have demonstrated that the length of this interval is closely connected to the influence of nonlinear terms coupling strain to relative rotations (in our case the terms with the coefficients $D_2^{(2)}$ and $D_2^{nw,(2)}$). There is a clear tendency that more nonlinear terms of this kind further increase the length of the reorientation interval. Accordingly, the observed stress-strain curve could also be modeled by a deformation of $S = 0$.

On the whole we will probably find a mixture of the two scenarios and intermediate states. We have to be aware, that the materials which are produced by the common techniques show a large degree of spatial inhomogeneities. Already by optical investigation one usually can detect some of these heterogeneities. Furthermore, also recent studies using NMR and calorimetry measurements have revealed the same scenario on a different length scale [72, 73]. Due to these inhomogeneities and the interaction of the various volume elements in the polymer material, we will find an elastic deformation which is to a large degree spatially heterogeneous. In addition, the boundary conditions of clamping the material induce further inhomogeneities in the deformation. Therefore, a macroscopically observed strain behavior will always be an average over varying strain behavior across the whole sample.

As a consequence, we must conclude that the degree of elastic shear deformation of one volume element does not only result strictly from minimizing its generalized energy. It seems to be more likely that the shear deformation is predominantly imposed onto the respective volume element by spatially inhomogeneous deformations. The local, spatially varying strain deformations have to arrange themselves in a way such that for the clamped edges of the elastomer we find the macroscopic displacement imposed from outside. Already by Fig. 1.1 in the introduction we have illustrated a corresponding

situation, in which the degree of shear deformation is strongly varying across the sample. However, we have demonstrated that both for suppressed shear deformation $S = 0$ as well as for the energetically favored shear deformation $S \neq 0$ the stress-strain curves can qualitatively be reproduced.

Next, concerning the original data points in Fig. 8.3, reproduced from Ref. [27], we would like to compare the final slope for high strain amplitudes to the initial slope at low strains. We find approximately the same value for the two slopes, although the elastomer is stretched perpendicularly to the director in the beginning and in parallel direction at the end. Consequently, we may conclude that the overall elastic behavior of the sample is virtually isotropic with respect to the orientation of the director field. This justifies our choice of the elastic part of the generalized energy density (8.1), in which we have neglected anisotropic elastic terms. The remaining difference between the initial and final slope of the curves in Fig. 8.5 can be explained by the influence of the relative rotations.

It is very important to address the slope of the data points in Fig. 8.5 for intermediate strain amplitudes as well. Here, we find a negative slope. On the contrary, we find a pronounced positive slope when we look at the overall stress-strain curves in Figs. 8.3 and 8.4. This means that, in the regime of intermediate strain amplitudes, the elastomer gains energy due to the reorientation of the director field on increasing strain deformation. However, during every step of increasing the strain, the intrinsic nonlinear part of the purely elastic deformation of the network of polymer backbones costs more energy than is gained from the process of director reorientation. Therefore, the slope of the overall stress-strain curve is positive. We have also analyzed other recently measured stress-strain data in the same way [74], and we have qualitatively obtained the same results.

We conclude that the underlying nonlinear elastic behavior of the network of polymer backbones can to a great extent be separated from the reorientation process. However, it has a major influence on the overall appearance of the stress-strain data. It prevents a plateau-like zero-slope intermediate region of the stress-strain curves. Due to its dominant contribution, it also seems to be justified to break down the interpretation of the stress-strain data to the spatially homogeneous behavior of one representative volume element: the nonlinear elastic behavior can mainly be attributed to every volume element of the material as a local effect, which does not arise from the nonlocal interaction of the different volume elements. The experimental data which we have selected in order to test our model clearly show this trend.

Possibly, oriented elastomer films in which this nonlinear elastic behavior plays a less dominant role can be produced. In this case, spatial heterogeneities become important for the macroscopic response of the system, and

the interaction between different volume elements is certainly essential. Scenarios similar to those found for polydomain samples may occur [75]. Then the connection between the homogeneous behavior of one volume element and the overall behavior of the whole elastomer becomes a challenging problem. Phenomenologically, it may be attacked by an averaging approach in a spirit similar to a Maxwell construction. These issues can be investigated in future studies on the basis of our model.

Chapter 9

Conclusions

The continuum characterization of the macroscopic behavior of side-chain liquid single crystal elastomers (SCLSCEs) has been the major topic of this thesis. In particular, we have concentrated on the response that these materials show when they are exposed to static or quasistatic external electric and mechanical fields. We have put the development of a nonlinear macroscopic description of SCLSCEs into the center of this work.

In chapter 1, we have introduced the materials under investigation – SCLSCEs, namely. Belonging to a new class of materials, SCLSCEs consist of chemically crosslinked polymer backbones, to which mesogenic units are attached as side-groups. The arrangement of the mesogenic units shows liquid crystalline order in a monodomain, which spans the whole sample. Consequently, SCLSCEs combine properties of liquid crystalline phases on the one hand, and the elastic mechanical behavior of crosslinked polymers on the other hand. In addition, they feature further specific properties, which make them unique. Above all, we should mention in the latter context their static (and quasistatic) macroscopic coupling between the liquid crystalline director orientation and elastic mechanical deformations.

It is a decisive feature of our continuum description that this coupling is taken into account explicitly. This is possible by including as macroscopic variables the relative rotations between the director orientation and the polymer network, the state of which is assumed to be connected to the mechanical deformations of the elastomers. A linear formulation of this model has first been given by de Gennes [36] and has been introduced in chapter 2. There, we have derived an expression for the generalized energy density in order to give a linear macroscopic characterization of nematic or cholesteric SCLSCEs when exposed to a static or quasistatic external electric or mechanical field. A current state of the respective elastomer is described by the field of director orientation on the one hand, and the displacement field characterizing the current state of mechanical distortion on the other hand.

We have first concentrated in chapter 3 on the investigation of an effect specific for cholesteric SCLSCEs, which has been named rotatoelectric for the following reason. When a spatially homogeneous external electric field is applied parallel to the cholesteric helical axis, and when the electric field amplitude is quasistatically increased or decreased, the director orientation has been predicted to rotate around the cholesteric helical axis relatively to the polymer network. The magnitude of this effect has been found to be linear in the external electric field amplitude and the wave number associated with the cholesteric helical structure. In particular, the sense of rotation should depend on the handedness of the cholesteric helix. We stress that the variables of relative rotations play a decisive role as generators of rotatoelectricity. Since the rotatoelectric effect has not been studied experimentally yet, we have discussed the ingredients important for an experimental observation, with a major focus on the boundary conditions of the director field.

Next, we have turned to the dielectric effects of cholesteric SCLSCEs in chapter 4. We have studied the same geometry as in the rotatoelectric case. The dielectric effects then become important at elevated external electric field amplitudes, if the director tends to align parallel to the electric field direction. From a linear stability analysis, we have predicted the competition of two qualitatively different instabilities at threshold. One of them corresponds to the instability of low molecular weight liquid crystals observed at the Fréedericksz transition, and it is spatially homogeneous in the directions perpendicular to the helical axis. We have shown that the influence of the boundaries, the cholesteric helical structure, as well as the anchoring of the director orientation within the polymer network determine the critical external electric field amplitude. On the other hand, the second instability we have identified is qualitatively different in that it features undulations in director orientation and distortion in at least one direction perpendicular to the cholesteric helical axis. This instability arises from the specific feature of SCLSCEs of coupling the director orientation to the elastic mechanical deformation. In particular, we have demonstrated and explained that this instability can be preferred over the Fréedericksz-like instability at threshold only for one specific sign of the material parameter which couples relative rotations to the strain deformations (D_2). In this context, we have also found that the linear continuum model includes the possibility of a specific set of values of the material parameters that allow a reorientation of the director field without distorting the elastomer. The results in this chapter are obtained formally identically in the case of an external magnetic field.

In chapter 5, we have studied elastic mechanical deformations of cholesteric SCLSCEs. First, we have focused on compressions and dilations imposed onto the elastomers parallel to the cholesteric helical axis. After that,

we have described the effects of compressive and dilative forces applied perpendicularly to the helical axis. In the latter case, we have predicted a twisting or untwisting of the structure of the cholesteric director orientation in general. If the elastomer is stretched or compressed perpendicularly to the cholesteric helical axis in two orthogonal directions by equal force densities, we find a compression or dilation of the cholesteric structure along the helical axis. This case is important from an application point of view, because it has been exploited for the construction of tunable mirrorless lasers.

Based on the linear picture, we have in both of these chapters, 4 and 5, suggested ways of experimental access to the values of the material parameters that are related to the variables of relative rotations (D_1 and D_2).

Naturally, the predictions made by the linear continuum model are in general restricted to small amplitudes of strain deformations and relative rotations. However, many of the unique features of SCLSCEs are connected to their nonlinear behavior. We have therefore developed a nonlinear macroscopic description of the materials in chapter 6, which can be viewed as the central part of our work. Our first step in this direction has been to generalize our macroscopic picture of nematic and cholesteric SCLSCEs to that of elastic materials of two coupled preferred directions. One of these directions is given by the liquid crystalline director. The other one is imprinted into the polymer network during the procedure of synthesis and is identified with the direction to which the director rotates back when the external forces are released. We have made the assumption that the orientation of the second direction is connected to the distortions of the polymer network. Our major task in this context has been to derive nonlinear expressions for the variables of relative rotations between these two directions, and to connect these expressions to the components of the director field and the displacement field. It has turned out that two sets of variables of relative rotations are necessary in order to respect the conditions of symmetry. Our nonlinear description contains the linear picture by de Gennes as a limiting case.

As a first application of our nonlinear model, we have investigated the static (or quasistatic) shear deformation of a nematic SCLSCE in chapter 7. The shear has been applied in a plane containing the director orientation. We have recovered the linear effect already analyzed in earlier work – a reorientation of the director due to the imposed shear deformation. As an additional nonlinear effect, however, we have found that the reorientation of the director acts back onto the elastic deformation and leads to compressive and dilative strains. Our analysis has been made using an expression of the generalized energy density to cubic order. We have demonstrated that all the effects are mediated by the variables of relative rotations and are not obtained without these variables. Significantly, the effects are qualitatively described

already by the quadratic terms in the generalized energy density when the nonlinear expressions for the variables of relative rotations are included.

Eventually, in chapter 8, we have turned to the inspection of the characteristic results obtained for nematic SCLSCEs during nonlinear stress-strain experiments. It has been found for nematic SCLSCEs stretched perpendicularly to the initial director orientation that their director reorients towards the stretching direction. Closely connected to this reorientation is a decrease in the slope of the stress-strain curve. We could demonstrate in chapter 8 that our model describes the experimentally observed behavior. In particular, we have semi-quantitatively compared the predictions of our model to the results obtained during recent stress-strain experiments which have been reported in Ref. [27]. We have shown that, within our model, the decrease in the slope of the stress-strain curve is associated with the coupling between the director orientation and the elastic mechanical deformation, described by the variables of relative rotations. As one result, however, we have found that a qualitatively different part of the elastic response dominates the overall appearance of the stress-strain curve. This is the kind of elastic response already present in the absence of relative rotations, which may be attributed solely to the elastic deformation of the network of crosslinked polymer backbones. Since this is a local effect, we could reduce our analysis to that of a single representative volume element. In addition, we have discussed the role of shear deformations during the stretching process. We have found that shear deformations do not qualitatively influence the overall response of the materials. Furthermore, we have demonstrated that both of the two sets of nonlinear relative rotations must be included in order to give a complete view of the experimental situation. This confirms our macroscopic picture of the materials.

In closing this summary, we mention that we have kept the introduction of our nonlinear model to be quite general. Also other materials of coupled preferred directions may be characterized in the same spirit, using nonlinear relative rotations between the preferred directions as the crucial variables. As indicated before, uniaxial magnetic gels appear to be natural candidates in this respect.

Concerning the future development of our model, one of the next steps would clearly be the extension to a dynamic description, which includes nonlinear strain deformations and the nonlinear variables of relative rotations. A possible application of such a dynamic picture can be found in the field of swelling dynamics of liquid crystalline elastomers. Various experiments have already been performed in this area, using low molecular weight liquid crystals as a swelling agent. A complete macroscopic characterization of these experiments is still forthcoming.

Appendix A

Variational derivatives of the generalized energy

In this appendix, we list the variational derivatives of the generalized energy $\mathcal{F} = \int F d^3r$ with respect to the five independent state variables u_x , u_y , u_z , n_z , and Δ . Here, the generalized energy density F is given by Eq. (3.6), and we use the abbreviations $\bar{c}_1 = e_1 - e_2 + \gamma_1 + \zeta^{(R)}$ and $\bar{c}_2 = \gamma_1 + \zeta^{(R)}$ introduced at the end of section 3.1. We neglect energetic surface contributions. In analogy to Eq. (3.6) we include the dielectric contribution, but we put it into squared brackets in order to indicate that its influence is not studied in chapter 3. Setting the resulting expressions equal to zero, we obtain

$$\begin{aligned}
0 = \frac{\delta \mathcal{F}}{\delta u_x} = & -c_1 \left\{ 2(\partial_x^2 u_x) + (\partial_y^2 u_x) + (\partial_z^2 u_x) + (\partial_x \partial_y u_y) + (\partial_x \partial_z u_z) \right\} \\
& -c_2 \left\{ (\partial_x^2 u_x) + (\partial_x \partial_y u_y) + (\partial_x \partial_z u_z) \right\} \\
& -D_1 \left\{ \frac{1}{2}(\partial_y \Delta) + \frac{1}{4}(\partial_y^2 u_x) - \frac{1}{4}(\partial_x \partial_y u_y) \right. \\
& \quad + \frac{1}{2}n_{ox} \left[(\partial_z n_z) + \frac{1}{2}n_{ox} \left((\partial_z^2 u_x) - (\partial_x \partial_z u_z) \right) \right. \\
& \quad \quad + \frac{1}{2}q_0 n_{ox} \left((\partial_z u_y) - (\partial_y u_z) \right) \\
& \quad \quad + \frac{1}{2}n_{oy} \left((\partial_z^2 u_y) - (\partial_y \partial_z u_z) \right) \\
& \quad \quad \left. \left. - \frac{1}{2}q_0 n_{oy} \left((\partial_z u_x) - (\partial_x u_z) \right) \right] \right. \\
& \quad \left. - \frac{1}{2}q_0 n_{oy} \left[n_z + \frac{1}{2}n_{ox} \left((\partial_z u_x) - (\partial_x u_z) \right) \right. \right. \\
& \quad \quad \left. \left. + \frac{1}{2}n_{oy} \left((\partial_z u_y) - (\partial_y u_z) \right) \right] \right\}
\end{aligned}$$

$$\begin{aligned}
& - D_2 \left\{ n_{ox} n_{oy} \left[- (\partial_x \Delta) - (\partial_x \partial_y u_x) \right. \right. \\
& \quad \left. \left. + \frac{1}{2} (\partial_x^2 u_y) + \frac{1}{2} (\partial_y^2 u_y) + \frac{1}{2} (\partial_z^2 u_y) \right] \right. \\
& \quad \left. - q_0 n_{ox} n_{oy} (\partial_z u_x) + \frac{1}{2} n_{ox}^2 \left[(\partial_y \Delta) + (\partial_y^2 u_x) + (\partial_z^2 u_x) \right] \right. \\
& \quad \left. + \frac{1}{2} n_{oy}^2 \left[- (\partial_y \Delta) - (\partial_y^2 u_x) \right] + \frac{1}{2} q_0 (n_{ox}^2 - n_{oy}^2) (\partial_z u_y) \right. \\
& \quad \left. + \frac{1}{2} n_{ox} (\partial_z n_z) - \frac{1}{2} q_0 n_{oy} n_z \right\} \\
& - \frac{1}{2} \bar{c}_2 q_0^2 \left\{ E_x (n_{ox}^2 - n_{oy}^2) + 2 E_y n_{ox} n_{oy} \right\}, \tag{A.1}
\end{aligned}$$

$$\begin{aligned}
0 = \frac{\delta \mathcal{F}}{\delta u_y} = & - c_1 \left\{ (\partial_x \partial_y u_x) + (\partial_x^2 u_y) + 2 (\partial_y^2 u_y) + (\partial_z^2 u_y) + (\partial_y \partial_z u_z) \right\} \\
& - c_2 \left\{ (\partial_x \partial_y u_x) + (\partial_y^2 u_y) + (\partial_y \partial_z u_z) \right\} \\
& - D_1 \left\{ - \frac{1}{2} (\partial_x \Delta) - \frac{1}{4} (\partial_x \partial_y u_x) + \frac{1}{4} (\partial_x^2 u_y) \right. \\
& \quad \left. + \frac{1}{2} n_{oy} \left[(\partial_z n_z) + \frac{1}{2} n_{ox} \left((\partial_z^2 u_x) - (\partial_x \partial_z u_z) \right) \right. \right. \\
& \quad \left. \left. + \frac{1}{2} q_0 n_{ox} \left((\partial_z u_y) - (\partial_y u_z) \right) \right. \right. \\
& \quad \left. \left. + \frac{1}{2} n_{oy} \left((\partial_z^2 u_y) - (\partial_y \partial_z u_z) \right) \right. \right. \\
& \quad \left. \left. - \frac{1}{2} q_0 n_{oy} \left((\partial_z u_x) - (\partial_x u_z) \right) \right] \right. \\
& \quad \left. + \frac{1}{2} q_0 n_{ox} \left[n_z + \frac{1}{2} n_{ox} \left((\partial_z u_x) - (\partial_x u_z) \right) \right. \right. \\
& \quad \left. \left. + \frac{1}{2} n_{oy} \left((\partial_z u_y) - (\partial_y u_z) \right) \right] \right\} \\
& - D_2 \left\{ n_{ox} n_{oy} \left[(\partial_y \Delta) + \frac{1}{2} (\partial_x^2 u_x) \right. \right. \\
& \quad \left. \left. + \frac{1}{2} (\partial_y^2 u_x) + \frac{1}{2} (\partial_z^2 u_x) - (\partial_x \partial_y u_y) \right] \right. \\
& \quad \left. + q_0 n_{ox} n_{oy} (\partial_z u_y) + \frac{1}{2} n_{ox}^2 \left[(\partial_x \Delta) - (\partial_x^2 u_y) \right] \right. \\
& \quad \left. + \frac{1}{2} n_{oy}^2 \left[- (\partial_x \Delta) + (\partial_x^2 u_y) + (\partial_z^2 u_y) \right] \right. \\
& \quad \left. + \frac{1}{2} q_0 (n_{ox}^2 - n_{oy}^2) (\partial_z u_x) + \frac{1}{2} n_{oy} (\partial_z n_z) + \frac{1}{2} q_0 n_{ox} n_z \right\}
\end{aligned}$$

$$-\frac{1}{2}\bar{c}_2q_0^2\left\{2E_xn_{ox}n_{oy}-E_y(n_{ox}^2-n_{oy}^2)\right\}, \quad (\text{A.2})$$

$$\begin{aligned} 0 = \frac{\delta\mathcal{F}}{\delta u_z} = & -c_1\left\{(\partial_x\partial_zu_x)+(\partial_y\partial_zu_y)+(\partial_x^2u_z)+(\partial_y^2u_z)+2(\partial_z^2u_z)\right\} \\ & -c_2\left\{(\partial_x\partial_zu_x)+(\partial_y\partial_zu_y)+(\partial_z^2u_z)\right\} \\ & -D_1\left\{-\frac{1}{2}n_{ox}\left[(\partial_xn_z)+\frac{1}{2}n_{ox}\left((\partial_x\partial_zu_x)-(\partial_x^2u_z)\right)\right.\right. \\ & \quad \left.\left.+\frac{1}{2}n_{oy}\left((\partial_x\partial_zu_y)-(\partial_x\partial_yu_z)\right)\right]\right. \\ & \quad \left.-\frac{1}{2}n_{oy}\left[(\partial_y n_z)+\frac{1}{2}n_{ox}\left((\partial_y\partial_zu_x)-(\partial_x\partial_yu_z)\right)\right.\right. \\ & \quad \left.\left.+\frac{1}{2}n_{oy}\left((\partial_y\partial_zu_y)-(\partial_y^2u_z)\right)\right]\right\} \\ & +D_2\left\{n_{ox}n_{oy}(\partial_x\partial_yu_z)+\frac{1}{2}n_{ox}^2(\partial_x^2u_z)+\frac{1}{2}n_{oy}^2(\partial_y^2u_z)\right. \\ & \quad \left.-\frac{1}{2}n_{ox}(\partial_xn_z)-\frac{1}{2}n_{oy}(\partial_y n_z)\right\}, \quad (\text{A.3}) \end{aligned}$$

$$\begin{aligned} 0 = \frac{\delta\mathcal{F}}{\delta n_z} = & D_1\left\{n_z+\frac{1}{2}n_{ox}\left((\partial_zu_x)-(\partial_xu_z)\right)+\frac{1}{2}n_{oy}\left((\partial_zu_y)-(\partial_yu_z)\right)\right\} \\ & +\frac{1}{2}D_2\left\{n_{ox}\left((\partial_zu_x)+(\partial_xu_z)\right)+n_{oy}\left((\partial_zu_y)+(\partial_yu_z)\right)\right\} \\ & -K_1\left\{n_{ox}(\partial_y\partial_z\Delta)-n_{oy}(\partial_x\partial_z\Delta)\right. \\ & \quad \left.-q_0n_{ox}(\partial_x\Delta)-q_0n_{oy}(\partial_y\Delta)+(\partial_z^2n_z)\right\} \\ & -K_2\left\{n_{ox}\left[-(\partial_y\partial_z\Delta)+n_{ox}(\partial_y^2n_z)-n_{oy}(\partial_x\partial_y n_z)\right]\right. \\ & \quad \left.-n_{oy}\left[-(\partial_x\partial_z\Delta)+n_{ox}(\partial_x\partial_y n_z)-n_{oy}(\partial_x^2n_z)\right]\right\} \\ & +K_3\left\{q_0n_{ox}\left[n_{ox}n_{oy}(\partial_y\Delta)+n_{ox}^2(\partial_x\Delta)+q_0n_{ox}n_z\right]\right. \\ & \quad \left.+q_0n_{oy}\left[n_{ox}n_{oy}(\partial_x\Delta)+n_{oy}^2(\partial_y\Delta)+q_0n_{oy}n_z\right]\right. \\ & \quad \left.-\left[n_{ox}^2(\partial_x^2n_z)+2n_{ox}n_{oy}(\partial_x\partial_y n_z)+n_{oy}^2(\partial_y^2n_z)\right]\right\} \\ & +\bar{c}_1q_0\left\{E_xn_{oy}-E_yn_{ox}\right\} \\ & \left[-\epsilon_aE_z\left\{E_x(n_{ox}-n_{oy}\Delta)\right.\right. \end{aligned}$$

$$+ E_y(n_{oy} + n_{ox}\Delta) + E_z n_z \Big\} \Big], \quad (\text{A.4})$$

$$\begin{aligned}
0 = \frac{\delta \mathcal{F}}{\delta \Delta} = & D_1 \left\{ \Delta + \frac{1}{2} \left((\partial_y u_x) - (\partial_x u_y) \right) \right\} \\
& + D_2 \left\{ n_{ox} n_{oy} \left[- (\partial_x u_x) + (\partial_y u_y) \right] \right. \\
& \quad \left. + \frac{1}{2} \left(n_{ox}^2 - n_{oy}^2 \right) \left[(\partial_x u_y) + (\partial_y u_x) \right] \right\} \\
& - K_1 \left\{ n_{ox} \left[n_{ox} (\partial_y^2 \Delta) - n_{oy} (\partial_x \partial_y \Delta) + (\partial_y \partial_z n_z) \right] \right. \\
& \quad \left. - n_{oy} \left[n_{ox} (\partial_x \partial_y \Delta) - n_{oy} (\partial_x^2 \Delta) + (\partial_x \partial_z n_z) \right] \right\} \\
& + K_2 \left\{ - (\partial_z^2 \Delta) + n_{ox} (\partial_y \partial_z n_z) - n_{oy} (\partial_x \partial_z n_z) \right. \\
& \quad \left. - q_0 n_{ox} (\partial_x n_z) - q_0 n_{oy} (\partial_y n_z) \right\} \\
& - K_3 \left\{ n_{ox} n_{oy} \left[n_{ox} n_{oy} \left((\partial_x^2 \Delta) + (\partial_y^2 \Delta) \right) + (\partial_x \partial_y \Delta) \right. \right. \\
& \quad \left. \left. + q_0 n_{ox} (\partial_y n_z) + q_0 n_{oy} (\partial_x n_z) \right] \right. \\
& \quad \left. + n_{ox}^2 \left[n_{ox} n_{oy} (\partial_x \partial_y \Delta) + n_{ox}^2 (\partial_x^2 \Delta) + q_0 n_{ox} (\partial_x n_z) \right] \right. \\
& \quad \left. + n_{oy}^2 \left[n_{ox} n_{oy} (\partial_x \partial_y \Delta) + n_{oy}^2 (\partial_y^2 \Delta) + q_0 n_{oy} (\partial_y n_z) \right] \right\} \\
& + \zeta^{(R)} q_0 E_z \\
& \left[- \epsilon_a (-n_{oy} E_x + n_{ox} E_y) \left\{ E_x (n_{ox} - n_{oy} \Delta) \right. \right. \\
& \quad \left. \left. + E_y (n_{oy} + n_{ox} \Delta) + E_z n_z \right\} \right]. \quad (\text{A.5})
\end{aligned}$$

Appendix B

Electrostrictive effects in cholesteric side-chain liquid single crystal elastomers

As mentioned in the main text of chapter 4, in this appendix we want to study the effect of the electrostrictive contribution $\tilde{\chi}_{ijkl}^E E_i E_j \varepsilon_{kl}$ to the generalized energy density F in Eq. (2.9). Therefore, we expand the electrostrictive tensor $\tilde{\chi}_{ijkl}^E$ assuming local uniaxial symmetry of the system. The symmetry axis is given by the components n_i of the director. In this way, we can rewrite the electrostrictive tensor as

$$\begin{aligned}\tilde{\chi}_{ijkl}^E &= \tilde{\chi}_1 \delta_{ij} \delta_{kl} + \tilde{\chi}_2 (\delta_{ik} \delta_{jl} + \delta_{il} \delta_{jk}) \\ &\quad + \tilde{\chi}_3 \delta_{ij} n_k n_l + \tilde{\chi}_4 \delta_{kl} n_i n_j \\ &\quad + \tilde{\chi}_5 (\delta_{ik} n_j n_l + \delta_{jk} n_i n_l + \delta_{il} n_j n_k + \delta_{jl} n_i n_k) \\ &\quad + \tilde{\chi}_6 n_i n_j n_k n_l.\end{aligned}\tag{B.1}$$

We then have to introduce this expression into the term $\tilde{\chi}_{ijkl}^E E_i E_j \varepsilon_{kl}$ and expand the result up to quadratic order in the five independent variables u_x , u_y , u_z , n_z , and Δ of the system. For this purpose we take into account that $E_i = E \delta_{iz}$, and we need the nonlinear expressions for the components of the Eulerian strain tensor ε up to quadratic order, which are given by $\varepsilon_{ij} = \frac{1}{2}(\partial_i u_j + \partial_j u_i) - \frac{1}{2}(\partial_i u_k)(\partial_j u_k)$ [41, 43]. After that, the variational derivatives of the resulting expression with respect to the five variables u_x , u_y , u_z , n_z , and Δ have to be calculated and added to Eqs. (A.1)-(A.5), where we once again neglect energetic surface contributions. We do not present the explicit calculations here because they follow the same procedure as those for the other terms arising from Eq. (2.9).

The results we have obtained in this way do not qualitatively differ from

those we have already presented in section 4. In the case of a laterally homogeneous solution (see section 4.2), the instability is still described by Eqs. (4.22)-(4.24) and (4.28)-(4.30), respectively, where only the amplitudes are slightly influenced by the external electric field: in these equations, the ratio $\frac{\alpha}{\beta}$ now has to be replaced following the scheme

$$\frac{\alpha}{\beta} \rightarrow \frac{\alpha - (\tilde{\chi}_3 + \frac{1}{2}\tilde{\chi}_5) E^2}{\beta - (\tilde{\chi}_1 + \tilde{\chi}_2) E^2}. \quad (\text{B.2})$$

Taking into account terms up to quadratic order, the expression for the amplitude of the critical external electric field turns into

$$E_c^2 = \frac{\alpha^2 - \beta A}{2\alpha (\tilde{\chi}_3 + \frac{1}{2}\tilde{\chi}_5) - \beta\epsilon_a - (\tilde{\chi}_1 + \tilde{\chi}_2) A}, \quad (\text{B.3})$$

where

$$A = D_1 + K_3 q_0^2 + K_1 \left(\frac{\pi}{d}\right)^2. \quad (\text{B.4})$$

Usually, for common nonpolar elastomers, the electrostrictive coefficients are very small compared to the other material parameters in Eq. (2.9). For example, Ref. [76] reports the measurement of electrostrictive coefficients of polyurethane, which shows unusually large electrostriction. The magnitude of the coefficients listed there does not imply any qualitative impact on our results. Consequently, we expect the expression for the threshold value E_c^2 to yield again Eqs. (4.21) and (4.31). This can be verified by taking the limit of $\tilde{\chi}_i \rightarrow 0$ ($i = 1, 2, 3, 5$) in Eq. (B.3).

Concerning the laterally inhomogeneous instability (see section 4.3), the results presented in the main text are neither influenced qualitatively by the electrostrictive corrections. Eqs. (A.1)-(A.5) including the additional terms arising from electrostrictive contributions can still be solved by ansatz (4.10), which implies the undulations we have found in section 4.3. When we then investigate the resulting set of ordinary differential equations numerically for a common nonpolar elastomer, it is a good approximation to set the electrostrictive coefficients equal to zero for the reasons already mentioned above.

Appendix C

Symmetry relations and an alternative definition of relative rotations

In the first part of this appendix, we discuss an alternative definition of the variables of relative rotations, which also takes into account the presence of the two local preferred directions $\hat{\mathbf{n}}$ and $\hat{\mathbf{n}}^{\text{nw}}$ in nematic and cholesteric SCLSCEs. The symmetry relations connected to these preferred directions play a major role in this context. After that, in the second part of the appendix, we demonstrate that the alternative definition of the nonlinear relative rotations leads to the same expression of the generalized energy density that we have derived in chapter 8 and used in order to characterize the nonlinear stress-strain behavior of nematic SCLSCEs.

Talking about the variables of relative rotations, it might be more suggestive at a first glance to start the construction of the macroscopic variables with a rotation matrix. In our case, the matrix should describe the rotation of the direction given by $\hat{\mathbf{n}}^{\text{nw}}$ to the direction given by $\hat{\mathbf{n}}$. We call this matrix \mathbf{W} .

As we have already explained in section 6.5, two spaces must be thought of in order to statically describe a distorted material in general. One is connected to the initial, undistorted state of the material and may be called the initial space, the other one is connected to the distorted state and may be called final space [41, 42]. Symmetry transformations in one of the two spaces do not imply the respective transformations in the other space. For example, this means that the transformation $\hat{\mathbf{n}}_0 \rightarrow -\hat{\mathbf{n}}_0$, which takes place in the initial space, does not imply $\hat{\mathbf{n}} \rightarrow -\hat{\mathbf{n}}$ in the final space, and vice versa. The same is true for $\hat{\mathbf{n}}_0^{\text{nw}}$ and $\hat{\mathbf{n}}^{\text{nw}}$.

We can see from definition (6.7) that \mathbf{S} is odd under the symmetry trans-

formations $\hat{\mathbf{n}}_0 \rightarrow -\hat{\mathbf{n}}_0$ and $\hat{\mathbf{n}} \rightarrow -\hat{\mathbf{n}}$, separately. From definition (6.8) we infer that \mathbf{R} is odd under the symmetry transformations $\hat{\mathbf{n}}_0^{\text{nw}} \rightarrow -\hat{\mathbf{n}}_0^{\text{nw}}$ and $\hat{\mathbf{n}}^{\text{nw}} \rightarrow -\hat{\mathbf{n}}^{\text{nw}}$, separately. A rotation matrix $\mathbf{S} \cdot \mathbf{R}$ describes how a direction parallel to $\hat{\mathbf{n}}^{\text{nw}}$ is rotated to a direction parallel to $\hat{\mathbf{n}}$, however, this product matrix is odd under $\hat{\mathbf{n}}_0 \rightarrow -\hat{\mathbf{n}}_0$, $\hat{\mathbf{n}}_0^{\text{nw}} \rightarrow -\hat{\mathbf{n}}_0^{\text{nw}}$, $\hat{\mathbf{n}} \rightarrow -\hat{\mathbf{n}}$, and $\hat{\mathbf{n}}^{\text{nw}} \rightarrow -\hat{\mathbf{n}}^{\text{nw}}$, separately. In order to set up a hydrodynamic-like Eulerian picture, the variables must be independent of the initial space. Formally, we thus have to insert an additional matrix that transforms $\hat{\mathbf{n}}_0^{\text{nw}}$ into $\hat{\mathbf{n}}_0$ according to $\hat{\mathbf{n}}_0 = \mathbf{T} \cdot \hat{\mathbf{n}}_0^{\text{nw}}$, so that we define $\mathbf{W} = \mathbf{S} \cdot \mathbf{T} \cdot \mathbf{R}$.

\mathbf{W} is the matrix we have been looking for, which rotates $\hat{\mathbf{n}}^{\text{nw}}$ to $\hat{\mathbf{n}}$. However, we cannot use the matrix \mathbf{W} directly as a macroscopic variable: as already mentioned in section 6.2, in a hydrodynamic-like Eulerian picture the macroscopic variables contributing to the generalized energy density must vanish when the system is in equilibrium and no external forces are applied. Subtracting unity from \mathbf{W} in order to satisfy this condition leads to problems, because \mathbf{W} is odd with respect to the transformations $\hat{\mathbf{n}} \rightarrow -\hat{\mathbf{n}}$ and $\hat{\mathbf{n}}^{\text{nw}} \rightarrow -\hat{\mathbf{n}}^{\text{nw}}$, separately. Consequently, the resulting object would not have a clearly defined symmetry behavior under these transformations. The problem cannot be solved by simple projections as those which have led to the definitions (6.1) and (6.2).

We therefore propose a different approach. All the information stored in the rotation matrix \mathbf{W} is given by the direction of the rotation axis and the angle of rotation. However, the same information is also provided by the cross product of $\hat{\mathbf{n}}^{\text{nw}}$ and $\hat{\mathbf{n}}$, so that, alternatively to Eqs. (6.1) and (6.2), in this appendix we define as variables of relative rotations

$$\tilde{\Omega}^{\text{alt}} := \hat{\mathbf{n}}^{\text{nw}} \times \hat{\mathbf{n}}. \quad (\text{C.1})$$

The components of $\tilde{\Omega}^{\text{alt}}$ read

$$\tilde{\Omega}_i^{\text{alt}} = \epsilon_{ijk} n_j^{\text{nw}} n_k. \quad (\text{C.2})$$

If we use this definition of the relative rotations, we can show that expression (8.1) for the generalized energy density F in chapter 8 is obtained identically.

It is straightforward to verify that

$$\tilde{\Omega}_i \tilde{\Omega}_i = \tilde{\Omega}_i^{\text{nw}} \tilde{\Omega}_i^{\text{nw}} = \tilde{\Omega}_i^{\text{alt}} \tilde{\Omega}_i^{\text{alt}}. \quad (\text{C.3})$$

For this reason, the terms in Eq. (8.1) with the coefficients D_1 , $D_1^{(2)}$, and $D_1^{(3)}$ are recovered.

Coupling $\tilde{\mathbf{\Omega}}^{\text{alt}}$ to the strain $\boldsymbol{\varepsilon}$ in lowest order and respecting the symmetry behavior of F leads to two terms

$$n_i \varepsilon_{ij} \epsilon_{jkl} n_k^{nw} \tilde{\Omega}_l^{\text{alt}} = -[n_i \varepsilon_{ij} n_j - n_i \varepsilon_{ij} n_j^{nw} (n_k n_k^{nw})] = -n_i \varepsilon_{ij} \tilde{\Omega}_j \quad (\text{C.4})$$

and

$$n_i^{nw} \varepsilon_{ij} \epsilon_{jkl} n_k \tilde{\Omega}_l^{\text{alt}} = -[-n_i^{nw} \varepsilon_{ij} n_j^{nw} + n_i^{nw} \varepsilon_{ij} n_j (n_k n_k^{nw})] = -n_i^{nw} \varepsilon_{ij} \tilde{\Omega}_j^{nw}. \quad (\text{C.5})$$

They correspond to the terms with the coefficients D_2 and D_2^{nw} in the generalized energy density F of Eq. (8.1). The terms with the coefficients $D_2^{(2)}$ and $D_2^{nw,(2)}$ in Eq. (8.1) are obtained in the same way.

Therefore, a characterization of the materials by the two definitions of relative rotations (6.1) and (6.2) on the one hand, and (C.1) on the other hand are identical as long as we confine ourselves to the terms listed in expression (8.1). In particular, the analysis presented in chapter 8 would be the same if one uses as an alternative definition of relative rotations expression (C.1).

Appendix D

Finite shear deformation of an elastically anisotropic nematic side-chain liquid single crystal elastomer

In chapter 7 we have studied the reaction of a nematic SCLSCE to an imposed static or quasistatic shear deformation. There, we have concentrated on the role the relative rotations play during this kind of deformation. Because of that we have assumed an isotropic elastic mechanical behavior of the materials in the case that no reorientation of the director occurs. We now demonstrate that an anisotropic elastic mechanical behavior of the elastomers does not qualitatively change the results derived in chapter 7.

If we want to include an anisotropic elastic mechanical behavior of the elastomers into our description, we have to supplement our expression for the generalized energy density (7.3) by some additional terms (compare, e.g., Refs. [77] and [78]):

$$\begin{aligned} & c_3 \varepsilon_{ii} n_j^{nw} \varepsilon_{jk} n_k^{nw} + c_4 n_i^{nw} \varepsilon_{ij} \varepsilon_{jk} n_k^{nw} + c_5 n_i^{nw} \varepsilon_{ij} n_j^{nw} n_k^{nw} \varepsilon_{kl} n_l^{nw} \\ & + \zeta_4 \varepsilon_{ij} \varepsilon_{ij} n_k^{nw} \varepsilon_{kl} n_l^{nw} + \zeta_5 \varepsilon_{ii} \varepsilon_{jj} n_k^{nw} \varepsilon_{kl} n_l^{nw} + \zeta_6 \varepsilon_{ii} n_j^{nw} \varepsilon_{jk} \varepsilon_{kl} n_l^{nw} \\ & + \zeta_7 \varepsilon_{ii} n_j^{nw} \varepsilon_{jk} n_k^{nw} n_l^{nw} \varepsilon_{lm} n_m^{nw} + \zeta_8 n_i^{nw} \varepsilon_{ij} \varepsilon_{jk} \varepsilon_{kl} n_l^{nw} \\ & + \zeta_9 n_i^{nw} \varepsilon_{ij} \varepsilon_{jk} n_k^{nw} n_l^{nw} \varepsilon_{lm} n_m^{nw} + \zeta_{10} n_i^{nw} \varepsilon_{ij} n_j^{nw} n_k^{nw} \varepsilon_{kl} n_l^{nw} n_m^{nw} \varepsilon_{mn} n_n^{nw}. \end{aligned} \tag{D.1}$$

It seems natural to use $\hat{\mathbf{n}}^{nw}$ as a preferred direction in these terms, because we have connected the orientation of the direction $\hat{\mathbf{n}}^{nw}$ to the macroscopic distortion of the elastomer characterized by the displacement field $\mathbf{u}(\mathbf{r})$. In this case, due to the transverse isotropy of the elastic terms with respect

to the direction $\hat{\mathbf{n}}^{\text{nw}}$, only nine of the ten terms with the coefficients ζ_i ($i = 1, \dots, 10$) are independent [77, 78]. We have checked that the terms associated with $\hat{\mathbf{n}}$ as a preferred direction do not qualitatively alter our conclusions below. Following the procedure described in section 7.2, we obtain the results listed hereafter.

Concerning the reorientation of the director field, Eqs. (7.15) and (7.17) are recovered identically. We find, however, that the amplitudes of the compression and/or dilation of the SCLSCE as given by Eqs. (7.18)-(7.20) are slightly modified in the anisotropic case,

$$\begin{aligned}
A_1 = & \frac{A_0^2}{8D_1^2(3c_1 + 2c_4 + 2c_5)}(4c_1D_1^2 + D_1\bar{D}_2^2 + \bar{D}_2^3 - 2\bar{D}_{2,n}\bar{D}_2^2 \\
& - 3\zeta_3D_1^2 + \phi_2D_1\bar{D}_2 + 2\phi_3D_1\bar{D}_2 + \psi_2\bar{D}_2^2 - 2\psi_3\bar{D}_2^2 \\
& + 4c_3D_1^2 + 6c_4D_1^2 + 8c_5D_1^2 - 4\zeta_4D_1^2 - 3\zeta_8D_1^2 \\
& - 2\zeta_9D_1^2 + D_2^{\text{nw}}\bar{D}_2^2), \tag{D.2}
\end{aligned}$$

$$\begin{aligned}
B_1 = & \frac{A_0^2}{16c_1D_1^2} \left(-4c_1D_1^2 + D_1\bar{D}_2^2 + \bar{D}_2^3 + 3\zeta_3D_1^2 - \phi_2D_1\bar{D}_2 + \psi_2\bar{D}_2^2 \right. \\
& - 2c_4D_1^2 + \zeta_8D_1^2 - D_2^{\text{nw}}\bar{D}_2^2 \\
& + \frac{c_1}{3c_1 + 2c_4 + 2c_5} \left(-4c_1D_1^2 - D_1\bar{D}_2^2 - \bar{D}_2^3 + 2\bar{D}_{2,n}\bar{D}_2^2 \right. \\
& \quad + 3\zeta_3D_1^2 - \phi_2D_1\bar{D}_2 - 2\phi_3D_1\bar{D}_2 - \psi_2\bar{D}_2^2 + 2\psi_3\bar{D}_2^2 \\
& \quad - 4c_3D_1^2 - 6c_4D_1^2 - 8c_5D_1^2 + 4\zeta_4D_1^2 + 3\zeta_8D_1^2 \\
& \quad \left. \left. + 2\zeta_9D_1^2 - D_2^{\text{nw}}\bar{D}_2^2 \right) \right), \tag{D.3}
\end{aligned}$$

$$\begin{aligned}
C_1 = & \frac{A_0^2}{16c_1D_1^2} \left(4c_1D_1^2 - D_1\bar{D}_2^2 - \bar{D}_2^3 - 3\zeta_3D_1^2 + \phi_2D_1\bar{D}_2 - \psi_2\bar{D}_2^2 \right. \\
& + 2c_4D_1^2 - \zeta_8D_1^2 + D_2^{\text{nw}}\bar{D}_2^2 \\
& + \frac{c_1}{3c_1 + 2c_4 + 2c_5} \left(-4c_1D_1^2 - D_1\bar{D}_2^2 - \bar{D}_2^3 + 2\bar{D}_{2,n}\bar{D}_2^2 \right. \\
& \quad + 3\zeta_3D_1^2 - \phi_2D_1\bar{D}_2 - 2\phi_3D_1\bar{D}_2 - \psi_2\bar{D}_2^2 + 2\psi_3\bar{D}_2^2 \\
& \quad - 4c_3D_1^2 - 6c_4D_1^2 - 8c_5D_1^2 + 4\zeta_4D_1^2 + 3\zeta_8D_1^2 \\
& \quad \left. \left. + 2\zeta_9D_1^2 - D_2^{\text{nw}}\bar{D}_2^2 \right) \right). \tag{D.4}
\end{aligned}$$

However, all terms appearing in these expressions directly depend on those coefficients of Eq. (7.3) that are directly related to relative rotations. This means that without including the variables of relative rotations compressive and dilative deformations are not found in this description at all. The material parameters ζ_5 , ζ_6 , and ζ_7 do not enter the expressions listed

above because the respective terms in the generalized energy density are of higher order due to incompressibility. From Eqs. (D.2)-(D.4) the special case of an isotropic elastic mechanical behavior of the elastomers is simply recovered by letting the coefficients appearing in expression (D.1) tend to zero.

Overall, we find that the results derived in this appendix for an elastically anisotropic nematic SCLSCE qualitatively coincide with those obtained in the isotropic case in section 7.2.

Appendix E

Highly ordered patterns of parabolic focal conics in lamellar lyotropic systems

In this appendix we report on the experimental observation of the formation of highly ordered parabolic focal conical patterns in lamellar surfactant solutions, and on some quantitative analysis of these patterns. This work is only loosely connected to the main topic of this thesis. However, it has been performed during the same period at the Universität Bayreuth in collaboration with Dr. Christian Wolf (Bayreuther Zentrum für Kolloide und Grenzflächen (BZKG), Physikalische Chemie I).

During this work, predominantly mixtures of sodiumdodecylsulfate, water, hexanol, and decane, located in the immediate vicinity of the region of the L_3 and L_α phase coexistence have been investigated. Experimental studies on the formation of the patterns and on their temporal development are described, which were mainly performed by Dr. Wolf [79]. We give a simple model picture for the underlying structure, corroborated by the experimental results. There appears to be only one independent length scale that controls the appearance of the whole respective pattern.

Our presentation of the subject in this appendix is closely connected to the one we have given in Ref. [80].

E.1 Introduction

The term “focal conics” refers to a special kind of defect structure that has been investigated since the beginning of the last century [81]. Focal conics can be observed, for example, in lamellar phases of smectic A liquid crystals [7,82]

and in those shown by various surfactant systems.

In an ideal lamellar system of infinite compressional layer modulus, which implies a constant layer thickness over the whole sample, these structures are modeled as families of so-called Dupin cyclides (see, e.g., Ref. [83] and references therein). The Dupin cyclides describe, for instance, a family of surfaces which are obtained in the following way: a pair of an ellipse and a hyperbola are chosen such that the plane containing the ellipse is oriented perpendicular to the plane containing the hyperbola. In addition, both lines run through a focal point of the respective other line. We then connect every point of the ellipse to every point of the hyperbola by straight lines, the so-called generators. Surfaces that are in every point oriented perpendicular to these generators contribute to the family of surfaces we are looking for. A focal conic domain structure can be described as a system of equidistant lamellae, obtained as Dupin cyclides. By construction, some of the lamellae form cusps located on the ellipse or hyperbola, respectively. The conical shape of these lamellae in the vicinity of the cusps gives rise to the name of the defect structures. Extensive effort has been made on calculating the curvature energy of these structures and their spatial arrangement [84–88].

Already in Ref. [81] the possibility that the ellipse and the hyperbola are degenerated into a pair of parabolae was pointed out, although not observed. The resulting defect structures are called parabolic focal conics (PFCs). These are the kinds of defect structures investigated in the following.

For this purpose, we have studied a lyotropic system in which highly ordered PFC structures could be observed. In particular, this was a mixture of sodiumdodecylsulfate (SDS) / water / hexanol / decane, the behavior of which has been examined in the immediate vicinity of the L_3 and L_α phase coexistence. For this kind of system it had been found that highly-arranged PFC structures can form, which are visible under the polarization microscope [89, 90].

It is well-known that ordered lamellar smectic phases can form PFC patterns by forced dilation [91, 92]. In the examined surfactant systems, the sample containers were, however, not dilated by an external mechanical stress. Nevertheless, well distinguishable PFCs were observed, and we suggest an explanation for the driving force behind their formation.

This appendix is organized as follows. In the next section, the procedure of generating the samples and their chemical composition will be described. After that, in section E.3, we will illustrate the experimental results obtained from the observation of these samples. In section E.4, we will relate the experimental data to the common model description of focal conical structures, and we will propose some quantitative analysis. Finally, we will summarize

our results.

E.2 Sample preparation

The following chemicals were used: SDS from Serva in quality p.a., hexanol p.a., and decane fraction without further purification. The water was demineralized.

Solutions of ten milliliters were produced for each sample. The alcohol and the hydrocarbon were added to a solution of water and approximately 15 wt-% SDS at 25 °C. The samples were then magnetically stirred for 10 minutes. In samples of coexisting L_α and L_3 phases, the phase volumes were determined after one day by visual observation. Microcuvettes (microslides from Camlab England) with a capillary thickness of 0.05 mm, 0.1 mm, 0.2 mm, 0.3 mm, and 0.4 mm were used for observations with a Leica DMR XE polarization microscope with the option of differential interference contrasting. The samples were homogenized by shaking, drawn into the microslides by capillary forces, and afterwards sealed with “Seal Ease Tube Sealer and Holder” from Becton Dickinson and Vacutainer Systems.

In order to study the influence of the composition on the velocity of formation of the textures, we also prepared samples from material that had not been homogenized by shaking before. Instead, the respective initial solutions had been equilibrated so that they showed fractions of the optically isotropic and lamellar phases, L_3 and L_α , respectively. Varying small amounts of L_3 material were then added to samples exclusively taken from material in the phase L_α .

A more detailed description of the preparation of the samples can be found in Ref. [79]. The following observations are based on the study of a few hundred microslide samples.

E.3 Experimental observations on the parabolic focal conical structures

For the investigation of the structure formation, samples were generated from the lamellar single phase and from the two-phase region, respectively. The samples were sealed in microslides of different thicknesses and observed using polarization microscopy. It was found that ordered lamellar structures did not form in the lamellar single phase region. All samples remained disordered and showed strong birefringence. However, when the lamellar phase was prepared from samples with a coexisting L_α and L_3 phase, pseudoisotropy

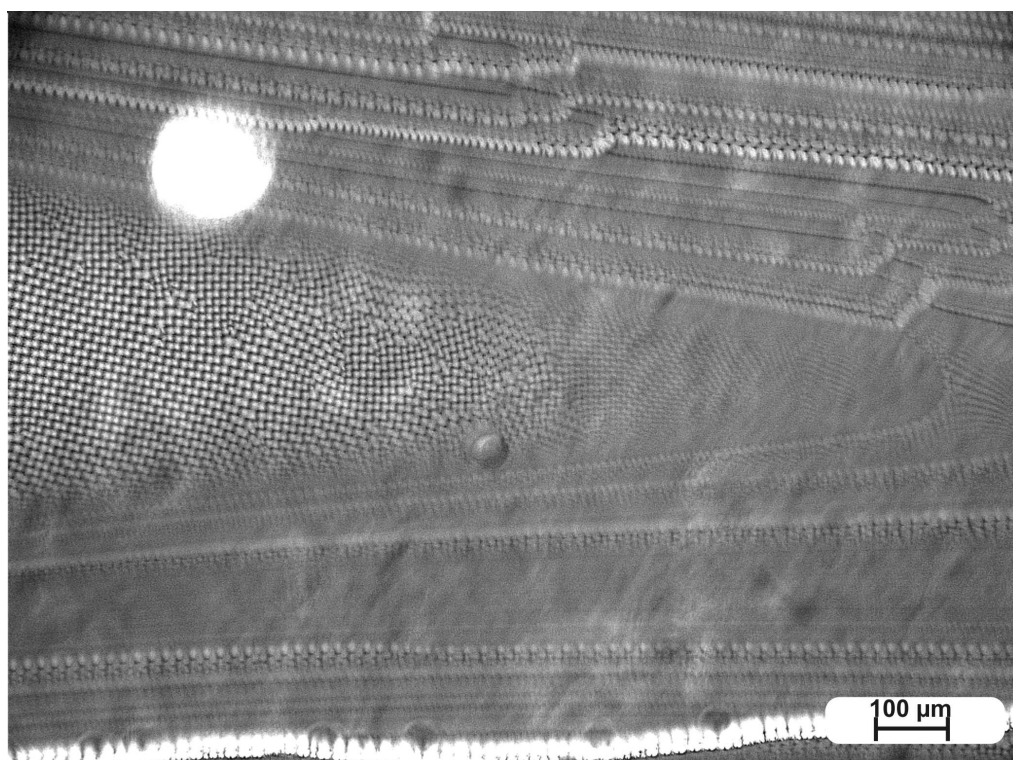


Figure E.1: Illustration of the formation process of highly ordered PFC domains. The PFC pattern develops from the wedge-like domain located in the central left part of the picture. On the whole, a flow of mass directed to the left was observed. Time of exposure: 2 sec.

developed in all cases within a short time. Bands of oily streaks vanished, and the sample appeared entirely dark under the polarization microscope. The duration of this process increased with the thickness of the microslides; it took about 10 minutes for the 0.1 mm microslides. Starting from the sealed edges of the microslides, a nebular haze began to grow into the capillary in the pseudoisotropic samples as depicted in Fig. E.1. The photo was taken next to one of the sealed edges of the microslide, where this edge was located close to the left of the pictured area. The wedge-like shaped haze grew towards the right of the pictured region. On the whole, a flow of mass towards the left of the pictured area and thus towards the sealed edge of the microslide could be identified. With a high magnification of the fog we could observe how ordered patterns formed from the diffuse structures. During the motion, the fog size, contrast, and order of these patterns increased strongly until

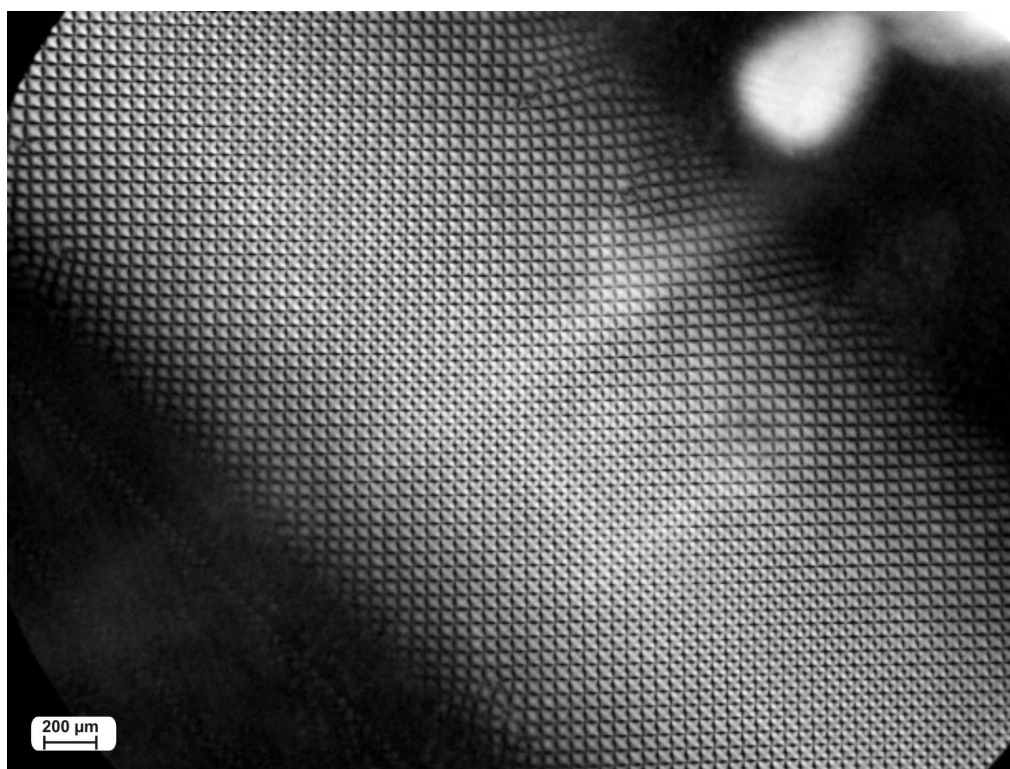


Figure E.2: Highly ordered pattern of PFCs (taken from Ref. [90]).

finally large ranges with almost perfect squares had developed. The growth of PFCs began as soon as the phase had become pseudoisotropic at the ends of the sealed microslides. Having chosen the method of preparation described above, it was possible to produce and observe highly ordered domains of perfect square patterns over the entire visual field of the microscope as shown in Fig. E.2. It could be verified that the orientation of the regular pattern to the direction of the flow is always the same.

In order to determine the driving force behind the formation of the PFC structures, the samples were prepared, sealed, and weighed in certain time intervals. A loss of mass was observed and after prolonged time gas bubbles were found within the surfactant phase. It was demonstrated by separate experiments that each of the three constituents water, hexanol, and decane are able to diffuse through the sealed microslides. The loss of decane, however, was significantly higher than that of water or hexanol as can be seen from Fig. E.3.

For illustration, we include the phase diagram Fig. E.4 as it had been

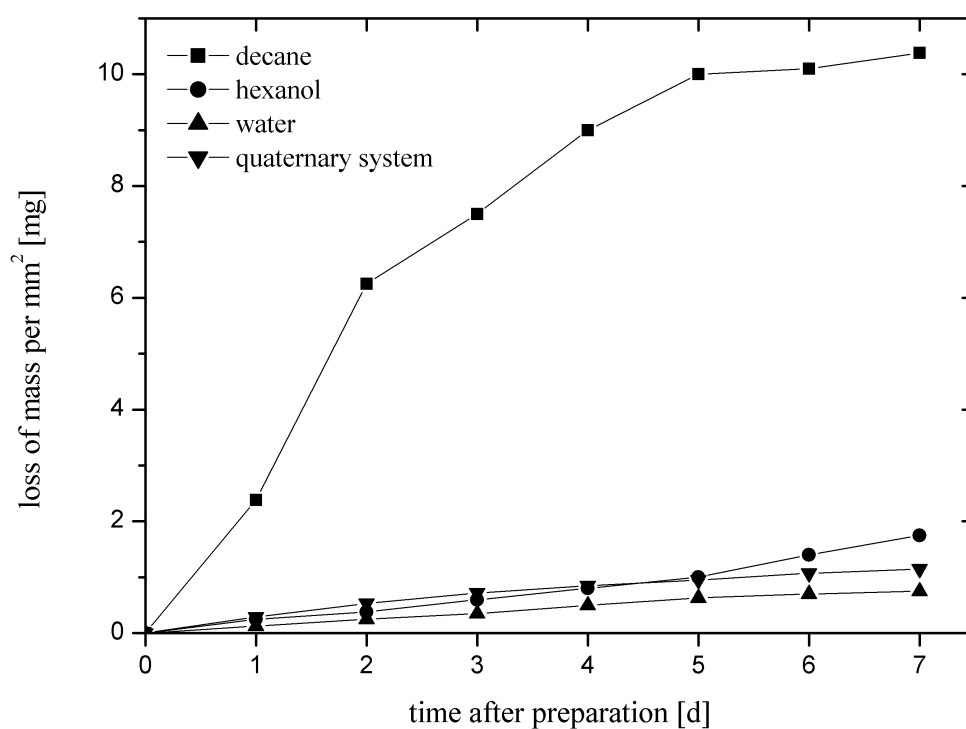


Figure E.3: Average loss of mass per area by diffusion through the sealings of 0.2 mm thick microslide samples as a function of time. The data points refer to the components decane, hexanol, and water, respectively, as well as to a quaternary system of a composition of 17 wt-% decane, 17 wt-% hexanol, 51 wt-% water, and 15 wt-% SDS.

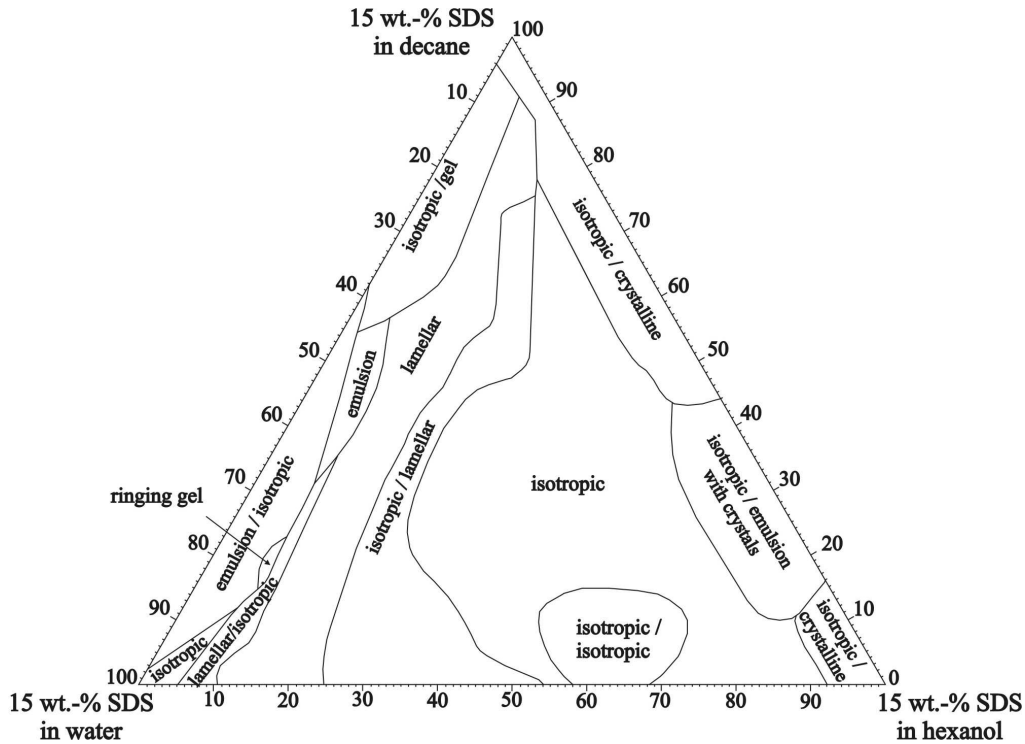


Figure E.4: Phase diagram for a quaternary system of 15 wt-% SDS and varying fractions of decane, hexanol, and water at 25 °C (taken from Ref. [90]). The scales on the upper left, upper right, and bottom edge of the triangle refer to the relative fractions of water, decane, and hexanol, respectively, besides SDS. This phase diagram has been determined via optical investigation, therefore the term “isotropic” refers to an optically isotropic state.

determined for a quaternary system of a constant fraction of 15 wt-% SDS and varying fractions of decane, hexanol, and water by A. Stark [90]. In our work we have concentrated on the regions indicated as “lamellar” and “isotropic/lamellar” in Fig. E.4, where the term “isotropic” refers to an optically isotropic state. It has been verified experimentally that the material shows the phase L_3 in the regions we have investigated. Potassiumdodecylsulfate turned out to be just as suitable as SDS, the lamellar phases occupy roughly the same portion of the corresponding phase diagram.

During the optical observations, polarizer and analyzer of the polarization microscope were oriented in perpendicular directions. Looking at the microslide from above, three characteristic planes of focus of the PFC struc-

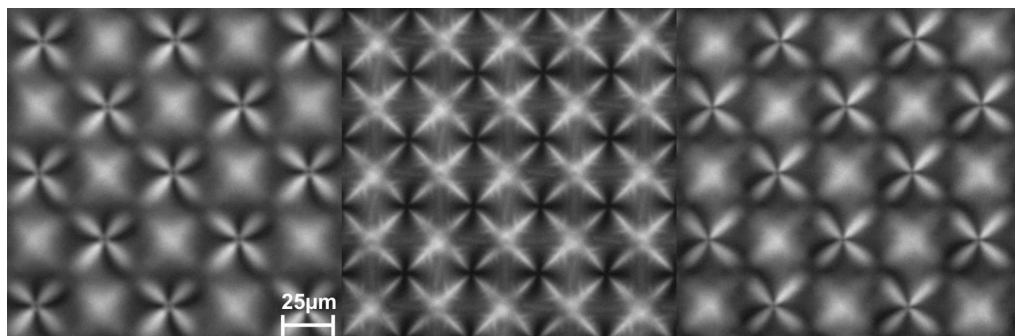


Figure E.5: The three characteristic planes that can be focused on with the help of a polarizing microscope as described in the text. Left: upper plane; center: middle plane; right: lower plane. The distance between the upper and middle plane, and between the middle and lower plane, was $21 \pm 1 \mu\text{m}$, respectively.

tures could be visualized at the exact center plane of the microslide and a few micrometers above and below, respectively. They are illustrated by the three pictures in Fig. E.5, and they can be obtained by orienting the long axis of the microslide parallel or perpendicular to the analyzer.

As we have observed, there are many factors which affect the growth of the PFCs. Investigating the samples that had been prepared by adding different small amounts of material showing the phase L_3 to material in the lamellar phase, we found that an increase of the portion taken from the phase L_3 during sample preparation leads to a faster development of the pseudoisotropy. However, smallest amounts of material taken from the phase L_3 were sufficient in order to observe the formation of the PFC textures.

Pentanol proved to be an appropriate cosurfactant like hexanol to form PFCs. When filled into microslides, the PFCs align themselves in a most perfect order when the weight ratio of cosurfactant and hydrocarbon was roughly 1 : 1 in the two-phase-region. The lamellar phases of the samples in this boundary area display the lowest viscosity and the lowest elastic moduli of all samples in the lamellar region.

An additional factor influencing the order and the propagation speed of the PFCs, is the quality of the sealing of the microslides. An improved sealing adds to a slow nebula propagation and a better order of the system.

Well developed patterns are very long transients in time. Mostly, they remain nearly unaltered for days or weeks, or even longer. Very slow movements of flow within the samples could be detected. Flows within the entire

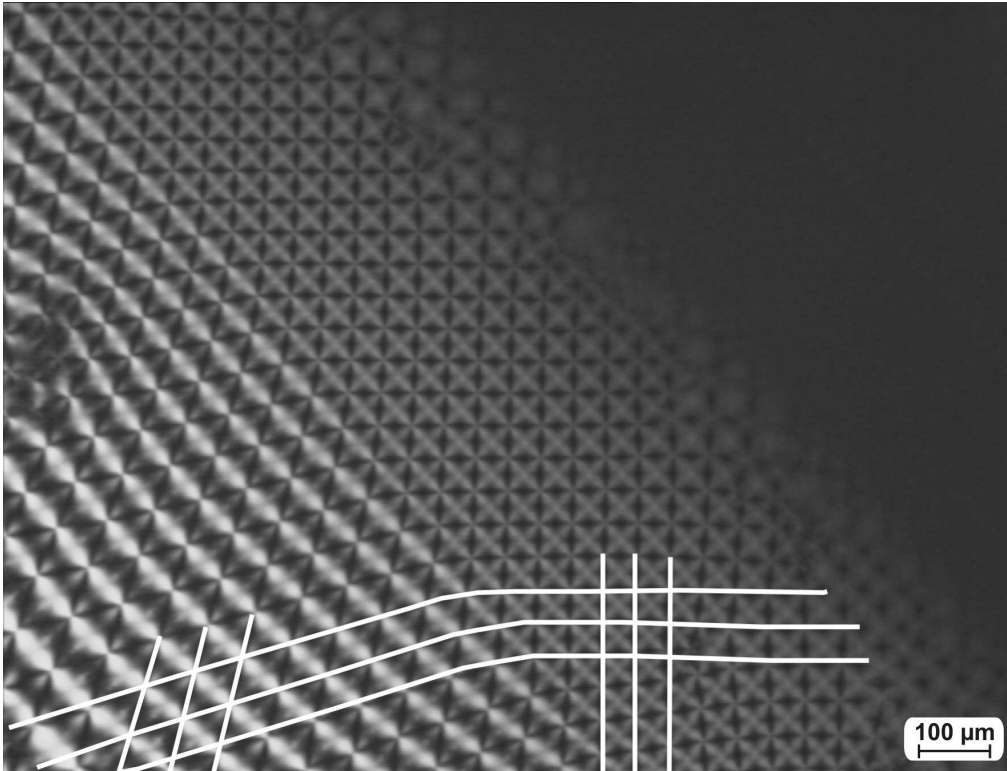


Figure E.6: Strain deformation of the PFC patterns a long time after formation. The characteristic squares of the previous pattern are continuously deformed to rhombi.

samples arise. The flow can be obstructed by defects in the texture such as bubbles. Thus distortions of the patterns are generated. It could be demonstrated that such distortions lead to the formation of a new rhombic lattice of a different symmetry: the 90° angle of the square corners of the previous undistorted pattern changes to a 60° angle as depicted in Fig. E.6. It is interesting to note that during this process the distinction of the three focal layers mentioned above disappears.

Finally, a transition to hexagonal structures could be observed. In particular, this was the case for samples that were predominantly composed of material showing the phase L_3 during sample preparation. Clearly, more investigations are necessary in order to further clarify this point.

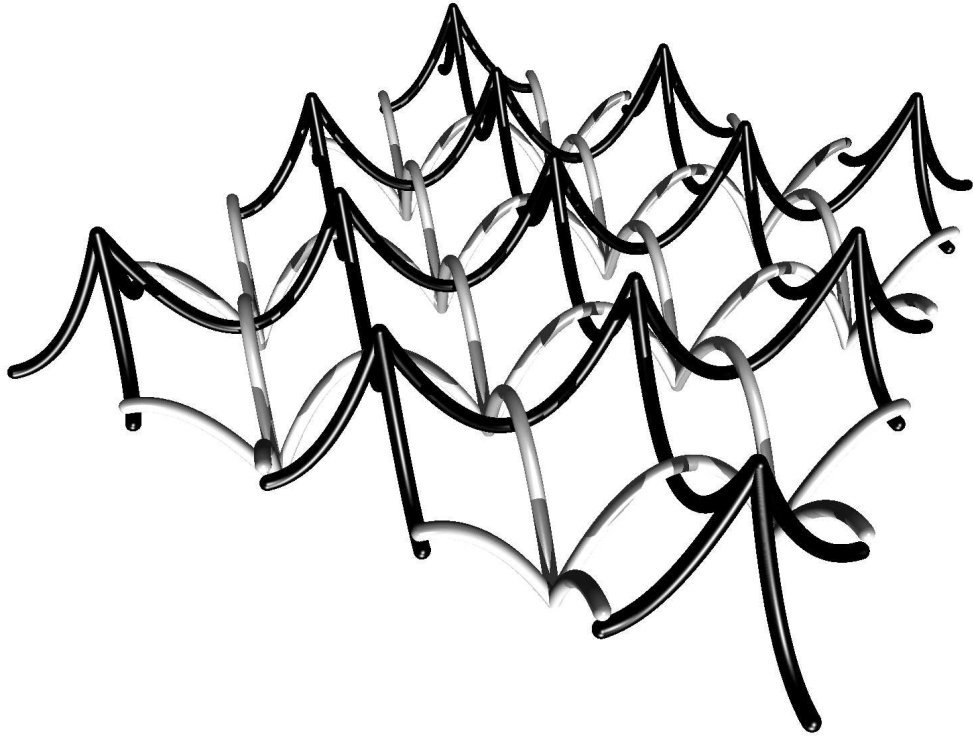


Figure E.7: Structure of the arranged parabolic focal conics, corresponding to the pattern depicted in Fig. E.5. Parabolae that open towards the reader in Fig. E.5 appear dark, the ones opening away from the reader in Fig. E.5 appear bright.

E.4 Discussion

Based on the experimental data presented in the last section and as already done in the previous sections, it is quite reasonable to interpret the investigated patterns as an array of ordered focal conical structures. The high symmetry of the patterns in all three dimensions, which is illustrated for example by Figs. E.2 and E.5, suggests that parabolic focal conics (PFCs) were observed. A model picture which corresponds to the array observed in Fig. E.5 is presented in Fig. E.7.

One single PFC consists of a pair of parabolae that can be parameterized in the following way: referring to Fig. E.5, we choose the z -axis of our Cartesian coordinate system such that it is pointing out of the plane towards the reader. The x - and y -axes are oriented in diagonal directions within the plane, following the bright arms of the crosses. In Fig. E.8 we have illus-

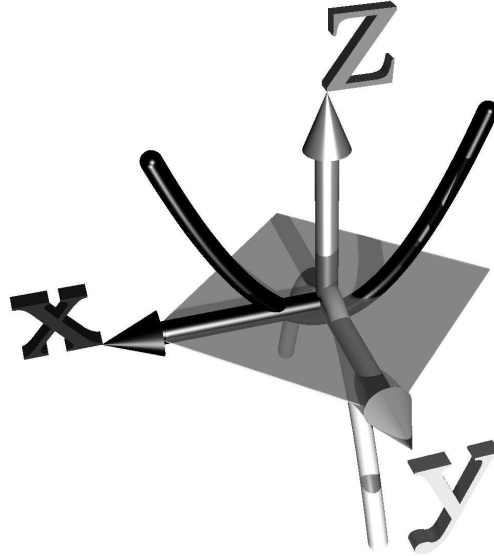


Figure E.8: Choice of the coordinate system in order to parameterize the pair of parabolae of one single PFC in Fig. E.5. The middle plane, which corresponds to the plane focused on in the center of Fig. E.5, is also indicated.

trated this choice of the coordinate frame, and we have also indicated the middle plane focused on in the center of Fig. E.5. We choose the origin of the coordinate system within the middle plane such that for the inspected single PFC the focal points of both parabolae can be found on the z -axis. The parabola which opens towards the reader in Fig. E.5 (dark in Fig. E.8) may then be parameterized by

$$z = -\frac{f}{2} + \frac{1}{4f}x^2, \quad y = 0, \quad (\text{E.1})$$

and the parabola that opens away from the reader in Fig. E.5 (bright in Fig. E.8) can be parameterized by

$$z = +\frac{f}{2} - \frac{1}{4f}y^2, \quad x = 0, \quad (\text{E.2})$$

f denoting the focal length of the parabolae.

The single PFCs are then arranged in a quadratic array in the way depicted by Fig. E.7. At each of the central points of the sharp crosses in the left picture of Fig. E.5, four of the parabolae opened towards the reader meet (dark in Fig. E.7). These points can be put into the focus of the microscope

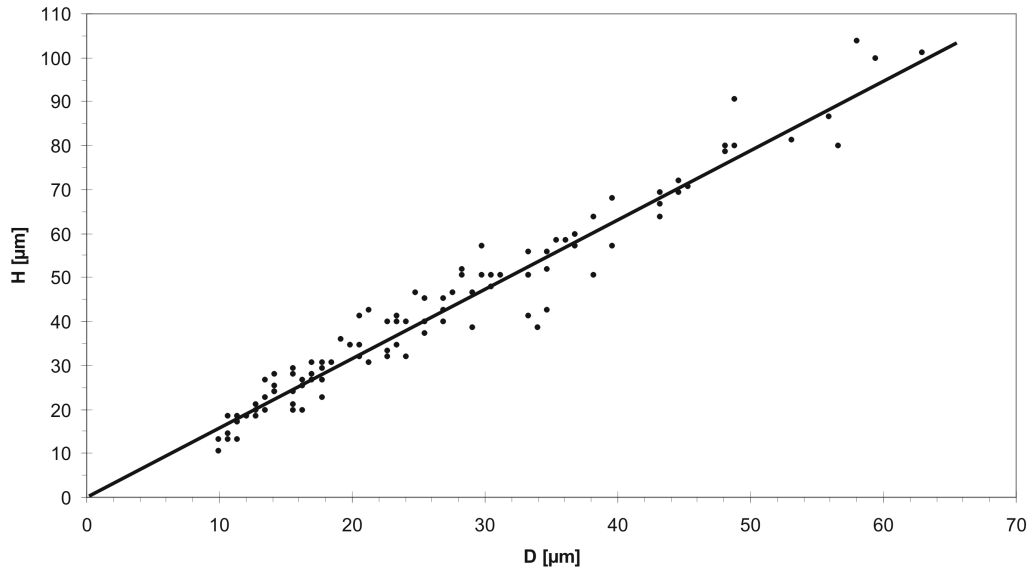


Figure E.9: Linear relationship between the characteristic lengths of D and H of the PFCs, as introduced in the text. Each data point represents the size of the PFCs in the respective sample investigated.

as was done in this picture. Between the sharp crosses, blurred crosses are observed, which however turn sharp on turning to the right picture of Fig. E.5. On the contrary, the sharp crosses of the left picture appear blurred in the right one. So we expect that on turning to the right picture, we put into the focus of the microscope the points where four of the parabolae opening away from the reader meet (bright in Fig. E.7). Focusing the plane in between, the intersecting points of both kinds of crosses become equally blurred (picture in the middle of Fig. E.5).

This concept is corroborated by the following analysis. The total height H of the PFC structure can be measured. In Fig. E.5 it equals the distance between the two focal planes on the left and on the right. In addition, within these focal planes, the opening distance D of one parabola (measuring the distance between the points where four parabolae meet) can be determined for each array of PFCs.

For various samples of the four different microslide thicknesses of 0.1 mm, 0.2 mm, 0.3 mm, and 0.4 mm, the total height H and the opening distance D of a relaxed PFC structure have been measured. The results are presented in Fig. E.9, which shows H as a function of D and suggests a linear relationship between the two lengths. This means that also the focal length f must

increase linearly with the opening distance D . f can be calculated from Eqs. (E.1) and (E.2) as

$$f = -\frac{H}{2} + \frac{1}{2}\sqrt{H^2 + \frac{1}{2}D^2}, \quad (\text{E.3})$$

and we find values of $f \approx 0.7 - 4.7 \mu\text{m}$ for the samples investigated.

We conclude from our results that for the systems under consideration there exists only one characteristic ratio for the values of lengths involved: $H/D \approx 1.60$, or $f/D \approx 0.07$, respectively. From this fact, we further conclude that the energy of the defect structure is minimized for these special values of the ratios, irrespective of the actual size of the underlying PFC structure. The pattern can scale in size only isotropically, and the knowledge of the value of one characteristic length determines the appearance of the whole structure.

Next, we want to address the issue of how the PFC structure is embedded in the surrounding texture. As we have described above, the PFCs form in the middle region distant from the upper and lower glassy boundary of the respective microslide. On the upper and lower glass surfaces of the microslides, homeotropic alignment prevails in the lamellar phase L_α . Thus, a lyotropic solution tends to orient its lamellae parallel to the glass surfaces.

On the other hand, the optical investigations of the samples indicate that the parabolic defect lines of the PFC structure end at least very close to the points where four of the parabolae meet. Above the upper and below the lower plane focused on in the left and right part of Fig. E.5, respectively, a crossover from the PFC to the lamellar structure then must occur. By construction, the arrangement of the layers becomes more and more planar with increasing distance from the middle plane of the PFC texture, so that a rather smooth crossover from a PFC structure to planar layers becomes possible far away from the middle plane.

However, above and below the points where the parabolae meet, respectively, some irregularities in the layer structure must occur. The appearance of focal defect lines that end on air surfaces – or on glass surfaces with homeotropic boundary conditions – has been discussed in the literature, predominantly for smectic A liquid crystals (see, e.g., Refs. [87] and [93]). It has been observed and suggested that some kind of dips occur in the layer structure at the ending points of the defect lines. We expect a similar behavior above and below the points where the parabolae meet, and we can think of two different scenarios. On the one hand, there may be a smooth crossover from the PFC to a planar texture by variations of the concentrations and thus of the layer thickness in the regions where the dips in the

layer structure are expected to appear. On the other hand, filling additional space by material in the state L_3 , the PFC texture can be embedded in the surrounding geometry. However, we were not able to distinguish between these two scenarios on the basis of our experimental results.

Of course, already the assumption of a focal conical domain structure of incompressible layers is an idealization. It has been shown for smectic A focal conics that, in particular close to the singular lines of the structure, the assumption of constant layer thickness does not hold [94]. However, the picture of the ideal focal conical structure has turned out to be very useful for the interpretation of many experimental results. For most of the coarse-grained discussion presented, the influence of a finite compressional layer modulus and thus the deviation from an ideal focal conical domain structure can be neglected.

There remains the question of how the PFC defect structure is formed. From the investigation of smectic A liquid crystalline phases the following results are known: stretching an oriented sample of a smectic A liquid crystal parallel to the smectic layer normal, there emerges an undulatory instability at a critical dilation [7,91,92]. Forming these undulations, the system can fill the additional space, avoiding as far as possible the energetically expensive dilation of the layers. When the sample is stretched further, there exists the possibility that a second critical point is approached. If this point is crossed, PFC structures can be observed [82]. Simple geometrical considerations show that forming a PFC structure leads to an extension of the system in the direction of dilation by a distance equal to the focal length f , when compared to the undisturbed ground state. Thus forming the PFC structure seems to be an effective way in order to relax the mechanical stress.

We interpret the appearance of the PFCs in our system taking into account these observations. As has been described in section E.3, the sealing of the microslides does not completely suppress the fractional loss of the included solution. Especially the hydrocarbons have been shown to slowly evaporate through the sealing. This drives the convection within the sample as has been explained for instance on the basis of Fig. E.1. Due to the resulting loss of mass, the system is effectively dilated, which forces the formation of the PFCs.

For microslides of a thickness of 0.2 mm, we measured the overall loss of mass of some of the samples as a function of time. In addition, we measured the loss of mass of sealed 0.2 mm microslides, containing only one of the pure components, respectively, as shown in Fig. E.3. Together with the known densities of the pure components we have then inferred the effective loss of volume ΔV in the samples. Finally, as a crude estimate, we have related the focal length f , the thickness d of the microslide, the loss of volume ΔV , and

the overall volume V of the microslide by

$$\frac{2f}{d} = \frac{\Delta V}{V}, \quad (\text{E.4})$$

where we follow the ideas outlined above. During that period after sealing the microslides in which PFCs could be observed, the values of f obtained from Eq. (E.4) amount to $f \approx 2 - 10 \mu\text{m}$. On the other hand, the values of f determined with the help of Eq. (E.3) by measuring the dimensions of the PFCs with the polarizing microscope were $f \approx 0.8 - 2.5 \mu\text{m}$. As the loss of volume ΔV is partly compensated by air bubbles in the microslide, the values obtained for f in the two different ways are comparable to each other. This underlines our scenario of analysis of the observed patterns.

The above mentioned investigations on the separate diffusion of the components through the sealings of the microslides revealed that the loss of material is dominated by the escape of decane, as demonstrated by Fig. E.3. More exactly, the loss of decane by weight is more than 10 times larger than that of water, and 5–10 times larger than that of hexanol, which changes the composition of our system. It has been demonstrated that a change in the composition of surfactant solutions can qualitatively influence their macroscopic behavior [95]. Varying the modulus of curvature may even change the phase present in the system [96]. However, in our case, a change of the phase in which the respective solution appears has not been observed. We find the reason for this behavior in the phase diagram Fig. E.4. The dominance of the loss of decane secures that for the observed overall loss of mass the system remains in the two-phase region which is indicated as “isotropic/lamellar”. This is the region in which the PFC structures form. To be sure, we determined the boundaries between the regions “lamellar”, “isotropic/lamellar”, and “isotropic” in the phase diagram once more with higher precision than the one used in order to acquire Fig. E.4. However, we roughly found the same positions for these boundaries.

Finally, we want to discuss the role of the flow in our samples. In section E.3, we have described the process of formation of the PFC texture. There, we have noted that a macroscopic flow can be observed which is directed towards the sealing of the microslides. A lot of work has already been performed in order to investigate the behavior of thermotropic and lyotropic lamellar phases exposed to macroscopic flow. In particular, the relations between macroscopic shear flows and mesoscopic structures have drawn a lot of attention [97, 98]. It has been noted in this context that the behavior of thermotropic smectic A liquid crystals and lyotropic systems can be very different. Shear flow enhances and suppresses fluctuations in the arrangement of the layers differently in thermotropic smectic A liquid crystals and

surfactant solutions, because in the latter case local variations of the concentration can play a crucial role [99]. In addition, thermotropic smectic A liquid crystals can show non-Newtonian behavior of varying viscosity already at low shear rates, where the formation of multilamellar cylinders elongated in flow direction has been observed [100]. On the contrary, lyotropic systems usually react to low shear rates in a Newtonian way with a constant viscosity, having the layers oriented parallel to the shearing surfaces. When the total shear flow is increased by either controlling the shear rate or the amplitude of the shear stress, the formation of multilamellar vesicles can take place in various lyotropic systems. The latter include solutions that contain the ionic surfactant SDS [95, 101, 102]. In certain systems multilamellar cylinders oriented with their axis parallel to the flow direction can be identified as an intermediate state, before the vesicle formation occurs [103]. For high shear rates, a transition to planar layers oriented perpendicular or again parallel to the shear plates could be detected in various systems [95, 97, 98, 101].

As mentioned above, the flow observed in our samples results from the evaporation at the ends of the microslides. Naturally, shear deformation is also involved in this motion. Due to the low velocity of this flow, the planar alignment of the layers near the surfaces of the microslides agrees well with the experimental findings for low shear rates summarized before. The formation of the PFC texture around the middle plane of the microslides, however, seems to be mainly related to another aspect. We think that here the procedure of effective dilation due to evaporation plays a major role.

A good test of our explanation for the formation of the PFC structures would of course be a mechanical control experiment. During this experiment, the samples should be mechanically stretched by increasing the distance between the boundary plates, whereas evaporation of the components should be avoided. Then, if the boundaries are moved slowly enough, similar patterns should form. Such an experiment, however, was beyond the scope of our work.

E.5 Conclusions

In this appendix, we have described and analyzed our investigations on the highly ordered patterns that we observed in lamellar lyotropic systems. From the signature of their optical appearance and the high symmetry in all three dimensions we conclude that PFCs determine the underlying structure of these patterns. Measuring the characteristic lengths of the pattern for different samples we found that the height of the PFCs and the focal length of the parabolae scaled linearly with their lateral extensions. This supports the

idea that there exists one energetically favored defect pattern, which adjusts to the overall size of the sample by varying only one independent length scale. Finally, we have given an explanation for the origin of the formation of the observed patterns. We suggest that the system is effectively dilated, and we have supported this picture by relating the corresponding loss of mass to the focal length of the PFC structure.

Bibliography

- [1] P. G. de Gennes, M. Hébert, and R. Kant, *Macromol. Symp.* **113**, 39 (1997).
- [2] M. Hébert, R. Kant, and P. G. de Gennes, *J. Phys. I* **7**, 909 (1997).
- [3] K. Urayama, S. Honda, and T. Takigawa, *Macromol.* **38**, 3574 (2005).
- [4] Y. Yu and T. Ikeda, *Angew. Chem. Int. Ed.* **45**, 5416 (2006).
- [5] G. Friedel, *Ann. Phys.* **18**, 273 (1922).
- [6] O. Lehmann, *Z. Phys. Chem.* **4**, 462 (1889).
- [7] P. G. de Gennes and J. Prost, *The Physics of Liquid Crystals* (Clarendon Press, Oxford, 1993).
- [8] D. Forster, *Hydrodynamic Fluctuations, Broken Symmetry, and Correlation Functions* (Perseus Books, 1990).
- [9] V. I. Kopp, B. Fan, H. K. M. Vithana, and A. Z. Genack, *Opt. Lett.* **23**, 1707 (1998).
- [10] B. Taheri, A. F. Muñoz, P. Palffy-Muhoray, and R. Twieg, *Mol. Cryst. Liq. Cryst.* **358**, 73 (2001).
- [11] A. Muñoz, P. Palffy-Muhoray, and B. Taheri, *Opt. Lett.* **26**, 804 (2001).
- [12] A. Saupe and W. Maier, *Z. Naturforsch.* **16 a**, 816 (1961).
- [13] G. Strobl, *The Physics of Polymers* (Springer, Berlin, 1996).
- [14] L. D. Landau and E. M. Lifshitz, *Theory of Elasticity* (Elsevier, Oxford, 1986).
- [15] H. Finkelmann, H. Ringsdorf, and J. H. Wendorff, *Makromol. Chem.* **179**, 273 (1978).

- [16] H. Finkelmann, H.-J. Kock, and G. Rehage, *Makromol. Chem., Rapid Commun.* **2**, 317 (1981).
- [17] J. Küpfer and H. Finkelmann, *Makromol. Chem., Rapid Commun.* **12**, 717 (1991).
- [18] J. Küpfer and H. Finkelmann, *Makromol. Chem.* **195**, 1353 (1994).
- [19] H. R. Brand and K. Kawasaki, *Macromol. Rapid Commun.* **15**, 251 (1994).
- [20] D.-U. Cho, Y. Yusuf, P. E. Cladis, H. R. Brand, H. Finkelmann, and S. Kai, *Jpn. J. Appl. Phys.* **46**, 1106 (2007).
- [21] A. Greve and H. Finkelmann, *Macromol. Chem. Phys.* **202**, 2926 (2001).
- [22] D.-U. Cho, Y. Yusuf, P. E. Cladis, H. R. Brand, H. Finkelmann, and S. Kai, *Chem. Phys. Lett.* **418**, 217 (2006).
- [23] C. H. Legge, F. J. Davis, and G. R. Mitchell, *J. Phys. II (France)* **1**, 1253 (1991).
- [24] G. R. Mitchell, F. J. Davis, and W. Guo, *Phys. Rev. Lett.* **71**, 2947 (1993).
- [25] S. T. Kim and H. Finkelmann, *Macromol. Rapid Commun.* **22**, 429 (2001).
- [26] A. Komp, J. Rühle, and H. Finkelmann, *Macromol. Rapid Commun.* **26**, 813 (2005).
- [27] K. Urayama, R. Mashita, I. Kobayashi, and T. Takigawa, *Macromol.* **40**, 7665 (2007).
- [28] K. Urayama, S. Honda, and T. Takigawa, *Macromol.* **39**, 1943 (2006).
- [29] J. Schmidtke, S. Kniesel, and H. Finkelmann, *Macromol.* **38**, 1357 (2005).
- [30] J. Weilepp and H. R. Brand, *Europhys. Lett.* **34**, 495 (1996).
- [31] J. Weilepp and H. R. Brand, *Macromol. Theory Simul.* **7**, 91 (1998).
- [32] P. Martinoty, P. Stein, H. Finkelmann, H. Pleiner, and H. R. Brand, *Eur. Phys. J. E* **14**, 311 (2004).

- [33] O. Müller and H. R. Brand, *Eur. Phys. J. E* **17**, 53 (2005).
- [34] H. R. Brand, H. Pleiner, and P. Martinoty, *Soft Matter* **2**, 182 (2006).
- [35] A. M. Menzel and H. R. Brand, *Eur. Phys. J. E* **26**, 235 (2008).
- [36] P. G. de Gennes, in *Liquid Crystals of One- and Two-Dimensional Order*, edited by W. Helfrich and G. Heppke (Springer, Berlin, 1980), pp. 231 ff.
- [37] P. C. Martin, O. Parodi, and P. S. Pershan, *Phys. Rev. A* **6**, 2401 (1972).
- [38] H. Pleiner and H. R. Brand, in *Pattern Formation in Liquid Crystals*, edited by A. Buka and L. Kramer (Springer, New York, 1996), pp. 15 ff.
- [39] H. R. Brand and H. Pleiner, *Physica A* **208**, 359 (1994).
- [40] L. D. Landau and E. M. Lifshitz, *Fluid Dynamics* (Elsevier, Oxford, 1987).
- [41] H. Temmen, H. Pleiner, M. Liu, and H. R. Brand, *Phys. Rev. Lett.* **84**, 3228 (2000).
- [42] H. Pleiner, M. Liu, and H. R. Brand, *Rheol. Acta* **39**, 560 (2000).
- [43] P. M. Chaikin and T. C. Lubensky, *Principles of Condensed Matter Physics* (Cambridge University Press, Cambridge, 1995).
- [44] T. C. Lubensky, *Phys. Rev. A* **6**, 452 (1972).
- [45] J. Küpfer, E. Nishikawa, and H. Finkelmann, *Polym. Adv. Techn.* **5**, 110 (1994).
- [46] S. Bohlius, H. R. Brand, and H. Pleiner, *Phys. Rev. E* **70**, 061411 (2004).
- [47] S. Bohlius, Diploma thesis, Universität Bayreuth, 2005.
- [48] W. P. Mason, *Physical Acoustics and the Properties of Solids* (Van Nostrand Reinhold, New York, 1958).
- [49] H. R. Brand, *Makromol. Chem., Rapid Commun.* **10**, 441 (1989).
- [50] A. M. Menzel and H. R. Brand, *J. Chem. Phys.* **125**, 194704 (2006).

- [51] T. C. Lubensky, R. Mukhopadhyay, L. Radzihovsky, and X. Xing, *Phys. Rev. E* **66**, 011702 (2002).
- [52] L. Golubović and T. C. Lubensky, *Phys. Rev. Lett.* **63**, 1082 (1989).
- [53] D. Rogez, G. Francius, H. Finkelmann, and P. Martinoty, *Eur. Phys. J. E* **20**, 369 (2006).
- [54] M. Warner and E. M. Terentjev, *Liquid Crystal Elastomers* (Clarendon Press, Oxford, 2003); and references therein.
- [55] R. Everaers and K. Kremer, *Macromol.* **28**, 7291 (1995).
- [56] E. Fried and S. Sellers, *J. Mech. Phys. Solids* **52**, 1671 (2004).
- [57] E. Fried and S. Sellers, *J. Appl. Phys.* **100**, 043521 (2006).
- [58] F. Ye, R. Mukhopadhyay, O. Stenull, and T. C. Lubensky, *Phys. Rev. Lett.* **98**, 147801 (2007).
- [59] A. M. Menzel and H. R. Brand, *Phys. Rev. E* **75**, 011707 (2007).
- [60] W. H. Press, S. A. Teukolsky, W. T. Vetterling, and B. P. Flannery, *Numerical Recipes in Fortran* (Cambridge University Press, Cambridge, 1999).
- [61] Y. Mao, E. M. Terentjev, and M. Warner, *Phys. Rev. E* **64**, 041803 (2001).
- [62] H. Finkelmann, S. T. Kim, A. Muñoz, P. Palfy-Muhoray, and B. Taheri, *Adv. Mater.* **13**, 1069 (2001).
- [63] P. Cicuta, A. R. Tajbakhsh, and E. M. Terentjev, *Phys. Rev. E* **65**, 051704 (2002).
- [64] I. Kundler and H. Finkelmann, *Macromol. Rapid Commun.* **16**, 679 (1995).
- [65] A. M. Menzel, H. Pleiner, and H. R. Brand, *J. Chem. Phys.* **126**, 234901 (2007).
- [66] A. M. Menzel, H. Pleiner, and H. R. Brand (submitted to *J. Appl. Phys.*).
- [67] I. Kundler and H. Finkelmann, *Macromol. Chem. Phys.* **199**, 677 (1998).

- [68] S. Conti, A. DeSimone, and G. Dolzmann, *J. Mech. Phys. Solids* **50**, 1431 (2002).
- [69] R. W. Ogden, *Non-Linear Elastic Deformations* (Dover Publications, Mineola, 1997).
- [70] P. D. Olmsted, *J. Phys. II* **4**, 2215 (1994).
- [71] L. R. G. Treloar, *The Physics of rubber elasticity* (Clarendon Press, Oxford, 1975).
- [72] A. Lebar, Z. Kutnjak, S. Žumer, H. Finkelmann, A. Sánchez-Ferrer, and B. Zalar, *Phys. Rev. Lett.* **94**, 197801 (2005).
- [73] G. Cordoyiannis, A. Lebar, B. Zalar, S. Žumer, H. Finkelmann, and Z. Kutnjak, *Phys. Rev. Lett.* **99**, 197801 (2007).
- [74] F. Brömmel and H. Finkelmann (unpublished).
- [75] N. Uchida, *Phys. Rev. E* **60**, R13 (1999).
- [76] F. M. Guillot and E. Balizer, *J. Appl. Polym. Sci.* **89**, 399 (2003).
- [77] O. Müller, Diploma thesis, Universität Bayreuth, 2001.
- [78] H. R. Brand and O. Müller, *Macromol. Theory Simul.* **11**, 154 (2002).
- [79] C. Wolf, Ph.D. dissertation thesis, Universität Bayreuth, 2007.
- [80] C. Wolf and A. M. Menzel, *J. Phys. Chem. B* **112**, 5007 (2008).
- [81] G. Friedel and F. Grandjean, *Bull. Soc. Franç. Minér.* **33**, 409 (1910).
- [82] C. S. Rosenblatt, R. Pindak, N. A. Clark, and R. B. Meyer, *J. Phys.* **38**, 1105 (1977).
- [83] G. H. Brown and W. G. Shaw, *Chem. Rev.* **57**, 1049 (1957).
- [84] M. Kléman, *J. Phys. (France)* **38**, 1511 (1977).
- [85] C. Blanc and M. Kléman, *Eur. Phys. J. B* **10**, 53 (1999).
- [86] M. Kleman and O. D. Lavrentovich, *Phys. Rev. E* **61**, 1574 (2000).
- [87] C. Blanc and M. Kleman, *Phys. Rev. E* **62**, 6739 (2000).
- [88] M. Kléman and O. D. Lavrentovich, *Eur. Phys. J. E* **2**, 47 (2000).

- [89] G. Platz and C. Thunig, *Langmuir* **12**, 1906 (1996).
- [90] A. Stark, Ph.D. dissertation thesis, Universität Bayreuth, 2001.
- [91] N. A. Clark and R. B. Meyer, *Appl. Phys. Lett.* **22**, 493 (1973).
- [92] M. Delaye, R. Ribotta, and G. Durand, *Phys. Lett. A* **44**, 139 (1973).
- [93] J. B. Fournier, I. Dozov, and G. Durand, *Phys. Rev. A* **41**, 2252 (1990).
- [94] J. B. Fournier, *Phys. Rev. E* **50**, 2868 (1994).
- [95] J. Zipfel, J. Berghausen, P. Lindner, and W. Richtering, *J. Phys. Chem. B* **103**, 2841 (1999).
- [96] T. D. Le, U. Olsson, and K. Mortensen, *Physica B* **276-278**, 379 (2000).
- [97] K. Mortensen, *Curr. Opin. Colloid Interface Sci.* **6**, 140 (2001).
- [98] W. Richtering, *Curr. Opin. Colloid Interface Sci.* **6**, 446 (2001).
- [99] R. Bruinsma and Y. Rabin, *Phys. Rev. A* **45**, 994 (1992).
- [100] P. Panizza, P. Archambault, and D. Roux, *J. Phys. II (France)* **5**, 303 (1995).
- [101] D. Roux, *Revue De L'Institut Français Du Pétrole* **52**, 145 (1997).
- [102] F. Nettekheim, J. Zipfel, P. Lindner, and W. Richtering, *Colloids Surf. A* **183-185**, 563 (2001).
- [103] J. Zipfel, F. Nettekheim, P. Lindner, T. D. Le, U. Olsson, and W. Richtering, *Europhys. Lett.* **53**, 335 (2001).

List of publications

Publications submitted during the course of this work:

1. A. M. Menzel and H. R. Brand,
“*Rotatoelectricity in cholesteric side-chain liquid single crystal elastomers*”,
J. Chem. Phys. **125**, 194704 (2006).
2. A. M. Menzel and H. R. Brand,
“*Cholesteric elastomers in external mechanical and electric fields*”,
Phys. Rev. E **75**, 011707 (2007).
3. A. M. Menzel, H. Pleiner, and H. R. Brand,
“*Nonlinear relative rotations in liquid crystalline elastomers*”,
J. Chem. Phys. **126**, 234901 (2007).
4. C. Wolf and A. M. Menzel,
“*Highly ordered patterns of parabolic focal conics in lamellar lyotropic systems*”,
J. Phys. Chem. B **112**, 5007 (2008).
5. A. M. Menzel and H. R. Brand,
“*Instabilities in nematic elastomers in external electric and magnetic fields*”,
Eur. Phys. J. E **26**, 235 (2008).
6. A. M. Menzel, H. Pleiner, and H. R. Brand,
“*On the nonlinear stress-strain behavior of nematic elastomers – materials of two coupled preferred directions*”
(submitted to J. Appl. Phys.).

I thank...

...Professor Helmut R. Brand, for making this work possible in the first place. For the various discussions and support during the whole course of this work. For the exceptional atmosphere within the group, and the manifold possibilities of scientific exchange. In particular, for the time and effort connected to my stay in Kyoto. For a lot of advice beyond the subject of this thesis.

...Professor Harald Pleiner, for the many stimulating and helpful discussions, and the support during the whole progress of this work; and, of course, for the invitations to the Max Planck Institute in Mainz.

...Professor Philippe Martinoty and his group, for their kind hospitality during my stays at Strasbourg, the cordial atmosphere, and the various helpful discussions.

...Professor Takao Ohta, for the time he spent and effort he made when hosting me in his group at the University of Kyoto. Professor Ohta and his whole group for the valuable discussions and their effort of introducing me to the Japanese way of living. Professor Shoichi Kai, Professor Mitsugu Matsushita, Dr. Nariya Uchida, and Dr. Makiko Nonomura, for their hospitality during my further trip through Japan.

...Professor Heino Finkelmann and his group, for the invitations to Freiburg and their seminars, which could always be characterized as an enjoyable combination of scientific and social exchange. And, of course, for synthesizing the background of this work.

...Professor Kenji Urayama, for the various helpful discussions, and for providing the data points of the stress-strain measurements, which have allowed a direct comparison of our model to the experimental results.

...Professor Gerhard Platz and Dr. Christian Wolf, for the fruitful collaboration during the work on the patterns of parabolic focal conics.

...Dr. Daniel Svenšek and Miha Ravnik, for organizing my stay at Ljubljana, which had significant impact on the course of this work, and Miha, for the trip to the Slovenian mountains.

...My parents and my brother, for their invaluable support beyond the immediate field of this work.

